

Caverns Measureless to Man: Interdisciplinary Planetary Science & Technology Analog
Research Underwater Laser Scanner Survey (Quintana Roo, Mexico)

by

Stephen Alexander Daire

A Thesis Presented to the
Faculty of the USC Graduate School
University of Southern California
In Partial Fulfillment of the
Requirements for the Degree
Master of Science
(Geographic Information Science and Technology)

May 2019

“History is just a 25,000-year dash from the trees to the starship; and while it’s going on its wild and woolly but it’s only like that, and then you’re in the starship.” – Terence McKenna.

Table of Contents

List of Figures	iv
List of Tables	xi
Acknowledgements.....	xii
List of Abbreviations	xiii
Abstract.....	xvi
Chapter 1 Planetary Sciences, Cave Survey, & Human Evolution.....	1
1.1. Topic & Area of Interest: Exploration & Survey.....	12
1.2. Incentives, Orientation, Motivation, & Significance	23
1.3. Hypothesis, Goal, Design, Phases, & Questions	29
1.3.1. Objectives	30
1.3.2. GIST PSTAR Thesis Blueprint.....	32
Chapter 2 Related Works	33
2.1. Exploration, Research, & Development in Planetary Sciences	39
2.1.1. Quantum: Spectrometry, & Biology - Scientific Synesthesia, & Holographic VRLs.....	43
Chapter 3 Data & Methods	51
3.1. Conceptual Framework.....	52
3.2. Schedule, Timeline, & Workflows	54
3.3. Research Design.....	62
3.3.1. Goals & Objectives	63
3.3.2. Phenomena & Sampling	64
3.3.3. Research Apparatus: Survey, Speleonation, & 3D GIST	64
3.3.4. Variables: Definition & Measures	80
3.4. Data Requirements & Sources	81

3.4.1. Datasets & Qualities	82
3.4.2. Origins & Physical Congruencies	82
3.4.3. Data-dictionary & Entity-Relationship Diagram	82
3.4.4. Limitations	83
3.5. Procedures & Analysis.....	88
3.5.1. Model Development & Analog PSTAR Operations Narrative.....	89
3.5.2. Expected Outcome	90
3.5.3. Equations, Weighting, & Schemes	97
3.5.4. Modus Operandi.....	99
3.5.5. Analytic Assumptions.....	100
Chapter 4 Results	101
4.1. Methods Evaluation	102
4.2. Facts	137
4.3. Evidence.....	150
4.4. Findings & Claims	175
4.5. Outcomes	199
Chapter 5 Discussion & Conclusions	201
5.1. GIST, QCED, Moduli Fields of Vacua, & Quasicrystals.....	203
5.1.1. Limitations of Accomplishments.....	204
5.2. Future Research	208
5.3. Summary of GIST Contributions.....	214
References.....	217
Appendices.....	231
Appendix A. Conceptual Periods in Speleogenetic Thinking	231

Appendix B. Glossary	241
Appendix C. Analog Martian & Terrestrial Atmospheric Environmental Contexts	245
Appendix D. Martian Kart of Noctis Labyrinthus and Robotic RS Survey Geohazards	246
Appendix E. International Union of Geological Science Holocene Subdivisions (Cohen et al 2018 update).....	247
Appendix F. Karst Geohydrological FOI Datasets & Definitions Table.....	248
Appendix G. Microsoft Access Karst Database.	258
Appendix H. ERD of cave system datasets (Daire et al. 2017).	259
Appendix I. GIST Project Schedule for ULS Cave Survey Deployment Table.....	260
Appendix J. Project Field Survey, Dive Plan, & Crew Procedures Table.....	271
Appendix K. Fractal Marble AgiSoft Parallel Projection & DEM Processing Parameters	296
Appendix L. Philosophies, Procedures, & Tools for Subaquatic Survey & Survival	301
Appendix M. Nebenhaus, Mayor, Daire, & Loew Spatial Datasets of Sistema Taj Mahal	302
Appendix N. Laser Classification & Safety Datasheet.....	303
Appendix O. Exported AgiSoft DTM for Full Cave Photoplethysmogram in Cloudcompare ...	304

List of Figures

Figure 1 Interdisciplinary Research Domains of Speleology with PSTAR Potential	2
Figure 2 Thesis Goal, Phases, Objectives, and Details	6
Figure 3 PSTAR Goal & Objectives.....	12
Figure 4 3D cross-section overlay of cenote karst map diagraming a Conceptual Model of Phreatic Karst Science Topics..	17
Figure 5 Yucatan Peninsula AOI Map.....	18
Figure 6 Cenotes proximate to highway 307	19
Figure 7 BRCA grade 1 AOI map with overlain FOI survey.	20
Figure 8 BRCA Grade 3 Map with .svg raw polylines-spheres	21
Figure 9 Research Benefits Matrix for Scientific Fields	26
Figure 10 Societal & PSTAR Benefits Matrix.	27
Figure 11 Epic Games Mars 2030 Mission Simulator.....	28
Figure 12 BRCA GIST Updated Grading Scale.....	35
Figure 13 Oceanic Karst Development.....	36
Figure 14 Karst Aquifer Network Flow Recharge.....	37
Figure 15 QCED Relativistic Commutating White Body Core – Black Body Shell Multidimensional Quantitative Chroma Spheroid-Wave Field Model	47
Figure 16 Project Workflow	57
Figure 17 Conceptual Phase.....	58
Figure 18 3D Printing for Sierpinski Octahedron.....	59
Figure 19 Disconnected-Outrigger & Spherical Underwater Survey Techniques.....	60
Figure 20 3D point cloud development from LiDAR and PhoDAR datasets.....	61
Figure 21 Photograph of traditional cave diving survey equipment.....	65
Figure 22 Photograph of diver propulsion vehicles for cave survey range extension.....	65

Figure 23 GIST equipment for remote sensing survey of cenotes and underwater caves with drones, VR, water quality, and fractal marbles.	67
Figure 24 Photo overlap series from FOI survey within the Deep Bone Room AOI.	69
Figure 25 2G Robotics ULS-200	70
Figure 26 Taylor Water Quality Test kit.....	71
Figure 27 MakerGear 3D printer.	79
Figure 28 3D Spatiometric-Spectrometric Sierpinski Octahedron Below, red, green, blue, contrast, and emergency fractal marker set.	79
Figure 29 Fractal Marble Parallel projection assessment in Agisoft Photoscan.....	79
Figure 30 Fractal Marble DEM analysis in Agisoft.....	80
Figure 31 Complex geometric features producing triangular irregular network imaging artifacts	85
Figure 32 Spatial Target coloration blending causing marker modeling invisibility image merge into AOI limestone texture located near paleontological remains	85
Figure 33 Scuba diver Off-gassing causing percolation and backscatter from sediment clouds.....	86
Figure 34 Diagram of four modulations of a Photonic Quantum Vortex (PQV) with different topological charged quantum electrodynamics (QED) phase-fronts.....	87
Figure 35 Photograph of Sistema Taj Mahal Cave Map on display at the cave entrance for crew navigation, mission planning, feature reference, & rescue response.	88
Figure 36 Preliminary modeling dataset geocoded surface survey coordinates in ArcGIS Pro AOI marked with a yellow dot.	92
Figure 37 Shearwater Petrel Dive computer datasets on depth, temperature, time, central CNS toxicity, breathing gas volume, PPN, and PPO LSS operational survey run time.	93
Figure 38 Preliminary PhoDAR dataset modeling of the DBR Interior restriction at entry within the red box, top down view as if entering chamber as a cave diver.	94
Figure 39 Preliminary modeling datasets	95
Figure 40 PhoDAR model of AOI interior from dive exit perspective with non-diffuse lighting causing voiding at shadows.....	96

Figure 41 PhoDAR AOI interior with contrast voids causing texting mapping distortions and bending in the 3D object.....	96
Figure 42 AOI PhoDAR image alignment for 3D Model QAC removing quality <.7.	97
Figure 43 ULS-200 Preparation with weighting & securing Fractal marker test.....	104
Figure 44 Sistema Taj Mahal, Cenote Taj Mahal Surface Survey, Rory collecting laser distance and ranging data.....	104
Figure 45 Sistema Taj Mahal, Cenote Sugarbowl, Field Camp.	105
Figure 46 Sistema Taj Mahal, Cenote Sugarbowl, GLONASS GPS data collection.	105
Figure 47 Cenote Mangrove survey with Fausto Tun Chx of Valladolid, Mexico.	106
Figure 48 Taylor water quality testing kit instructions, field, notes, and site sketch.....	107
Figure 49 Diver crew Dr. Marceline Nebenhaus (Blue helmet) & Natalie Gibbs (White helmet) prepare abseiled equipment and discuss mission plan prior to surge.....	108
Figure 50 Marceline Nebenhaus preparing to collect scanner with buoyant dive light providing operations area illumination.....	108
Figure 51 Sistema Taj Mahal, Cenote Sugarbowl, Field Camp and rope-ladder to entrance.....	109
Figure 52 ULS-200 scan of Cenote Sugarbowl entrance, vertical perspective looking down on divers from surface at 6m height.....	110
Figure 53 Lidar point cloud of .1cm scan resolution accuracy.....	111
Figure 54 Marceline Nebenhaus verifying survey North direction with contrast Black-White fractal marker & wrist compass.....	112
Figure 55 Astronaut-Scientist Sean Thompson confirming nominal IVA Suit function & communications for polar mesospheric cloud experiment simulation.	113
Figure 56 Photogrammetric model of the Deep Bone Room Entrance Restriction.....	114
Figure 57 Right, extracted Digital Elevation model of AOI from inside the Deep Bone room, up the restriction, and along the corridor from left to right.....	115
Figure 58 Astronaut-Scientist polar mesospheric cloud experiment mission plan, timing for synchronization, and relevant safety notes.....	117
Figure 59 Project PoSSUM Astronaut-Scientist polar mesospheric cloud experiment simulation cockpit data recorder for flight statistics, mission planning, & CRM.....	117

Figure 60 Craft simulated flight data for operation evaluations.	118
Figure 61 Patty Wagstaff Aerobatics Flight School Extra Flugzeugbau EA300 monoplane capable of unlimited category competition & G-force simulation..	120
Figure 62 Author & EA300 pilot Jeff simulating a polar mesospheric cloud experiment flight 5G to 0G-force, craft inverted & looping	120
Figure 63 Redundant sidemount rebreathers for advanced cave diving & survey.	121
Figure 64 Embry-Riddle University VRL Director Zach instructing Astronaut- Scientist in International Space Station simulation to prevent synesthesia sickness.	121
Figure 65 Astronaut-scientist flight simulation control under hypoxia Astronaut	123
Figure 66 Project PoSSUM hypoxia simulation training for astronaut-scientist crews at the Southern AeroMedical Institute with Dr. Paul Buza assessing	123
Figure 67 Photogrammetric resolution calculations for fractal marker assessment.	124
Figure 68 Esri, City Engine regional extraction for VRL contextual development and ULS point cloud integration.	127
Figure 69 ArcGIS Pro 3D regional scene with shuttle radar topography mission synthetic streams converted to 3D submerged tubes for point cloud integration.....	128
Figure 70 City Engine regional extraction for VRL contextual development & point cloud integration related to infrastructure & cadastral datasets.	128
Figure 71 Distance measurements of fluid turbulence from ULS-200 rotational axis on point cloud during data collection.	129
Figure 72 Cenote Sagrado cross-sections of anatomical planes in red, extracted from surveyor torso for scale determination for first response imaging.	130
Figure 73 Deep Bone Room cross-section with reference height, width, & length.	131
Figure 74 Two horizontal & vertical stitched cross-sections of openwater of Cenote Sugarbowl, Sistema Taj Mahal karst aquifer entrance	132
Figure 75 ULS-200 extracted Kd-tree planes as raw data in Cenote Sugarbowl	132
Figure 76 Semi-supervised image classification of fracture, distortion, & either-or schema of Kd-tree planes in fluid dynamics, QED, & matrix topography	133
Figure 77 Facet classification structure for fracture detection NDI representing dissolution-cleavage edges	133

Figure 78 A rope ladder imaging artifact quantum buoyant friction shadow.....	134
Figure 79 ULS non-linear optics extractions representing fractures or distortions requiring supervision for classifications related to PQVS & KHI	134
Figure 80 Histogram of cenote density to synthetic streams NDI correlating to winter tree canopy cover from IceSat datasets indicating cave presence.	135
Figure 81 Heat map of derived karst-NDI data of caves compared to canopy density	136
Figure 82 Earth Stratigraphic Atmosphere Model.....	138
Figure 83 Earth Atmospheric Carbon Density.....	139
Figure 84 Remote Sensing signal range & environmentally induced interference	140
Figure 85 Polar mesospheric cloud simulations of atmospheric dynamics.	141
Figure 86 Polar mesospheric cloud simulations of Density-shear KHI.....	142
Figure 87 Laser goggles attached to cave-diving helmet for eye-safety	145
Figure 88 ArcGIS Pro 3D polygon development of surveyed cenote entrances related to synthetic stream locations and heat density mapping.....	146
Figure 89 ArcGIS Pro map development of unsurveyed cenotes in region of future exploration interest.	146
Figure 90 ArcGIS Pro development of cenote entrances related water table depth.	148
Figure 91 ULS-200 Ceiling percolate backscatter influencing scan accuracy..	149
Figure 92 Water sample analysis for alkalinity, hardness, & pH from the DBR	151
Figure 93 Salt water sample analysis for chlorine, copper, nitrates, & nitrites..	151
Figure 94 ULS transverse scan of KHI related to karst topographic profile & halocline, outer-square, & flow direction.....	153
Figure 95 A plot of an instantaneous Gaussian beam around a focus at an instant of time, showing two intensity peaks for each wavefront	156
Figure 96 Relationship diagram between properties of harmonic waves: frequency, period, wavelength, angular frequency, & wavenumber.....	157
Figure 97 Cross-section of matrix wall & roof collapse with Hele-Shaw Flow inducing KHI Turbulence.....	158

Figure 98 ULS raw data in Cenote Sugarbowl openwater entrance bearing quantum buoyancy & friction.....	159
Figure 99 Boresight perspective PQV induced QTK in ULS pulse bearing hypergeometric-Gaussian mode & comodulating-commutating spiral vertexes	160
Figure 100 Rear offset perspective ULS camera with visible PQVS QTK interference peaks, +40% brightness and -40% contrast variation highlighting of the original photo..	161
Figure 101 Rear offset perspective ULS camera with visible PQVS beam troughs preceding QTK, -40% brightness and -40% contrast of the original photo.....	162
Figure 102 Rear offset perspective ULS camera visible PQVS QTK beam decay, -40% brightness and +40% contrast of the original image.	163
Figure 103 Rear offset perspective ULS camera with visible PQVS beam QED dynamics, 40% brightness and 40% contrast of the original image..	164
Figure 104 ULS scans presentng backscatter and imaging noise extracted as non-linear optics distortions Kd-tiles.....	165
Figure 105 Yellow box presenting planarized facet of naturally occurring photonic quantum vortex from sunlight	166
Figure 106 One of sixteen perspective orientations of holographic inverted reflections bearing accurate volumetric holonomies from a homothetic core at 1-1.5m scale	167
Figure 107 Two of sixteen perspective orientations of holographic inverted reflections bearing accurate volumetric holonomies from a homothetic core at 1-1.5m scale	168
Figure 108 Three of sixteen perspective orientations of holographic inverted reflections bearing accurate volumetric holonomies from a homothetic core at 1-1.5m scale	169
Figure 109 Four of sixteen perspective orientations of holographic inverted reflections bearing accurate volumetric holonomies from a homothetic core at 1-1.5m scale	170
Figure 110 Five of sixteen perspective orientations of holographic inverted reflections bearing accurate volumetric holonomies from a homothetic core at 1-1.5m scale	171
Figure 111 Six of sixteen perspective orientations of holographic inverted reflections bearing accurate holonomies from a homothetic core at 1-1.5m scale	172
Figure 112 Informal 16D PQVS Harmonized Fibrational Phase Index Orbifold.	174
Figure 113 Semiformal 16D PQVS Harmonized Fibrational Phase Index Orbifold.....	178
Figure 114 3D Apollonian Sphere Packing	185

Figure 115 Vertex transitive omnishub icosahedral honeycomb $s\{3, 5, 3\}$ with a sunb dodecahedron, octahedron, & tetrahedron that cannot be produced via uniformity	186
Figure 116 Order-3 regular icosahedral honeycomb sphere model $\{3, 5, 3\}$ Semiformal Multiresolution-Multiphasic Orbifold Index	187
Figure 117 Penrose Diagrams of various blackhole slutions for topologically flat spactime & time-like wormholes.....	189
Figure 118 Wadabasin fractal developed in Mandelbub 3D fractal generator for 6 16D reflective inversions, with holonomic transliterations via a homothetic center	192
Figure 119 Fractal developed in Mandelbub 3D fractal generator with Complex Julia Set Dynamics for representative topobathic lidar TPU conceptual model.....	192
Figure 120 Project PoSSUM Astronaut-Scientist Candidate in an underwater VRL International Space Station spacewalk simulation with ULS-200 scanning.	196
Figure 121 MC tomography experiment IVA full simulation Scientist-Astronaut operating GIST toolkits & Embry-Riddle Pilot-Astronaut controlling suborbital spacecraft flight. ...	196
Figure 122 Lightweight, compact, underwater drones promote future research projects operating as diving black boxes & rescuse tools	197
Figure 123 Yucatan Peninsula 3D Cave Density Geohazard Heat Map	198
Figure 124 Full cave ULS photoplethysmogram in Cloudcompare PhoDAR overlays, these materials can be exported into mapping files for full display	206
Figure 125 Models of human muscle proteins that degrade during astronautics missions, myosin, actin, & collagen.....	213

List of Tables

Table 1 Laser Crystal Topologies & Considerations	73
Table 2 Geovisual Hierarchy for AR/MR/VR and 3D Cartography	76
Table 3 ULS Survey Resolution Chart	143
Table 4 Sistema Taj Mahal Survey Water Quality Assessment for Cenotes Taj Mahal, Sugarbowl, & Sagrado in parts per million	152
Table 5 Photonic Quasicrystal - Vacua Unit Orbifold LiDAR Calibration & DTFE Quasi-Triangulation QCED Reference.....	179

Acknowledgements

Thanks to my family, Emery Nolasco, Richard Gerdes, Joseph Taraski, Kevin Galli, Dan Rapacki, Brandon Cook, Nicole Nir, John Sabin, and Dr. Veronika Puisa for inspiring discussions and development to produce survey tools. To my research advisors Dr. Jennifer Bernstein, Dr. Laura Loyola, Dr. Steven Fleming, and Dr. Su Jin Lee of University of Southern California Spatial Sciences Institute. Dr. Darrin York of Rutgers University Center for Integrative Proteomics Research York Laboratory. To Christine Loew, Diving Caves Owner, Razor Sidemount & TDI Cave Instructor for training, equipment, facilities, repair tools, and survey support. To Natalie Gibbs, Under the Jungle Owner, Explorer, Razor Sidemount & TDI Cave Instructor for training, equipment, facilities, repair tools, and lots of coffee. To Jeronimo Aviles, Director General of The Institute of Prehistoric Americas and the Museum of the Desert for laboratory space, locality access, remains assessment, equipment, and diving support. To Dr. Marcelin Nebenhaus of Under the Jungle for his cave line survey map of Sistema Taj Mahal (2017). To David Mayor for his Mnemo line survey data of the Taj Mahal system. To Dirk Penzel, of Cenote Diving, for access to ancillary reference exit markers for survey. To Rory OKeefe of the Quintana Roo Speleological Society for surveying in the rain at night, twice. To Don Feliciano Tun Tah and his family for site access. Finally, to Bil A. Phillips (1955-2017) cave diving researcher, explorer, instructor, and innovator, Explorers Club Fellow, and owner of Speleotech for his support, training, guidance, recommendations, and planning critiques of this project concept, *requiem in pacem aeternam*.

List of Abbreviations

μm	Micrometer
ρ	Fluid Density
AOI	Area of Interest
APE	Area of Potential Effect
BQP	Bounded Error Quantum Polynomial Time
BRM	Behavior Related Modification
CAA	Confidential Archaeological Addendum
CAL	Confidential Archaeological Letter
CCPR	Contamination Control Plan and Requirements
CIRM	Crew and Individual Resource Management
CIRMSS	CIRM Survival and Safety
CRM	Crew Resource Management
CRSI	Cohort Remote Sensing Instruments
CSV	Comma Separated Value
CTH	Complex Topography Hypothesis
DARPA	Defense Advanced Research Projects Agency
DBR	Deep Boone Room
D&E	Design & Engineering
DEM	Digital Elevation Model
DIM	Digital Image Model
DOF	Degrees of Freedom
DPFAR	Developmental Problem/Failure Anomaly Reporting
DPO-LIBS	Dual Pulse Orthogonal Laser Induced Breakdown Spectrometry
DTFE	Delaunay Tessellation Field Estimator
DTM	Digital Terrain Model
EES	Extended Evolutionary Synthesis
EQA	Environmental Quality
ETE	Extraterrestrial Environment
ETRR	Environmental Test Readiness Review
FCR	Fire Cracked Rocks
FOR	Field of Regard
FOV	Field of View
FXB	Filename Extension Bank
Ga	Gigaannum
GHR	Ghyben-Herzberg Relationship
GIS	Geographic information system
GISci	Geographic information science
GIST	Geographic information science & technology
GSE	Ground Support Equipment
HBE	Human Behavioral Ecology
H/W	Hardware
HQ	Headquarters
HSF	Hele-Shaw Flow

HUD	Heads-up-display
IARPA	Intelligence Advanced Research Projects Activity
IOP	Intraorbital planetary
IR	Infrared
ISS	International Space Station
ka	Kiloannum
KHI	Kelvin-Helmholtz Instability
LASER	Light Amplification by Stimulated Emission of Radiation
LIBS	Laser Induced Breakdown Spectrometry
LiDAR	Light Detection and Ranging
LULC	Land Use and Land Change
LXO	Low Xenoplanetary Orbit
ma	Megaannum
MEL	Master Equipment List
MXD	Map Exchange Document
NASA	National Aeronautics and Space Administration
NDI	Normalized Difference Index
NISN	NASA Integrated Services Network
Nm	Nanometer
Ns	Nanosecond
ORT	Operational Readiness Test
PCA	Principal Components Analysis
PETR	Post-Environmental Test Review
PFAMR	Problem/Failure Anomaly Management & Reporting
PLEOP	Post-landing Environment Operational Procedures
PMC	Polar Mesospheric Cloud
PPDE	Planetary Protection Design & Engineering
PP-CR	Psycho-Physiological Contingency Response
PPP	Planetary Protection Plan
Ps	Picosecond
PQV	Photonic Quantum Vortex
PQVS	Photonic Quantum Vortex Slipstream
PSTAR	Planetary Science and Technology through Analog Research
QAC	Quality Assurance and Control
QB	Quantum Buoyancy
QCED	Quantum Chromo-Electro Dynamics
Qi-Fi	Quantum Information Transmission Fidelity
QTK	Quantum Topological Knotting
RASP	Rapid Acquisition Sampling Package
RS	Remote Sensing
SASER	Sound Amplification by Stimulated Emission of Radiation
SCH	Submerged Cultural Heritage
SoNAR	Sound Navigation and Ranging
SSI	Spatial Sciences Institute
SVG	Scalar Vector Graphic

SWORT	Strength, Weakness, Opportunity, Risk, & Threat
TBD	To Be Determined
TPU	Total Propagated Uncertainty
TRN	Terrain-Relative Navigation
ULS	Underwater Laser Scanner
USC	University of Southern California
USGS	United States Geological Survey
UTM	Universal Transverse Mercator
UV	Ultraviolet
V&V	Verification & Validation
VRL	Virtual Reality Laboratory
VRV	Virtual Reality Vertigo
VTD	Voronoi Tessellation Diagram
WQ	Water Quality
XML	Extensible Markup Language

Abstract

This work outlines an underwater laser scanner (ULS) operational readiness test (ORT) demonstrating the efficacy of ULS-200 in response to National Aeronautics and Space Administration (NASA) Planetary Science and Technology through Analog Research (PSTAR) Program knowledge gaps. This geographic information science and technology (GIST) project advises stakeholders on extravehicular activity (EVA) design and engineering (D&E) via cave diving. Analog surveys define strengths, weaknesses, opportunities, risks, and threats (SWORT) in three-dimensional (3D) remote sensing (RS) detection and ranging (DAR) via light (LiDAR) and photogrammetry (PhoDAR). Sidemount cave diving procedures and life-support systems (LSS) facilitate paleontological, hydrogeological, and microbiological evidence sampling, mitigating crew resource management (CRM) risks. 3D geographic information systems (GIS) toolkits produce LiDAR and PhoDAR digital terrain models (DTM) that require British Cave Research Association (BCRA) GIST quality assessment and control (QAC) modernization.

Research outcomes included survey cost reductions, a $< .15$ cm precision $\approx 2,000\text{m}^3$ karst photoplethysmogram (volumetric LiDAR cavity system measurements) scan completed in < 5 days and a GIST human-robotic (H-R) CRM PSTAR D&E SWORT ORT. Products included geohazard maps, a regional karst network 3D GIS, a LiDAR photonic quasicrystal-vacuum orbifold indicatrix, and 3D underwater imaging artifact characterizations. Analog extraterrestrial environmental (ETE) analysis occurred in Cloudcompare, datasets were unable to be uploaded for virtual reality laboratory (VRL) simulation in Esri City Engine. This work provides PSTAR D&E references in high-fidelity EVA simulations, H-R ergonomics, quantum physics, and area of potential effect (APE) planetary protection design and engineering (PPDE).

Chapter 1 Planetary Sciences, Cave Survey, & Human Evolution

Speleonauts (cave diving scientists) and astronauts incur risks while surveying extreme environments and mitigate hazards through detailed references, simulations, and technological innovation (Reimuller et al. 2015; Carney et al 2013; Neufeld and Charles 2015). Inundated cave surveys have been limited in terms of physical accessibility and contextual quality due to remote distribution, geospatial inaccuracy, extreme environmental hazards, and CRM accidents (Andreo et al 2015; Klimchouck et al. 2000; Armstrong 2017). In the past, solar system and phreatic karst survey both required return-to-sender environmental quality (EQ) sampling for isotopic analysis in laboratories (Hunsaker 2001). PSTAR ULS SWORT ORT cave surveys signify high-fidelity planetary sciences, scientific communication, biogeographic human behavioral ecology (HBE), LSS, H-R CRM ergonomic dynamics, CIRM (Crew and Individual Resource Management), CIRM Survival and Safety (CIRMSS), and other EVA analogies (Cruz et al. 2015).

Light amplification by stimulated emission of radiation (LASER) technologies are extending laboratory quality spectrometry to *in situ* domains for research field application and GIST project management (Fortes et al 2013; Obermeyer and Pinto 2008). ULS require detailed calibration assessments for total propagated uncertainty (TPU), Unruh effect, quantum buoyancy (QB), photonic quantum vortex (PQV), quantum topological knotting (QTK), quantum chromo-electrodynamics (QCED), fractal dimensional analysis, and other phenomena (Mandelbrot, B. 1983; Law & Rennie 2015; Larocque et al 2018; Freire et al 2017; Feng et al 2017; Takeuchi 2015; Hod 2011). Figure 1 presents interdisciplinary research domains of speleology within GIST surveys which meet PSTAR needs for development of educational materials through analogous operations providing invaluable references for scientific literacy in the future. ULS

deployed for LiDAR cave surveys promote trilateral synergistic developments for GIST, PSTAR, and underwater speleology.

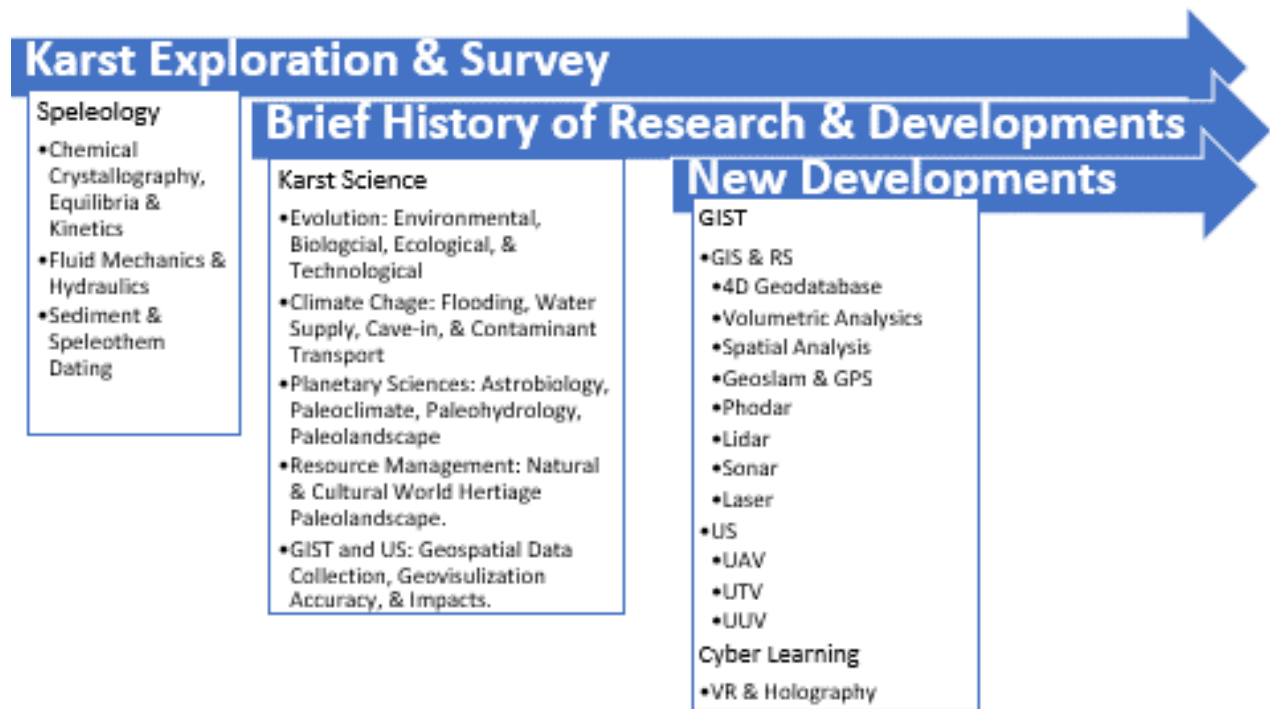


Figure 1. Interdisciplinary Research Domains of Speleology with PSTAR potentials

The Earth’s sphere is approximately 30% terrestrial, 70% aquatic. 70% of the total liquid H₂O on Earth is subterranean, 25% of that drinking water resides in karst aquifers (Benson and Yuhr 2016). Cave environments are research focuses of planetary sciences because of their interrelationship with our species, *Homo sapiens*, as shelters and water access point for millions of years (Nunn 2011; Jaubert et al 2016; Stinnesbeck 2018. 2017; Daire et al 2017). Current research in cave formation, extremophile microbiology, human genetics, and niche construction theories concurrently developed with aerospace technologies, while subaquatic cave RS field incurred a 50-year deployment lag time (Winder et al 2013; Laland 2015; Nunn 2011).

Developments in GIST are providing new perspectives into environmental and human

coevolution through ULS and 3DGIS. These are promoting new geochronological scale classifications and improved planetary science field survey methodologies (Alvey et al 2010; Pořízka et al 2012; Sakka et al. 2012). There is crucial need for scientific references development related to these concepts as human activities impact planetary environments through unforeseen agencies (Spidle et al 2013; Morwood 2005). Unless sampled via ULS laser ablation molecular isotopic spectrometry (LAMIS) beforehand, planetary science evidence within caves on geoheritage, biodiversity, and linguistics will be lost to humanity (Diaz-Bolio 1975; Blamey et al. 2016; Parks and Mulligan 2010).

Capacities to overcome environmental and training obstacles are converging via GIST (Weidner et al 2016). ULS dual pulse orthogonal – laser induced breakdown spectrometry (DPO-LIBS), 3DGIS, and VRLs expedite innovative interdisciplinary research. ULS improve dataset accuracy collection standards for karst modeling by providing $\approx 5,400$ LiDAR ranging points per line (PPL). ULS 5m radii cylindrical cross-section scans at 5m line segments along the caveline transect provide high quality data collection. A maximum observed ULS pulse environmental quality (EQ) sampling distance of ≈ 25 m provides geospatial accuracy at $< .15$ cm PPL within sampling radii.

Hydrogeological, hydrochemical, paleontological, and microbiological evidence collected during transects via LiDAR can be integrated with PhoDAR overlays for stereoscopically realistic photoplethysmogram reconstructions. Planetary sciences interests relate to numerous factors within HBE activity, occupation, and exploration phases into caves over hundreds of thousands of years. PSTAR requires GIST ULS deployments, applications, and simulation products to overcome past research obstacles. Each project phase, objective, and

element are considered and evaluated through the Heilmeier catechism against the final PSTAR EVA ULS ORT for SWORT analysis.

George Heilmeier, Defense Advanced Research Projects Agency (DARPA) director (1975-1977), crafted the "Catechism" to help DARPA and Intelligence Advanced Research Projects Activity (IARPA) officials think through and evaluate proposed research programs. This mantra includes, explaining what the research aims by articulating its objectives without jargon. The catechism elicits inquiry on how operations are conducted today and the present limitations. The doctrine then requires clarification of the new approach, and estimations of potential success. It assesses the audience of interest related to the systems and concerns. It conducts a pensive ORT SWORT review of the implementation benefits, risks, costs, and duration. The framework finally aims to determine success via mid-term and final evaluations.

With the Catechism set as a guide post, the research goal aimed to conduct and assess a successful ULS EVA analog survey ORT deployment for speleonator and astronautic survey SWORT assessment. Phase 1 identified and defined a safe and successful ULS EVA analog survey deployment developed with a jargon free explanation of the project aim along with references on research questions. Figure 2 presents a clockwise-radial Catechism diagram extending from the project goal. Phase 2 subsequently assessed risks, existing systems reviews, geodatabase (GBD) management, DTM developments, geoanalysis techniques, products QAC, and a modified BCRA EVA analog SWORT ULS survey metric for achievement assessment. Phase 2 also required an exhaustive review of existing apparatus, datatypes, metadata, logistics, costs, benefits, time requirements, and limitations for a cohort RS instruments (CRSI) analog survey deployment. PSTAR mission planners, topobathic LiDAR engineers, DARPA and IARPA officials, urban planners, speleologists, microbiologists, paleoclimatologists, geophysicists,

urban planners, and world heritage conservators were identified as the concerned technical audience. Phase 2 then conducted the survey by consolidating, calibrating, and deploying subaquatic LiDAR, PhoDAR, and LSS for a karst hydrogeological chemistry EQ sampling ORT for environmental GBD construction utilizing analogous master equipment list (MELs) required for PSTAR ETE EVA operations. Phase 3 employed the research methodologies on products from the ORT survey for environmental reconstruction for SWORT progress benchmarks pre, mid, and post mission. These evaluations on deployments elucidate mitigative solutions for APE planetary protection plans (PPP), CRM risk reductions, and LiDAR improvements. Phase 4 vetted the impacts, concerns, and limitations against mapping product BRCA benchmarks. The project conducted a success analog research survey from the developed timelines, NOAA Diving Standards, implemented toolkits, and sampling techniques. Phase 5 SWORT assessment and discussion of ULS analogs highlights potential and limitation in terms of CRM, H-R, RS, and science, technology, engineering, art, and mathematics (STEAM) educational and research reference developments. SWORT assessment, prefaced by a terse history of speleology and biogeography provides a bridge between past obstacles, current needs, and future PSTAR MEL inclusions and STEAM references (NASA ROSES PSTAR 2018).

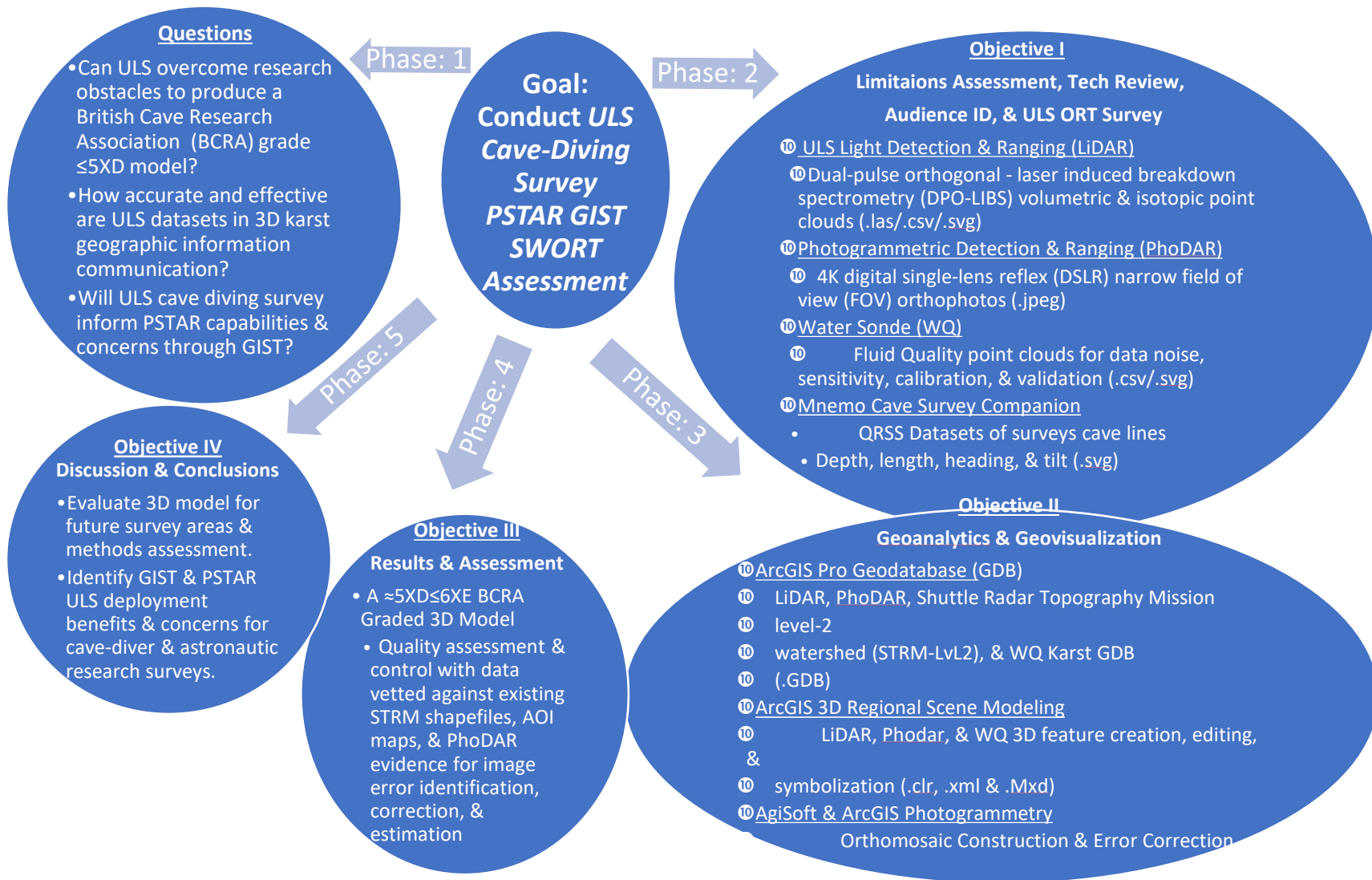


Figure 2. Clockwise divergent-radial Heilmeier Catechism diagram developed for high-fidelity ULS EVA analogs.

Early biogeographic observations resonated within western academia as ancient groups began relating cultural myths to locations to explain their position and understanding of the natural world. Ancient Greek geographers began crafting maps of the known world and providing explanation on differences of regional groups of people. Overtime concepts, research, and access have grown with generations of biogeographers employing new tools and techniques by means of education and research. Appendix A provides a terse history of biogeography and speleology which provides a bridge between past obstacles, current needs, and future GIST PSTAR equipment applications. Appendix B provides a technical glossary related to relevant to scientific concepts and apparatus in GIST, PSTAR, and cave diving. The glossary presents a relevant review of the terms required for a karst data dictionary and GDB to evolve over time with identification of new specimens, AOIs, and FOIs (geochemistry, bioperturbation, paleoenvironments, etc.). These two Appendixes serve as resources for reflections on limitations and conversations on new system potentials afforded to current RS surveys extending beyond the Earth Sphere.

These broader classical concepts are historical footnotes in modern sciences relative to current discussions and serve as contextual reflections for evolving perceptions and developments in topics and tools for planetary sciences, evolutionary biogeography, hydrogeomorphology, and paleolithic HBE. GIST surveying translates a thematic progression of planetary sciences with interdisciplinary speleology, anthropology, and PSTAR over the millennia intersecting within ULS surveys. These historical observations denote past limitations and current potentials of CRSI technologies to reconstruct our species lost historical narratives and evolutionary contexts related to globally inundated paleolithic landscapes. HBE relationships

provide comparatives and evidence for recognition of lost cultural narratives, HBE responses to climate change, and relative sea-rise induced Paleolithic LULC.

Protohistoric periods possessed neither biogeographers nor ethnographers, the archaeological filter (e.g. unsuccessful preservation destroying evidence sets) impedes paleoenvironmental reconstructions of lifeways and perspectives from humanities paleolithic past. These paleolithic narratives inform current climate change resilience, Earth systems management, and urban planning schemas. Paleolithic HBE and LCLU reflect cultural loss that extends an analogy that translates to paleoenvironmental-paleolithic restructuring and HBE coevolution related to sea-level fluctuations, and caves and continental shelf habitat flooding (UNESCO 2002; Jones & Christal 2002; NMAI. 2017; National Park Service, 2017). Prehistoric, historic, and formative research periods of karst studies over human history related to geospatial cognition, geoheritage awareness, and planetary sciences dynamics. This summary references the diverse historic settings of planetary sciences fields and cave research concepts set in a context to inform PSTAR and GIST deployment, development, and research planning. ULS accommodates heightened spatial cognition of subaquatic and subterranean environments by providing high accuracy EQ sampling via Nanosecond (Ns) LAMIS Rapid Acquisition Sampling Package (RASP) *in situ* analysis.

Applications of LDAR LAMIS on Earth provides lessons on ETE EVA for D&E PSTAR references. ULS promote effective sampling by producing photoplethysmograms with a minimum of quality of BCRA grade 3 modeling. ULS reduce survey cost, mitigate risk, expedite accurate and precise volumetric EQ sampling, and facilitate high quality 3D modeling. Cave system photoplethysmograms extend mapping standards beyond subterranean geographic communication and temporal analysis limitations. Appendix B provides a glossary of scientific

research concepts in underwater speleology, LSS, RS, biogeography, extended evolutionary synthesis (EES), niche construction hypothesis, complex topographic hypothesis, and paleolithic HBE climate change response (Clark 2000; Jacřková, K and Romportl 2008). Paleolithic communities utilizations of caves included water access, protective habitats, funeral grounds, and ambush hunting sites. Relative sea-level fluctuations induced HBE dynamics as Pleistocene landscapes were inundated and paleolithic communities were forced to displace and adapt to new lifeways. Understanding past climates promotes understanding of organismal and environmental coevolution on Earth, which in turn promotes PSTAR area of interest (AOI) field of regard (FOR) selection related to topography and water access for planning surveys, space habitat construction, and astrobiological ‘first contact’ interactions via anthropology and archaeology (Vakoch 2014). This assessment focused on geoarchaeology and paleoanthropology to contextualize current concerns and future research afforded by ULS-200 PSTAR cave deployments.

Water has been a locus of HBE and astrobiology research, life-as-we-know-it does not exist without water. Recent discoveries of liquid water on Mars require subaquatic cave RS SWORT assessments for impending EVAs into the regions for H-R RS surveys (Orosei et al 2018; Boston et al 2008). Seasonal watertable fluctuations relate to cave habitat access, utilization by paleolithic communities, and contemporary RS cave research surveys (Anita et al 2013). Regional rain cycles (e. g. seasonality) impose seasonal structural load capacity fluctuations on caves corresponding to hydrogeologic stress and failure Ghyben-Herzberg Relationship (GHR) zoning depth across individual karst aquifers (halocline, thermocline, chemocline, etc). These seasonal environment and structural factors relate to karst aquifers via

Archimedes of Syracuse fluid dynamics essays and proofs from *On Floating Bodies* circa 250BCE, approximately 2.268ka (*kilo annum* - thousands of years ago).

Archimedes' Principle on buoyancy provides metrics for karst load bearing and failure related to implosion or explosions (cave-ins or blowholes), and also provides methods to extrapolate total fluid volume, composition, and density of a karst aquifer. Fluid density (ρ – rho) of fresh water is 1000 kg/m³ and salt water is 1025 kg/m³. Each 1m of fresh or salt water gained or lost by an aquifer impacts regional depths and is subsequently gained or lost in load bearing capacity at $\approx 1010 \text{ kg/m}^3$ per m³ of fluid volume. Fluctuations induce failures periodically and chaotically, relative to the intensity and frequency of seasonal rain fall and evaporation, with human-karst environment coevolution causing accelerated cave formation dynamics. The regional maps and VRLs promote effective field methods development and implementations in analogous PSTAR education, simulation, modeling, and planning for survey and geohazard identification (Vassiliou 2007; VRARA 2017). This research project aimed to conduct an experimental speleonator ULS LAMIS survey for *in situ* real-time 3D hydrogeomorphometric photoplethysmogram AOI EQ sampling. ULS cave surveys of extremophile microbiomes, hydrochemistry fluid dynamics, karst structural fractures, complex topography, and submerged cultural heritage (SCH) BRM FOI respond to PSTAR knowledge gaps via high fidelity GIST D&E (NASA ROSES PSTAR 2018).

The survey methods and datasets produce AOI exploration and geohazard heat maps, as well as stereoscopic stratigraphic cross-sections for PSTAR ETE comparative analysis.

Appendix C presents a stratified Martian atmosphere diagram with polar mesospheric cloud (PMC) formation analogous to Earth's which currently impede orbital operations in the upper atmosphere. Atmospheric diagrams promote climate change assessments on Earth and provide

PMC comparatives for orbital entry debris avoidance on Mars. Appendix D displays a chronostratigraphic impact map of the Martian surface with karstic bearing features detected from RS, robotic exploration landing sites, PSTAR geohazards for cave-ins and steep slopes >15° avoidance, and a focus on the 10,000 km² area similar to the Grand Canyon - Noctis Labyrinthus - for landing site suitability, and H-R operational geohazards for equipment and habitat deployment considerations developed from the United States Geological Survey (USGS) HiRISE Martian chronostratigraphic universal transverse Mercator (UTM) impact crater LiDAR map (Tanaka et al 2014; Daire 2018).

This PSTAR analog and these two appendices translates to a pilot-astronaut and scientist-astronaut crew conducting a Martian LXO CRSI sorties via spacecraft or satellite. The astronauts produce AOI survival resource estimates and habitat site suitability maps related to Appendices C and D. They identify structurally sound landing points, conduct an orbital entry problem-tree mesospheric cloud risk analysis, land a robotic system or spacecraft near an AOI, deploy a space habitat, and finally conduct a H-R Martian EVA CRSI cave photoplethysmogram scan for PSTAR BCRA grading (Virrantaus et al 2009; Domagal-Goldman et al. 2011). Problem/Failure anomaly management & reporting (PFAMR) provides CRM contingencies to off-nominal conditions for accident response. Analog surveys promote comparative capabilities assessments of H-R principal component analysis (PCA) VRL comparatives for transect sampling simulations (Denson 2016). A SWORT post-environmental test review (PETR) distills experiences on benefits, costs, externalities, hazards, and obstacles related to post-landing environment operational procedures (PLEOP) with existing toolsets (Charles 2013; Neufeld and Charles 2015). Figure 3 presents three fidelity objectives of NASA PSTAR analogs present with ULS surveys as high fidelity PETRs (NASA ROSES PSTAR 2018).

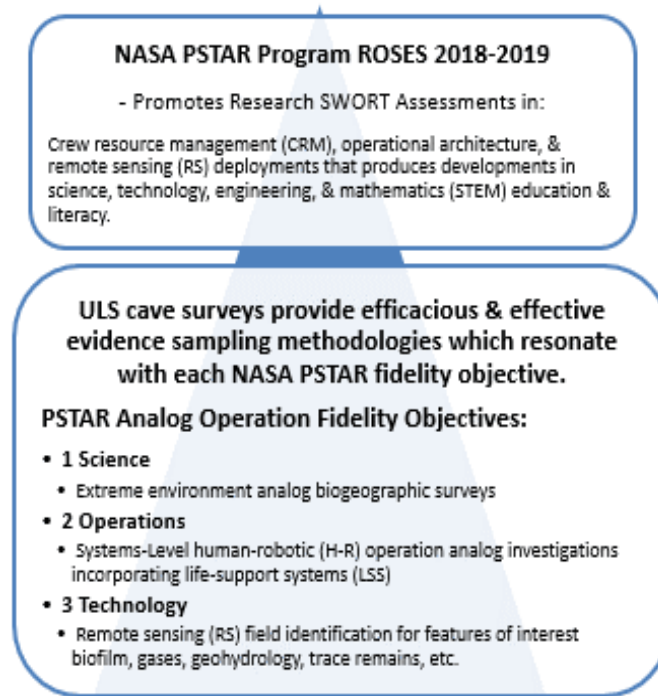


Figure 3. NASA Research Opportunities in Earth & Space Sciences (ROSES) PSTAR Goal & Fidelity Objectives ULS SWORT PETR ORT Diagram

1.1. Topic & Area of Interest: Exploration & Survey

Cave researchers have collected datasets in Yucatan Peninsula karst with increasing interest since the 1980s. The cave community’s exploration reports, survey logs, maps, and dive data have been compiled, curated, and organized by the Quintana Roo Speleological Society (QRSS) since 1985. The QRSS has promoted collaboration with volunteer divers conducting cave mapping projects, and also provides surveyors for research operations. Cave systems, geoheritage sites, and maps are discrete datasets. The datasets are discrete in terms of quantitative planetary science evidence, and confidentiality for world heritage conservation.

Confidential archaeological addendums (CAAs) and confidential archaeological letters (CALs) are primary tools in cave conservation etiquette and accident prevention but CAAs and CALs hinder research surveys. Containing knowledge of cave entrances, locations of remains,

and AOI maps deters harmful entries and accidents (Exley 1986). This system has worked in the past, with explicit agreements forged between private property owners and cavers, protecting sites and cavers (Carney et al 2013). Increasing interest in the cenotes as areas of recreation and ecotourism are placing numerous pressures upon the cave systems. These in turn are causing restrictions on diving activities on all fronts as land owners aim to limit access to prevent accidents, mitigate public health concern, and prevent endangered species losses in regional caves (Yoshizawa and Jeffery 2008).

The area of interest (AOI) is a cenote (sinkhole) on private land with access, by daily fee, for diving or swimming. The project team was allowed free access by the landowner with explicit permissions to conduct research. Cenote Tajma Ha, renamed from Taj Mahal by the land owners, has a volume of $\pi r^2 h = \pi \times 5\text{m} \times 15\text{m} \approx 3534.29\text{m}^3$, Cenote Sugarbowl possesses a volume of $\pi \times 6\text{m} \times 20\text{m} \approx 7539.82\text{m}^3$, Cenote Sagrado has a $\pi \times 5\text{m} \times 10\text{m} \approx 1570.79\text{m}^3$, and Cenote Mangrove has a volume of $\pi \times 5\text{m} \times 30\text{m} \approx 14137.16\text{m}^3$. Sistema Taj Mahal is comprised of a series of epiphreatic caves exposing the water table (QRSS1985). These four cenotes provide access to the karst aquifer for research, cave diving training courses, and ecotourism.

The cenotes are connected by labyrinthine, sponge work, collapsed, epiphreatic, and phreatic types of flooded passages with volume reducing as depth increases. Numerous hydrogeological, microbiological, and paleontological features of interest (FOIs) occur throughout the AOI and within the Deep Bone Room (DBR). The AOI is an admixture of karst, paleokarst, and pseudokarst in various stages of evolution. The Yucatan Peninsula is a limestone outcrop exposure, that was formerly a reef. Appendix E presents the most recently updated chronostratigraphic reference scale with the Holocene epoch now represented with the newly added conferred Anthropocene subdivision as it presents a new global stratigraphic reference

layer (Cohen et al 2018). The Yucatán plateau and reef experienced geologic uplifting over the period of 143Ma (*Mega annum* – millions of years ago) to 63Ma (Bonet and Butterlin 1962; Vázquez-Domínguez and Arita 2010). The reef has remained tectonically inactive providing stable chronostratigraphic calibration point for radiometric analysis of global planetary sciences datasets that benefit from these ULS chronostratigraphic scan training references.

Conducting ULS surveys provides datasets, calibrations, and techniques for equipment and environmental modeling developments for geohydrologists and PSTAR mission planners to access novel evidence and reference materials (Refsgaard et al 2007; NASA ROSES PSTAR 2018). These hydrogeochemical datasets also promote predictive dissolution modeling of karst systems. Experimental dissolution rates presented by Benson and Yuhr (2016) underestimate observed field dissolution conditions in the Yucatan, anthropogenic activities may be related to the discrepancy as they account for rough 60% of new sinkhole formation (Benson and Yuhr 2016; Spilde et al 2013).

Land use and land change (LULC) dynamics are putting literal and metaphorical strain on the regional karst platform. Pollution, deforestation, and development are accommodating global urbanization for growing populations, inducing and exacerbating regional speleogenesis. Dissolution increases are likely due to point source pollutant presence in the aquifer, as well as acidification and deoxygenation along oceanic-karst interfaces from HBE activity. Karst EQ monitoring mitigates water contamination by locating pollution sources and restricting them (Alcocer et al 1998; Martínez-Navarrete et al 2011). Karst matrix structural loading capacities on air and water filled caves relate to sinkhole formation related to pollution modeling via Archimedes' principle. ULS help to plan future urban developments related to flood plains,

sinkholes, karst fractures, water contamination, and geoheritage conservation by sampling and characterizing site suitability and structural weakness (Bostenaru et al 2014).

In the archaeological record water resource concerns, decision-making, and planning have been linked to the waxing and waning of various cultures. Illegal hotel development causing cave-ins, cave excavations to provide ecotourists recreation, and world heritage looting are all dynamics interacting karst geoheritage through increasing anthropogenic impact and exacerbation of speleogenesis. Indiscriminate and illegal building, deforestation, water extraction, and sewage disposal all exacerbate speleogenetic processes on the Yucatan Peninsula karst system by direct and indirect aquifer modification. Geoheritage evidence on paleontological, palaeoclimatological, paleoenvironmental, and biogeographic evolution are at risk due to anthropogenic activity.

Relative sea-level rise from carbon emission and looting are restricting site access as well as destroying world heritage. Figure 4 presents a 3D cross-section overlay conceptual model illustrating topics relating to planetary phreatic karst science sciences processes occurring since the 66ma Chixulub impact on the peninsula. The Chixulub near Earth object (NEO) impact created a series of radiating fractures & cave systems in the Yucatan region. The impact induced the Cretaceous – Paleogene (K-Pg) extinction event boundary which is one of several chronostratigraphic calibration points in Earth's 4.5Ga (billions of years) evolutionary history. The NEO and its ejected iridium-layer acts as a reference for subsequent biogeographic evolution and relative sea-level rise for research sites globally. Figures 5 through 8 represent the AOI on finer scales with increasing accuracy to highlight subaquatic cave survey and mapping progressions related to GIST. These map highlights the efficacious GIST applications in cave diving and PSTAR survey for accuracy improvements, risk mitigations, and cost reductions

(Stafford et al 2017). Figure 5 presents a map of the Yucatan peninsula, with NEO impact crater located 50km north of the city of Merida. This celestial impact is analogous to impact points on extraterrestrial surfaces of Mars and the Moon, providing a baseline for analog PSTAR ULS microgravity and LSS missions translating to effective EVA proving grounds. Figure 6 presents regionally extrapolated cave system synthetic stream networks and AOIs within a 5km buffer of Federal Highway 307. These caves possess geheritage evidence and represent infrastructure geohazards. Figure 7 is the first extant British Cave Research Association (BCRA) grade 1 survey sitemap of the Sistema Taj Mahal AOI certified by the QRSS. This map was produced with traditional subaquatic cave survey tools and techniques by Nebenhaus (2017). The map is the primary geospatial reference of DBR AOI and a BRCA research assessment benchmark. Figure 8 presents volunteered geographic information (VGI) of the most recent, accurate, and rapidly produced AOI grade 3 BCRA map with juxtaposed raw Mnemo scalar vector graphic (.svg) DTM datasets. QRSS VGI was presented to this research by the principle surveyors for a photograph and is the most accurate and more rapid cave line survey of the AOI by any team over the past 15 years of active exploration. This VGI was provided with the stipulation of non-disclosure of exact site locations to the public, the .svg datasets represent surveyed cave lines and tie-offs station collected via underwater velocimeter, declination compass, and level. The .svg datasets can be exported in filename extension bank (.fxb), extensible markup language (.xml), comma separated values (.csv), and map exchange document (.mxd) which provide interoperable thematic layers for analysis, research, and 3D modeling. These datasets are not exhaustive and substantial portions of the cave remain unsurveyed. These features and remains took tens of thousands of years to form or become fossilized and possess detailed and undocumented paleoclimatological and paleoecological evidence.

Quintana Roo, Mexico



Figure 5. Yucatan Peninsula Map AOI marked within orange box, submerged paleolithic sites relate to \approx -130m relative sea-level (Daire et al 2017).

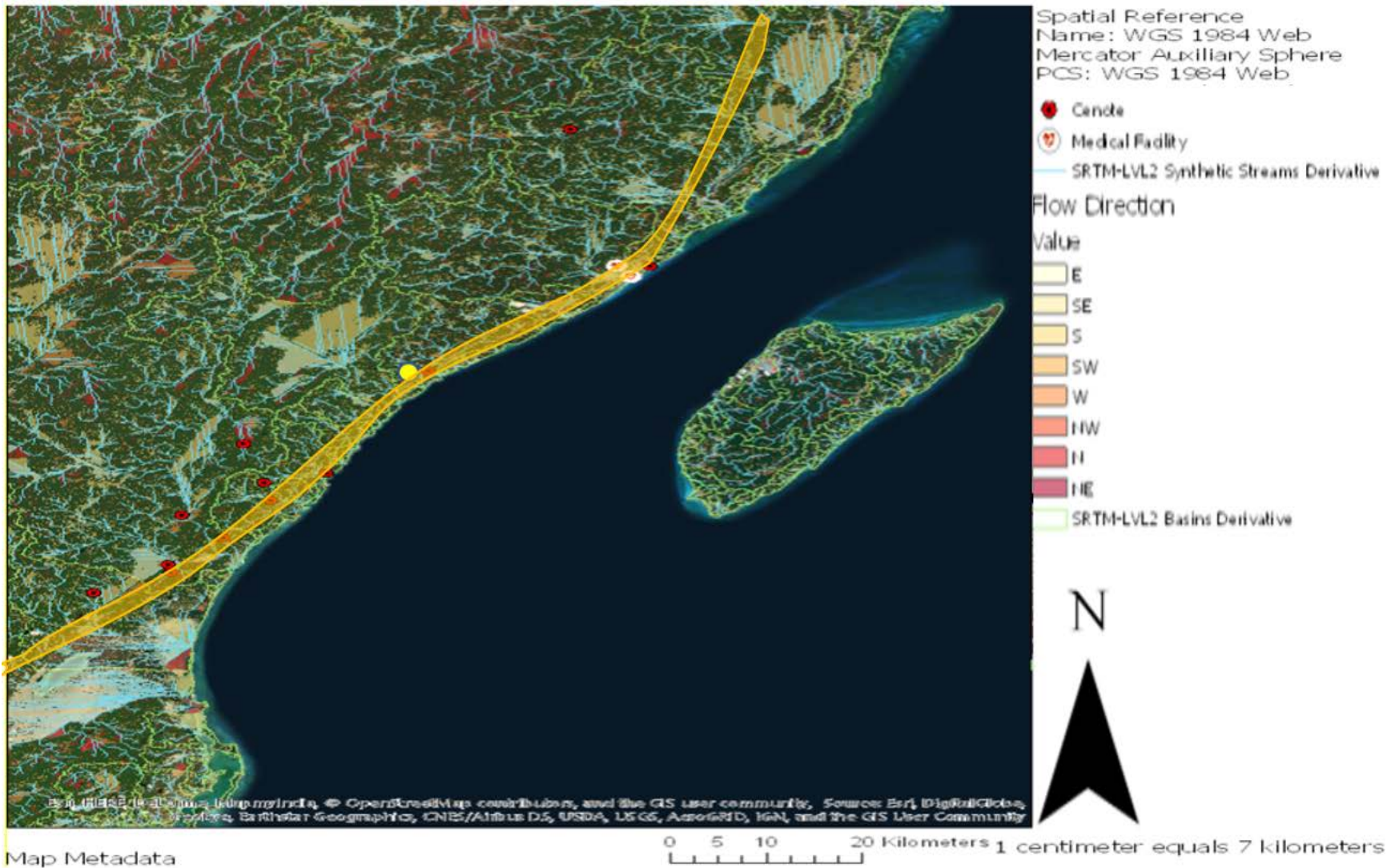


Figure 6. Cenotes proximate to Federal Highway 307 buffer, in orange, presenting geohazards. AOI marked in yellow circle on right with regional cave systems are shaded underneath to represent flow direction (Daire et al 2017).

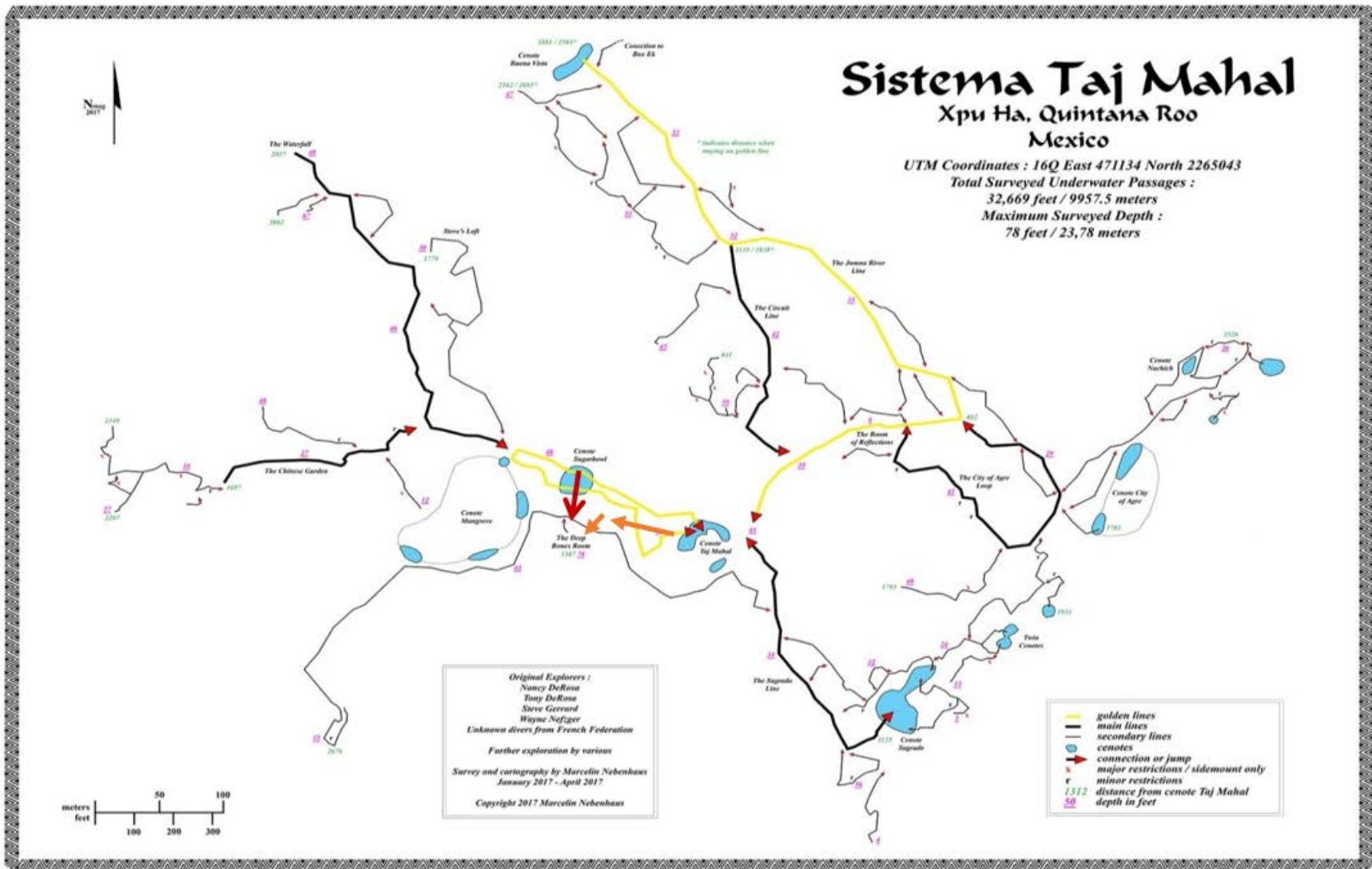


Figure 7. BRCA grade 1 AOI map with overlain FOI survey lines marked in orange for 2017 photogrammetry field season, and red for ULS-200 survey 2018 field season (Nebenhaus 2017).

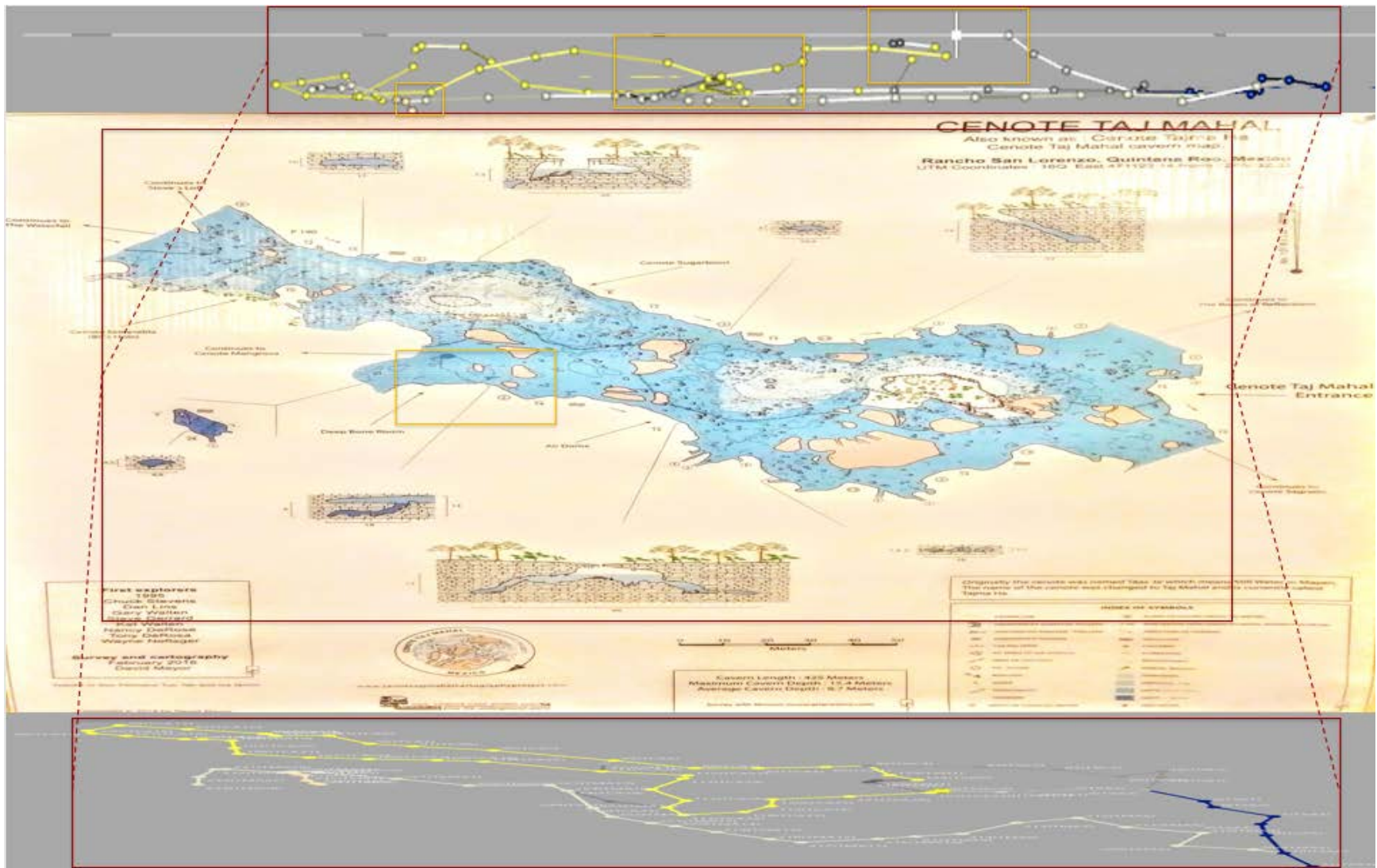


Figure 8. BRCA Grade 3 Map photographed at cave entrance with the juxtaposed .svg polyline-sphere data presenting the spatial primitives developed from survey data as a benchmark for ORT progress assessment, FOI marked orange. (Mayor et al. 2018)

Planetary science evidence formed in the AOI caves during subsequent periods of sea-level fluctuations with expansions and recessions of 130 to 140m in depth (Vázquez-Domínguez and Arita 2010; Villasuso-Pino et al 2011). Sea-level fluctuations from the last glacial maxima unleashed and restricted large quantities of the global hydrosphere into ocean water or ice sheets, which then froze and evaporated, exposing or flooding global paleolithic cave systems over millennia. These restrictions and abundance of water beckoned and deterred various organisms into or out of the caves for survival. EES provides insight into behavioral ecology related to mating, behavioral related modification (BRM) fire cracked rocks (FCR), and subsistence methods exploited by cave life causing natural and bioperturbation to speleogenetic processes. Complex Topographic hypothesis and new archaeological evidence of global anthropogenic cave activity provided new comparatives for extreme environment and human coevolution. Currently, there are no rivers on the Yucatan Peninsula, paleolithic fresh water sources were located within the cave systems >25m below ground. Human occupation of the Yucatan began \approx 20-16ka and provides a locus on human genetics research on migration, cave lifeways, and paleolithic isotopic environments.

As time has progressed access and utilization of the regional caves has modified in several ways through paleolithic habitation, local globalization, karst research, and ecotourism. A series of Late Pleistocene climatic glacial fluctuations, and subsequent marine transgressions occurring \approx 18ka to the present have been causing further inundation to the regional caves, with anthropogenic activity fueling new cave formation. Evidence of natural and anthropogenic HBE are observable at various cave depths by watertable marks of increasing depth, fire pits, and FCR on the limestone surface in various locations across the karst platform.

The AOI Cenote Taj Mahal of Sistema Taj Mahal Xpu Ha, Quintana Roo, México provides access to various features of interest (FOI) within the Yucatan karst platform. These FOI include paleontological remains, late Pleistocene HBE evidence in the Deep Bone Room, and various sections of moonmilk (*Streptomyces* carbonate formations), speleothems, and cave-in features. This system has been under active survey for fifteen years, by the author and various groups, had has produced novel datasets. Recent research developments in the Yucatan platform and global karst systems have been extending scientific bodies of knowledge on numerous levels. Growing appreciation of the position of karst topology in evolutionary studies is developing alongside technological progressions in GIST data collection and digital modeling for subterranean sciences. These series of global archaeological caves sites in Daminisi, Georgia, Biunique, France Atapuerca, Spain, Sterkfontein, South Africa, Padge-Landson, United States, and Yucatan, Mexico are providing extensive insight into karst HBE, human evolutionary genetics, and novel paleolithic species remains (Jaubert et al 2016; Stinnesbeck 2017, 2018) Cave sites are producing paleontological evidence on cave community HBE. Continued cave research from Daminisi, Georgia favors arguments against cladistic differential splitting are forwarding Goethe's uniformitarian lumping phylogenetic schema for genus grouping and subdivisions (Flannery 2005; Suslick 2012).

1.2. Incentives, Orientation, Motivation, & Significance

The scientific record lacks ULS survey references for astronauts and speleonauts, as well as >5 grade BCRA maps. These knowledge gaps prevent research, as well as search and rescue, which requires the presented methodologies in survey, geoanalysis, and presentation of geohazards, geoheritage, and biodiversity datasets for planning, research, and response to

promote climate change resilience & future PSTAR GIST applications in cave surveys (Xiong et al 2017). NASA PSTAR requires LiDAR and PhoDAR surveys to provide datasets and identify potential imaging indexes, field methods, and training for scientists, surveyors, and engineers. Lack of scientific literature on ULS laser induced breakdown spectrometry (LIBS) prevent TPU calibration in RS and climate change analyses. ULS surveys are desperately required for VRL & 3D GDB development, as $\approx 10,000,000$ km of cave systems exist globally, approximately occupying 75% of United States, and possess karst topology proximate to most regions of urban development (Weary and Doctor 2014). ULS provide real-time geospatial RS observation for *in situ* karst spectrometric analysis of natural isotopes, nanoparticles (pharmaceuticals & plastics), and vector point clouds (x, y, z volumetric measurements) which promote unprecedented inundated cave hydrogeological modeling, geohazard site assessment, urban planning, LiDAR calibration, and geohazard (cave-in) modeling (Stevanovic 2015; Stevanovic and Milanovic 2015). Research, geohazard awareness, spatial cognition, and GIST quality assessment and control (QAC) benefit from karst ULS survey to develop future PSTAR VRLs.

Astrobiology, bioastronautics, xenolinguistics (e. g. foreign planetary languages), xenohydrogeology (e. g. foreign planetary hydrogeology), xenoplanetary sciences (e. g. foreign planetary sciences), quantum physics, and other science fields benefit from analog ULS cave surveys and VRLs due to the immersive factors that govern both cave surveys and VRLs in terms of biogeographic evolution, open or closed circuit LSS, formative Mayan hieroglyphic systems, paleokarst formations, cave habitation, LiDAR applications, and fluid dynamics. Immersive factors also need to consider inclusive binomial nomenclature modifications for native Mayan dialects and geospatially contextualized vocabularies as they retain and revive traditional ecological knowledge (TEK) which assists in niche specific descriptions.

Incorporating Latin, Greek, Sanskrit, Mayan, and other language families into taxonomy promotes holistic STEAM literacy and assists in site and feature identifications, characterizations, and classifications. An example being the recently discovered *Xibalbaonyx oviceps* (the taxonomic name is derived from the admixture of the Mayan Xibalba for God of the Underworld, and Greek onyx for egg or stalk) which facilitates regional TEK language retention.

PSTAR and geographic information science (GISci) VRLs provide applications domains and development contexts beyond past limitations. Analog records provide PSTAR mission planning technical evaluation metrics. Numerous research topics benefit from developments of PSTAR references in GIST, LSS, and HBE. Earth analog AOI identification, colonization site selection, and operations geohazard RS mitigation promote avoidance engineering and GISci map references developments of the Martian Surface (Reimuller et al. 2015; Daire 2018). Figures 9 and 10 present matrices on benefits and developments of phreatic karst ULS survey and VRL development. Figure 9 denotes a research benefits matrix related to science, technology, engineering, art, and mathematics (STEAM) education references for the presented fields and domains. Figure 10 presents a Societal & PSTAR Benefits Matrix with serendipitous comparatives for xenoenvironments RS deployments in numerous PSTAR settings including hydrogeochemistry characterization and biogenic assay. PSTAR cave diving analogs serve as scalable orbital to subaquatic-subterranean microgravity exploration projects that can be assessed for PSTAR H-R training and research. Figure 11 presents Mars 2030 VRL providing PSTAR STEM platform for testing tools developments, CRM, and surveys. ETE analogs possess development potentials for baric trauma response, extraterrestrial RS, aphotic RS environments, scientist-astronaut microgravity performance, PPDE, lifeline safety in high-flow fluid velocity, and LSS contingency planning (Charles, J. B. 2013).

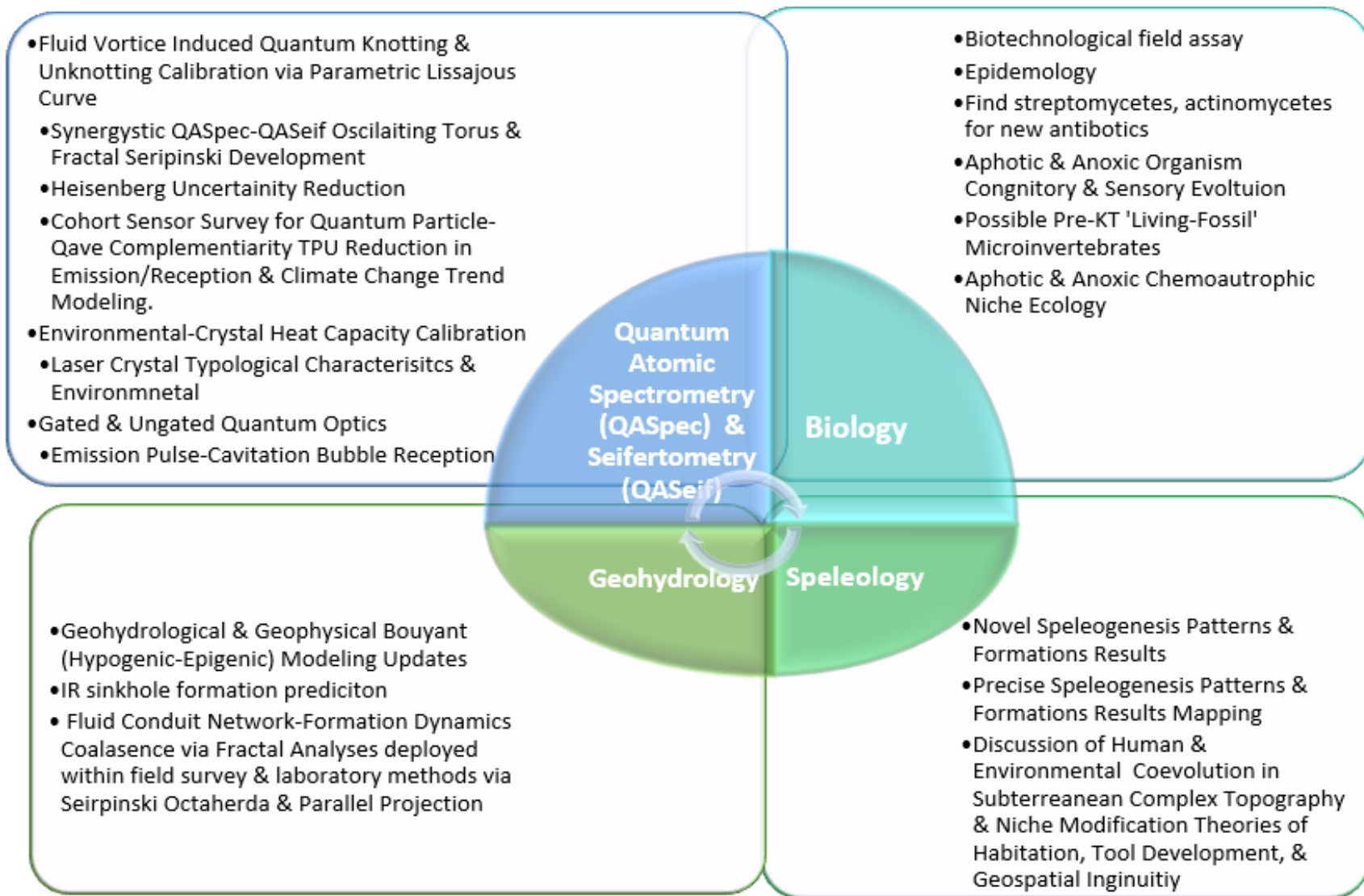


Figure 9. Research Benefits Matrix for Scientific Fields.

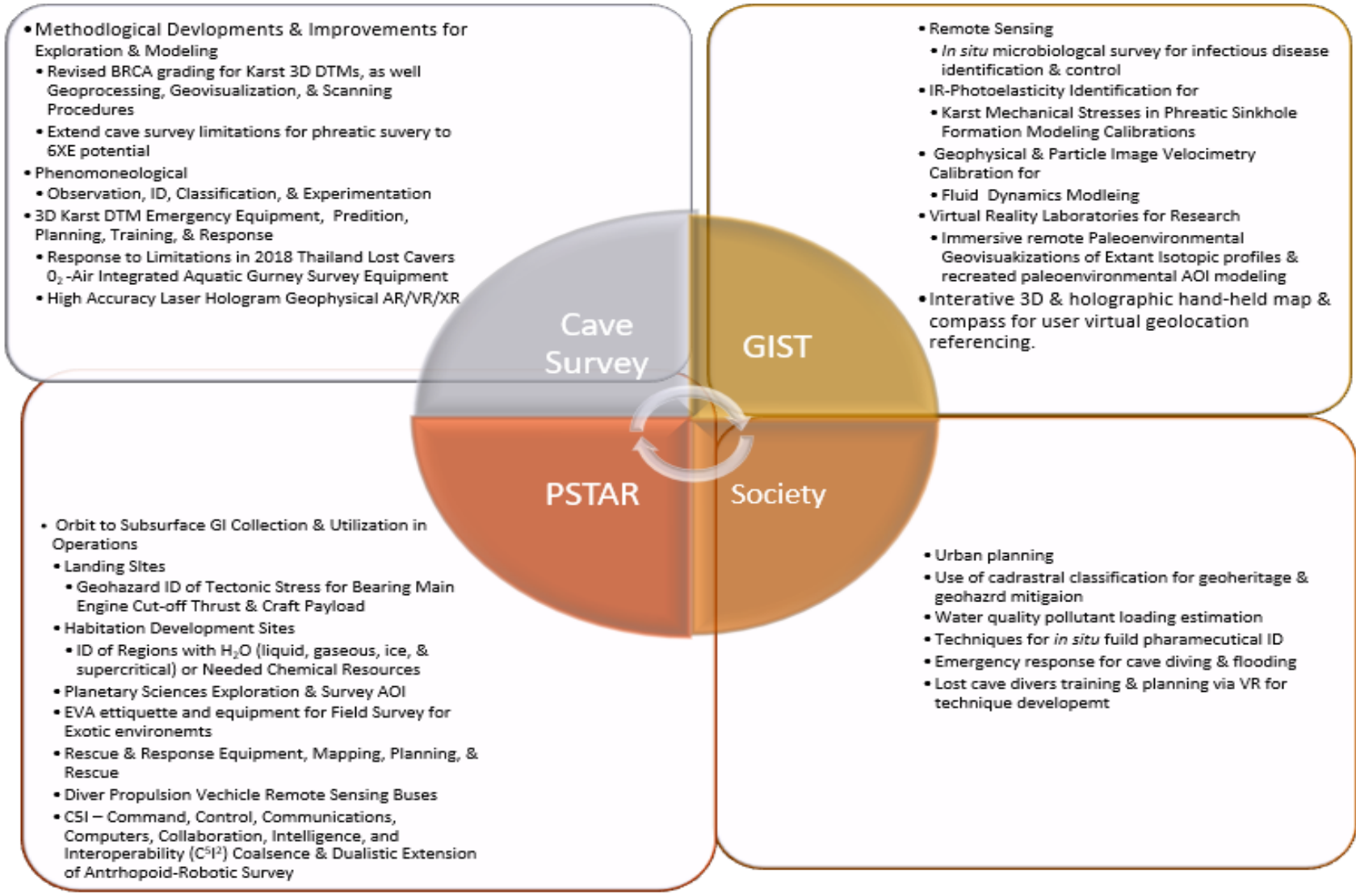


Figure 10. Societal & PSTAR Benefits Matrix.

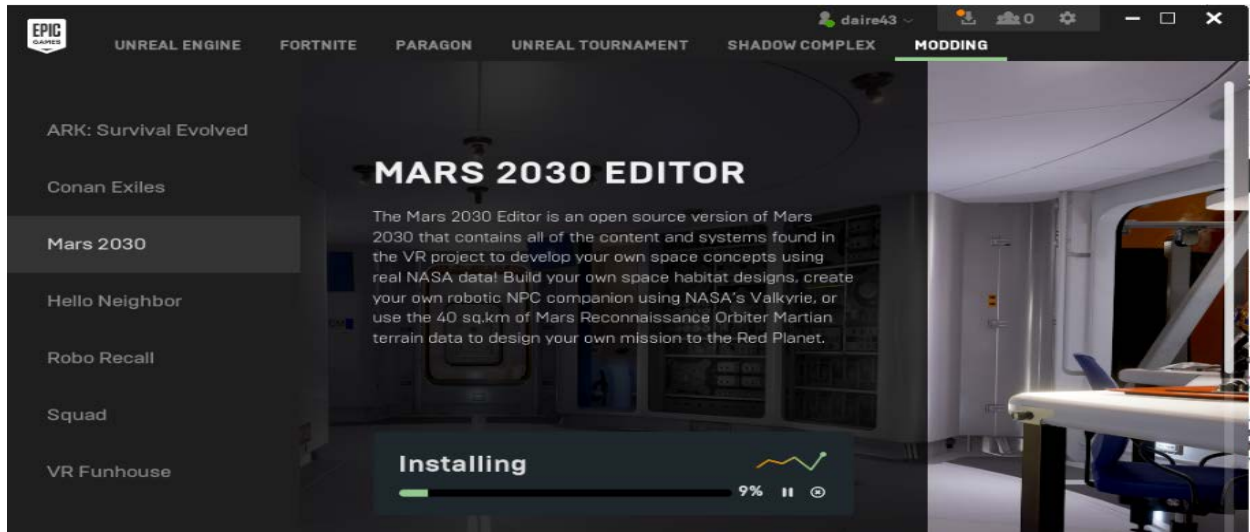


Figure 11. Epic Games Mars 2030 Mission Simulator (Unreal Studios 2017)

GIST and PSTAR developments all relate to improvements in survey accuracy and precision for geographic communication of prehistoric environments, humans that survived and evolved within paleolithic karst communities HBE parallel astronaut experience with isolation, life in confined space, and zero-reference spatial disorientation, which all inform future PSTAR survey and survival in extraterrestrial environments. Analogous surveys improve NASA Integrated Services Network (NISN) communication systems for dive and ground support equipment (GSE) CRM on field surveys via PSTAR command, control, communications, computers, collaboration, intelligence, and interoperability (C⁵I²) VRL assessments and innovations for future collaborative H-R research deployments and techniques developments (Alberts et al. 2009; Obermeyer & Pinto 2008).

ULS represent a factorial progression in ease of survey by speleonator, astronaut, and robotic systems which have diverse research applications within laboratory and field settings. ULS require further field deployment for several reasons. ULS have minimal cave deployment

references with scant methodological transitions from industrial to scientific scanning contexts. Cave environments are more geometrically complex than mine shafts by orders of magnitude and improve mine scanning (Schiller & Pfeiler 2015). Transition from laser scanning data to virtual reality formats is relatively simple and provide unprecedented 3D mapping capabilities for underwater caves in stereoscopic formats (Weidner 2016; Schiller & Pfeiler 2015). References are required to promote LiDAR developments related LASER RS holograms of objects and environmental reconstruction via omni-angular parallax LAMIS volume measurements and PhoDAR overlays. These technologies and visualization methods afford digital cartographers, geographic information scientists, and the public to have access to capabilities of vector data collection, scalar data format conversion, holographic geovisualization modeling, and virtual reality (VR) products via Microsoft HoloLens of underwater cave environments. (Gale Group. 2011; Feng 2017)

1.3. Hypothesis, Goal, Design, Phases, & Questions

Concurrent ULS, photogrammetry, and water quality data collection conducted by speleonauts overcome traditional obstacles preventing progressions beyond grade 3 cave mapping in phreatic systems. The enhanced survey methodologies improve survey success by decreasing workload, improving collection variety and accuracy, and simplifying field surveyor task loading (Exley 1986; Carney et al 2013; National Oceanic and Atmospheric Administration Diving Program (U.S.), and Joiner 2011). ULS surveys improve cave conservation by coherently providing unrecorded datasets to assess the natural and cultural resources as they stand, before time impacts them further. The evidence and data on karst morphology and matrix geochemistry promote future karst hydrogeological modeling and PSTAR GISci survey planning.

1.3.1. Objectives

The project goal is to conduct an ULS 3D geographic information systems (GIS) survey for karst modeling assessment and PSTAR analog reference materials development for future astronautic mission planning. Near-infrared (N-IR) provides Brillouin Scattering photoelasticity analysis of structural tension, fluid density, and zones of fracture via ULS LAMIS survey. LIBS provide geochemical, hydrochemical, and biochemical identification and classification via partial PCA and modified-optimal scale fractal analyses (Pardo-Igúzquiza et al 2015; Feng et al 2017).

The data collected from the survey toolkits and techniques provide novel environmental data in a BCRA grade 6 phreatic karst survey map (Day 2002). Development of the sampled evidence produces semi-guided, geomorphological tour of the AOI datasets which provides site access from a cave researcher field of view (FOV) (Blaser 2015; NMAI 2017; National Park Service 2012.; National Park Service n. d.). The interface of speleonator and astronaut mission simulations and assessments provide referential materials for dialog on PSTAR GIST survey methods on Earth and other celestial bodies (Charles 2013). References must be improved on QTK, PQV, TPU, and other accuracy impacts via ULS cave deployments in terms of bore sighting & plasma pulse propagation and degradation.

Effects of PQV identified by this research and cave ULS imaging artifacts must be referenced for future LiDAR and ETE modeling improvements. Field assessments for ULS accidental over-ablation of microorganisms during surveys is required to confirm laboratory testing assessments. Apparatus and human factors limitations in deployment success require VRLs training simulations for hypoxia/hyperoxia physiological awareness, psycho-physiological contingency response (PP-CR) (e. g. psychosomatic – mind-body), breathing gas narcosis mitigation, geospatial disorientation in zero reference geospatial Terrain-Relative Navigation

(TRN) (aphotic, acelestial, ageomagnetic) and other ETE dynamics. VRLs developed in ArcGIS Pro 3D provide research access points for stereoscopic ULS data visualization for regional speleogenesis, paleokarst processes, isotopic spectrometry, radiometric dating, geoheritage protection, and paleolithic HBE VRLs GDB management.

Geocoded ULS datasets and geospatial construction materials are stored and managed in a 3D karst GDB for map and animation developments. The GDB development products provide a detailed map of hydrogeomorphology for a conduit section to FOIs. A semi-guided, first-person geomorphological tour of the AOI from the perspective of a speleonator promotes cyber PSTSR GIST education of researchers, stakeholders, and students. The final 3D products allow karst researchers and cave diving instructors to take a partially guided tour along the caveline, with high quality geomorphological feature scans, points of potential cave-in, and geospatial dimensions in the AOI for awareness and accident analysis (Armstrong 2017). Geospatial information including a stratigraphic cross-section, chemical datasets, and fossil remains developed for representation increase research access and provide materials for simulation developments in VRLs.

This PSTAR GIST ULS survey utilizes karst researcher cave diving training requirements to extend experiential and geospatial comprehension of phreatic karst processes, size, magnitude, and importance for inclusive input and dialog on cave research. PSTAR GIST ULS surveys inform future public participation GIS for speleonators, astronauts, and stakeholders on how, when, where, what, and why to collect survey datasets and metadata for research. These efforts promote AOI reconstruction, along with providing methods developments for RS and VRL. VRL GDBs exported to and from, ArcGIS, Unreal Engine, and CloudeCompare promote interoperability via Esri City Engine production in the future.

1.3.2. GIST PSTAR Thesis Blueprint

Chapter One introduces the AOI, PSTAR cave diving analogs, a contextual appendix, a technical glossary, and a Heilmeyer Catechism on the project goal, phases, objective, tools, potentials, limitations, grading, and audience. Chapter Two cites aspects surrounding exploratory survey in cave diving for PSTAR ULS SWORT ORT, GIST D&E, field sciences concepts, and quantum non-linear optics dynamics in H-R deployments. Chapter Three outlines the PSTAR ULS survey methodology, workflows, scientific apparatus, 3D GIS elements, and CIRM PPDE LSS requirements. Chapter Four provides a procedural analysis of the deployment, examines evidence collected by the LiDAR and PhoDAR generated datasets from the experimental PSTAR methodology, and LiDAR calibration and GIS product outcomes. Chapter 5 expands on the quantum quasiperiodic crystal transform circuit identified in Chapter 4. This circuit is an antiphotonic-photonic quasicrystal that is an edge and vertex transliterate toroidal flow propagating within a viscous holographic Moduli Fields of Vacua Orbifold hyperspace inducing coherently complexifying holonomic extensions from the original homothetic vacuum through PQVS harmonized QCED automorphic Random Matrix Theory (RMT). Photons operate trilaterally on a serialized dodecaphonic harmonized quasiperiodic crystalline vortex slipstream through a curvilinear worm-hole of time-like past and future via vertex and edge transitive present time-space. This volumated holographic quasicrystal-vacua-orbifold QCED space, quasi-triangulable Delaunay tessellation field estimator (DTFE), and QCED conceptual model facilitates the GIST and PSTAR thesis discussion. The thesis concludes with future works in spatial sciences, LiDAR research, H-R field methodology, SWORT ORT productivity evaluation, PPDE disengagement techniques, CIRMSS, proteomic countermeasures, and VRL simulations for astronaut and cave diver PSTAR education.

Chapter 2 Related Works

PSTAR and karst surveys require continuing ULS cave deployments and GIST techniques improvements in terms of *in situ* EQ PCA field analyses to promote data collection, analysis, and presentation beyond historic geographic communication limitations in environmental research (Andero et al. 2017; Reimuller et al 2015). Science (e. g. physics, geology, hydrology, biology, and aeronomy) has benefited from remote sensing advancements on all fronts. Extant cave maps are scarce and provide invaluable data on formation, system topology, paleoclimatology, HBE dynamics related to EES BRM, and search and rescue procedures (White 2012; Pardo-Iguzquiza et al 2015; Padilla & Pulido-Bosch 1995; Denton et al. 2016). PSTAR requires H-R ORT karst surveys to synergistically improve RS methods, and in turn, tool operational extensions and domain applications that facilitate GIST and karst research (Dixon 2018).

Evidence of the tempos and magnitudes of sea-level rise and dissolution events are present in numerous paleolithic cave sites (Cruz et al 2015). Late Pleistocene marine transgression inundated 130m of continental shelves globally as sea-level rise that began roughly 20ka globally with the end of the last glacial cycle. Mounting progress in dispersal, radiation, and infiltration of RS, GIST applications, and GISci techniques across numerous fields of science facilitate observations, modeling, and presentation. GIST progressions are promoting understanding in planetary sciences, HBE, paleoclimatological coevolution, and karst BRM via EES forces that guided our species evolutionary trajectory in novel ways. Global paleoclimatic, human genetics, and LULC research is promoting an appreciation of early Hominidae expansion out of Africa related to evidence of human tool production, biogeographic range extensions, and

population interactions on larger timescales and social networks than previously perceived (Harmand et al. 2015; King 2013; Ashley 2013; Stinnesbeck et al 207; Laland et al 2015).

ULS LIBS karst stratigraphic sampling provides critical information for paleoenvironmental reconstruction of correlated global conditions (geochronologic, oceanic, atmospheric, etc.). Evaluations of map product quality can be completed with BCRA survey grades. Figure 12 depicts updated BCRA survey grading rubric with considerations and recommendations for GIST ULS surveys (Day 2000). The updates promote higher quality modeling requirements extending from nominal ULS-200 sampling accuracy. They are based on the authors five years of evolutionary anthropology and Darwinian medicine research, four years of underwater archaeology field work in various environments with >200 dives, three years of experience in cave diving survey, and GIST master's certification from the University of Southern California (USC).

GIST modernization relates to multiple toolsets for research and benefit environmental reconstructions for analysis of paleoenvironmental isotopes and EQ *in situ*. ULS provides novel sampling for theories of planetary formation and biogeographic evolution through cave survey. Figure 13 presents a paleokarst speleogenetic model with hydrogeological dynamics occurring via Ghyben-Herzberg Relationship (GHR). GHR effects karst aquifer buoyancy as a dynamically interfacing series (time-slices) of oversaturated viscous matrix flows mediated by density differences between the fluid and geologic crystalline interface. Figure 14 diagrams karst aquifer network flow recharge patterns. Karst networks correlate to HBE caves activity in the Paleolithic (Klimchouk et al. 2000). Paleolithic HBE related to paleoclimate seasonal rain kernel potentials provide habitation site suitability survey and geohazard maps via karst fracture fractal network topology assessments (Benson & Yuhr 2016; Pickering et al 1999).

GIST revised BCRA Karst Line Survey Grading			GIST revised BCRA Karst Detail Grading			
Grade	Requirements	Notes	Class	Level of Karst Detail	Notes	
1	Low accuracy sketch - no measurements.	<p>❖ Survey grades given must be read in conjunction with these notes.</p> <p>1. Grades 2 & 4 define impractical re-survey or physical cave conditions preventing any stage of survey from attaining all requirements for the next higher grade.</p> <p>2. Descriptions & Reports on GIST georectification, remote sensing techniques, geovisualization techniques, geospatial accuracy assessment, & error mitigation strategies.</p> <p>3. <u>Caving organizations reproduction of this table in publications is encouraged; permission is not required from BCRA or the author</u></p> <p>4. <u>This table should be reassessed every 5 years for quality updates.</u></p>	A	Passage details based on memory.	1. The accuracy of the detail should be like the accuracy of the line.	
2 (see note 1)	Intermediate accuracy sketch, between 1 – 3.					
3	Magnetic Survey <ol style="list-style-type: none"> horizontal & vertical angles measured to $\pm 2.5^\circ$ distances measured to ± 50 cm station position error < 50cm. Clinometric measurements $\pm 2.5^\circ$ 		4 (See note 1)	B	Passage details estimated & recorded in cave.	1. Normally only one of the following combinations of survey grades should be used: 1A, 3B or 3C, 5C or 5D, 6D, XA, XB, XC, XD, or xE
4 (See note 1)	Surveys that are more accurate than a grade 3 and fail to attain all grade 5 requirements.					
5	Magnetic survey <ol style="list-style-type: none"> Horizontal & vertical angles measured to $\pm 1^\circ$. Distances recorded to the nearest centimeter. Station positions error < 10cm. Instrument calibration. All measurements of stations within 10cm sphere Geospatial Analysis for length, width, height, depth, slope, volume, and surfaces. 		6	C	Only survey stations measurements.	
6	Magnetic surveys more accurate than 5. <ol style="list-style-type: none"> Compass and clinometer accuracy to $\pm 0.5^\circ$ Station position error $< \pm 2.5$ cm. Use of tripods or fixed station spatial-volumetric markers. 					
X (See note 2)	Accuracy beyond Grade 6 <ul style="list-style-type: none"> Recommending Disconnected-Outrigger 3D Network Survey Measurement angles of $45^\circ \leq X \leq 135^\circ$ Theodolite, GIS total station, ULS, & Mnemo 			D	Measurements at survey stations & FOIs	1. Represent significant geohydrochemical changes & passage dimensions.
		E				

Figure 12. BCRA GIST Updated Grading Scale for ULS Surveys

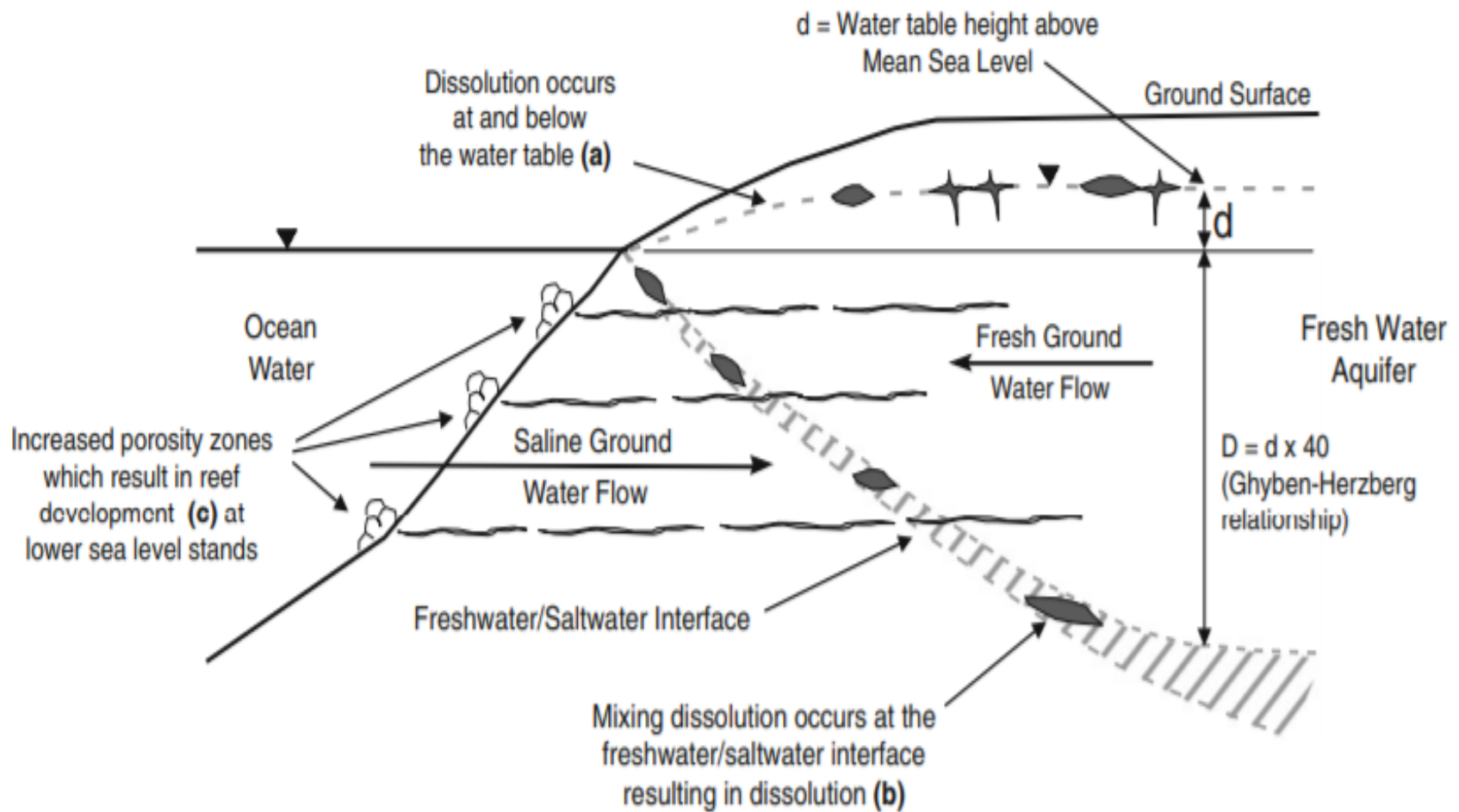
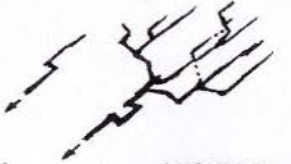
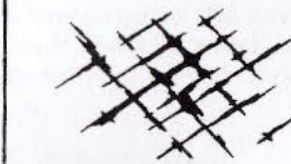
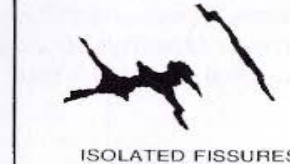
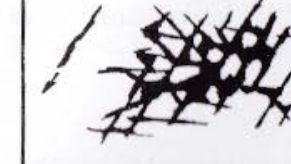
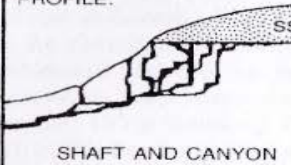
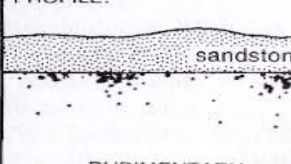


Fig.2.2 A fresh water lens is found along the coast and on islands and its thickness is determined by the Ghyben-Herzberg relationship. Dissolution of limestone occurs near the surface of fresh water (a) and at the freshwater saltwater interface (b)

Figure 13. Oceanic Karst Development (Benson & Yuhr 2016).

		TYPE OF RECHARGE				
		VIA KARST DEPRESSIONS		DIFFUSE		HYPOGENIC
		SINKHOLES (LIMITED DISCHARGE FLUCTUATION)	SINKING STREAMS (GREAT DISCHARGE FLUCTUATION)	THROUGH SANDSTONE	INTO POROUS SOLUBLE ROCK	DISSOLUTION BY ACIDS OF DEEP-SEATED SOURCE OR BY COOLING OF THERMAL WATER
BRANCHWORKS (USUALLY SEVERAL LEVELS) & SINGLE PASSAGES		SINGLE PASSAGES AND CRUDE BRANCHWORKS, USUALLY WITH THE FOLLOWING FEATURES SUPERIMPOSED:	MOST CAVES ENLARGED FURTHER BY RECHARGE FROM OTHER SOURCES	MOST CAVES FORMED BY MIXING AT DEPTH		
DOMINANT TYPE OF POROSITY	FRACTURES	 ANGULAR PASSAGES	 FISSURES, IRREGULAR NETWORKS	 FISSURES, NETWORKS	 ISOLATED FISSURES AND RUDIMENTARY NETWORKS	 NETWORKS, SINGLE PASSAGES, FISSURES
	BEDDING PARTINGS	 CURVILINEAR PASSAGES	 ANASTOMOSES, ANASTOMOTIC MAZES	PROFILE:  SHAFT AND CANYON COMPLEXES, INTERSTRATAL SOLUTION	 SPONGEWORK	 RAMIFORM CAVES, RARE SINGLE-PASSAGE AND ANASTOMOTIC CAVES
	INTERGRANULAR	 RUDIMENTARY BRANCHWORKS	 SPONGEWORK	PROFILE:  RUDIMENTARY SPONGEWORK	 SPONGEWORK	 RAMIFORM & SPONGEWORK CAVES

3.4 Figure 10. Cave patterns and their relationship to types of recharge and porosity. Maps are plan views unless otherwise noted. They are generalized to illustrate the dominant patterns. Many caves exhibit rudimentary forms, multiple stages of development, or combinations of more than one type (from Palmer, 1991).

Figure 14. Karst Aquifer Network Flow Recharge Patterns (Klimchouk et al. 2000)

Buoyancy is a complex phenomenon involving millennia of intuition, observation, experimentation, modeling, and research since Archimedes' first observations and related the GHR as caves saturate and empty (Benson & Yuhr 2016). Karst buoyant forces vary based on fluid depth, density, cation-anion composition, temperature, pressure, and proximity to littoral (coastal) regions (Baldini, Mcdermott, and Fairchild 2006). Beringia (Bering Strait), Sundaland (Sunda Shelf), Sahul (Sahul Shelf), Doggerland (North Sea), Middle Atlantic Bight (Lower Hudson Bay), the Yucatan Cave Systems (Campeche Bank), and other continental shelf regions represent global Late Pleistocene biogeographic habitats utilized by our ancestors that have been lost to humanity via ocean rise that require 3D GIS ULS reconstruction (Halligan et al 2016). *A posteriori* analysis of karst ULS datasets also provide, given appropriate calibration, modification, and data-dictionary formation, an ability to extract and geovisualize numerous phenomenon and datasets. Understanding these elements and factors are critical for site identification, characterization, classification, and demarcation for future land use or disuse in karst regions (Goldscheider and Drew 2007; Ford and Williams 2007; Moore and Wade 2013; Blamey et al 2016).

Speleogenetic processes occur throughout karst matrixes from surface to bed rock, from the inside out, along paths of least resistance topobathically (flowing contiguous from terrestrial topographic and subterranean substructure into subaquatic bathymetric systems (Benson and Yuhr 2016; Padilla, Pulido-Bosch, & Mangin 1994). Microbiological and hydrogeological laboratory chemical analyses have developed ULS geochemical, astrobiological, EQ analysis techniques but require controlled LiDAR survey field testing in underwater cave survey for geospatial RS QAC.

Explorations and surveys provide evidence for dataset conversion, reference for field methods improvements, and analytic ORT assessments for RS planetary impact assessments. Unified RS scanning techniques provide high detail, real-time, dataset collection methods on previously disparate evidence for planetary science survey field analysis developments but are lacking in research deployments and field work references. (Jac̃ková and Romportl 2008; Parks and Mulligan 2010; Spilde 2013; Gray 2014).

These topics resonate with PSTAR solar system surveys methods, systems, techniques, and analysis developments for ULS AOI analysis for PSTAR and GIST references and discussions. The research narrative highlights the continued need for underwater cave exploration to develop high-quality maps to define geospatial accuracy concerns, protect water resources, inform CRM via high-fidelity simulations, formulate EVA H-R emergency responses, and develop unstudied narratives of human-karst coevolution via 3DGIS (Jiménez-Madrid et al 2012; King 2013; Stinnesbeck 2018; Angelo 2017; Dixon 2018; Charles 2013; Boston et al 2008).

2.1. Exploration, Research, & Development in Planetary Sciences

Recent publications in karst science are shedding light on karst system dynamics. Unified sound navigation and ranging (SoNAR), LiDAR, and PhoDAR CRSI scanning provide high detail collection methods on previously disparate datasets for new analysis development into >5 BRCA grade maps. These research topics are intertwined in terms of comprehension of PSTAR ORTs for future deployment in solar system H-R C^5I^2 and cave diving surveys (Raggett & Jacobs 2018; Pronk et al 2009; Perrin 2003; Perrin & Andreassian 2001; Scanlon et al 2003). The body of works presented cite contemporary state-of-the-art survey methods, techniques,

technologies, tools, and concepts in GISci. These references include fractal modeling, GDB development, stereographic geovisualization, and spatial analysis.

Andreo et al (2015) published a comprehensive review of current karst hydrogeology and environmental studies and materials including Pardo-Igúzquiza (2015), Paredes (2015), Cabeza, Hidalgo, and Carrera (2015), Schiller & Pfeiler (2015), and other authors. E. Pardo-Igúzquiza, J.J. Durán, P.A. Robledo-Ardila and C. Paredes (2015) conducted fractal modeling for karst porosity estimation to develop conduit flow and dissolution frameworks. Mandelbrot Set fractal self-similar geometry have statically comparable distributions within various naturally occurring phenomena with dynamic Julia set variables (Mandelbrot 1967). Cabeza, Hidalgo, and Carrera (2015) determined the interrelationship between dissolution and sequential wormhole growth in preferential conduit flow drainage development. These works enumerate on passages that are fit for exploratory H-R survey, and those that are geohazards for infrastructures. Feng et al. (2017) presents on the connotations of pixel-based scale effect in RS and the modified fractal-based analysis method applicability for use in optimal scale mapping. Fractal scale modeling based on a constant 1:1 imaging-visual pixel-surface area schema that facilitates high quality texture development from point clouds and subsequent 3D and VR product developments for cave simulations. These have been developed via LiDAR and PhoDAR individually. The schema lacks cohort RS instrument (CRSI) survey for data congruency and quantum imaging calibrations indicatrix for aberration reductions and mitigation.

Schiller and Pfeiler (2015) conducted preliminary phreatic karst laser scanning surveys utilizing industrial scanning methods. Their paper is brief and lacks specific information on the methodological framework, type of laser, and other pertinent information for survey replication. The report praises the scanner on accurate and rapid scanning but does not include accuracy

assessments or deployment methods. Lack of methodological references highlights the need for a field research framework for karst ULS survey. Weidner (2016) develop a stereoscopic 3D photogrammetry cave survey methodology and cave model reconstruction for computer science research. The work covered the concepts required to utilize VR for karst reconstruction for virtual reality development (Bowens 2009). This work details survey efforts and optics imaging via dive propulsion vehicle (DPV) PhoDAR which serves as an analog to EVA-RS craft and tools development for rapid data acquisition as a pushbroom CRSI array for DTM development (Exley 1986; Carney et al 2013; NOAA and Joiner 2001; Armstrong 2017).

Hollingsworth's (2009) thesis calls for integration of regional karst GDBs into a comprehensive global karst GDB for geoh heritage and biodiversity conservation. Weary and Doctor (2014) proposed a Karst GDB for the continental United States. Their works proposes a metadata methodological frame work for geospatial storage and cave comparisons applicable to the Yucatan Peninsula AOI (Bauer-Gottwein et al 2011; Bonnet & Butterlin 1962; Chica-Olmo & Luque-Espinar 2003; Joint Committee of American Society of Civil Engineering, American Congress on Surveying and Mapping, and American Society of Photogrammetric and Remote Sensing 2011).

Jaubert et al (2016) located structures produced by *Homo neanderthalensis* in caves of southwestern France. This work represents developments in understanding in karst science, built environments, technology in HBE, BRM, and human evolution. It provides evidence that promotes the works of Laland (2015), Holdaway (2015), and Winder (2013) in terms of the ESS, NCT, and CTH in human evolution. Evidential extensions of human fire, tool, and land use and development related to cave living can be extended to PSTAR ETE space habitat survival

analogies for site suitability selection and water source identification (Harmand et al 2015; Ashley 2013; Stinnesbeck 2017; Stinnesbeck a, b 2018; Daire et al 2017).

PSTAR PPDE of laser ablation cratering on microbiomes need to be evaluated in the field (Pořizka et al 2012). Laser plasma pulse width, intensity, and wavelength methodological calibrations for microbiological survey can prevent misidentification and accidental destruction of exobiotic evidence (biogenic gas, cell structure, trace evidence, etc). The Outerspace Treaty (1967) serves as an analog for cave survey etiquette and continuing considerations for remote sensing development (Boston et al 2008). Transition from laser scanning dataset to virtual reality formats is simple in terms of CloudCompare 3D DTM development but relates to numerous LiDAR quantum dynamic paradoxes. These paradoxes relate to photonic quasicrystals propagating instantaneous QCED RMT via supersymmetric hyperspatial photonic quasicrystal in a Moduli Fields of Vacua orbifold. LIDAR scanning inherently produces holograms of the remotely sensed objects, these provide omni-angular parallax, as well as plasma ablation spectrometric measurements which promote precision replication of the object and environment (Feng, J. C. 2018; Encyclopedia of Emerging Technologies 2011). PSTAR and suborbital space research can be identified and compounded upon within and between human and robotic EVA planning, cave diving, and GIST technologies and techniques which facilitating new methods for data collection and spatial sciences communication. These references set a context for analog cave PSTAR ORT surveys to promote effective and productive underwater tool and technique developments for operational EVA field sciences with next generation GIS deployment of EVA vehicles, H-R, and LSS. These works highlight new technologies abilities to promote sampling, assessment, and broadcasting for research evolutions to the public via subaquatic-subterranean regions RS for PSTAR (Boston, 2008; Reimuller et al 2015).

2.1.1. Quantum: Spectrometry, & Biology - Scientific Synesthesia, & Holographic VRLs

Since the 1960s laser and sound amplification by stimulated emission of radiation (SASER) research and developments have promoted data exploration, identification, and sampling in physical sciences. Lasers provide numerous benefits to experimentation and testing in quantum mechanics, quantum nonlinear optics, as well as in photonics and phononics (technologies related to properties and transmission of photons – light and phonons – sound). These have interdisciplinary concepts in terms of industrial and research applications and domains including, but not limited to PSTAR analogs, surgery, and Massachusetts Institute of Technology - Laser interferometric gravitational-wave observatory (MIT LIGO).

These applications of photonics and phononics are prompting research developments via GIST RS toolkits. Development of LiDAR and Phodar products with CloudCompare, ArcGIS, and AgiSoft Photoscan allow for photoset alignments, dense cloud extraction, triangular irregular network (TIN) construction, and 3D orthophoto texturing in reconstruction development, which are finally exported for VRL (Villasuso-Pino et al 2011; Vassiliou 2007). LAMIS occurs via point cloud sampling with fractal survey markers assisting processing by providing alignment, mesh, and texture construction references. These reconstructed environments then provide contextual settings for immersive paleoenvironmental VRLs for research in PSTSR and GIST for the scientific community and general public via ULS cave scanning. Marius Vassiliou's (2007), continuing works in the human display interaction are promote VRL developments. VRLs provide visualization techniques for new perspectives on concepts providing innovative developments in all fields of research.

Lasers present new potentials of dataset collection in terms of accuracy, speed, and versatility with inclusive parameters for extensive variables detection and identification in all

scientific fields. ULS data collection tools are the next generation of utilitarian RASP toolkits for cave survey and PSTAR. Lasers emit and detect entangled quantized photons and assess PCA for radiometric, isotopic, and other evidence by producing plasma on the surface of an object or in the water column. The sensor energy emission and absorption emerge from symplectic groups, quantum paradoxes, observational evidence in physics and fluid thermodynamics. Elements of some quantum and fluid mechanics can be addressed, other dynamics require continued research extending beyond the scope of this work. Causality inherently relates to these paradoxes induces series of GIST phenomenological dynamics in terms of quantum photonic and phononic environments producing automorphic Random Matrix Theory (RMT) environmental noise.

Energy released by ULS for RS sampling causes destruction to provide ablation dataset holograms and environmental RMT entropy at the scan instant. As the ULS operates it induces viscous fluid thermodynamics which effect scanning accuracy. ULS provides profound impact in field evaluations of capacities, capabilities, and impacts which require further PSTAR GIST assessments in QB, the Unruh effect, TPU, and QTK (Law & Rennie 2015; Hod 2011; Larocque et al 2018; Freire et al. 2017). ULS represent a factorial progression in survey potentials by H-R system scale deployment and have diverse applications within laboratory settings. ULS require further field deployment for several reasons. ULS have minimal use in the field speleology, with scant methodological transition from industrial to research scanning. This lack of domains application includes mapping karst and LiDAR calibration unknowns. Pre-deployment considerations are required to assess a series of variables for calibration framework development and spectrometric signature and sub-band identification and classification. The laser scanner, field methodology, and environmental context influence RS data validation frameworks in karst survey that need QCED considerations.

Fortes et al (2015) is a primary reference on LIBS with definitions and evaluations of numerous applications in various domains. Alvey et al. (2010) covers laboratory testing LIBS for mineral identification and fingerprinting for field application. This work signifies the high accuracy laser mineral classification. They reflect on geochemical training samples requirements for robust identification. They note presence of chemically similar cation and anion bonding on the sample surface from ablation causing sample misidentification (Sakka et al. 2012).

Pořízka et al. (2012) experiment with LIBS for biofilm chemical analysis which provides a design frame work for ULS with design considerations aimed to meet GIST needs and PSTAR goals. The work covers high accuracy biochemical classification within water columns and ablation cratering effects on microorganism surfaces. They include a scanning tunneling microscopic image of the resultant plasma ablation impact crater. These materials present preliminary calibrations for laser deployment PPDE in astrobiological survey (Paschotta 2008; Cristoforetti et al 2012; Freire et al 2017; Boston et al 2008).

Visualization of phenomena beyond the scale and range of natural human sensory organ systems has been a continued area of perception exploration research and development in STEAM education. Computers and sensors produce algorithmic visualization through various means and modes, they do not provide understanding of phenomenological dynamism of form and function, nor do they consider causality in scientific intuition (Solcum 2009; Campbell and Wynne 2011). STEAM modeling and presentation are all concepts at the center of ULS cave mapping. Presenting the unseen is an intersection of observational, educational, and philosophical inquiry that relate to Goethe's works on scientific aesthetic, phenomena modeling, and communication (Flannery 2005; Suslick 2012). Phenomenological inquiry and classification-taxonomy evolved via Goethe's developments on Baruch Spinoza's *natura*

naturans. Continued conjecture in natural philosophy, physical sciences, and linguistics benefited from the subsequent dialogs on the phrase, which translates from Latin as nature naturing. Elaborating on *natura naturans* concept, veracity and realism in phenomenological observation, taxonomic classification, and scientific communication extend from scientific observers whose perspectives are open to all influence of new information. One of the most profoundly obfuscating and enlightening delves into reality that has occurred in science is the progression towards cohesion of a Newtonian-Relative-Quantum (Unified Field Theory) worldviews in the light of quantum gravity and dynamics. Quantum mechanics is incomprehensible on the macroscopic scale, yet it is beginning to divulge coevolutionary mechanisms between organismal biology and quantum physics in photosynthesis, sensory perception, and metabolic free energy modeling. Reconciliations between longstanding arguments, and reflections on Goethe's proactive scientific lifeway perspective on phenomenological ineffability of nature and knowing call for a suspended disbelief in light of quantum dynamics (Flannery 2005; Suslick 2012; Lambert et al. 2012)

Elaboration in scientific technology occurs along continuums of scale, scope, and sensitivity. Unified field theory is a recent concept in physics with juxtaposed datasets from gravitational waves, QCED, and spatial sciences. Figure 15 presents a conceptual model of a multidimensional quantitative and qualitative QCED commutating white body core – black body energetic wave-spin functions extending from the orbifold harmonics (Corcovilos 2018; Penrose 2005; Nielsen 2018; Bhattacharya et al 2017; Smithey et al 1993; Çengel et al. 2002; Nielsen and Shoom 2018; Dyson 1956). This QCED conceptual model presents a photonic quasicrystal propagating a complete-hyperspatial-filling moduli fields of vacua orbifold.

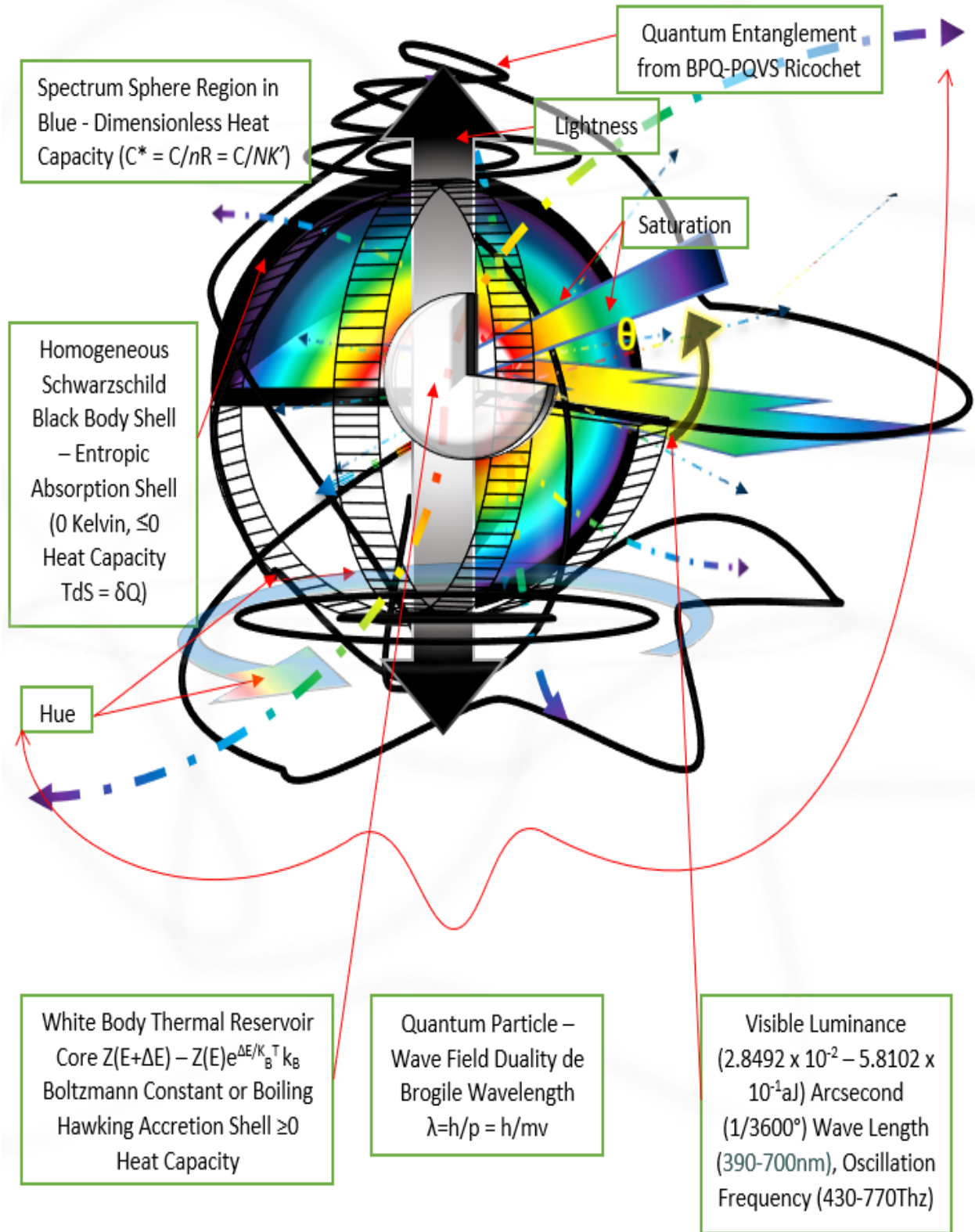


Figure 15. Conceptual QCED White Body-Black Body Spheroid-Orbifold Wave-Field Diagram.

Quantum wavefield spatial distributions related to the adiabatic theorem – uncertainty distributions of phenomena within and between quantum wave – extending from particle continua presenting energetic ordering, disordering, and entropy of a system at a given LiDAR observation. TPU relates to LiDAR sampling of the particle or spinning wavefunction asynchronously. LiDAR Holography stands to profoundly impact life, karst survey, and geographic information science as an emergent technology but requires continuing improvement.

In the standard model of elementary particle physics experimentation related to quanta, fermions – (Fermi-Dirac obedient $\frac{1}{2}$ integer spin), gauge bosons (Bose-Einstein obedient 1 integer spin), and Higgs bosons – (Higgs obedient 0 integer spin), and so on require research PSTAR and GIST references (Dyson 1956). As LiDAR and PhoDAR interact with the environment the systems produce intermediate subatomic virtual particles and emergent phenomena that can interact detection, ranging, and random matrix theory (RMT).

Elementary and subatomic particle models and indexes of these phenomena require consolidation to promote developments in quantum computing, quantum information sciences, LiDAR calibration, and VRL holographic environmental reconstruction. Ineffabilities relate to quantum uncertainties in the use of GIST, LiDAR, PhoDAR, SoNAR, and other apparatus as well as transition phases in terms of understanding complex quantum system fluid dynamics degrees of freedom (DOF) (Penrose 2005; Neilsen 2018; Bhattacharya et al 2017; Smithey et al 1993; Çengel et al. 2002; Larocque et al 2018; Freire et al 2017; Sakka, T. et al 2012; NIST 2017). This confluence of incomprehensible impressionistic realism can promote or deter scientific research due to the presumptions and experiences of the subjective researcher working towards an objective goal.

Referential experience and techniques continue to build with laser scanning technologies deployed *in situ* that will mitigate laboratory practices that are not reflective of natural systems in question. Doppler velocity logs are preventing the Unruh Effect, CRSI surveys are deterring the observer effect, and comprehension of quantum wave-particle duality into a complementary perspective that is progressively allowing for more accurate and precise impressionistic models deterring Heisenberg Uncertainty fault-tree propagation (FTP) (Smithey et al.1993; New York: Springer, 2001; Çengel et al. 2002; Bhattacharya et al. 2017; Law & Rennie 2015).

Measurement of number-phase uncertainty relations of optical fields relates to geospatial sensor wave-particle detection uncertainty and will benefit from habitual fractal-dimensional analysis within mapping. Quantum paradoxes extend to GIST as it interacts with an environment-emitter-sensor-display-developer-user continua environments and datasets through coinciding uncertainties in GIST LiDAR systems effects.

"... it's a product of the fractal laws that govern the world at an informational level. There is no deeper truth." – Terence McKenna (Davis 2011)

Virtual laboratory development requires reflection on any models to be presented, as well as their format content to be an intuitively simplistic user experience. Considerations for parallax vertigo of complex features, light distortions effects on spatial perception, and slow frame rate induced virtual reality vertigo (VRV) all need to be identified and mitigated to promote 3DGIS user-experience PSTAR analog simulations related to VR emergent sensory stimulation. Organismal sensory organs developed in relation to existence, or survival stressors, and pragmatic utilitarian exploitation of natural quantum particle-wave function complementarity corresponding to evolutionary biological systems phylogenetic response. Each organismal

response subsequently developed relative to the electromagnetic magnetic spectrum via deferral & discrimination of vibro-oscillating, cyclic-flux quanta-magnetic field activities. Various developments in caudal portions of the brain in homo sapiens, aves, fish, etc. prevented or enhanced sensory receptors interference or synergy allowing reception or amplification of audio-visual (sight-sound-smell) waves, as well as haptic-gastrointestinal (touch-gut) cognizance, and so on. (Lambert et al. 2012; Yoshizawa & Jeffery 2008).

Construction of precise geovisualizations affects user experience and synesthesia in virtual environments in positive, and negative ways as well, which require developments to serve as useful PSTAR educational simulation toolkits. Virtual reality development requires assessment for geometric accuracy, 3D feature snapping, geovisual texture precision, lighting objective consideration, data compactification, relative scale, and virtual reality sickness reduction. These are best accomplished in the virtual environment via Unreal Engine for production. Texture formation is a critical element in model production and development of intermediate geospatial products via LiDAR and PhoDAR. AgiSoft Photoscan modeling via photoset improves alignments, dense cloud extraction, TIN mesh construction, and orthophoto texturing. Intermediate products, datasets, and metadata are exportable for VRL development. CloudCompare LiDAR modeling expedites alignment, mesh, and texture reconstruction. VLRs provide creative means for PSTAR and cave surveys scientific communication, modeling, and low risk simulations in underwater VRLs for survey microgravity, zero-visibility, and contingency training. Stereographic images and holographics extend to cultural fascination, government need, and academic research for PSTAR and GIST cave survey references with immersive high-fidelity synesthesia simulations.

Chapter 3 Data & Methods

A karst aquifer is a branching geologic substructure that acts as a drainage basin network for groundwater that flows completely below ground to bed rock. Karst aquifers are points of PSTAR and GIST research interest in terms of HBE, geoheritage, water resources management, urban planning, and exploration. Aquifer networks consist of interconnecting tributary conduit flows via an enhanced porosity lithic matrix, typically made of carbonate minerals. Discharge from headwaters flows into perennial springs, which seep into caves, and exhaust into oceanic conduits. Salt and fresh water intermixes relate to the GHR with Hele-Shaw Flow (HSF) propagating forms of weathering in caves via Kelvin-Helmholtz Instability (KHI). Sediments, gases, or fluids flush and abrade cave surfaces and consolidate materials into downstream sinks (e.g. sediment cavities, air filled pockets, and waterbodies). Abrasions expose more surfaces to wearing by sediments, gases, and fluids which in turn, induces more distributed weathering along the hydrogeological matrix relative to the GHR evapotranspiration cycles. Hydrogeologic conditions associated with karst aquifer systems include: chemical dissolution equilibria, sinking streams, springs, estavelles, dolines, conduits, karst network recharge, and path of least resistance flow within a lithological matrix.

Water dissolution chemistry and conduit surface chemistry are required for comprehension of karst decomposition. Speleogenetic processes can operate individually or in concert. Formational processes include fracturing, fissuring, dissolution, mechanical wearing, thermodynamics, and others and are analogous across planetary sciences. Karst geospatial processes are dependent upon a range of factors and occur throughout the topography from surface to bed rock, in spatially homogeneous or heterogeneous distribution. Physical definitions

of heat capacity of water, refraction index of salt and fresh water, and dissolution chemistry inform calibration requirements for ULS survey. Volumetric geospatial datasets include photoplethysmogram - depth, width, length, height, volume, inclination, length, and azimuth through ULS vector point cloud sampling.

3.1. Conceptual Framework

Understanding the series of natural and anthropogenic speleogenetic processes in sinkhole formation provides insight on cave fragility, geohazard forethought, and natural resource management in urban planning and PSTAR. By examining and identifying APE on karst geospatial distributions, natural processes, and anthropogenic exacerbations can be mitigated, improving urban planning, preventing injury, and reducing private and public infrastructure loss by charactering karst topography.

“Everything is related to everything else, but near things are more related than distant things.” - Tobler’s 1st Law (Miller 2004).

Recent karst surveys have indicated a formation biases of approximately 60% to 40% for anthropogenic to natural cave formation processes. This reflects rapid LULC induced speleogenesis related to globalization compared to deep geologic processes. Relative buoyant forces acting on karst matrixes and unconsolidated materials correlate to respective differences in regional climatic seasonalities. Other factors are also involved in cave formation, and others are unknown to science.

Buoyancy is an extensive, complex topic involving millennia of intuition, observation, experimentation, modeling, and research. Karst buoyant forces vary based on fluid depth, density, cation-anion composition, temperature, pressure, and proximity to littoral regions. The variations on these elements equate to matrix structural loading capacities and tolerances of matrix structural loading from flooding, evapotranspiration, and hydraulic pumping.

Anthropogenic hydraulic pumping activities introduce novel feedback loops into the speleogenetic process. These loops exacerbate water table dynamics increasing drought depression and recharge rebound potential energy gradients, promoting geophysical stresses, impacts, and destruction. Understanding these elements and factors are critical for site identification, characterization, classification, and demarcation for future land use or disuse.

The more the anthropogenic perturbation within a given system, the greater the amount of phenomenological and optical aberrations occur that during ULS RS dataset collection. These perturbations signify novel datasets on water chemistry, flow, planetary impacts, and other phenomena. Datasets categorized to reflect existing karst geomorphological feature definitions promote identification of water quality (WQ) components of caves, known pollutants, and paleontological records as described in Klimchouck et al (2000) and Andreo et al (2015).

These features can be identified, classified, and symbolized based on ULS plasma ablation spectrometry of the karst geomorphology and dissolution hydrodynamics for geologic assessment of conduit formation. UNESCO World heritage resource protection and cave protection etiquette prevent disclosure of human remains locations within paleoanthropology but can be publicly displayed in a VRLs for education that masks the specific AOI geospatial references (UNESCO 2002; VRARA 2017). World heritage resource protection parallel PSTAR needs and can be utilized as a comparative reference for insightful PPDE via contamination

control plan and requirements (CCPR). Public datasets on phreatic karst are not available for public record due public safety prevention of cave accidents, geoheritage, endangered species, and other reasons.

3.2. Schedule, Timeline, & Workflows

A study period of eight months total provides timing to conduct a ULS cave survey for karst stratigraphic profiling. Conducting ULS cave surveys with photogrammetric and water quality scans of submerged cave site of interest provides high quality, fruitful datasets at micrometric (μm) accuracy through an omni-angular LiDAR imaging parallax. The project planning and ULS survey can be completed within 3 months of research and a two-week field survey period to meet the project goal. The surveying provides detailed site datasets on field evidence for considerations in efficacy of ULS utilization within an analog field context for their environmental recording qualities, characteristics, concerns, and impacts related to PSTAR.

A safe survey takes precedence over all other project goals, safety supersedes mission planning and incites diversion to crew contingency planning on-the-fly. The project safety requirements must be in accordance with the community standards for cave and scientific diving (NOAA Diving Program (U.S.) & Joiner 2001; Carney et al 2013). The core members of the team consist of surface support and survey crew members. All members of the team are qualified in Technical Diving International (TDI) Sidemount Full Cave Diving standards and have an extensive amount of field experience as underwater cave surveyors and scientific divers. Upon project initiation, the entire team possessed current Diver Medical, First Aid, CPR and O2 provider certificates, the copies of are kept on file at the survey site for emergencies. Following the schedule and proposed work flows for the overall project promotes rapid geospatial dataset

acquisition, spatial analysis, digital image model (DIM) production, and finally PSTAR discussion. Figure 16 presents the total project workflow for a ULS survey. This world heritage 3D EQ sampling presents referential GIST PSTAR survey briefs and debriefs to elucidate ULS performance in phreatic caves survey and potential analog tool developments. Figures 17 PSTAR analog ULS cave survey and GIST GDB conceptual development period prior to tool selection, site selection, and field work preparation. All those taking part in the operations were required to be familiarized with the dive site, local hazards, applicable first response procedures, and locations of regional medical facilities. The entire team is informed, trained, and practiced in the requisite CIRMSS equipment and techniques necessary to fulfil all operational aims, and mitigate all or contend with contingencies that arise from Murphy's Law during underwater exploration. Figure 18 presents the workflow for fractal survey marker development and production. Equipment was supplied personally by the divers for the survey, as well as the ULS-200 from Protean GIST Solutions, LLC. Figure 19 displays a modified Underwater 3D disconnected-reconnected-outrigger network survey diagram for movement and RS scanning through restrictions (i. e. orange outline, unfilled block) with speleonators following the black line in, red line out for methodological LiDAR and PhoDAR survey image collection of cave interior surfaces and exterior of FOIs on land or underwater (Bowens 2009). Operations did not take place unless the surveyors and supervisor were comfortable with the on-site conditions, team dynamics, and contingency planning. Figure 20 presents the workflow diagram for 3D point cloud development from LiDAR and PhoDAR datasets collected during the project PSTAR survey for cave interior modeling. This GIST ULS LiDAR survey method translates to PSTAR in productive ways for utilitarian ETE analysis. These methods of 3D surveying and model

development highlight SWORT FTP, mission cessation events, contingency procedural requirements, tools capabilities, CRM experience, and H-R points of synergy.

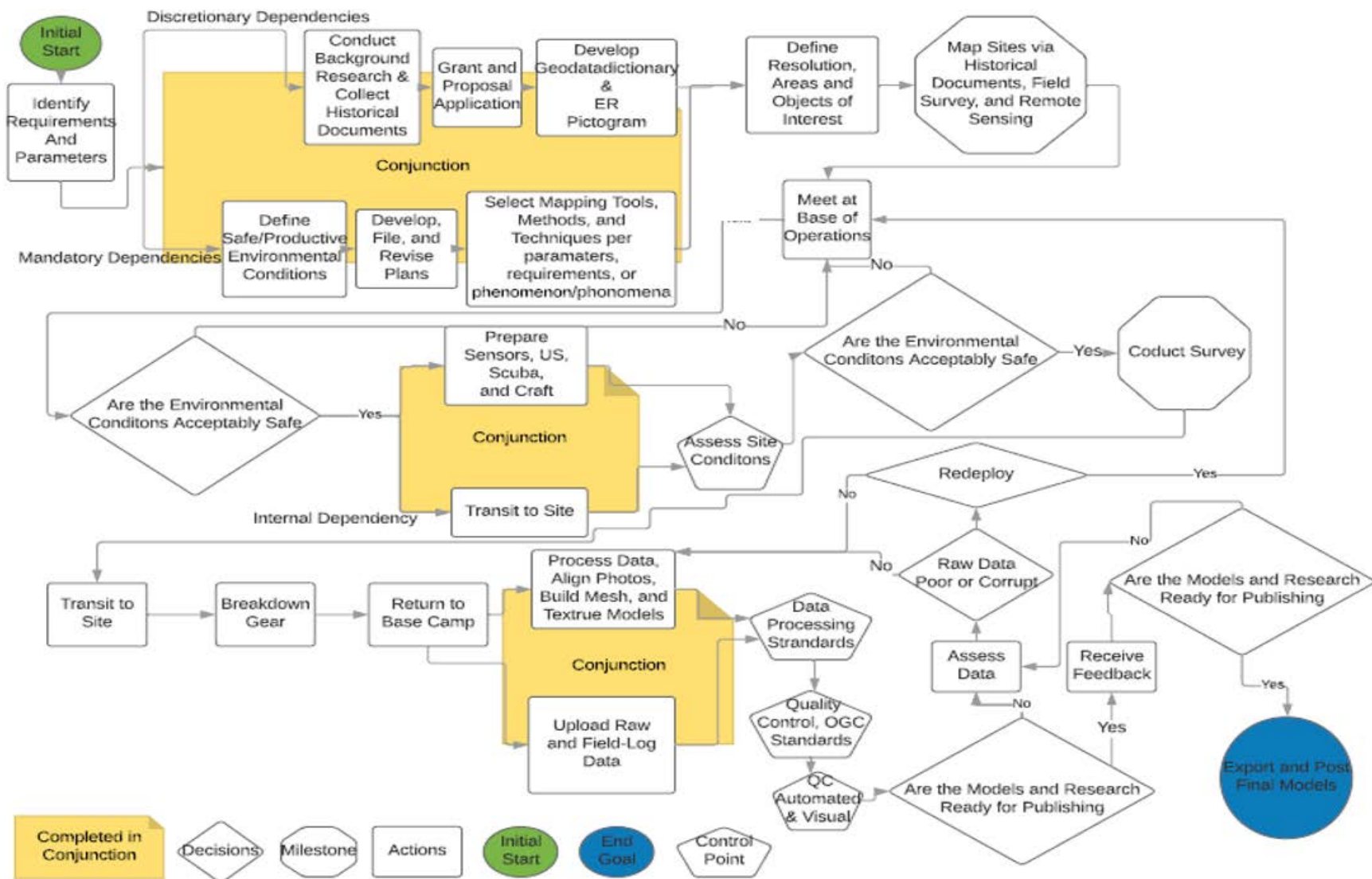


Figure 16. Project Workflow including: Conceptual Phase, Positively Abated Risk Assessment, H-R field deployment, and DTM production, and DTM QAC represented in the conjunction segments, respectively.

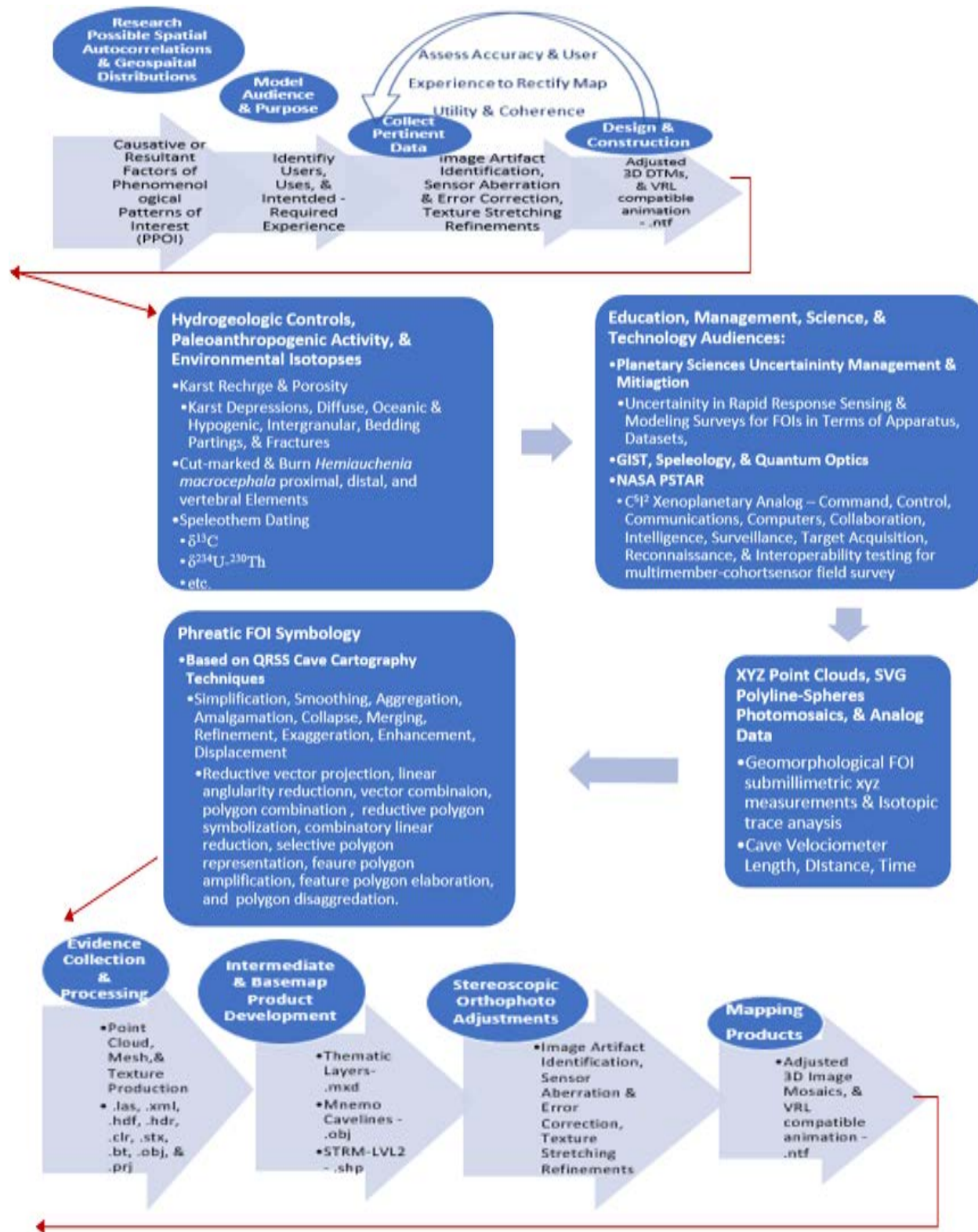


Figure 17. Conceptual Phase: Audience Identification FOIs, sensor types, dataset considerations, and development formats.

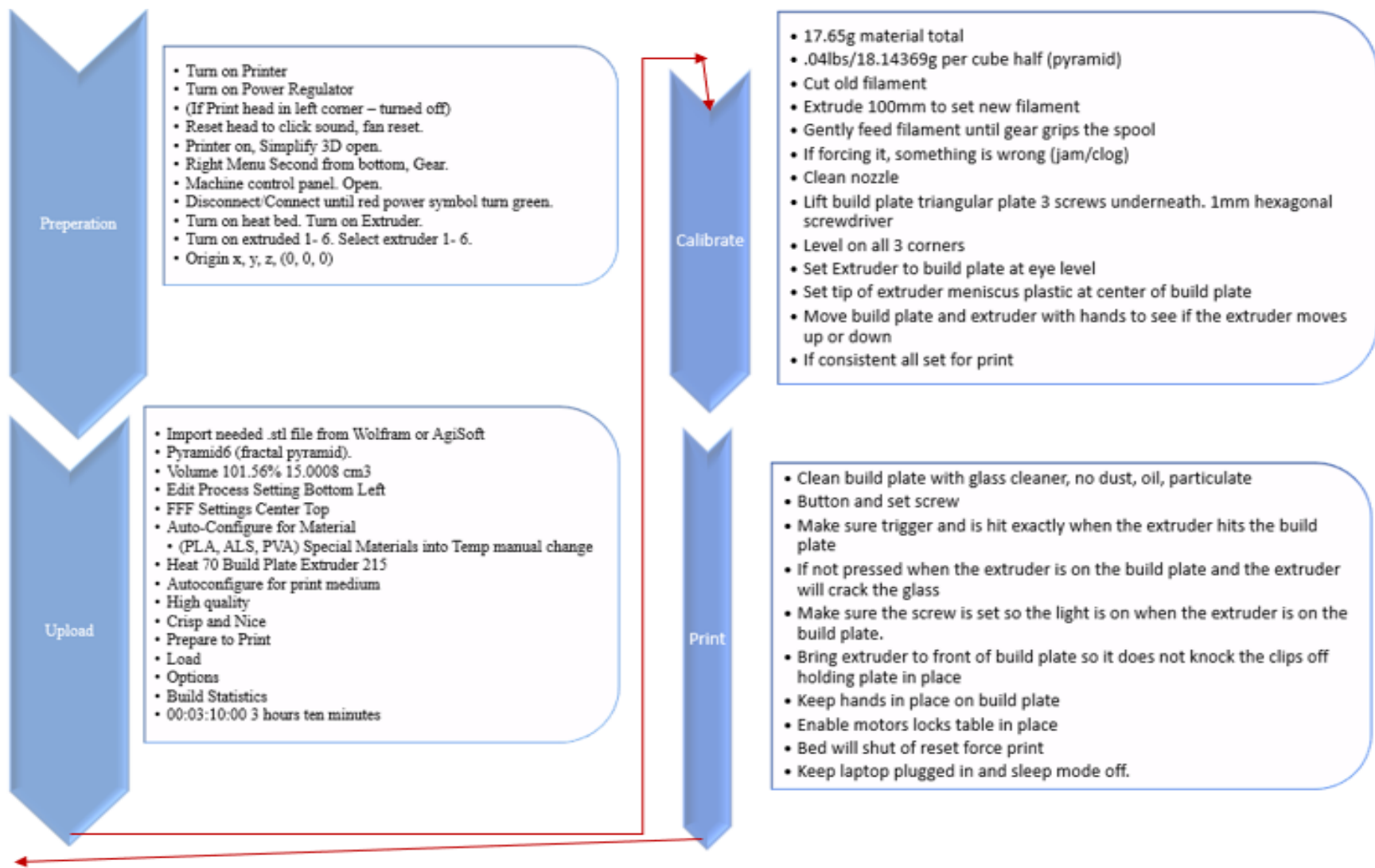


Figure 18. Conceptual Phase: 3D Printing Procedures for Sierpinski Octahedron Fractal Survey Markers, color dependent upon the PLA utilized.

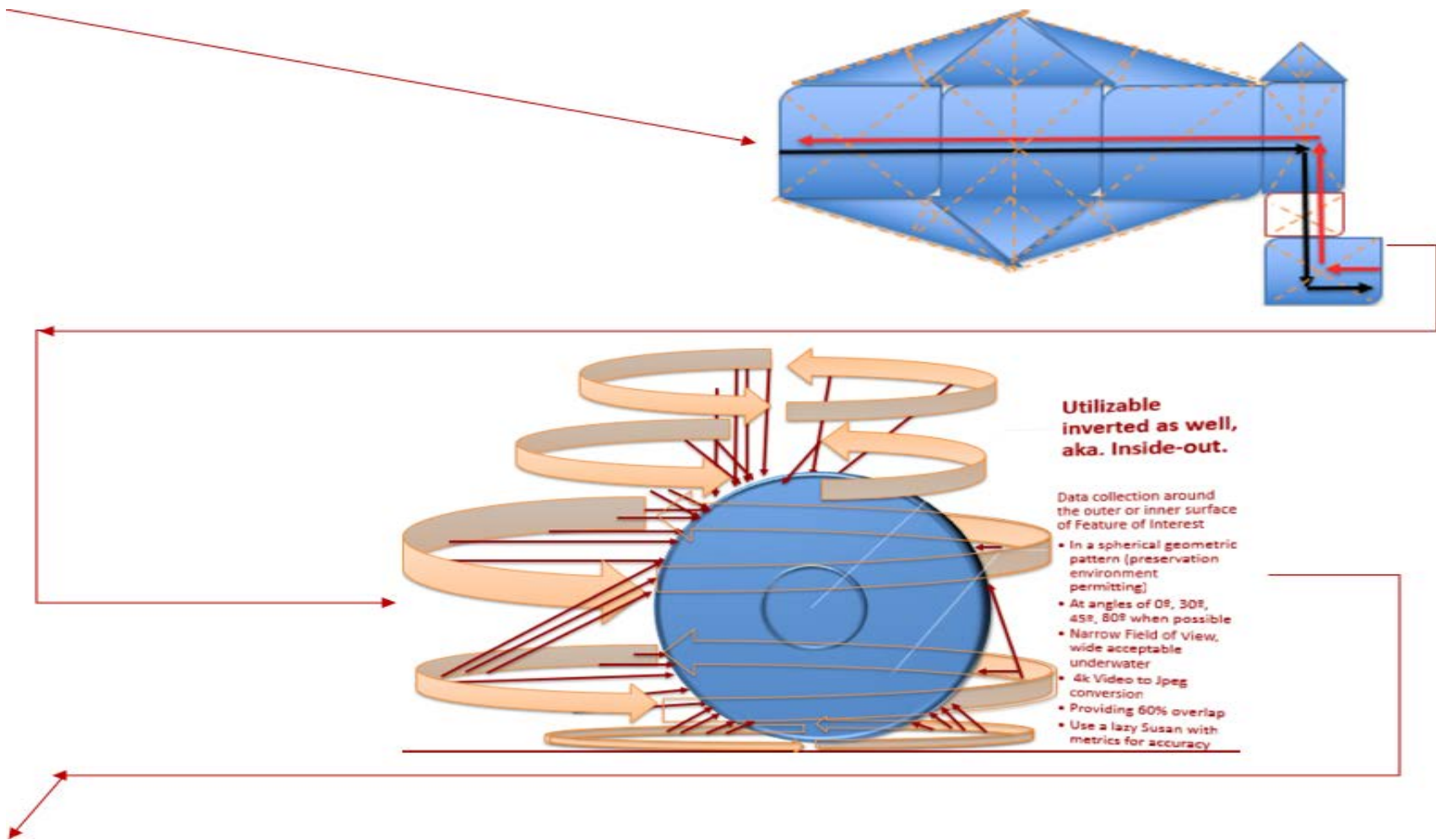


Figure 19. Displays a modified 3D disconnected-reconnected-outrigger network survey diagram for passage and RS scanning through restricted underwater spaces in nominal environmental conditions (i. e. orange outline, unfilled block). Speleonauts follow the black line in, red line out of the cave for methodological survey LiDAR and PhoDAR image collection. Top, Disconnected-reconnected-outrigger network surveys cave interior surfaces and spherical, bottom, scans exteriors of FOIs on land or underwater (Bowens, A. 2009).

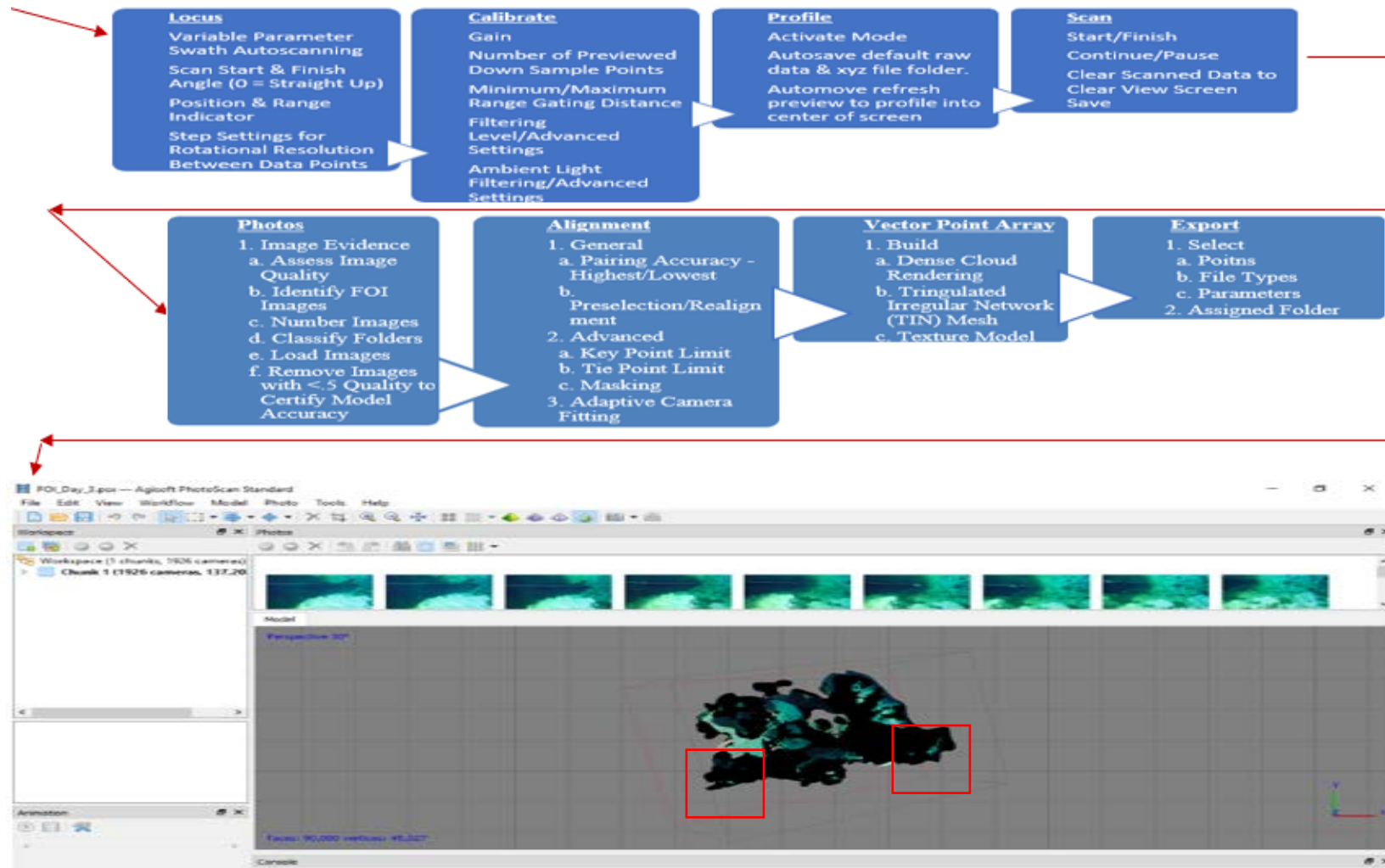


Figure 20. DEM QAC for 3D point cloud development from Cloudcompare LiDAR and Agisoft PhoDAR interior surface datasets observed from a perspective outside and directly above the survey site, the cave restriction entrance/exit is on bottom right, FOI paleontological remains on the left. The model shape matches Mayor et al 2018 mapping products, validating methods potential.

Utilization of this workflow and preliminary products improves previous survey methodologies, as well as project time management which promote success of the primary objectives toward the overall mission goal, which forward future productions of 3D phreatic cave survey (Borkovec et al 1993; Pardo-Igúzquiza et al 2015; Mandelbrot, 1983; Feng et al 2017). Maps and models of unprecedented geovisual precision and accuracy can be produced within project research timeline of 8 months to plan, survey, digitally preserve, and exhibit datasets to enhance the interpretation of phreatic cave geoheritage. These methods provide new narratives on caves survey and evolutionary biology for patrons, institutions, the public, and stakeholders interested in the materials invested in long-term subterranean surveys and PSTAR analogs. Moreover, these provide the basis for follow-up scans of these sites to monitor their cave processes of formation, evolution, looting, and rates of degradation as a time-series through full scale 3D aquifer surveys.

3.3. Research Design

This project model assists karst researchers without cave diving training to experience and comprehend phreatic karst processes and input dialog on the research via 3D GIS datasets collected from an exploratory ULS cave field survey PSTAR analog. It informs future public participation GIST for cave researchers and explorers on how, where, what, by what means, and why to collect and upload their survey metadata for recognition and development. This promotes considerations for training, techniques, and PPDE etiquette in PSTAR and GIST survey. These GDB stratigraphic and paleontological 3D GIS datasets and materials can be exported to and from ArcGIS and Unreal Engine or Unity promoting interoperability and increases to cave research access. These methodological developments promote metanalysis and digital karst

reconstruction methods to be developed for 3D RS and cyber analysis materials for PSTAR, GIST, and STEAM education and developments (Skanect. Nd. 2017; AgiSoft, Inc. 2018; 2GRobotics 2018).

3.3.1. Goals & Objectives

The project goal aim to conduct an exploratory ORT ULS 3D GIST imaging survey for karst modeling assessment and PSTAR analogs reference discussions for future astronautic mission planning. Project phases include sensor selection, sensor calibration, accuracy assessment, data dictionary development, GDB preparation, dataset coding, spatial analysis, map construction, product development, and a final discussion on GIST and PSTAR research potentials. GDB modeling in ArcGIS Pro 3D regional scene provides an unprecedented VR research access point for research and simulation on regional speleogenesis, paleokarst processes, isotopic spectrometry, radiometric dating, geoheritage protection, and HBE datasets for geospatial analysis.

The geocoded and processed survey evidence of cave passage sizes, FOIs, and extracted Kd tree-fracture facets provides data for construction in CloudCompare. A 3D karst GDB for a VRL simulated environment, a LiDAR indicatrix, photoplethysmogram cross-section, PhoDAR of paleontological & hydrogeological FOIs, and cave-in geohazard references were all outcomes. The geomorphology GDB can be utilized for development of a detailed map of conduit sections of interest. A semi-guided, speleonator FOV geomorphological tour of the AOI from the perspective of a cave diver, developed for cyber education of researchers, stakeholders, and students transmitting geographic information on the geoheritage site improves public knowledge of subterranean resources, cave diving LSS and safety requirements.

Final maps produced from this project are survey grade 4x products, which enhance and extend existing datasets beyond previous karst survey limitations (Mayor et al 2018; Nebenhaus, M. 2017). Virtual reality products allow karst researchers and cave divers to take a partially guided speleonator FOV tour along the caveline, with accurate point clouds of hydrogeological features, geomorphological features, chemistry composition, and geospatial dimensions in the AOI. These include chemical datasets for representation of dissolution water quality for photogrammetry and LiDAR image artifact identification and correction. After model assessment final discussion on GIST & PSTAR research SWORTs can be assessed from the perspective of an experienced analog survey crews' responses to ULS cave survey and potentials for GIST improvements.

3.3.2. Phenomena & Sampling

The survey sampling frame work will operate based on multiphase calibrations to verify and utilize in data collection. ULS will be calibrated by test scanning in air, fresh water, and salt water in the laboratory accompanied by the water quality sensor. These datasets will be evaluated for accuracy and precision of both instruments, confirmation of their operation, and calibration for deployment. The ULS and water samples in the fresh and salt water strata of the cenote allow for assessment prior to model deployment for QAC in imaging artifact identification, hydrogeological stratigraphic assessment, and Kd-tree geological fracture facet extraction.

3.3.3. Research Apparatus: Survey, Speleonation, & 3D GIST

Speleonauts and astronauts require specific equipment sets to safely and effectively complete operational goals that are analogous in terms of RS, LSS, and other factors (Armstrong

2017; Bowens 2009; NOAA and Joiner 2001). Figure 21 presents TRN H/W, recording devices, survey scales, and personal protective equipment. Figure 22 presents open-circuit sidemount scuba LSS and diver propulsion vehicles (DPV) to reduce dive transit costs. These figures present the equipment utilized by speleontors on deployment for safety and geospatial reference collection, traditionally.



Figure 21. Photograph of traditional cave diving survey equipment including, left to right, top to bottom, light integrated helmet, 150m survey reel, solar panel, TRN H/W, survey slate with compass, level, and pencil, spare pencil and TRN markers and photogrammetry survey targets.



Figure 22. Photograph of diver propulsion vehicles (DPV) to reduce swimming fatigue and pen circuit self-contained breathing apparatus (SCUBA) sidemount tanks for cave survey range extension at the system entrance of Cenote Taj Mahal (Gibbs 2018).

Speleonauts tandemly survey the AOI by LiDAR and PhoDAR for geospatial FOI sampling. While conducting the survey, diver 2 act as EVA leader. Diver 2 and diver 1 operate as individuals within a crew structure for safety. Diver 1 leads the dive entry and tails on the exit, diver 2 tails on the entry and leads on the exit. Diver 1 deploys the survey reels, PhoDAR markers, collects video evidence films, and assists diver 2 with ULS deployment. Diver 2 deploys the ULS system, lays fiber optic cables, ensures system leveling and stability, and finally deploys fractal survey markers. The speleonaut crew is in direct command of mission abort procedures, with diver 1 and 2 possessing equal authority to end operations at any time, for any reason. End of operations can extend from equipment malfunction, psychosomatic events, stochastic environmental events, or spatial disorientation.

These improvements to methods and safety all pale in comparison to geospatial data collection improvement in technique, productivity, and accuracy which serves to reduce each risk individually and in concert via ULS deployments and simulation developments. Figure 23 presents digital cave survey toolkits standing as improvements to cave survey equipment from analog tools that provide inadvertent mitigation strategies to historic cave diving risk assessments and planetary science mission planning concerns. AOI surveys collect data with calibrations and assessments modifications based on image artifacts observed daily for rectification. ULS fiber optic cables are deployed in Velcro straps to facilitate swimming. Cave survey stations, fractal markers, and surveyors represent georectification survey points in scans.



Figure 23. GIST equipment for remote sensing survey of cenotes and underwater caves with drones, VR heads-up-display (HUD), solar panels, water quality, fractal marbles, and 3D scanned and printed paleontological remains.

LiDAR improves methods for crew and surface communication, which decreases work and stress-loading, and improving real-time cave-in risk assessment for analog contingency planning. ULS scale, precision, metadata, and accuracy all play vital roles in cave datasets as high-quality geospatial information is of vital necessity in speleontor exploration and geohazard avoidance. Need for engineering grade GDBs for assessment are critical for urban planning and accident analysis and should aim towards $<10\text{cm}^3$ geospatial accuracy. These GDBs also promote PSTAR objectives by serving as analog mission planning tools and simulators for operations architecture and RS operator assessments based on science objectives, GIST capabilities, equipment limitations, risk mitigation, and other requirements for developmental problem/failure anomaly reporting (DPFAR).

3.3.3.1. Cohort Remote Sensing Instrument (CRSI) Array

Zero-visibility remote sensing survey training, microgravity peak performance buoyancy standards, EVA lifeline concerns, PPP etiquette, microorganismal laser impact mitigation (lowest mJ for sensing) parallel effect exploratory underwater cave and PSTAR surveys. PSTAR

and GIST both require for training datasets in imaging biofilms, hazardous chemicals, geohazards, etc for identification, characterization, and classification. Appendix L presents cave etiquette parallels for PSTAR PPDE to prevent negative anthropogenic due to operations, which also promotes survey dataset quality outcomes.

In cave diving these include induced zero-visibility (silt storm), delicate feature damage, harmful ablation of organisms, & anthropogenic chemistry modification. Cave diving restrictions prevent >3BCRA survey by causing speleonauts to have to swim or squeeze single file through passages 1m or smaller and wait for crew members to gather on the exiting side. Divers rely upon personal redundant LSS to navigate complex geometric phreatic systems of $\approx <1\text{m}^3$. Divers must abate or adapt to existing survey methods deficiencies on-the-fly while on mission. VR, LiDAR, PhoDAR, and robotic technologies are serving to offset past survey methods limitations with H-R rescue, TRN H/W, and contingency response Appendix G. (Bartos et al 2014; AgiSoft Inc. 2013; 2GRobotics Inc. 2018)

LiDAR, PhoDAR, water quality, and dive computers employed through underwater 3D Disconnected-reconnected-Outrigger network surveys, allows for CRSI scans through restrictions (i. e. orange outline, unfilled block) while swimming along the black line in, red line out (Bowens 2009). ULS survey mitigates negative cave and planetary impacts through cognizant PPP training. These promote LiDAR and PhoDAR stereoscopic imaging methods, while mitigating collection concerns. Figure 24 presents PhoDAR survey video measurement angles of $45 \leq X \leq 135^\circ$ to highlight collection methods listed below:

- i. Collect LiDAR and PhoDAR evidence from center of caveline facing the cave walls, ceiling, floor, or FOIs in and out for the total cave-line length.

- ii. Deploy Mnemo survey tool along caveline and FOIs along the survey line to collect .svg central survey line.
- iii. Mark each meter of caveline and collect LiDAR and PhoDAR at 90° angles to the cave walls, ceiling, & floor from the cave line at 5m transect increments.
- iv. Collect at 1m perpendicular transect increments vertically, dependent upon, wall or FOI heights.
- v. Hand-extinguished light and computers for LiDAR scanning & deploy 60000 lumen Big Blue Dive lights for PhoDAR video collection. Allow for various light levels as agreed upon by the crew for calibrations, operational, and safety needs.

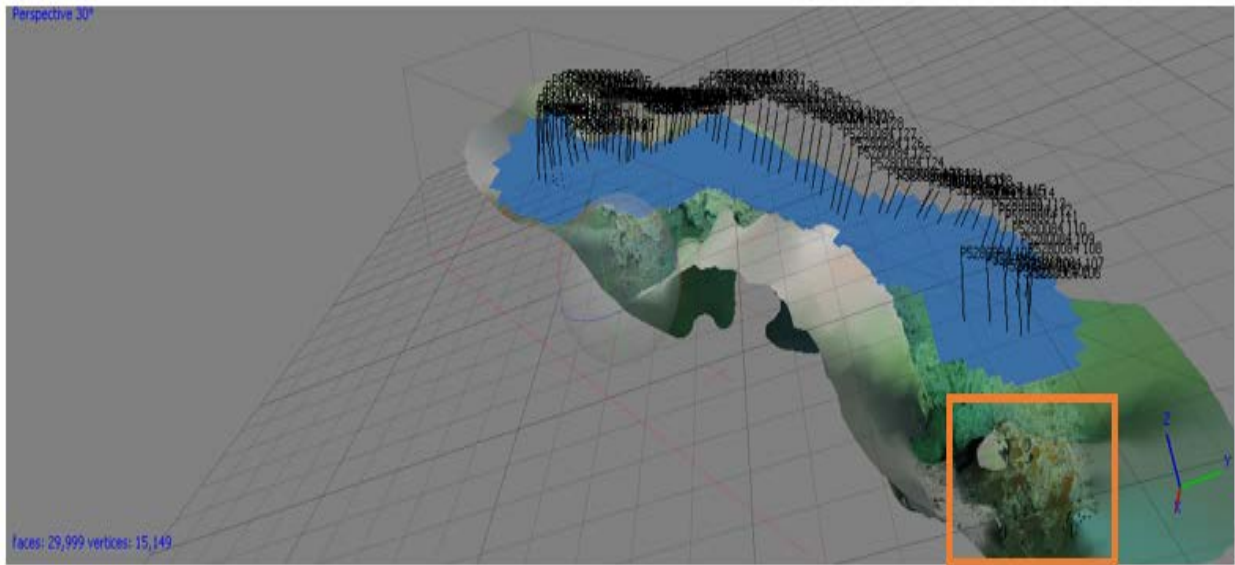
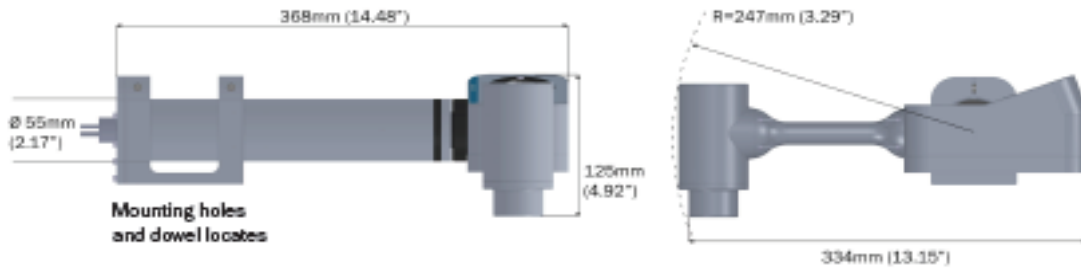


Figure 24. PhoDAR overlap series from FOI survey within the Deep Bone Room AOI with Paleontological remains at the opposite end of the cave restriction entrance in the orange box.

The methods and skills necessary to produce the project include photogrammetry and ULS phreatic karst survey by experienced cave divers. Development of karst hydrogeomorphology GDB via ULS and water quality modeling promote VR environment creation. Figure 25 provided details on the ULS. Figure 26 presents methods for data collection with Taylor water sampling surveys kits. These stand to serve as deployment environment references for 3D GIST karst analysis and modeling correction with CRSI PhODAR, LiDAR,

and hydrochemistry. Results of the ULS dataset quality and water quality samples are assessed against existing survey datasets from the QRSS and BCRA Grading.

ULS-200 Specifications



Performance		
Scan Range	Minimum: 0.36m (1.2') Maximum: 2.5m (8.2')	
Points Per Line	480	
Laser Coverage	50° (in water) 68° (in air)	
Rotational Coverage	360°	
Laser Line Resolution	0.1042° (in water) 0.1412° (in air)	
Rotational Resolution	0.018°	
Range Resolution	0.01mm at 0.21m 0.2mm at 1.4m 0.6mm at 2.5m	
Sample Rate	Up to 4750 points/sec 9.9 profiles/sec	
Electrical		
Power Output/ Laser Class	50 mW/ Class 3R	
Wavelength	440nm	
	Vehicle Integration	Direct Tether to 2G Robotics Junction Box
Power Consumption	5 Watts (Max), 12-24 VDC	8 Watts (Max), 120/240 VAC
Data Interface	RS-485 half-duplex	USB
Mechanical		
Weight in Water	1.6 kg (3.5 lbs)	
Weight in Air	3.9 kg (8.6 lbs)	
Depth Rating	350m	
Connectors	SubConn 4 pin MCBH4M	
Operating Temperature	-10°C to 40°C	
Software		
Data Acquisition Software	Included	
Export Data Formats	.xyz (CSV)	
Custom Integration	API Available	

Figure 25. 2G Robotics ULS-200 Specifications (2G Robotics, Inc. 2016).

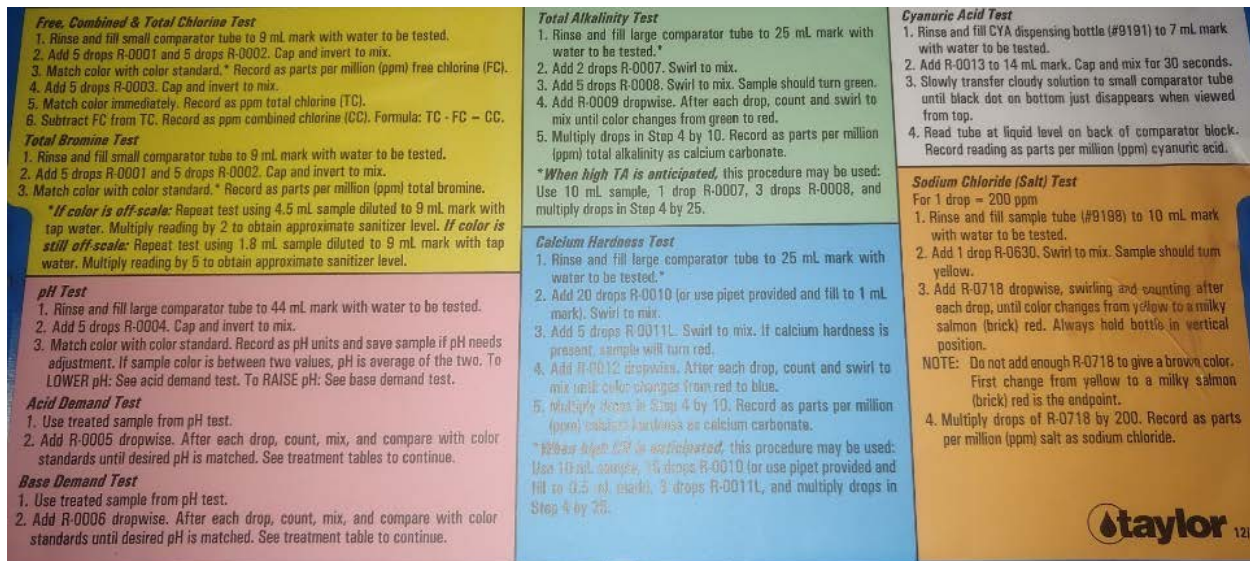


Figure 26. Taylor Water Quality Test kit (Taylor, Inc. 2018).

Energy requirements, sensing environment, systems contexts, phenomena of interest, and other properties are at play in sensing, collection, and analysis of geospatial and ULS survey data. GSE H/W included energy production from a hardline car battery as a power source and a laptop to fire the ULS-200. ArcGIS, AgiSoft Photoscan, Unreal Engine, and CloudCompare are all applications that can be utilized for management, development, and analysis of geospatial datasets require experienced QAC. DSRL cameras, in conjunction with a water quality sonde and other equipment promote high detail environmental scanning. ULS utilizes and depend upon a variety of factors for their deployment and application.

Laser scanners deployment methods and application domains are reliant upon a series of production and human factors including the phenomena of interest, environment, dopant, crew, and crystal. Laser crystals include a varying series of transparent, ionized dopant monocrystalline gain media matrices for non-linear optics data collection. Doped crystals enable wavelength-specific, optical pump stimulated photonic amplification for scanning emission and absorption of

plasma ablation from scanned surfaces. The ULS-200 utilizes a titanium doped sapphire operating in a blue light range to detect ablated targets in aphotic underwater conditions.

Crystals scanning effective can be compared to glass and ceramic linear and non-linear optics in several terms and have relative benefits and deficits. Lasers offer higher band transition cross-sections and thermal conductivity, as well as a smaller electromagnetic bandwidth absorption and emission range than glass or ceramic. Laser efficiency can be hampered by several factors if prior considerations have not been prepared for in terms of dopant agent, agent uniformity, agent concentration, monocrystalline host matrix property, matrix geometry, matrix surface quality, optical pump source, pump geometry, optical pump energy, photon wavelength, power source, and other factors, Table 1. Birefringence in crystals may also occur which can affect scanning accuracy and requires considerations for ULS calibration.

Table 1: Laser Crystal Typologies & Considerations

Doping Agent	Period Block	Monocrystalline Host Matrix	Wavelength Emission Ranges in μm	Crystalline Structure & Atomic Constituent Properties
Ti ³⁺ (Titanium)	d-block; Group 4, Period 4	a) Sapphire (α -AlO)	0.650 – 1.100	a) Anisotropic, high hardness, high thermal conductivity
Cr ²⁺ (Chromium II)	d-block; Group 6, Period 4	ZnS, ZnSe, etc (Zinc chalcogenides)	2.0 – 3.40	Mid-Infrared
Cr ³⁺ (Chromium III)	d-block; Group 6, Period 4	a) Ruby (AlO) b) LiCaAlF (LiCAF), LiSrAlF (LiSAF), LiSrGaF (LiSGAF).	0.800 – 0.900	a) Anisotropic, high hardness, high thermal conductivity b) Broad Gain Media
Cr ⁴⁺ (Chromium IV)	d-block; Group 6, Period 4	a) Forsterite (MgSiO) b) YAlO (YAG)	a) 1.10 – 1.37 b) 1.35 – 1.65	a) Broad Gain Width; b) Isotropic, hard, chemically inert materials, high thermal conductivity
Nd ³⁺ (Neodymium)	f-block; Group N/A, Period 6	a) YAG; b) YAlO (YALO); c) YLiF (YLF); d) Tungstates KGd(WO) & KY(WO) e) YVO (Vanadate)	a) 1.064; b) 1.047; c) 1.342; d) 0.946; e) 1.053	a) Isotropic, hard, chemically inert, high thermal conductivity; b) Anisotropic, high hardness, high thermal conductivity; c) Good UV transparency; birefringence, large energy storage; d) High thermal conductivity, high cross-sections, and large gain bandwidth; e) Anisotropic, very high cross-sections

Yb ³⁺ (Ytterbium)	f-block; Group N/A, Period 6	a) Apatites (SYS); b) Borates (BOYS, GdCOB); c) Sesquioxides (YO, ScO); d) YAG	a) 1.020 – 1.070; b) 1.030	a) Isotropic, high hardness, and high thermal conductivity;
Er ³⁺ (Erbium)	f-block; Group N/A, Period 6	a) YAG b) YLF	a) 2.9 b) 1.6	a) Good UV transparency; birefringence, large energy storage;
Tm ³⁺ (Thulium)	f-block; Group N/A, Period 6	YAG	1.9 – 2.1	Isotropic, hard, chemically inert, high thermal conductivity;
Ho ³⁺ (Holmium)	f-block; Group N/A, Period 6	YAG	2.1 – 2.94	Isotropic, hard, chemically inert, high thermal conductivity;
Ce ³⁺ (Cerium)	f-block; Group N/A, Period 6	LiCAF, LiLUF, LiSAF, & YAG	0.28 – 0.33	Broadband Gain Media

The intended final products of the project include a high-quality survey dataset for accurate geospatial analysis and precise geovisualization in ArcGIS Scene and virtual reality environment for karst hydrogeologic research and exploration. Other products include cave geomorphology from a vertical perspective, stratigraphy from a horizontal perspective, and a 3D printed fractal survey marker for parallel projection, a LiDAR photoplethysmogram, PhoDAR paleontological dataset, and a regional 3d heat map for potential cenote locations for future analog research missions, a 3D geohazard modeling for potential cave-ins, and a LiDAR pulse calibration indicatrix. The software necessary for developing a karst 3D GIS is an admixture of open source and proprietary products based on need, access, and toolsets provided. Proprietary Esri CityEngine and ArcGIS Pro, or open-source QGIS utilized for 3D spatial analysis and construction promotes extended 3D capabilities and are utilized for this project. AgiSoft photoscan and Cloudcompare Stereoviewer for ULS and photogrammetry are used to develop 3D functionality which provides interoperability formats for point cloud, texture, and object development and exportation to other software suites.

Virtual phreatic karst environment could be visualized in numerous head mounted displays to allow platform independent research access through computers as well. These planning considerations promote metanalysis and digital 3D karst reconstruction methods to be developed for GIST and cyber analysis materials. These GDB materials require assessment for geometric accuracy, 3D feature snapping, geovisual texture precision, lighting objective consideration, data compactification, relative scale, and VRV. These are best accomplished in the virtual environment and promote the use of the final 3D products.

3.3.3.2. GIS, 3D Modeling, & 3D Printing

Numerous considerations are required for 3D data collection, modeling, and presentation.

Table 2 presents the visual or drawing hierarchy for an open-source Unreal Engine, CityEngine, or Unity VRL which provides relatively automated construction and quality validation in virtual reality for 3D model development and texture generation (Solcum 2009).

Table 2: Geovisual Hierarchy Levels for 2D, 3D, & AR/MR/VR Map Design			
Level	General Interest	Thematic	Augmented
1	<ol style="list-style-type: none"> 1. Title Screen 2. Generic Symbology 3. Artistic, Basic, & International Standard Labels 4. Key Reference Data 5. Legend - Information Window 	<ol style="list-style-type: none"> 1. Title or Splash Screen 2. Methodological Symbology 3. Descriptive Labels 4. Key Reference Data 5. Information Window 6. Detailed or Interactive Legend 	<ol style="list-style-type: none"> 1. Title or Splash Screen 2. AOI Overview Animation 3. Interactive Labels & Legend 4. AR/MR/VR Symbology 5. Spatio-Temporal Reference 6. Key Reference Data
2	<ol style="list-style-type: none"> 1. Generalized 2D Paper & Web Basemap 2. Navigation Tools: North Arrow, Scale, & Coordinate Reference System 2D-3D DTM Conversion 	<ol style="list-style-type: none"> 1. Highly detailed 2. Navigation Tools: North Arrow, Scale, Pan, Zoom, Rotate, & Coordinate Reference System 3. 3D DTM – 4D Time Series Conversion 	<ol style="list-style-type: none"> 1. 3D Paper & Web Basemaps 2. Navigational Tools: North Arrow, Scale, Pan, Rotate, Zoom, & Coordinate Reference System 3. 4D – VR Time Series Conversion for VRL
3	<ol style="list-style-type: none"> 1. Dissemination Tools: Print, Email, Share, & Like 	<ol style="list-style-type: none"> 1. Dissemination Tools: Print, Email, Share, & Like 	<ol style="list-style-type: none"> 1. Dissemination Tools: Print, Email, Share, & Like
4	<ol style="list-style-type: none"> 1. FOI Reference Identifiers 	<ol style="list-style-type: none"> 1. Interactive Geolocator: 	<ol style="list-style-type: none"> 1. Interactive Geolocator:

	2. Multimedia Inlay & Overlay	Compass, Map, & Dive Computer 2. Reference Information 3. Statistical Charts or Graphs 4. Multimedia Inlays & Overlays	Compass, Map, & Dive Computer 2. Reference Information 3. Statistical Charts or Graphs 4. Multimedia Inlays & Overlays
5	1. Reference Notes 2. Attributes 3. Copyrights, Limitations, & Deductions 4. Neatlines, Grids, & Graticules 5. Tools, Tips, Help, & Information	1. Reference Notes 2. Attributes 3. Copyrights, Limitations, & Deductions 4. Neatlines, Grids, & Graticules 5. Tools, Tips, Help, & Information	1. Reference Notes 2. Attributes 3. Copyrights, Limitations, & Deductions 4. Neatlines, Grids, & Graticules 5. Tools, Tips, Help, & Information

This hierarchy coupled with 3D image corrections promote and improve QAC methods for 3D GIS and VRL simulations through fractal analysis. These GDB materials can be exported to and from ArcGIS and Unreal Engine or Unity promoting geovisual hierarchy interoperability. Utilization of Wolfram Mathematica Sketchup produces digital illustrations of a fractal marble geometry to export and 3D print with the Makergear printer.

The code to produce the octahedron from MatLab and 3D print as a .stl file is

```
vect[1] = {0, 0, 0};
```

```
vect[2] = {1, 0, 0};
```

```
vect[3] = {0.5, 3^0.5/2, 0};
```

```
vect[4] = {0.5, 1/3*3^0.5/2, ((3^0.5/2)^2 - (1/3*3^0.5/2)^2)^0.5};
```

```

Tetron[{i_, j_, k_}] :=
Tetrahedron[{vect[1] + {i, j, k}, vect[2] + {i, j, k}, vect[3] + {i, j, k}, vect[4] + {i, j, k}]];
SiPyramid[0, {i_, j_, k_}] := {Tetron[{i, j, k}]];
SiPyramid[n_, {i_, j_, k_}] :=
Module[{s = {}},
Do[s = Union[s,
SiPyramid[n - 1, 2^(n - 1)*vect[u] + {i, j, k}], {u, 4}]; s];

```

Figure 27 presents a Makergear 3D printer for fractal survey marker development from Wolfram Mathematica recursive function procedure products, which produces a Sierpinski Octahedron 3DGraphic image and is convertible to .stl for 3D printing object formats. Figure 28 presents a Sierpinski Octahedron fractal survey marker set. The resultant fractal octahedron serves as a valuable, novel geospatial-spectrometric LiDAR and PhoDAR scale that can be utilized for *in situ* 4D LAMIS spectrometric calibrations underwater. They act as edge-detection vertex confirmations for point cloud-surface area & spectral signature accuracies in 3D environment texture and color QAC. PhoDAR point cloud quality is evaluated via automated process in AgiSoft based on the parameterized photo optic lens settings, quality values of < .5 are removed from modeling to prevent aberrations. Parallel projection assessments of cave sites with fractal markers serve as effective methods for 3D model QAC. Figure 30 displays 3D imaging artifacts reduction in a DTM or digital elevation model (DEM) parallel projection square which is perfectly filled with parallel rays on the point of contact with the survey markers. The AgiSoft processing report for the fractal marker DEM is provided in Appendix K.

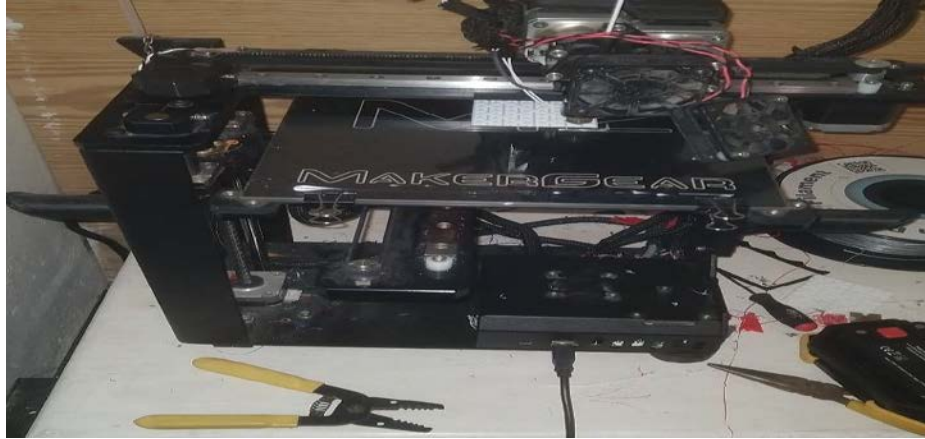


Figure 27. MakerGear 3D printer producing white portion of black-white contrast survey marker.

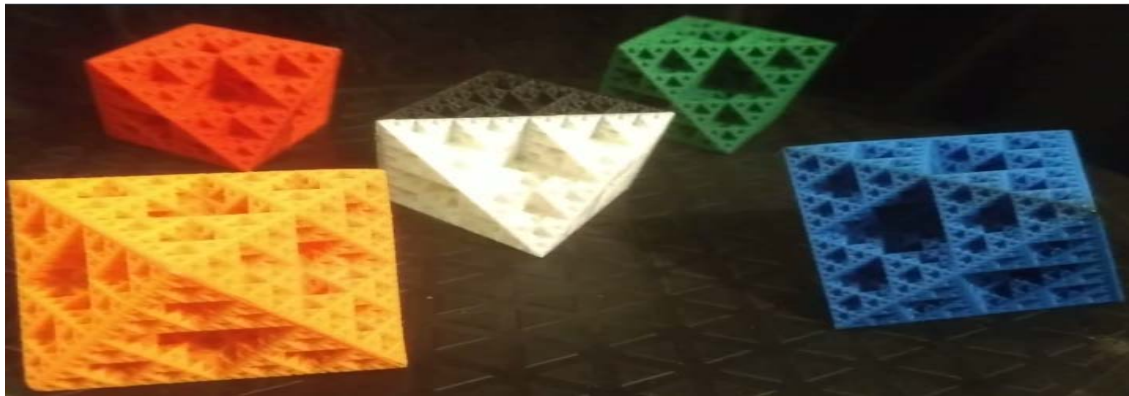


Figure 28. 3D Spatiometric-Spectrometric Sierpinski Octahedron. Red, green, blue, black-white contrast, and reflective orange survey marker set.

Camera Calibration

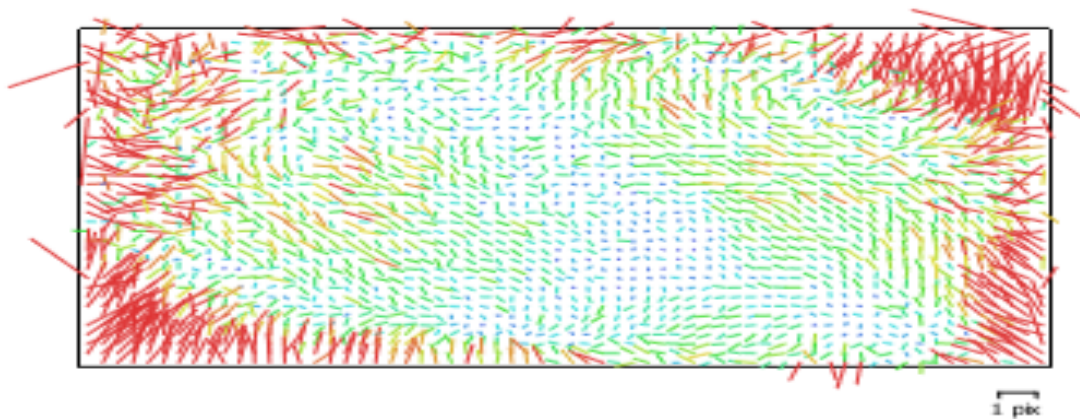


Figure 29. Fractal Marble Parallel projection assessment in Agisoft Photoscan. Red represents background scatter, blue represents fractal edge-detection assistance at 1-pixel resolution.

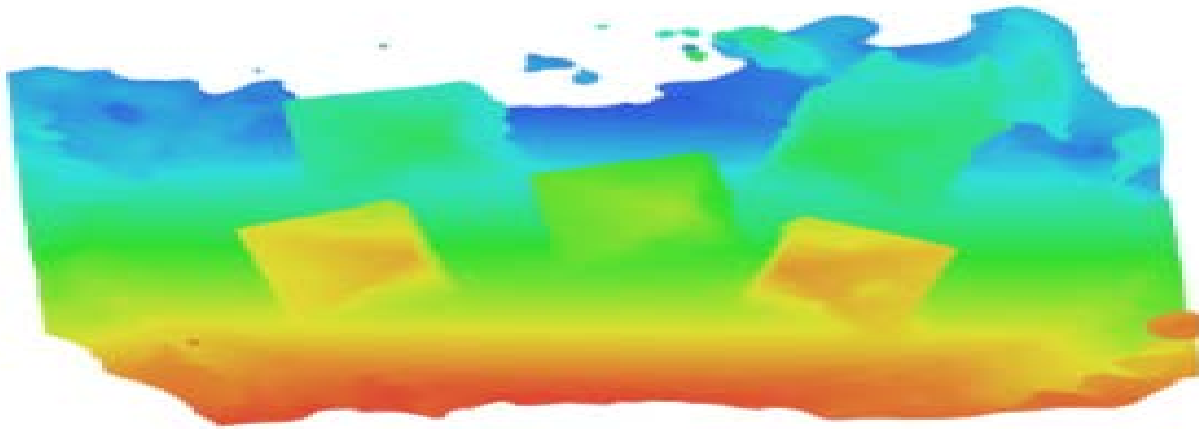


Figure 30. Fractal Marble DEM analysis in Agisoft Photoscan.

The Makergear M2 3D Printer produces μm precision print quality for dual extrusion printing in both PLA and ABS plastics. The system is complicated to use, requires ample tending, but provides high quality printing products with engineering grade print accuracy. These products improve RS imaging and provide underwater survey markers that are less complicated to deploy than traditional tools.

3.3.4. Variables: Definition & Measures

Optical variables include the refractive index in terms of fresh and salt water for cameras and lasers. The pulse, wavelength, timing, and duration of plasma ablation all effect RS datasets collected by the ULS-200 and require documentation as well. Data categorized to reflect existing karst geomorphological feature definitions, identified hydrochemical components of caves, known pollutants to karst aquifers, and paleontological records as described in Klimchouck and Andreo based on karst geomorphology and dissolution hydrodynamics require annual updates for GDB spatial data veracity and completeness.

3.4. Data Requirements & Sources

The geospatial datasets exist as a series of physical phenomena of hydrological and lithic processes that can be surveyed by eye and remote sensing equipment deployed by scuba divers (NOAA and Joiner 2001; Carney et al 2013; 2G Robotics Inc, 2016). Water dissolution chemistry and conduit surface chemistry are required for comprehension of karst decomposition. Physical definitions of heat capacity of water, refraction index of salt and fresh water, and dissolution chemistry are needed for environmental contexts. Volumetric geospatial data includes depth, width, length, height, volume, inclination, length, azimuth, and survey vector point clouds. The unforgiving environmental conditions have deterred previous survey tools, technologies, and access to develop phreatic cave survey maps. No map greater than BCRA grade 1 existed before 2017 for the Cenote Taj Mahal Phreatic system, though survey attempts have been mounting for 15 years. Phreatic cave maps in the Yucatan Peninsula have not yet progressed above grade 3 based on the BCRA survey grades and notes.

The virtual reality application aims to provide a semi-guided first-person tour of the AOI from the perspective of a cave researcher. Virtual reality development requires assessment for geometric accuracy, 3D feature snapping, geovisual texture precision, lighting objective consideration, data compactification, relative scale, and virtual reality sickness reduction. Focused application development incorporates karst researchers without scuba diving experience into the research dialog to comprehend phreatic karst processes. It assists in informing future public participation GIS for cave researchers and explorers on how, where, what, and why to collect and upload their survey metadata for recognition and 3D development.

3.4.1. Datasets & Qualities

The definitions described in Benson & Yuhr, Klimchouck, and Andreo based on karst geomorphology and dissolution hydrodynamics guide the data dictionary for this work. Water dissolution chemistry and conduit surface chemistry are required for comprehension of karst decomposition. Physical definitions of heat capacity of water, refraction index of salt and fresh water, and dissolution chemistry are needed. Volumetric geospatial datasets, and FOI PhoDAR point cloud datasets vetted for QAC quality are modeled to prevent aberrations and promote high quality DTMs development.

3.4.2. Origins & Physical Congruencies

Overlapping photos, combined with analog survey measurements promote high photo alignment for photogrammetric model development. Alignment quality promotes geometric modeling consistency throughout the cave environment to compensate for hindering photo-optic aberrations and assess their impacts for later mitigation or investigation. Deliberate scanning of surveyors in the scanning radius promotes image artifact identification and volumetric measurement estimates. Assessing ULS datasets and pulse firing dynamics from complementarity wave-spin-particle function perspective improves imaging analysis of the holographic ULS point cloud datasets based on an omni-angular point cloud collection perspective.

3.4.3. Data-dictionary & Entity-Relationship Diagram

Cave explorers, surveyors, and researchers have collected datasets in the area since primary cave discoveries in the late 1980s, early 1990s. Database management for karst regions via GIS, structured query language (SQL), and python scripting provides promotes 3D spatial

analysis and long-term resource references. Appendix F presents the data dictionary, definitions, datatypes, formats, storage elements, description and validation for sampling and apparatus types. Related to speleological formations, formational mechanisms, speleothem products, and other information. FOIs evidence existing for this project within the AOI were recorded within a Microsoft Access Database for data management, geospatial analysis, and long-term storage. Appendix G presents the SQL and Python enabled Microsoft Access database with information on AOIs of the region with their related geoh heritage materials. Datasets are in the forms of personal and community exploration notes, survey logs, maps, dive computers, remote sensors, photos, and videos from the QRSS. Appendix H presents entity-relationship diagram (ERD) necessary for an effective implementation of 3D karst research GDB for planetary sciences evidence collection, research surveys, and accidental events leading to injury or death for risk assessment and mitigation.

3.4.4. Limitations

ULS cave survey datasets are not freely available for several reasons. ULS have one recorded deployment in phreatic karst to the knowledge of the author related to this proposal in Schiller and Pfeiler (2015). Underwater laser scanning data is not available and requires collection with concurrent water quality data for calibration confirmation. Public datasets on phreatic karst are not available for need of public safety prevention of cave accidents.

The costs to purchase a ULS-200 is approximately 40,000 dollars, rental of the system is 1,200 dollars a day. Cave diving survey costs approach 200-500 dollars a day depending upon cave entry fees, diver breathing gas mixes, environmental hazards, and other costs. Other equipment needs for the exploration include 3D printed spatial markers which require 8 hours of production per marker and cost 320 dollars each. A flight to the area of interest costs 400 dollars

and requires a day of travel to reach the site. The datasets were developed over the course of a one-and-a-half-week period of survey with seven to eight-hour days of survey. Data processing was limited by power outage, ArcGIS Pro malfunctioning, imaging artifacts, and ambiguity of ULS scanning position without post dive debrief confirmation by the dive team.

Optical variables effecting and deterring categorization of karst geomorphological features were numerous. These variables were observed, recorded, identified, and indexed as photonic quantum vortex (PQV) fluid dynamics, topological laser pulse (quantum) singularities QTK, hydrogeochemical components of cave haloclines, pollutants within the aquifer's water column, and other factors. Figures 39 presents in the Complex Geometric Survey Environment Collection with stalagmites, flowstone, Boxwork, cave-in, cave survey line, and paleontological remains. The environment presents non-diffuse lighting obstacles to mapping which deter edge detection in PhoDAR, and mask or agitate LiDAR point cloud volumetric results.

Figure 31 presents photographic evidence of fresh/salt image refraction & fluid vortex imaging artifacts related to HSF propagating GHR dissolution along the cave central path of least resistance at the halocline with silt paleosols and collapsed ceiling deposited on the cave floor. It also depicts the supra-sub, halocline interface and fluid dynamic KHI shearing related to conduit floor, wall, and ceiling topography producing imaging artifact refringence and birefringence in the red box. Figure 32 represents the one of the needs for fractal markers LiDAR and PhoDAR spatial target survey deployments to prevent coloration blending. Figure 32 located near the paleontological remains of butchered and cooked *Hemiauchenia macrocephalus* proximal tibia and scapula $\approx 11\text{Ka}$ with in red box, also presents coloration blending. Coloration blending occurs when image artifacts merging causes 3D modeling as AOI limestone texture-marker invisibility.

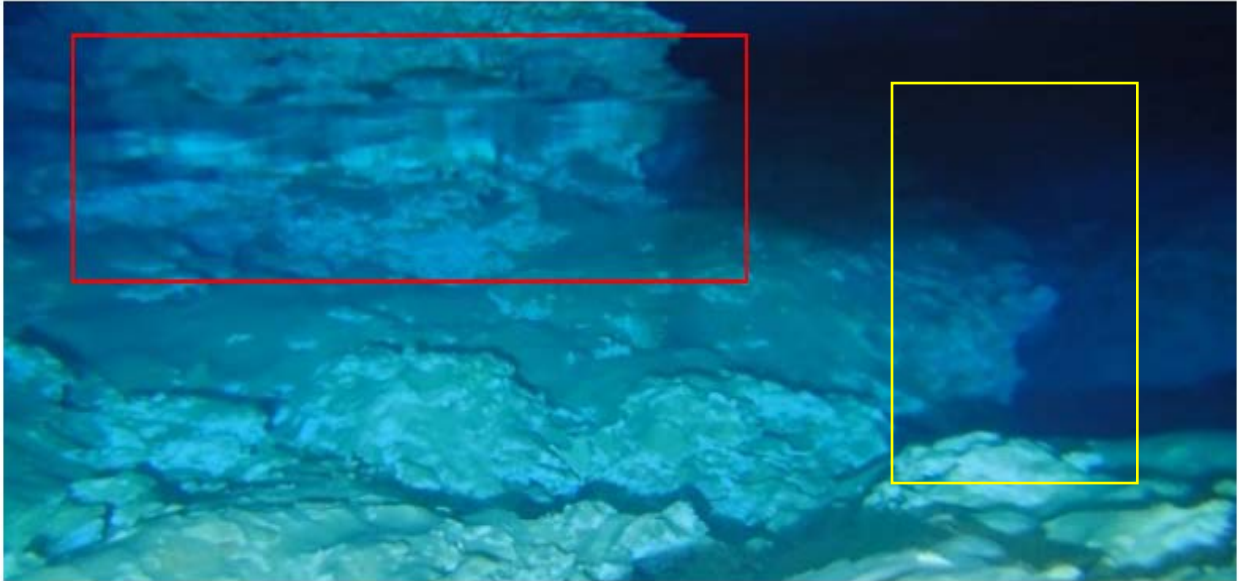


Figure 31. Halocline image slip in the red box, and non-diffuse lighting edge-loss in yellow. Topographically correlated GHR HSF KHI thermodynamic cave-in & paleosols stratigraphy.

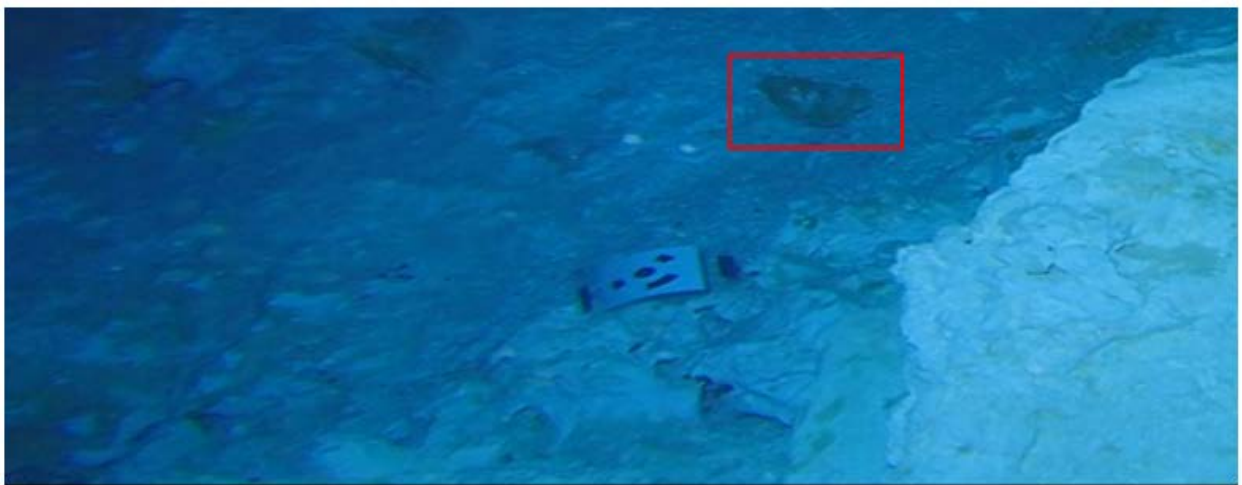


Figure 32. Spatial target coloration blending causing 3D texture merge into limestone, located near HBE remains of *Hemiauchenia macrocephalus* proximal tibia $\approx 11\text{Ka}$ with in red box.

Figure 33 presents a minor silt storm from scuba diver off-gassing and swimming causing percolation and backscatter from increased dissolution. RS observations of silt storms can inform dissolution mechanics studies via calculation of fluid suspension. Figure 34 presents a diagram

of an optical Photonic Quantum Vortex (PQV) with different topologically charged electrodynamic phase-fronts radiating in a helix excitation.



Figure 33. Scuba diver Off-gassing causing percolation and backscatter from sediment clouds.

PQV prevent applied RS LiDAR, PhoDAR, and SoNAR systems sampling accuracy-precision in terms of sensor-target synchronization to spin-wave-particle dynamics. Figure 34 presents a multiphasic singularity, PQV, which at zero intensity $m = 0$ bears a non-massive centralized hypergeometric-Gaussian mode (HyGG) $\psi = \alpha e^{im\phi} e^{-r^2}$ paraxial wave function in an oscillating viscous toroidal flow. PQV is similar to the Lissajous curve special case of $\delta = 0$, bearing curvilinear energy transmission over curvilinear knot-modulations that translate as emanated QCED. QCED are based on PQV phononic and photonic dynamics of a specific plasma product resonating or coalescing in quasiperiodic spin-wave-particle ordered and disordered structures within a vacuum continuum. LiDAR systems attempt to accurately detect the elementary quasiperiodic spin-wave-particle structures for 3D reconstruction, with inaccuracies related asynchronous environmental LiDAR plasma generation and sampling. (E-Karimi 2011).

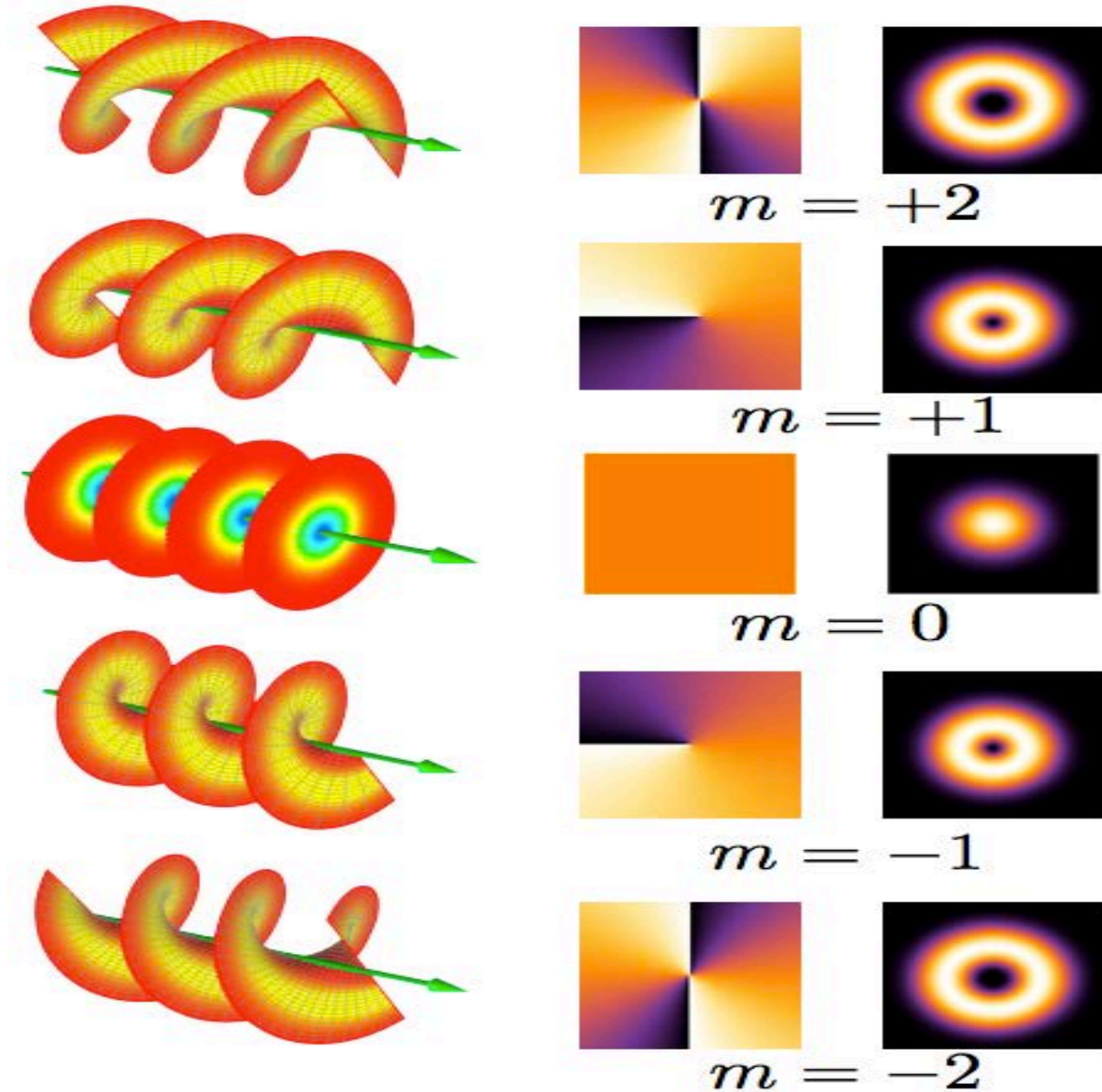


Figure 34. Photonic Quantum Vortex (PQV) diagram with different topologically charged QCED radiating from phase-fronts $m = +2, +1, -1, \text{ and } -2$ in a helix excitation. (E-Karimi 2011).

Relating geographic information to RS datasets for geovisualization is a complicated process, a map is a single presentation of a conceptual instant of infinitely complex dynamic processes. Figure 35 presents a photograph of Sistema Taj Mahal Cave Map symbology on display at the cave entrance for parallels in 3D cave symbolization (Mayor 2017). Map

symbolization relative to figure 33, 34, and 35 forward the cartographic reality that no one map possess all information, nor the perfect picture; a map simply provides a specific amount of vital information in the most productive way on a spatial information system. Selection of geometric and other markers for translation is vital and complicated. ULS cave surveys improved karst geographic information techniques and fractal-scale LiDAR edge-detection methods which reduce needs for symbolic representation through RASP CRSI ground truthing.

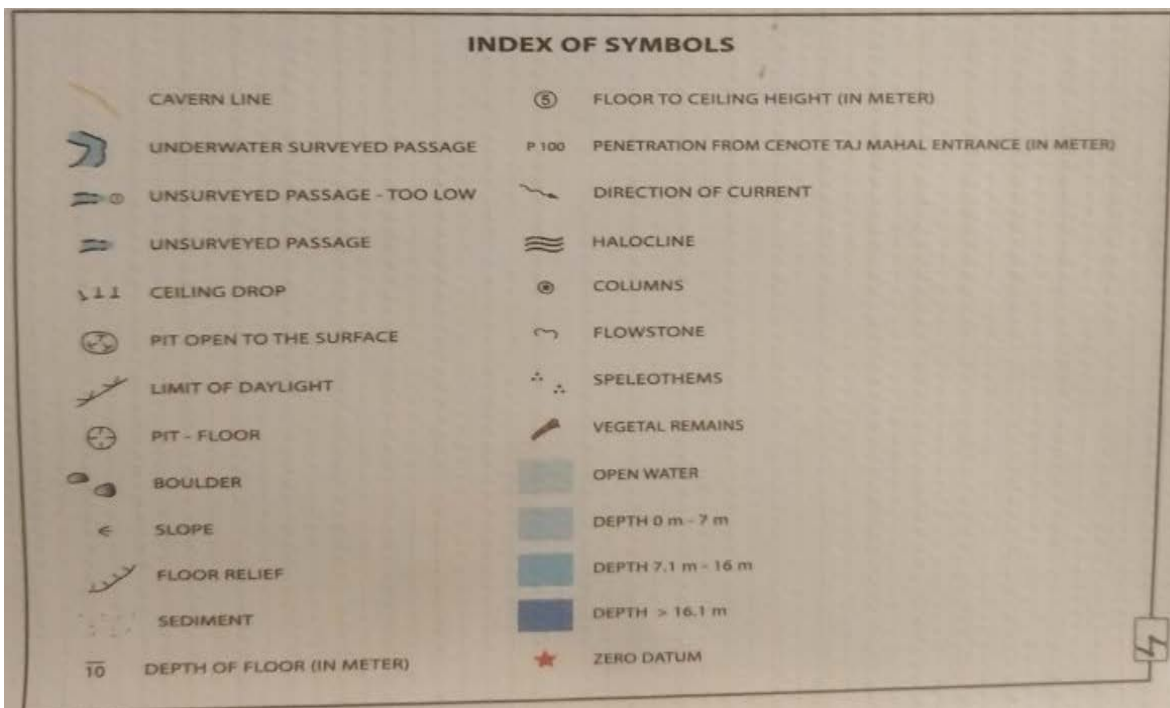


Figure 35. Photograph of Sistema Taj Mahal Map symbology on display at the cave entrance for dive TRN, mission planning, feature reference, and rescue response (Mayor 2017).

3.5. Procedures & Analysis

Model development and analysis occurs in multiple, interdependent stages. These require organization, coding, processing, construction, analysis, visualization, editing, and final presentation. Each model requires the same set of procedures, and each requires unique

calibrations to mitigate various environmental and optical scanning artifacts for each symbolized feature.

3.5.1. Model Development & Analog PSTAR Operations Narrative

The course materials and simulation experiences provided and highlighted ULS cave survey and astronautic PSTAR consideration parallels in LSS planning, scientists-astronaut microgravity etiquette, airborne G-force analogs, FAA hypoxia awareness and training certification, extravehicular activity (EVA) suit testing, and extreme environment RS operations simulations for PSTAR considerations and parallels. The time lines are outlined in Appendices I and J. Appendix I presents the total research times lines as it is related to the goal of a ULS-200 ORT cave survey for PSTAR analog SWORT developments. Appendix I presents logistics, research review, mid-project assessments, analog experiential references on EVA analogs and VR simulations, and writing phases. Appendix J presents the field procedures, CRM reference information, individual crew tasks, responsibilities, and functional roles during survey.

Model development requires several days per model. Photo alignment in low accuracy promotes model development in underwater environments by mitigating backscatter effects. These modifications to alignment decreases matches between foreground particulates in suspension and improves matching of background features of interest.

Later revisions can be implemented to force photo alignment if automated selection lacks significant congruence. Dense cloud formation also varies from model to model with high to low quality and depth filtering depending upon the scanning environment. Mesh and texture formation from a high face count promotes scanning geometrically complex features and requires unique calibration for each model.

Once AgiSoft model development is complete models are exported from AgiSoft to Unreal Engine, Microsoft 3D viewer, and ArcGIS for geovisualization and virtual laboratory development. Object orientation, lighting, scaling, texturing, and geocoding all become the focus in terms of communicating geographic information. The project schedule including research, planning, preparation, survey, calibration, survey, and finally astronaut analog courses and simulations with Project PoSSUM at Embry-Riddle Aeronautical University in Daytona, Florida.

3.5.2. *Expected Outcome*

Preliminary PhoDAR full cave modeling suggests this method PhoDAR coupled LiDAR survey forward cave modeling beyond traditional survey and research limitations. Figure 36 presents the geocoded region in ArcGIS Pro. The maps and models produced from ULS phreatic survey verification & validation (V&V) can be compared against existing maps and analogous PSTAR CRM requirements. Figure 37 diagrams Shearwater Petrel Dive computer datasets including depth, temperature, time, and central nervous system toxicity readings related to LSS run time, operation depth, and O² pressure during Taj Mahal site surveys. Survey video evidence facilitates verification & V&V of datasets *post hoc* for identification of imaging artifacts. Figure 38 displays the preliminary modeling photogrammetry dataset of the Deep Bone Room Interior Model restriction entry within the red box, top down view as if entering chamber as a cave diver. Figure 39 presents the modeling datasets at the survey line end in red box and *Hemiauchenia macrocephalus* burnt and cut osteological remains in yellow, viewed from the perspective of a cave diver swimming head towards floor, feet towards ceiling (Daire et al 2017). Figure 40 PhoDAR model of AOI interior from dive exit perspective with non-diffuse lighting causing edge detection voiding (Daire et al 2017).

The final products include a geomorphological stratigraphic cross-section, regional geohazard heat map of the cave-in potential, and 3D maps and animations of the regional cave systems for long-term GDBs. Figure 41 PhoDAR AOI interior with contrast voids causing text mapping distortions and bending in the 3D object related to speleonaut scuba off-gassing bubbles which effect images and DEM QAC (Daire et al 2017). GDBs materials accessible provided via web and paper formats, as well as a 3D geovisualization virtual reality environment for stereographic display overcome past modeling obstacles. These relate to survey blood chemistry modifications through LSS to provide safe access to extreme environments for survey and exploration.

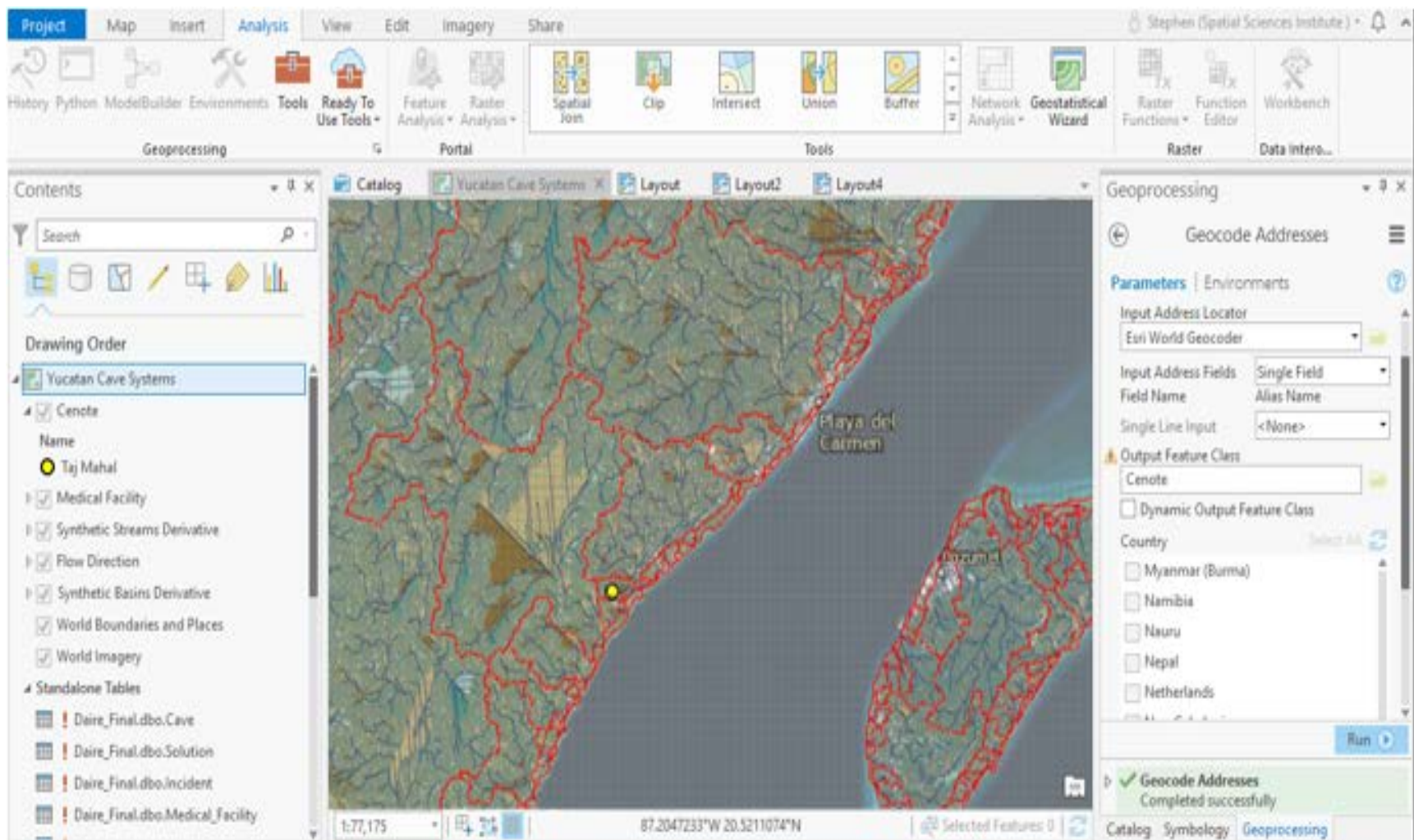


Figure 36. Preliminary modeling dataset geocoded surface survey coordinates in ArcGIS Pro AOI marked with a yellow dot.

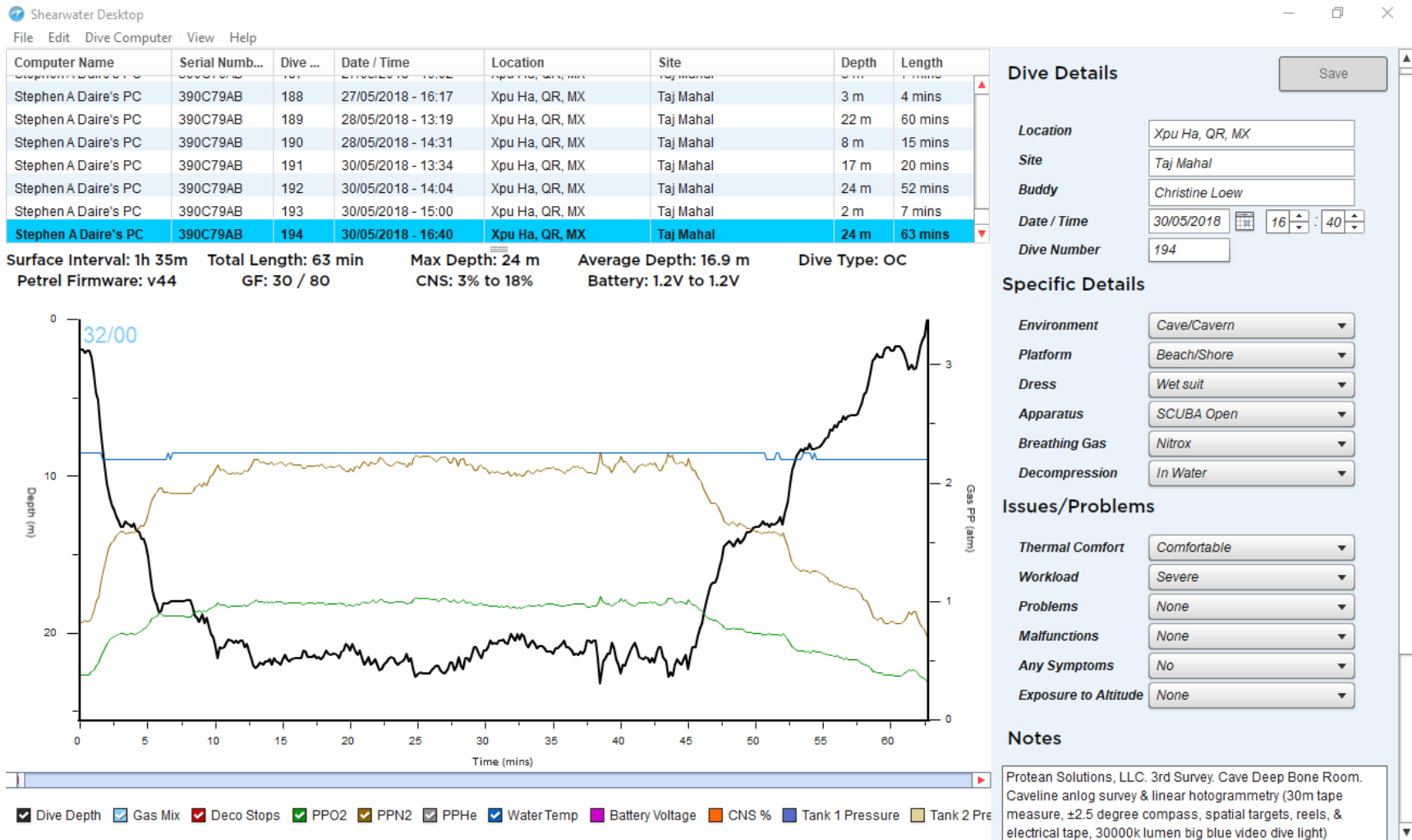


Figure 37. Shearwater Petrel Dive computer preliminary modeling dataset depth, temperature, time, and central nervous system (CNS) toxicity, breathing gas tank readings, partial pressure nitrogen (PPN), and partial pressure oxygen (PPO), related to life support systems run time, operation depth, and O² pressure during Taj Mahal system surveys.

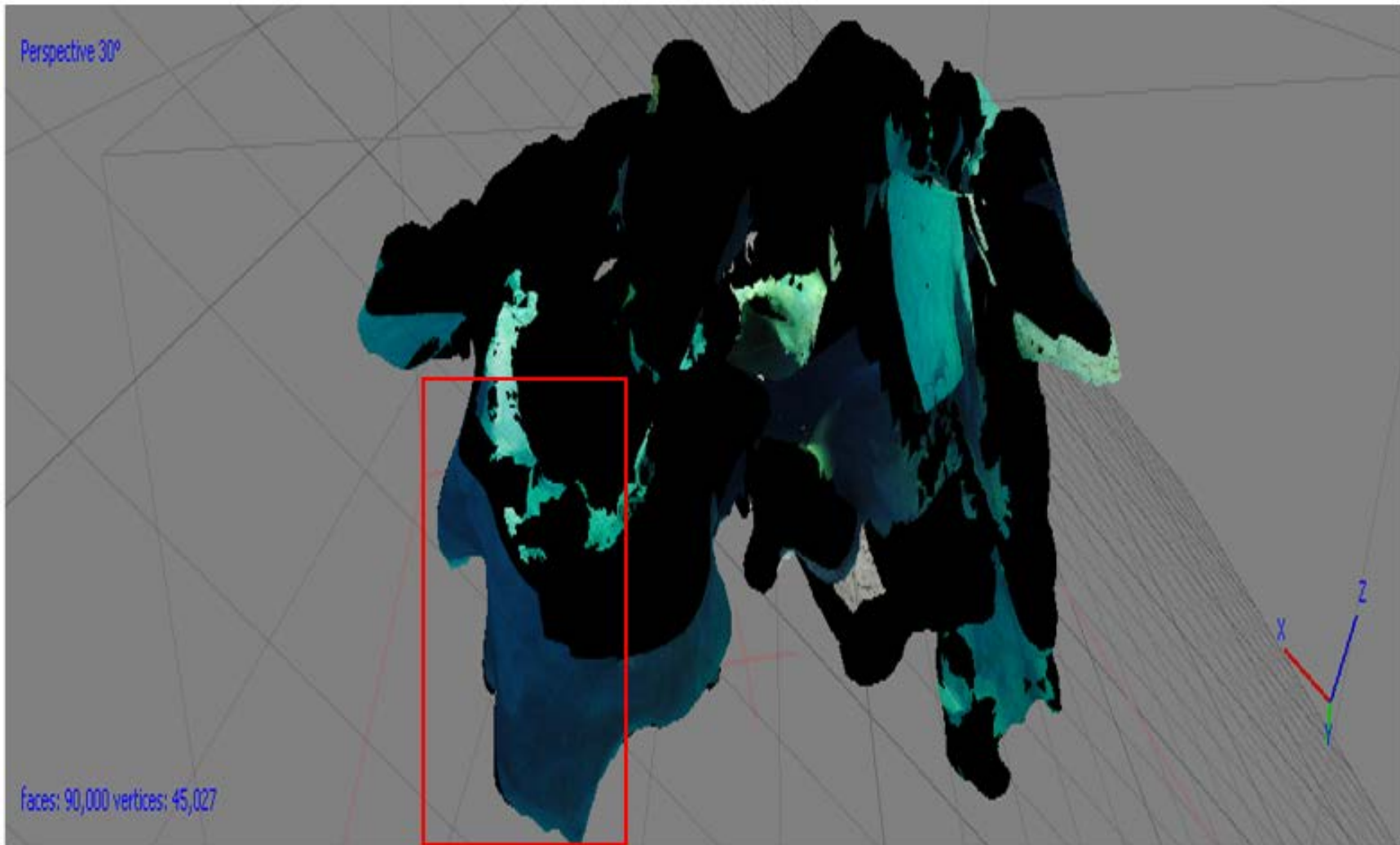


Figure 38. Preliminary modeling photogrammetry dataset of the Deep Bone Room Interior Model restriction entry within the red box, top down view as if entering chamber as a cave diver.

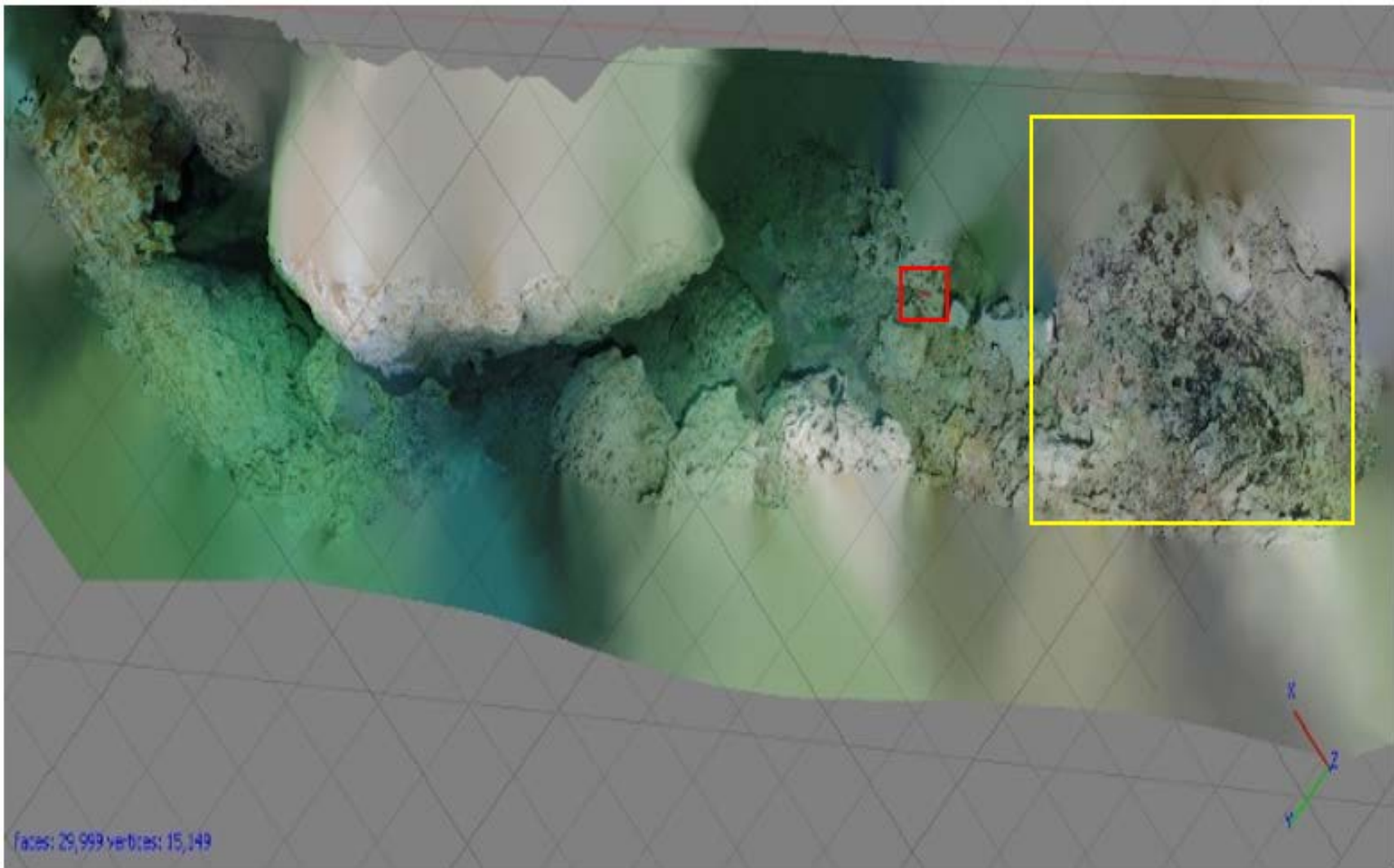


Figure 39. Preliminary modeling dataset cave line end in red box and *Hemiauchenia macrocephalus* burnt and cut osteological remains in yellow, viewed from the perspective of a cave diver swimming head towards AOI on cave floor, feet towards ceiling.

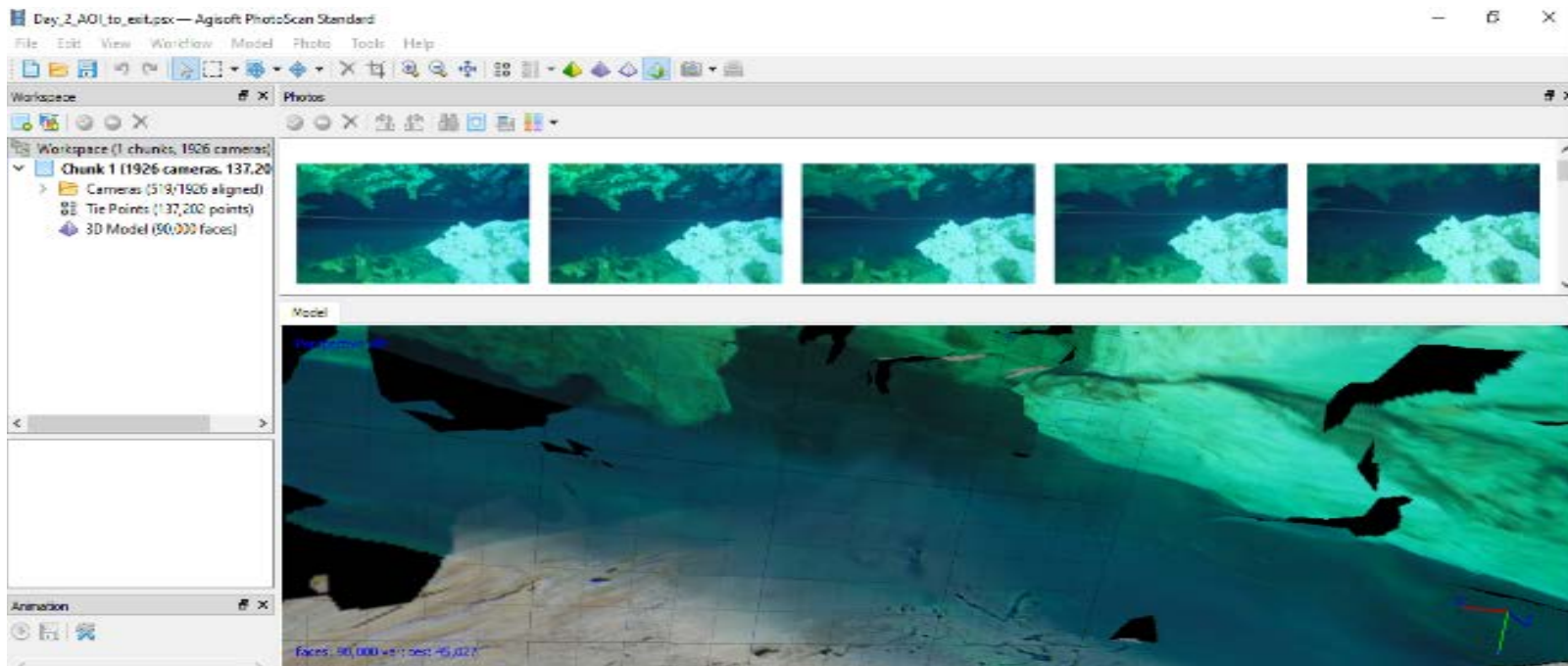


Figure 40. PhoDAR model of AOI interior from dive exit perspective with non-diffuse lighting causing voiding at shadows.



Figure 41. PhoDAR AOI interior with contrast voids causing texture mapping distortions and bending in the 3D object.

3.5.3. Equations, Weighting, & Schemes

Automated photo and point cloud alignment promotes dataset congruence. Dense cloud formation also varies from DEM to DEM with high to low quality images and depth filtering depending upon the scanning environment lighting. Figure 42 presents mesh and texture QAC in AgiSoft Photoscan. 3D reconstruction occurs via formation of a high vertex-face count which promotes scanning geometrically complex features and requires unique calibration for each model in terms of karst sites for image quality.

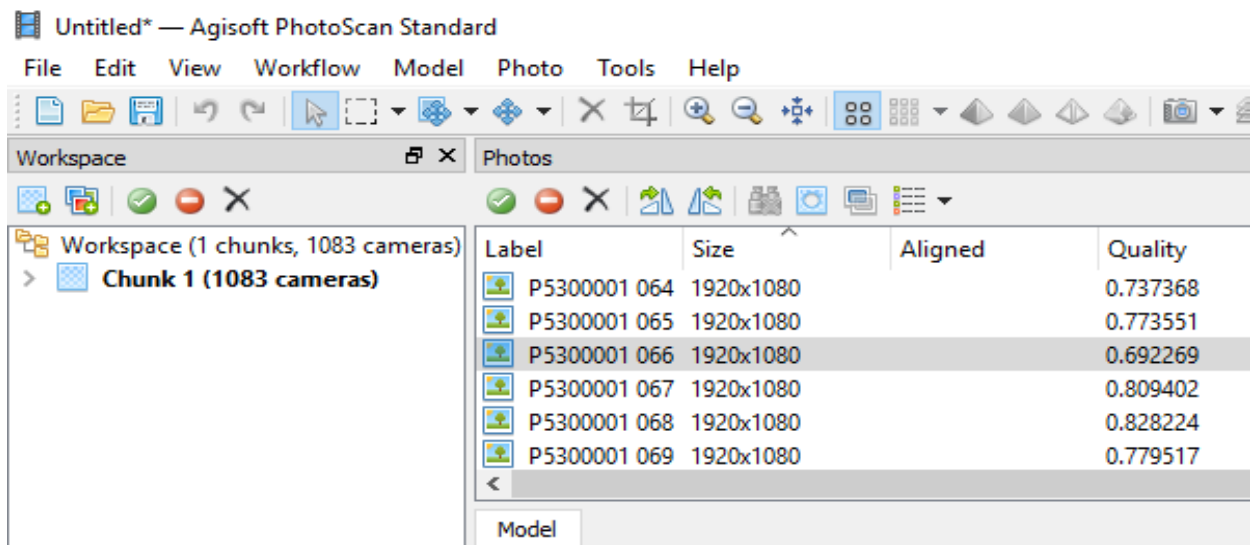


Figure 42. AOI PhoDAR image alignment for 3D Model QAC removing quality <.7.

ULS calibration prior to survey assists in contending with QTK (Larocque et al 2018). QTK occurs where the laser beams literally knot along their linear transit and over ablate the fluid instead of the FOI surface. Corrections for QTK related to harmonic principles in phononics, the use of sound in technological sensing apparatus. Lissajous harmonic curve

parametrization $x = A\sin(at + \delta), y = B \sin(bt)$, possess high triangular side length a: b ratio sensitivity. In special cases the harmonic curve produces an ellipse where a: b = 1 and a for lines when $\delta = 0$. These particular cases serve as a correction for ULS to mitigate the pulse sensor effects in the wave-spin-particle function field causing QTK in gated, isotopic threshold detection, and, unmitigated detection ungated LIBS. When $\delta = 0$ is viewed from the origin on a rotation perspective (x, y, z), (x, y) presents a (a:b) uniphasic oscillation for quantum wave-field perturbation induced vortex with lamniscate and torus mitigating vacuum space via pulse electrodynamic calibration.

This means that from a head on perspective the laser pulse seems to occur as a single point from the ULS, and from an off-set perspective the laser pulse is observed as a straight curvilinear segment at the same time. The seeming disparities of perspectives is related to differences in instants of plasma stream observation representative undulating quantum spirals, with pulsating waves and troughs that slipstream, overtake, ricochet, or interfere with one another instantaneously. This topological quantum dynamic requires indexing for ULS calibrations in cave survey scanning to identify, characterize, and mitigate imaging artifacts in point cloud datasets (Larocque et al 2018; Freire et al 2017; Sakka, T. et al 2012; NIST 2017; Portugal et al 2014).

LaGrangian trojan point vortices from relative gravitational differences may cause ULS gravitational lensing between sensor and environment for FOI detection. The Mandelbrot set function $\int_c(z) = z^2 + c$ does not diverge when iterated from $z = 0, \int_c(0), \int_c(\int_c(0))$ (Mandelbrot 1983) Sierpinski 3D analog octahedron present a fractal dimensional volume reduction of height L by $\frac{1}{2}$ per iteration towards 0, maintains constant total surface area through

the reduction series $L^2\sqrt{3}$. Initial surface area assessment (Reduction – 0), $4L^2\sqrt{3/4} = L^2\sqrt{3} = (L/2)^2\sqrt{3}$ with unlimited 1:1 surface area-volume reduction via a complex curvilinear topology matches the Hausdorff dimension of $\log(4)/\log(2) = 2$. If the ULS-200 is functioning efficiently & accurately with environmental calibration and DPO-LIBS techniques implemented an outer edge parallel projection should fill exactly fill a $L^2\sqrt{3}$ sided square. Deviations from 100% fill for the square can then be addressed for performance and enhancements for QAC related to imaging artifacts. A parallel, or line-of-sight, projection utilizes a ray diagram constrained within a uniform square to assess completeness of surface area-volume imaging.

3.5.4. Modus Operandi

Experiment Operations Plan (EOP) develops a contagious photoplethysmogram model from each individual imaging series and point cloud series overlays. Appendices I and J outline the reproducible research EOP in complete detail for future development additions and improvements. The Appendix J EOP also notes the AOI description, crew member information, operational period, purpose, logistics, contingencies, daily time table, equipment, gear management, dive plan, and daily goals for ORT SWORT reviews by the crew and interested stakeholders. Appendix M presents spatial metadata sets collected during surveys of the AOI over the past 3 years for meta-analysis of survey improvements and limitations in the future. A DTM developed from each individual survey chunk can be produce into a reliably interoperable 3DGIS format for mapping products display and eventual VRL developments.

Texture formation is a critical element in DTM production and VRL environment development benefits from the congruency of high-quality survey data collection tools and effective spatial reference metric deployment and placement near FOIs. Texture reconstruction is

time consumptive, computationally complicated, and mission critical. Survey planning utilizing the methods and procedures presented decrease survey investments and processing costs, along with increasing in dataset accuracy and long-term GDB productivity related to texture reconstruction. Appendix K geospatial DEM fractal marker accuracy promotes PhoDAR texture reconstruction productivity reducing survey reconstruction costs. Fractal-dimension optimized-scale edge detection promotes CRSI extreme environment surveys by facilitating high quality survey sampling on the first go, that also provide in image corrective references for subsequent reconstruction developments.

3.5.5. Analytic Assumptions

Development of a single DTM from each survey compared to BCA model developed from each individual survey model chunk allows for site reconstruction. The more precise, reliable model will be utilized for final product mapping virtual reality development. Texture formation is a critical element in model production and virtual environment development that derives from the congruency of survey data. Karst exploration and mapping can only occur where access to the subterranean cavity or aquifer is human sized, .5m x .5m and larger. The few cave maps in existence provide a series of information on known caves and surveyed conduit networks. Explorations provide evidence for dataset conversion in several forms but are limited based on space, distance, and equipment limitations. Preliminary photogrammetric full cave modeling processing requires several weeks of data organization, coding, processing, development, refinement, and formatting. The process is trial-error, and final product creation is non-linear. It must contend with TPU in data collection and visualization inaccuracies due to numerous factors including but not limited to RS selection, QTK, FOIs, environmental dynamics, and surveyor ergonomics via GIST analog PSTAR operations for refences production.

Chapter 4 Results

ULS represents a dynamic shift in underwater cave mapping technologies, the methods presented prompt rapid deployment, collection, assessment, and modeling of extreme environments in record time on multiple scales of scientific interest for planetary sciences field surveys (Fortes et al 2013; Mandelbrot 1983; Feng et al 2017). Concurrent CRSI data collection conducted by cave diver survey overcomes traditional obstacles preventing >5 BRCA mapping grades. Thesis objectives included ULS phreatic cave survey, GBD development, data coding, dataset processing, imaging artifact identification, model calibration indexing, 3D GIS map construction, and discussion of GIST and PSTAR research intersections with VRL simulators for CRSI field survey. The project outcomes and products include 3D site tour animations, identified imaging artifacts, high accuracy phreatic cave data, a hand drawn informal photonic quasicrystal orbifold, and semiformal photonic quasicrystal- moduli fields of vacua QCED LiDAR and PhoDAR indicatrix for optics assessments that requires conversion into a detailed interactive .svg index.

ULS cave survey corresponds to the fidelity objectives of NASA PSTAR for comparative capabilities assessment, Figures 1 through 3. ULS cave surveys serve to produce novel datasets of numerous unobserved phenomena in various fields of science from exotic and remote environments (Alvey et al 2010; Pořízka et al 2012). As analogs for planetary sciences research ULS deployment incorporates numerous aspects of GIST and PSTAR concerns in terms of remote sensing technique development, CRM procedural training, equipment evaluation, PPDE, and mission readiness from exploratory cave diving and survey. These technological and methodological developments benefit geoh heritage preservation, evolutionary biology, cave rescue, urban planning, PSTAR comparatives, and quantum non-linear optics field research

(Hunsaker 2001; Orosei et al 2018; Domagal-Goldman et al. 2011). PSTAR ULS ORTs allow for SWORT PETRs to be delineated that can be referenced from underwater caves and terrestrial contexts onto extraterrestrial environments and astronautic planning for continued technological innovation, crew vigilance, and mission architecture improvements

CRSI speleonator and astronaut suborbital PSTAR surveys present possibilities to experimentally develop RS techniques, tools, and procedures for various *in situ* scientific applications, domains, and environments (Federal Grant: NASA ROSES PSTAR 2018; Boston et al 2008; Vakoch 2014). Both subaquatic cave and suborbital environments possess novel analogous structures for survey, with similar methodological needs for field CRSI operations, especially in LSS and planning for emergency or environmental contingencies (Charles 2013; Neufeld and Charles 2015). CRSI is deficient in methods of specific entropy calculation in pulse detection due to lack of detailed research and calibration for QB, TPU, and other errors in underwater ULS LiDAR survey (Hod 2011; Sakka et al. 2012; Law & Rennie 2015; Larocque et al 2018; Freire et al 2017; Takeuchi 2015; redata.org 2014). CRSI arrays being to surmount wave-particle complementarity dualities, promote data congruency, reduce survey risk and time, and enhance collection sensitivity of exotic and novel datasets from Earth proxy ETE survey simulations (Vassiliou, M.S. 2007; Jones & Christal 2002; Denson, T. J. 2016; 2015; Anita et al 2013).

4.1. Methods Evaluation

The research methods and fieldwork proactively and reactively respond to Murphy's Law, what can go wrong will go wrong, and promoted survey safety, efficiency, and effectiveness. Successful nanometric (nm) accuracy (0.7 - to .05mm) sampling was conducted via LASMIS RASP CRSI data collection and benefited from pre-survey calibration for PSTAR

PLEOP SWORT ORT modeling. Preliminary test scans and debriefing over three days on land provided experiences in crew development with training datasets, equipment preparation, risk identification, safety concerns, and logistic responses. Debriefs and mission architecture defined mission success and safe working conditions requirements with considerations on ULS pulse power, ULS step rotation size, LSS risk and range limits, operational obstacles, environmental hazards, equipment restrictions, and other survey crew resource management needs.

The methods presented extend LiDAR field survey techniques and provide benefits and induce limitations in various ways that inform PSTAR and cave field research dynamics. They serve as a comparative parallel for future PSTAR considerations in planetary science, RS, and mission architecture development. The mitigate microgravity through sidemount

cave diving CRM and overcome LSS obstacle with redundant rebreathing systems.

These methods parallel planetary sciences field survey concepts and provide SWORT ORT assessment parallels.

ULS survey represents a marked progression in cave site measurement and improved crew safety via reduction of task loading, equipment requirements, and survey inaccuracy. Preliminary survey assessments promoted underwater analog success with system preparation, scan calibration. A simulated aphotic ULS test in a surface sinkhole opening at night promoted supervised imaging characterization with references. Figure 43 depicts a photograph of ULS-200 preparation with weighting and system fastening with fractal markers on bookshelf, second shelf from the top, being scanned in Under the Jungle dive shop for presurvey calibration assessments. Figure 44 presents a photo from day 1 of Sistema Taj Mahal, Cenote Taj Mahal Surface Survey with QRSS surveyor Rory OKeefe collecting data with a modified Lecia laser distance and ranging system at night from Cenote Taj Mahal to Cenote Sugarbowl for preliminary automated

3D site modeling overnight. Mission planning provided GLONASS GPS positioning of the sites along with a modified Lecia Geosystem laser range finder, compass, and declination calculator of each of the surface sections, and the datasets were recorded by hand and then added to the 3D GIS after fieldwork.



Figure 43. ULS-200 Preparation with fractal markers on bookshelf, second shelf from the top. Fractal marker ULS scan test on bookshelf in Under the Jungle dive shop classroom.



Figure 44. Sistema Taj Mahal, Cenote Taj Mahal Surface Survey, Rory collecting 140m of linear laser distance and ranging AND GLONASS GPS data from Cenote Taj Mahal to Cenote Sugarbowl.

Mangrove, Sugarbowl, Taj Mahal, and Sagrado Cenotes of Taj Mahal cave system occur Northwest to Southeast with $\approx 100\text{m}$ separating each doline, the cenotes are several km from the highway and coast. Figure 45 depicts the survey field camp daily setup in the for each ULS scan, hazards of note included fall-hazards, hurricanes, *Bothrops asper* (fer-de-lance), *Panthera onca* (Jaguar), and *Metopium brownei* (*Chechen* in Mayan, aka. Black poisonwood). Figure 46 presents GIST project RS mission planning for optimal global positioning satellite (GPS) connection for spatial data QAC. The sites were accessed on foot and scanned within 4 hours each. After the two-night scans, three days of survey were organized out of Cenotes Taj Mahal and Sugarbowl.



Figure 45. Sistema Taj Mahal, Cenote Sugarbowl, Field Camp.



Figure 46. Sistema Taj Mahal, Cenote Sugarbowl GPS Collection

Equipment abseiled from 6m above, down to the team at the beginning and up at the end of survey in Sugarbowl, reduce equipment loading and deter negative environmental impacts. Figure 47 highlights the climb into Cenote Mangrove representing the dive teams need to utilize a safe watertable access points in Cenote Taj Mahal, as well as diver propulsion vehicles (DPV) to reach the Cenote Sugarbowl staging area.



Figure 47. Cenote Mangrove survey with Fausto Tun-Chx of Valladolid, Mexico standing on a broken staircase providing entry to the watertable.

Subterranean collection covered 50m of linear passage on a bearing Nm 175° from the open water of Cenote Sugar Bowl (N 20.48408° W 87.27804°) at -7 m depth to the Deep Bone Room at -27 m depth. 5 m diameter cross sections with an average of 500 points per line per 4 m line segment were collected throughout the system producing a real-time 2,000m³ cave photoplethysmogram. The Cloudcompare processing log with AgiSoft imported 3D .obj overlays on the ULS point cloud is presented in Appendix O.

The most distantly detected points extended to a maximum range of 25m in the sun exposed open water of Cenote Sugar bowl, with the most proximate points recorded at a distance of <math><0.015\text{ mm}</math> for each day in saltwater and freshwater sections, halocline induced sensor noise and clouded the point cloud with birefringent reflections and optic distortions. The cave system showed variation in pH on a basic range of 7.2 to 8 from fresh to salt water and a relatively stable water hardness of 23-24 grain, 40ppm. Figure 48 presents Taylor water quality testing kit instructions, field, notes, and site sketches created daily due to lack of Wi-Fi and a power outage to prevent digital dataset loss. No other contaminants were present that may deter potability in the freshwater for this system.

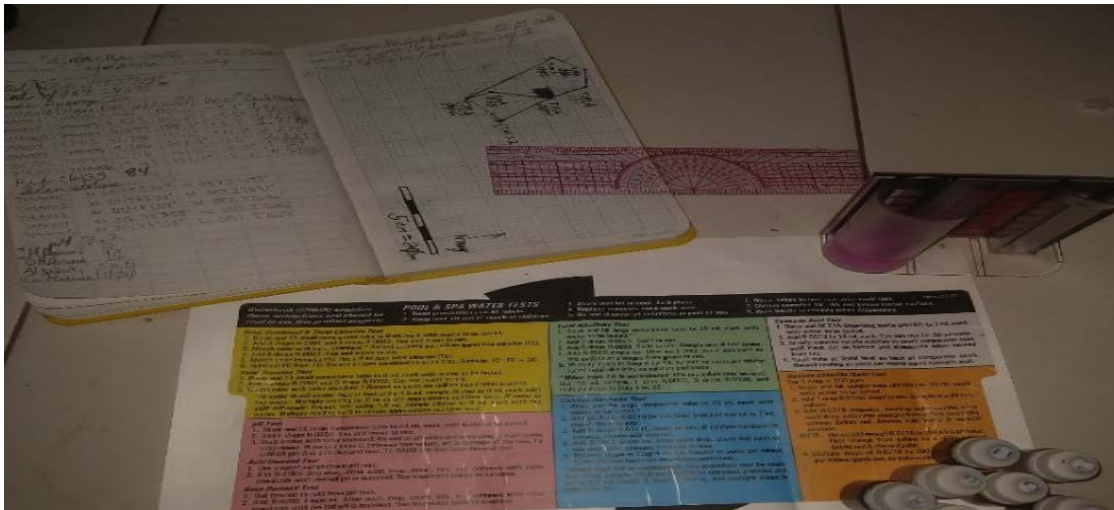


Figure 48. Taylor water quality testing kit instructions, field, notes, and site sketch.

The saltwater test produced null results for microbial contaminants and require resampling. Figure 49 shows dive crew Marceline Nebenhaus (Blue helmet) and Natalie Gibbs (White helmet) preparing abseiled equipment in Cenote Sugarbowl and discuss mission plan prior to survey. Water quality testing instructions govern diver EQ sampling mission architecture

requirements to include longer passages of halocline survey, and to allow access to the site by other dive teams. Figure 50 depicts Marceline deploying ULS-200 in for scanning, optical distortions due to halocline. Figure 48 through 50 represent the transition from traditional analog cave survey equipment to new digital technologies with extensions for future research applications in GIST RS and robotics. Photoplethysmogram LiDAR datasets were obtained with accompanying water quality samples and result in improvements to ULS calibrations for future deployments in cave surveys with LiDAR indexing.



Figure 49. Dive crew Marceline Nebenhaus (Blue helmet) and Natalie Gibbs (White helmet) prepare abseiled equipment in openwater and discuss mission plan prior to survey.



Figure 50. Marceline Nebenhaus preparing to collect scanner with buoyant light providing area illumination for transect scanning. optical distortions due to halocline.

Figures 51 and 65 presents past obstacles that ULS 3D Disconnected-reconnected-outtrigger network transects for cave diving survey responds to restrictions and obstacles preventing >3BCRA grade survey allowing teams to adapt the survey plan to accommodate various forms of unanticipated karst restrictions, sizes, superstructures, and FOIs that may have impeded prior surveys. Figures 52 represents a vertical down surface surveyor perspective of the ULS point cloud datasets from scans of the Cenote Sugarbowl staging area. Figures 52 and 53 presents the ULS stratigraphic cross-sections of Cenote Sugarbowl. ULS produce and profile a Kd-tree cave collapse fracture maps along 10cm cross-section extracts. Figure 53 presents draperies scanned from Figure 52 for future system paleoclimate dissolution modeling estimates.



Figure 51. Cenote Sugarbowl, ground support field camp, and 6m rope-ladder to watertable.

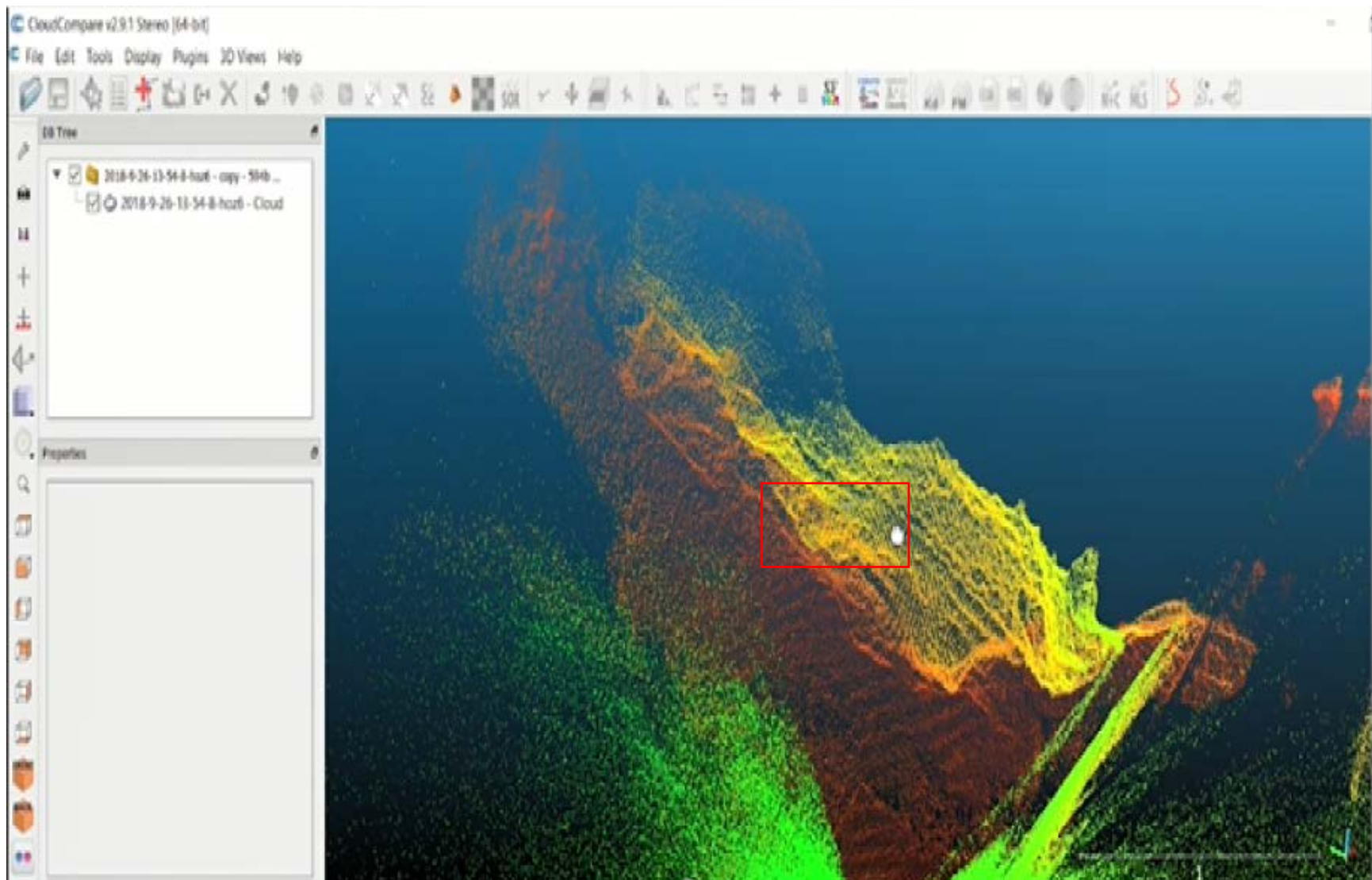


Figure 52. Lidar point cloud of hydrogeological stratigraphy at 1m resolution scan accuracy with stalactite and drapery features in the red box, presented in finer resolution in figure 53.

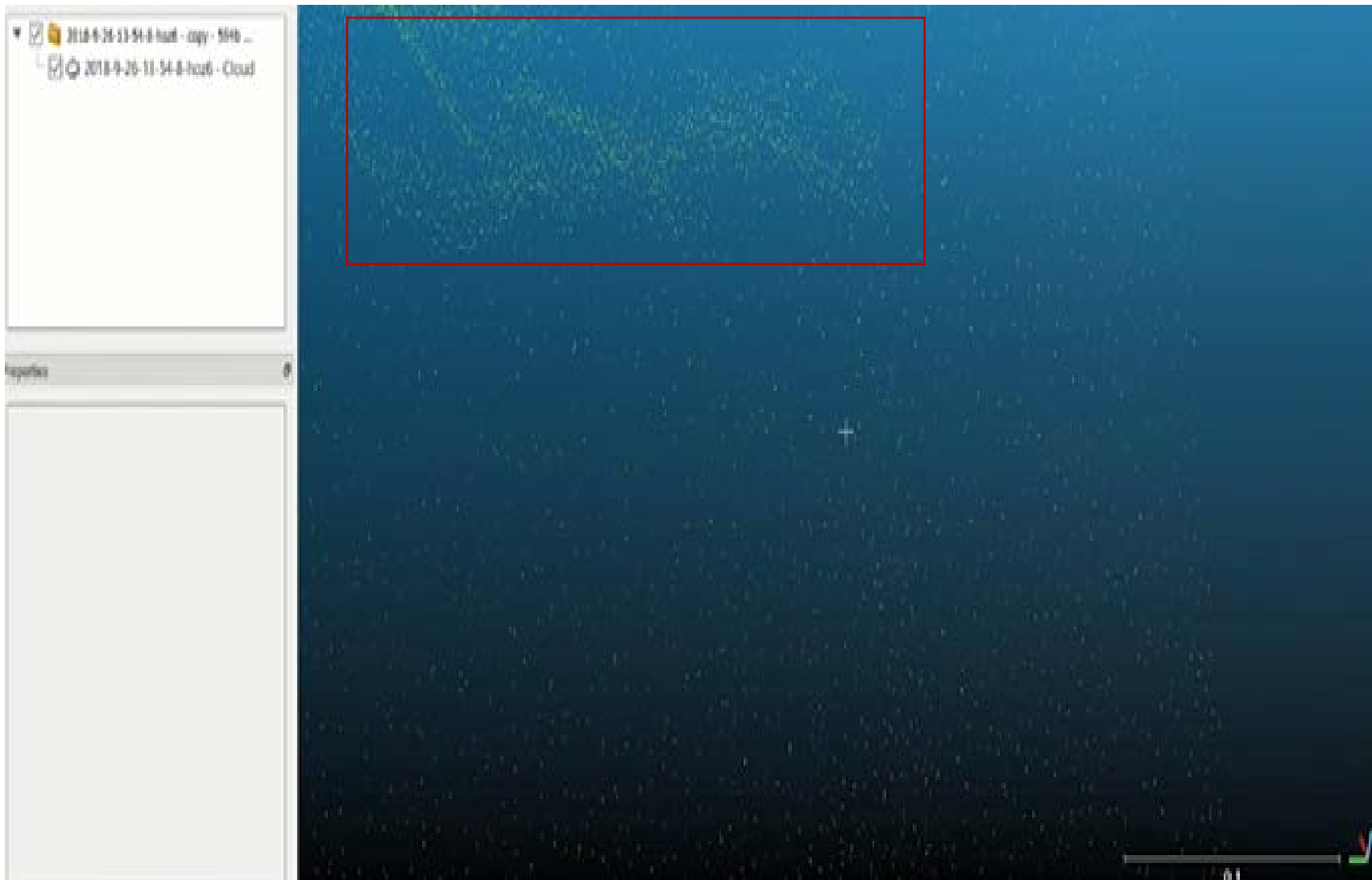


Figure 53. Lidar point cloud of stalagmites and flowstone draperies in the upper right in the red box at 0.1m scan resolution from above in figure 52.

The methods developed within this research promoted two separate, two-person dive teams to conduct a simultaneous laser, video, and water quality survey in a rapidly effective manner with minor debriefing over one evening. One surface support crew member acting as supervisor fired the laser and abseiled equipment to and from the divers. Communication was maintained via predefined cave-diving procedures for hand and light signaling and extended to use of visual communication between the surface and subsurface teams for safety and synergy (Carney et al 2013; Bowens 2009; NOAA and Joiner 2001). Crew and Individual (CIRM) reliant redundant LSS, diver propulsion vehicles (DPVs), and sidemount scuba training were able to conduct the surveys with minor difficulties extending from fiberoptic cable management underwater. Figures 54 and 55 present CIRM synchronization methods between surface and subsurface members to promote efficiency, as well as reduce inaccuracies and risks by predefined H-R C⁵I², dive plan timing, ULS positioning, and survey markers placement for site imaging reconstruction references. These methods are reproducible when conducted by an experienced cave diving team with training in underwater research, cave exploration, crew resource management and survey dataset collection. Safety, communication, and accuracy concerns between RS operators and dive crews are directly reduced via adaptive procedures.



Figure 54. Diver 1 survey V&V of North with contrast fractal marker & wrist compass for GSE crew reference.



Figure 55. Final Frontier Design IVA suit technician Van Wampler & Astronaut-Scientist Sean Thompson LSS & communications V&V for PoSSUM Project PMC tomography simulation.

GIST and communication systems parallels are as mission critical as LSS for CRSI field surveys in cave diving as they are for astronautics. Figure 71 Communications systems reflective of astronautics radios in ULS cave diving allow for off-nominal conditions communication to be transmitted. Speleonator CIRM utilizes hand and light signals, as well as written notes for communication between members while surveying. Lasers stand to serve speleonators as long-range subaquatic communications devices.

The laser provides communication between mission control and survey crews via laser pulsing in sequences of 3 pulses, in asynchronous firing, or Morris code to modify or discontinue operations. Synergistic mission planning for surveying from the farthest cave section to the open water allows for dives of 60min on 3 tanks of 32% Nitrox with little to no decompression requirements incurred by crew members and >1/3 of their remaining breathing gases remaining for emergency exit, crew member out of air emergency crisis, equipment failure, or loss crew member search and rescue related to Appendix L.

The preliminary setup timing of 10-15 min deployment phases, followed by 5 min horizontal scans, 2 min resets, 5 min vertical scans, and a 5 min swim reset in-between repositioning were safe, efficient, and effective for data collection. Figure 56 and 57 present PhoDAR DEM of Diver One AOI scans. The AOI was marked at the North with the contrast cube and RGB cubes against the highest contrasting color in the scan area. The ULS mounted on the weighted tripod, ensured stability, and detected the deployed fractal cubes.

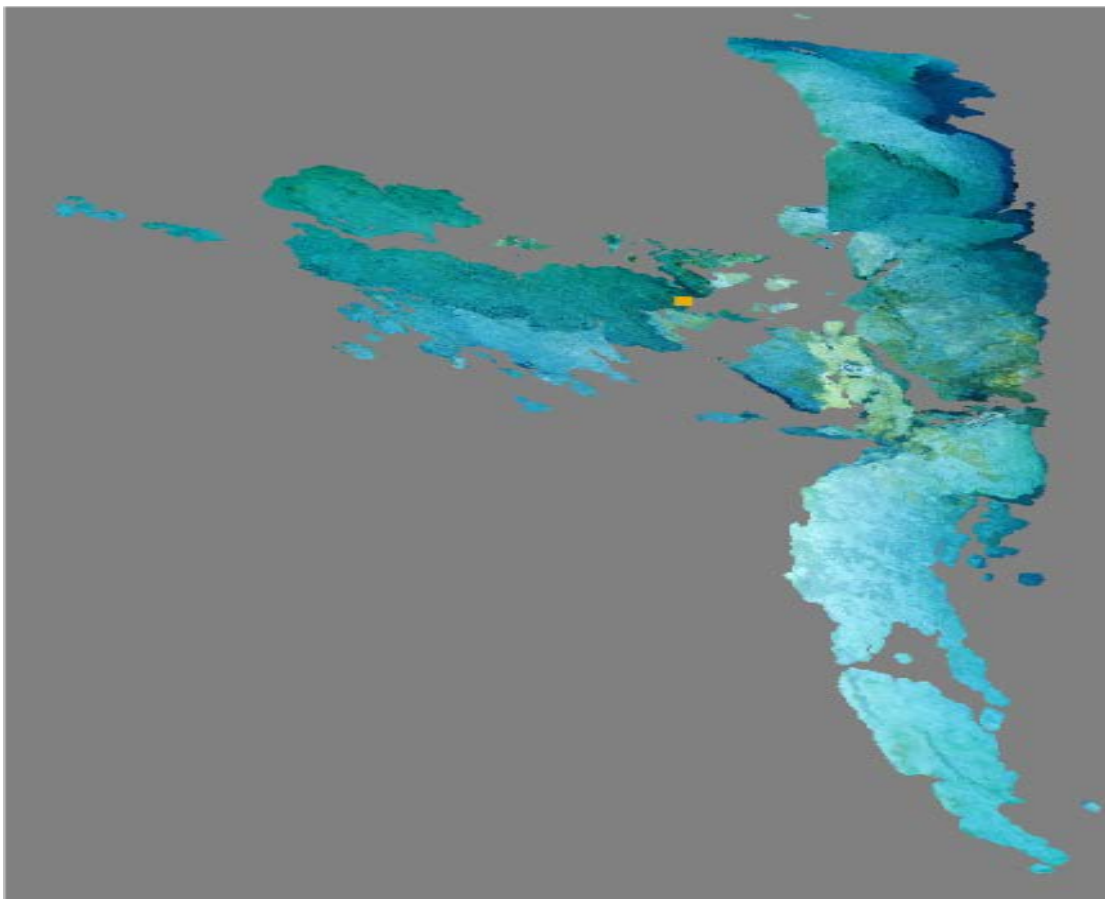


Figure 56. Photogrammetric model of the Deep Bone Room Entrance Restriction.

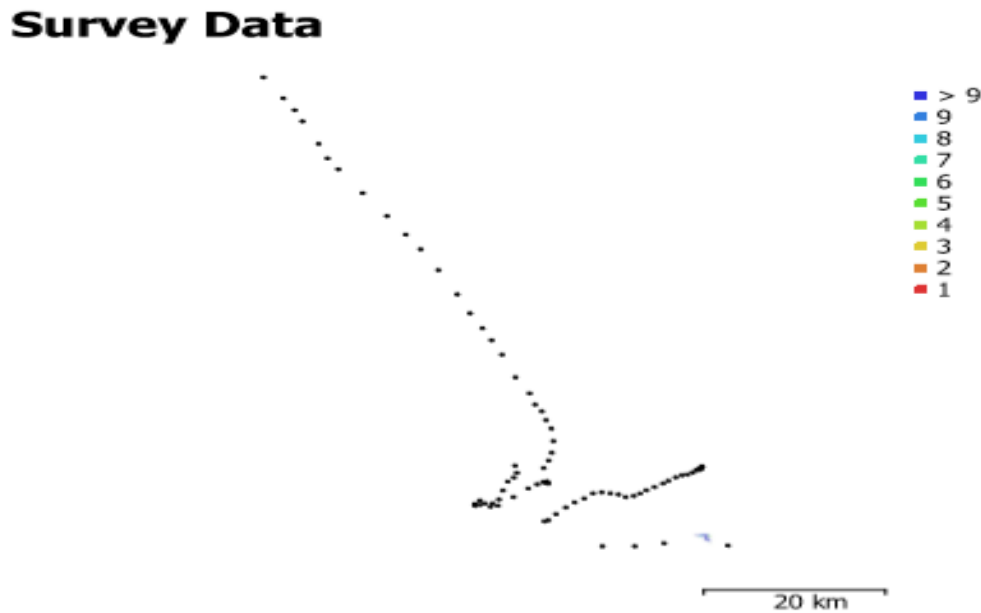


Figure 57. Extracted digital elevation model from figure 72 of AOI from inside the Deep Bone room, up the restriction, and along the corridor from left to right.

Diver two deployed the fiberoptic cable, collected video evidence, and water quality samples while keeping wet-notes on depth, temperature, and time. Prior crew training in cave diving and cave conservation etiquette allowed for coherent communication of environmental conditions, crew concern, and survey requirements related to cave protection. Training in zero-visibility remote sensing survey, peak performance buoyancy, and cave etiquette standards all promoted minimal impact on the site relative to dataset collection analogous to PPDE.

Methods with training of future survey crews for speleology and astronautics for hydrogeological and biological research related to EVA lifeline concerns, planetary protection etiquette, microgravity training, microorganismal laser impact mitigation related to lowest effective mJ for sensing, and exploratory exoplanetary sciences survey benefits and risk reduction via the CRSI survey skill sets presented via peak performance buoyancy and cave etiquette training. Silt storms were prevented, minor ceiling percolation occurred from diver

induced turbulence. These methods intended to observe natural and anthropogenic halocline disruption as it is unavoidable during survey intersections and induce novel imaging distortions.

These distortions are relative to fluctuation of the diver's position in the water column as they are breathing and floating up and down. The divers motion produces a vibratory pattern of the diver's relative position within ULS point clouds. Density and temperature difference of the fluid admixtures produced refringent patterns, natural light produced spiraling helixes in open water and fill cave surveys. ULS induced PQV QTK occurred as anticipated. Trimetric fractal marbles promote sensor evaluation and allow for *in situ*, on-the-fly corrections for measurement of unanticipated novel datasets by surface based remote sensing operators, and do not burden cave crews with excessive measuring tools.

The communication, and imaging corrections, coupled with trained scientific survey teams provide detailed digital and physical evidence sampling records. Figure 58 PMC mission plan for operations synchronization, science objectives, and safety notes for contingencies related to main engine cutoff (MECO), free-fall RS sampling windows, G-force awareness, no-stall-glide knots indicated air speed (KIAS), and safe landing window 50 nautical miles downrange at Eielson Airforce Base (Reimuller et al 2015). Mission planning for PSTAR operations benefit from GIST integration and cave diving field survey techniques paralleled in extraterrestrial EVA planning, communications, timing, operations, equipment, and microgravity RS procedures during risk inductive research. Figures 58 through 60 presents the Project PoSSUM suborbital spaceflight simulator and flight data for focused CIRM development, ETE CIRMSS, and contingency response for science objectives. These suborbital science operations and simulators that parallel PSTAR cave diving surveys mission planning and needs related to survey windows of access related to LSS, environmental conditions, and synchronization.

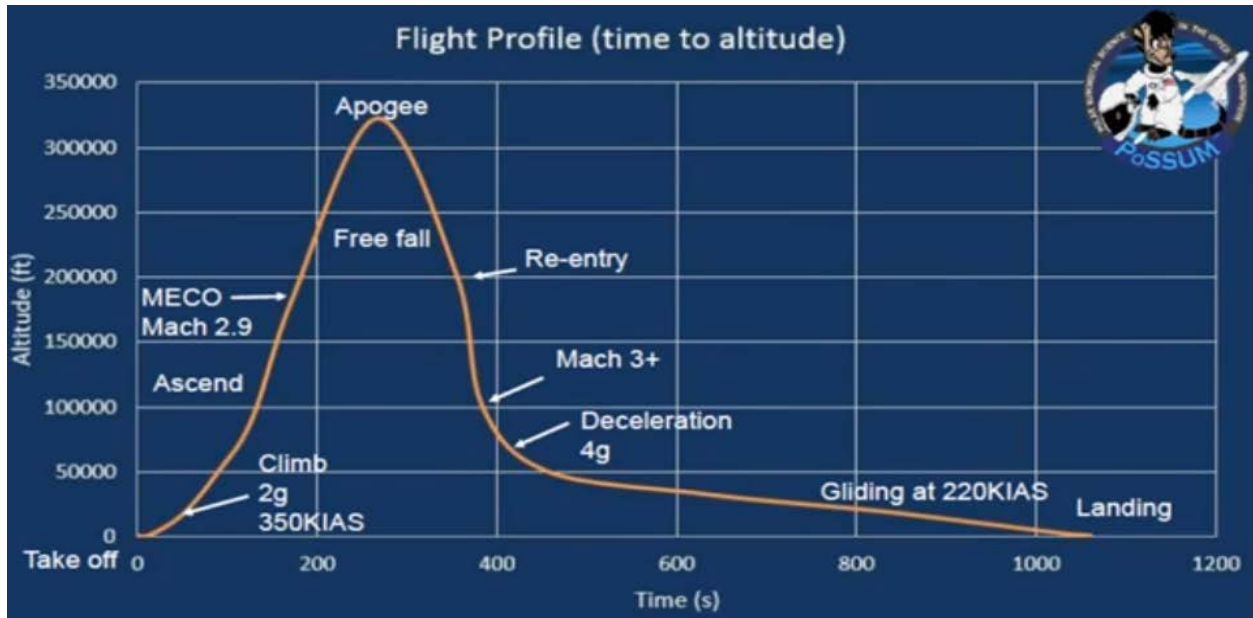


Figure 58. Project PoSSUM PMC tomography mission plan for flight operations synchronization (Reimuller et al 2015).



Figure 59. Photograph of the Project PoSSUM Astronaut-Scientist PMC simulation cockpit data recorder flight statistics, mission planning, & crew acclimation for suborbital mission operations.

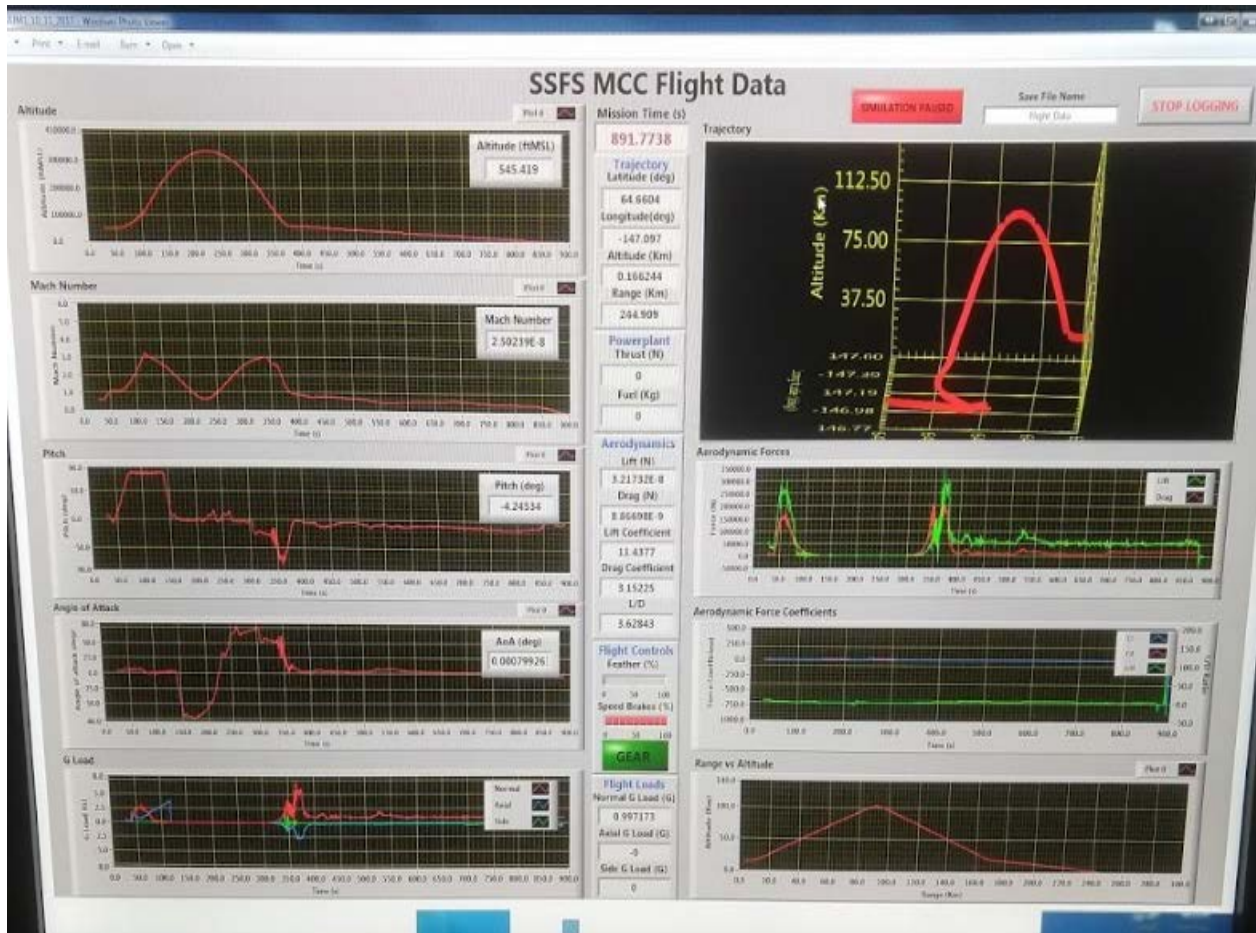


Figure 60. Photograph of the Lynx Cor or Virgin Galactic spacecraft simulated flight data for operational evaluations and developments.

The number of images collected, CRSI-station alignment, CRSI altitude, tie point number, ground resolution, coverage area, and reprojection error all impact survey data. These methods benefit from methodological GIST field techniques in planetary sciences. As images referenced along the survey line, at perpendicular 5m marks, and via modified 3D disconnected-reconnected outrigger survey these methods surpass prior survey and mapping errors by providing means to correlate CRSI array cinematic, photographic, volumetric, molecular, and spectrometric datasets for rapid, accurate 3D and VR modeling. Error estimates, fractal dimension analyses, and spectrometric verification completed via *in situ* trimetric marker FOI

assessment promote rapid 3D karst survey and modeling, overcoming prior research survey limitations and geohazards. These allow for geometrically complex natural FOIs to be directly assessed for RGB color scales as well as geospatial point cloud collection accuracy and geovisual precision. These also provide novel collection of halocline cross-sections for assessment of interface dissolution in caves. These datasets can be utilized to create high detail, high accuracy map products for numerous applications in VRL simulators, 3D mapping, and 3D printing for astronautics applications in education, research, and survival (NMAI. 2017; VRARA. 2018; UNESCO 2002; National Park Service, 2017; Virrantaus et al 2009).

The systems and methods utilized represent analogous needs and responses in terms of remote sensing survey, LSS equipment, microgravity etiquette, pressure emergency, G-force stress, breathing gas toxicity symptoms, and blood chemistry fluid dynamics for discussion in relation to training courses for scientist astronauts and speleonauts. Figure 61 through 66 present simulation and LSS system materials as the promote direct PSTAR analog assessments in cave diving and astronautics. Primary concerns for management of LSS supersede all other mission parameters in PSTAR analogs and cave diving which require ample training and evaluations to prepare for and contend with them efficiently and effectively. Figure 61 is a photograph of an EA300 two-seat aerobatic monoplane capable of G-force simulations for physiological reflex response training. Simulations in G-force stress awareness and mitigation techniques promote PSTAR analog education and RS mission success in research operations (Reimuller et al 2015). Figure 62 presents a cockpit camera operated by the author to take an image of the pilot and copilot, upside down at +4 G-force in an inverted loop headed into a microgravity chandelle stall, while upside down in high g-force blood pools into the ocular cavity causing a visual synesthesia

as a color grey out. A chandelle is a steep climbing turn executed in an aircraft to gain height while changing the direction of flight.



Figure 61. Patty Wagstaff Aerobatics Flight School Extra Flugzeugbau EA300.



Figure 62. Author & pilot Jeff Rochelle, background, simulating psychosomatic stress mitigation in a PMC 5 to 0 G-force loop, author's eyes bearing G-force sclera distortions causing grey-out.

These simulations promote spatial awareness and physiological limitation of the body during RS PSTAR analogs related to vision grey outs, microgravity, g-stress, limb immobility, and cardiac hypertension. Figure 63 is a photograph of cave LSS sidemount rebreather systems which utilized carbon-dioxide scrubbing salts to allow divers to recycle their lung volume with mixtures of oxygen, nitrogen, and helium to off-set effects of hyperbaric water pressure on the body while surveying or exploring. PSTAR analogs and GIST all benefit from immersive 3D

and VR simulations for preparedness training and contingency response reflexes in RS. Figure 64 presents Embry-Riddle University VRL Director instructing Astronaut-Scientist Tatsunari Tomiyama in use of HTC Vive International Space Station simulation (ISS) for acclimation and prevention of VRV synesthesia sickness. CRSI data collection and mission success stem from LSS functionality, effective communication, and procedural assessments of equipment, crew psycho-physiological conditioning, navigation tools, and safety procedures reiterated in simulations and pre-mission, intra-mission, and post-mission debriefs.



Figure 63. Redundant sidemount cave diving LSS rebreathers for underwater RS survey.



Figure 64. Embry-Riddle University VRL director Zach instructing Astronaut-Scientist Tatsunari Tomiyama in HTC Vive ISS simulation for VRV prevention.

Synchronicity, crew experience, equipment planning, and debriefing directly overcome communication black outs between surface support and survey teams during remote sensing operations in cave diving and astronautics. Planning on timing, sensor placement, contingency response, and communication methods via land survey training and debriefings promote successful missions via proactive CIRMSS. Improvised cave diving contingency procedures deter ineffective survey between surface support and survey crews allowing for on-the-fly survey stops, changes, touch ups, and contingency responses for inclement weather patterns and other potentially hazardous scenarios.

Simulations on land, in virtual reality, and underwater provide training extensions for cave surveys to improve standards, safety, and technique in cave diving and astronautics microgravity mission planning. Simulations provide realistic, immersive exercises for crew resource management and development in numerous settings and for various field applications. Figure 65 is a photograph of a data recorder for an extended Federal Aviation Administration (FAA) scientist-astronaut hypoxia certification simulation in the Southern AeroMedical Institute hypobaric chamber. Simulations allow crews to grow accustomed and acclimated to environmental conditions, mission stressors, equipment operations, operations dynamics, and communication structure. Figure 66 presents medical personnel directing and monitoring scientist-astronaut biometric conditions for individual symptoms onset during hypoxia simulation at 80% oxygen, the staff also act as air traffic controllers and direct the students in maintaining their flight paths. Dr. Paul Buza assessing CIRMSS hypoxia symptoms awareness & response. Simulators allow crews to develop responsive motor reflexes in terms of G-force, microgravity, and high turbulence data collection settings which promotes mission success and crew safety and related to underwater cave surveys and PSTAR analog ETE data collection.



Figure 65. Astronaut-Scientist Merit Bibawy wearing an oxygen mask under hypoxic conditions simulating pilot perspective of cockpit instruments & operations control (Lamaison 2018).



Figure 66. PoSSUM Astronaut-Scientists Merit Bibawy, Lycourgos Manolopoulos, & Bethany Downer CIRMSS hypoxia simulation in the Southern AeroMedical Institute. (Lamaison 2018).

Turbulent, loud, high flow, high pressure, hypothermic, hypoxic, hyperoxic, microgravity, negative buoyancy, and low visibility all impact operator error and the available tools and techniques to image macroscopic or microscopic phenomena rapidly and efficiently by hand or craft with RS. Fractal markers improve scans while maintaining or improving mission safety parameters for dataset collection, 3D modeling, and mapping. Figures 68 through 70 present 3D GIS and VR preliminary developments. Figure 68 depicts the ESRI City Engine for regional cadastral context extraction for VR development. Figure 69 displays the ArcGIS Pro 3D regional karst scene with z-value enabled synthetic streams presenting host polylines for future point cloud spatial joins which correlate with known cave systems, color saturation and polyline weight which represent symbolized stream order number from 4, headwaters, to 1, a major stem. IceSat LiDAR data for winter jungle canopy were utilized to correlate stream order 1 to areas of dense winter vegetation for assessment of near surface caves with water access for development of future ULS cave datasets for research, education, and international stakeholders (Stafford et al 2017; Denton et al 2016). Figure 70 presents the extracted regional City engine scene with local infrastructure enabled as a VRL basemap for 3D GIS imports.

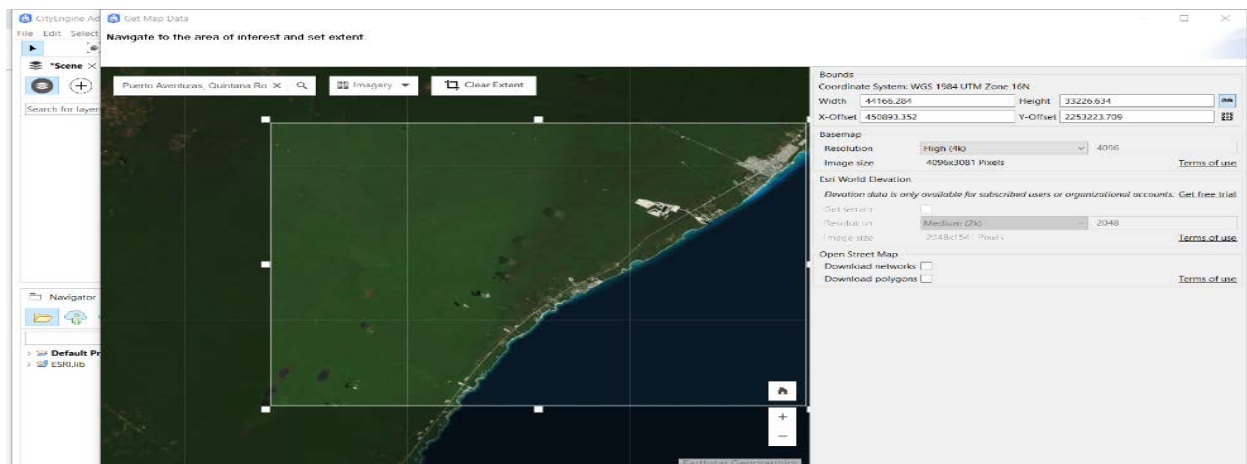


Figure 68. Esri, City Engine regional contextual extraction for map development.

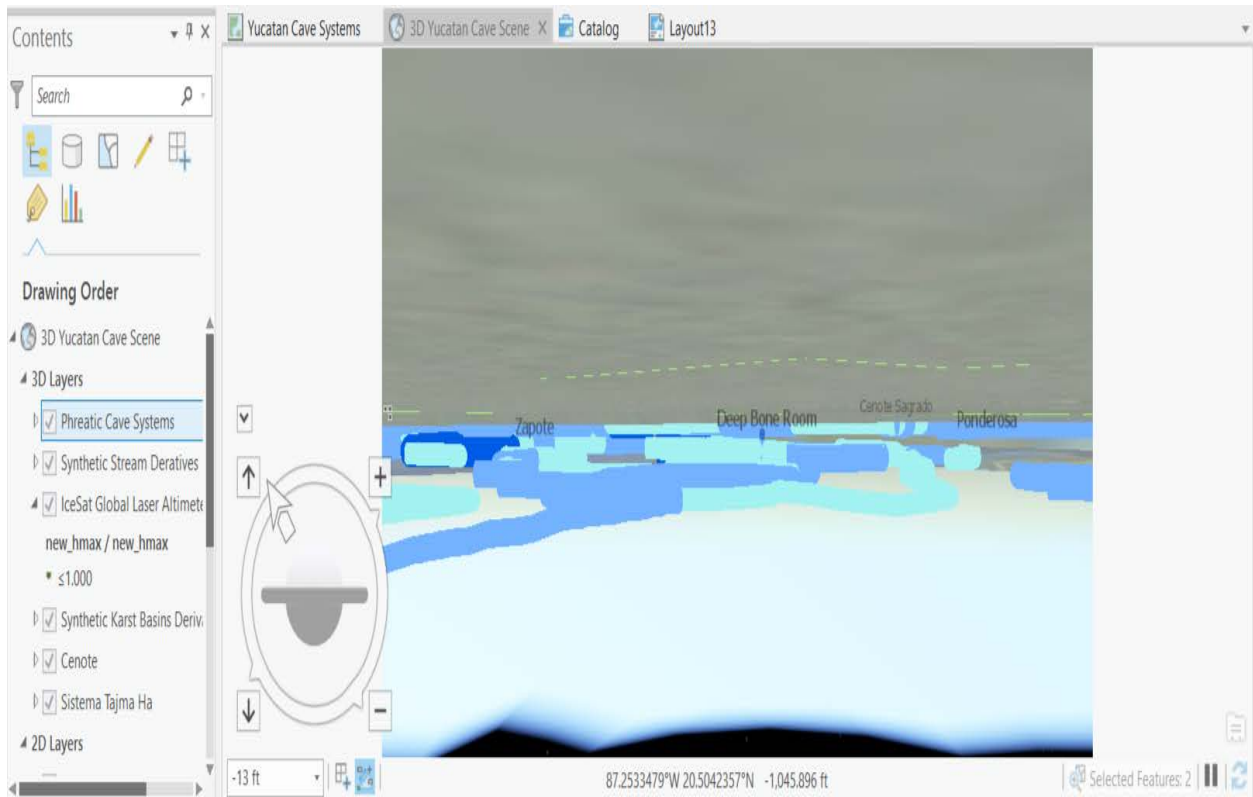


Figure 69. ArcGIS Pro regional scene with STRM-LVL2 synthetic streams converted to 3D tubes and submerged into the landscape for point cloud integration.

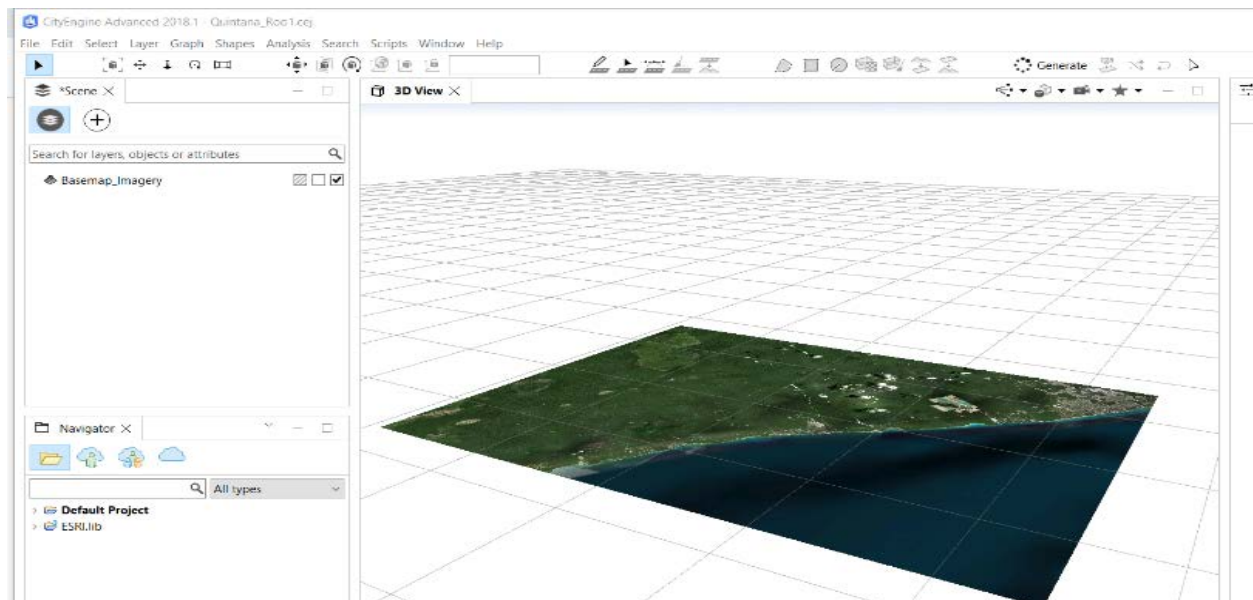


Figure 70. Esri, City Engine regional extraction for ULS point cloud integration of Sistema Tajma Hal related to infrastructure and existing VR cadastral datasets.

CRSI array datasets provided high QAC quality geospatial information on the caves, as well as the surface sites although the ULS was not calibrated for the refraction index of air and produced imaging errors on land. Calibrated datasets were inspected within 2G Robotics ULScanViewer and CloudCompare programs. Figure 71 displays distance measurements of fluid turbulence generated by ULS-200 rotational spin on point cloud during collection. Potential ULS search and rescue scanning presented with anatomical planes extracted from the surveyor mid-scan was extracted from data of Cenote Sagrado's openwater area in Figure 72. Figure 73 depicts AOI horizontal cross-section with reference height, width, wall, and divers lengths represented with arrows. ULS measurements extended from an omni-angular quantum quasicrystal singularity at the intersections of height and width planes related to the deployed ULS centroid to complete a $< .15\text{cm}$ radius scan. Figure 74 shows two horizontal and 2 vertical stitched cross-sections of openwater of Cenote Sugarbowl used to create the stratigraphic profile and animations. ULS-200 non-linear optics Gaussian extracted raw data noise and distortions in Cenote Sugarbowl are presented Figure 75. Figure 76 represents semi-supervised image classification for fracture, distortion, and either-or classification of fracture and turbulence detection of Gaussian extracted Kd-tree planes in geohazards, fluid dynamics, and QCED for model corrections. Figure 77 shows Kd-tree facet classification structure for detection on a PPL/Kd-tree normalized difference index (NDI) representing geohazard sections with more mass and density on external dissolution-cleavage edge. Figure 78 provides referential supervision for image processing as a rope ladder imaging artifact identification, scale estimates, and QAC. Figure 79 displays ULS dataset extractions that represent fractures or distortions requiring

supervision for clarification and classification related to PQV, KHI, and HSF. Figure 71 through 79 serve as reference material for ULS classification and optics calibration improvements.

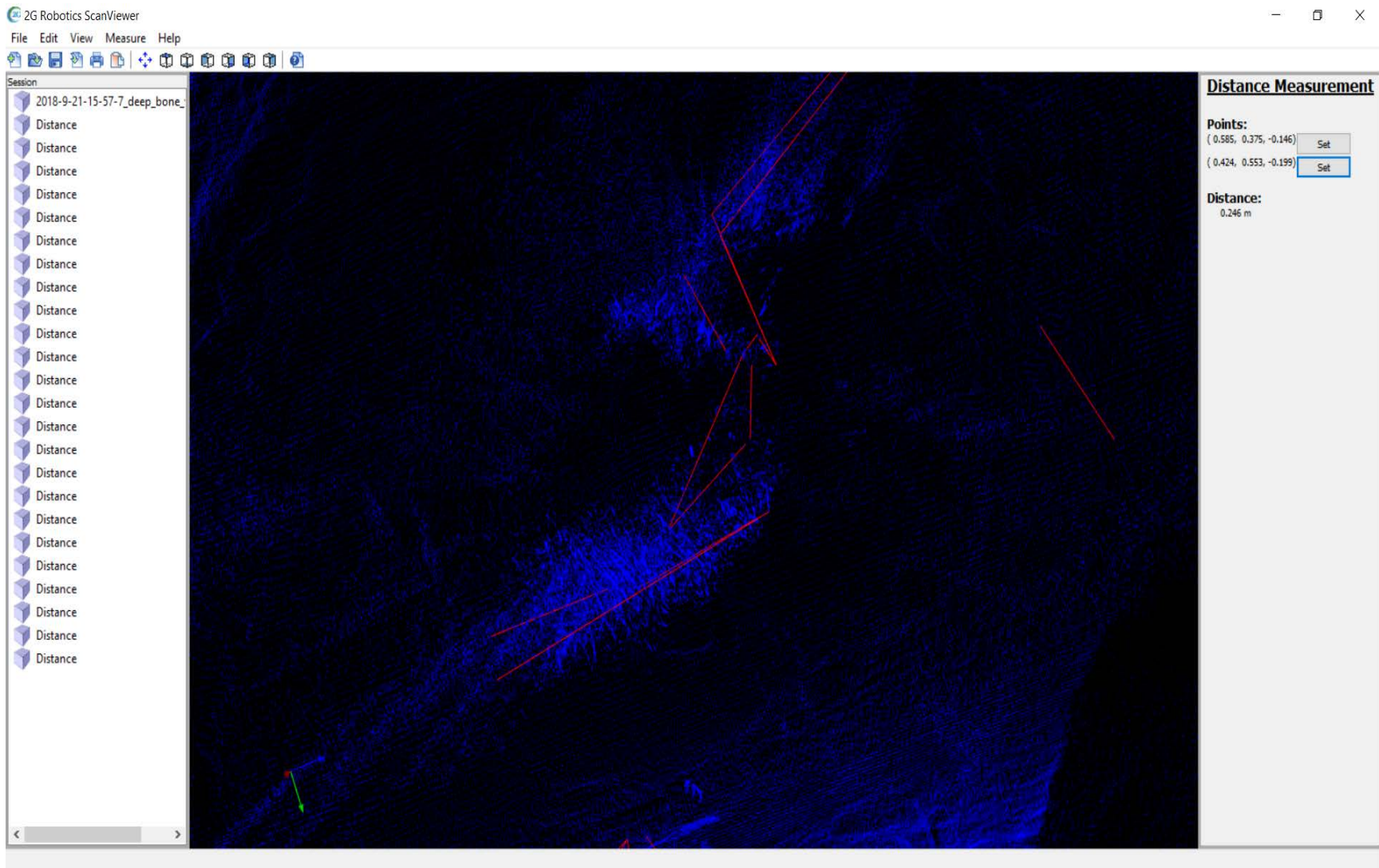


Figure 71. Distance measurements of fluid thermodynamics effects from ULS-200 rotation on point cloud during sampling.

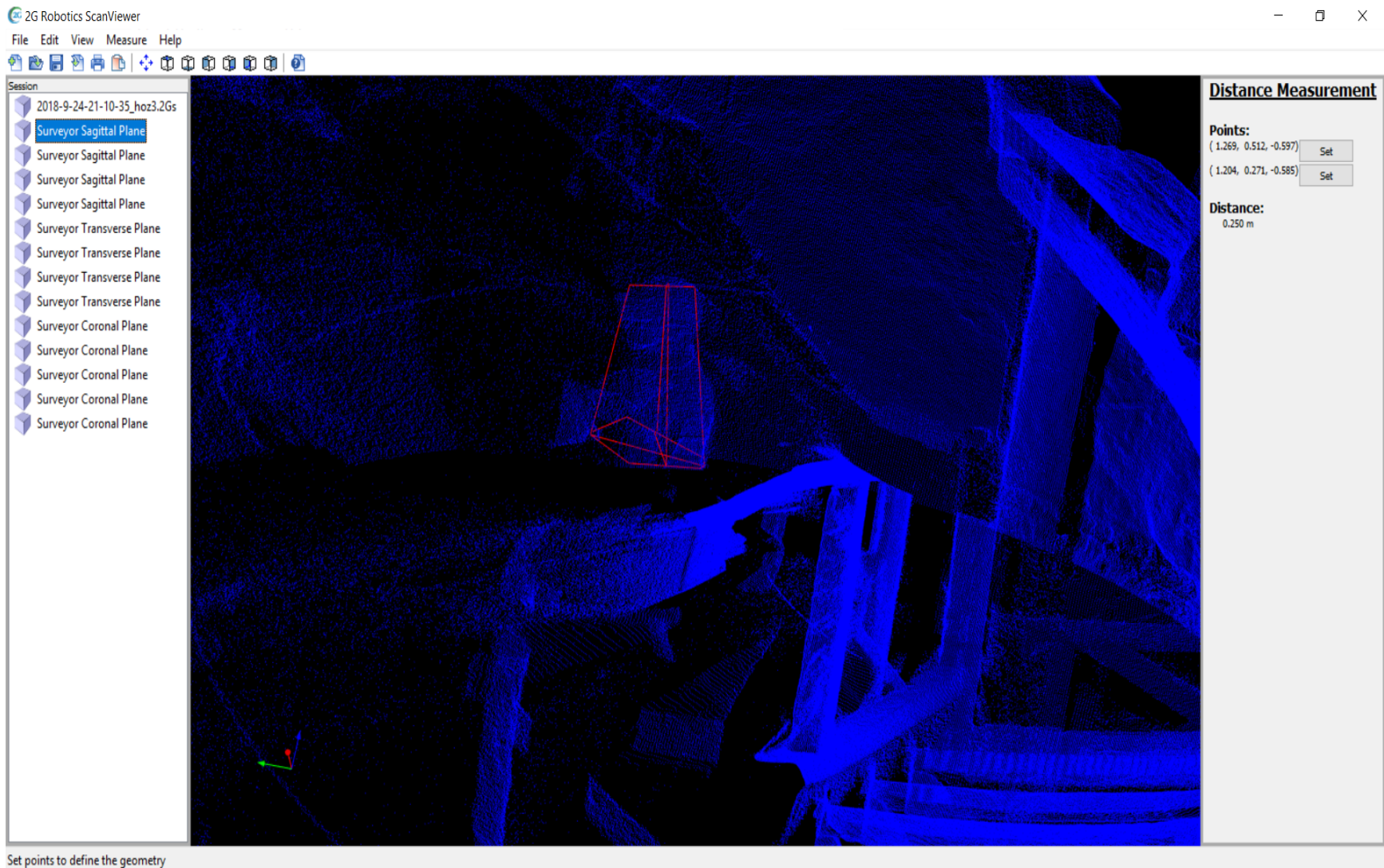


Figure 72. ULS scan with surveyor anatomical planes (torso sagittal, transverse, and coronal) extracted in red for SWORT RASP CIRMSS H-R emergency imaging.

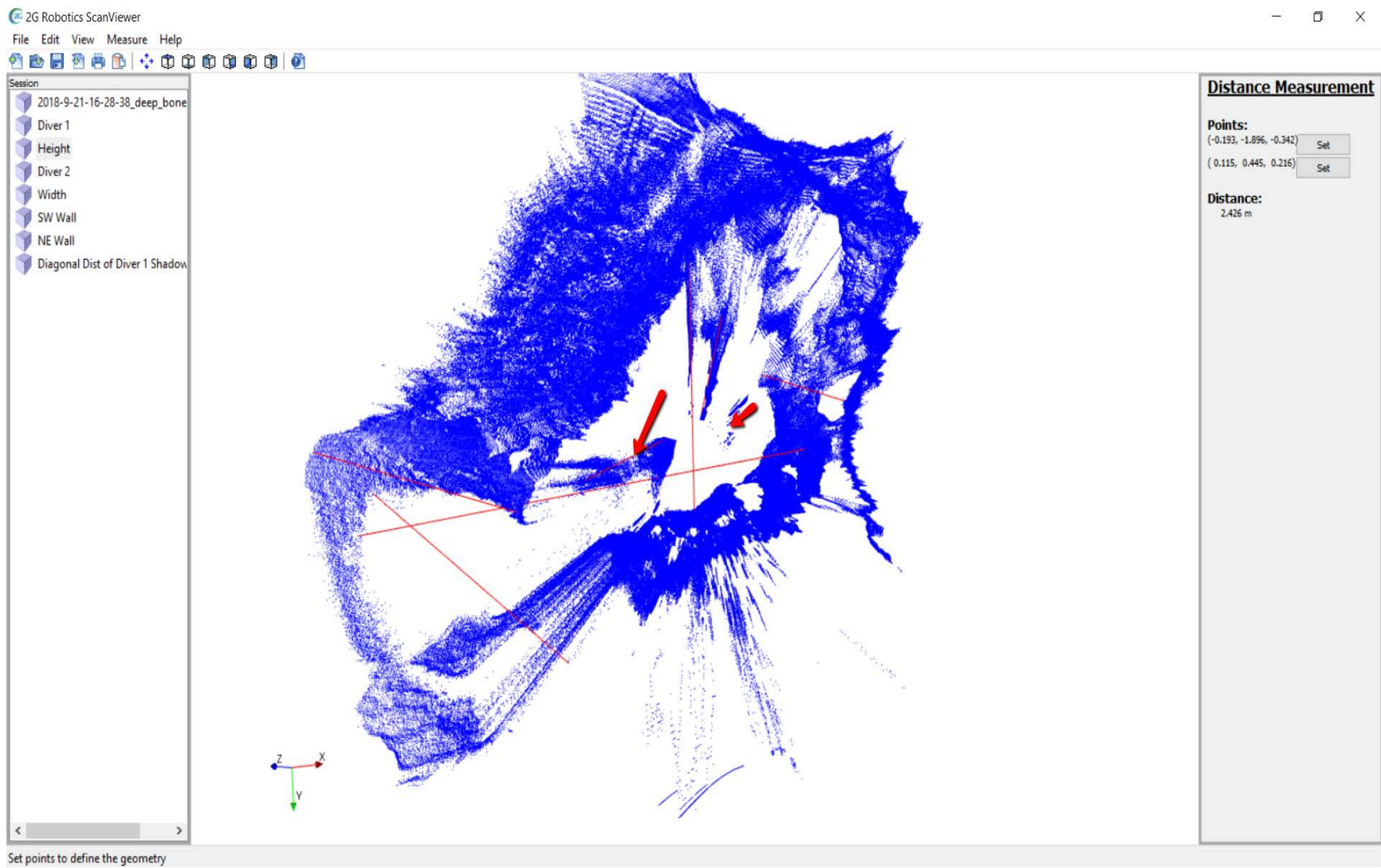


Figure 73. AOI, DBR cross-section with reference measurements divers represented by arrows and a PQV extending from the intersections of height & width planes related to the ULS centroid.

1

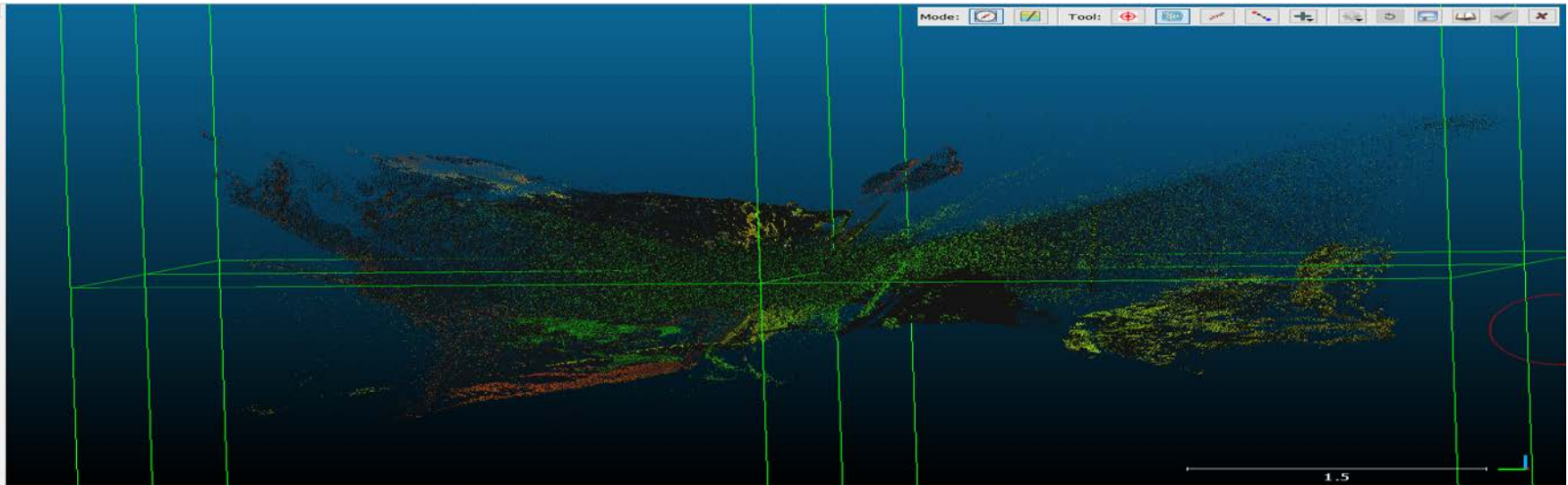


Figure 74. 2 horizontal & 2 vertical stitched cross-sections of of Cenote Sugarbowl, Sistema Tajma Hal karst aquifer entrance.

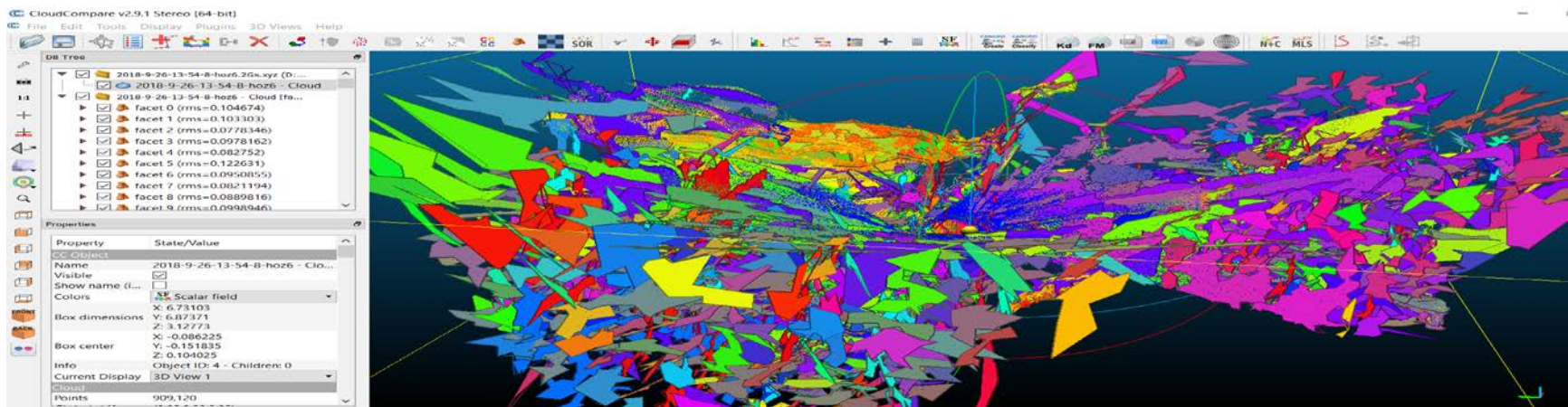


Figure 75. ULS-200 non-linear optics Gaussian extracted Kd-tree planes as raw distortions in Cenote Sugarbowl.

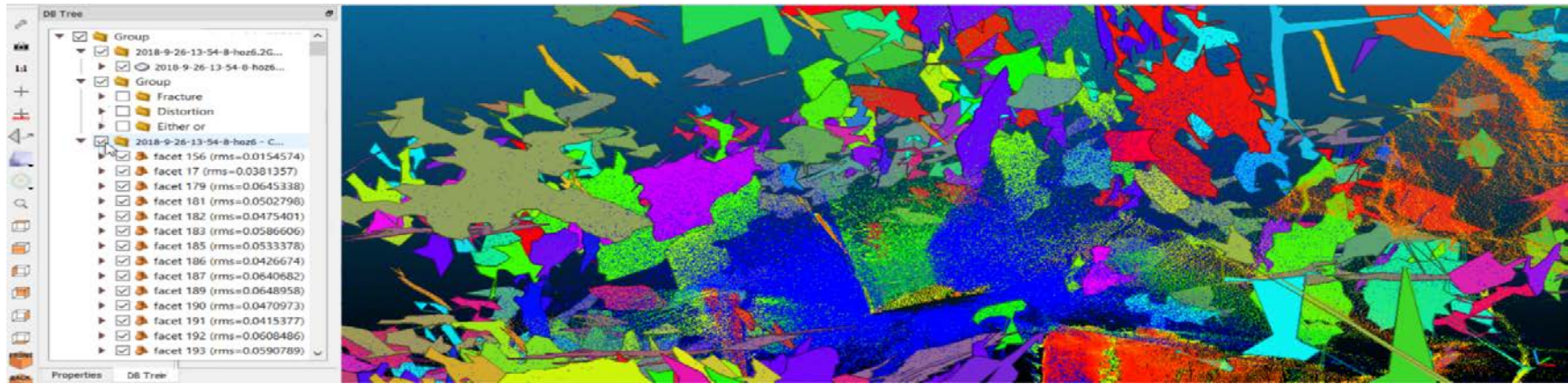


Figure 76. Semi-supervised classification of fracture, distortion, & either-or classification geohazard detection schema via Gaussian extracted Kd-tree planes for fluid thermodynamics, QCED, & topography.

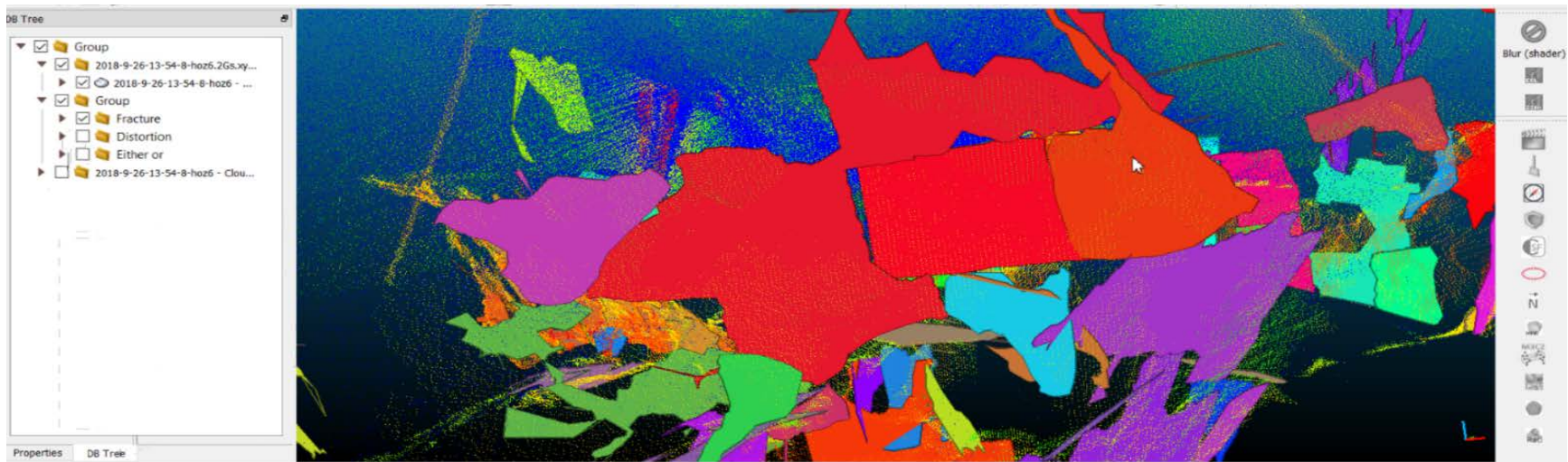


Figure 77. Facet classification for a PPL to NDI plane detection on sections with more density on the external dissolution-cleavage edge representing geohazard collapse points.

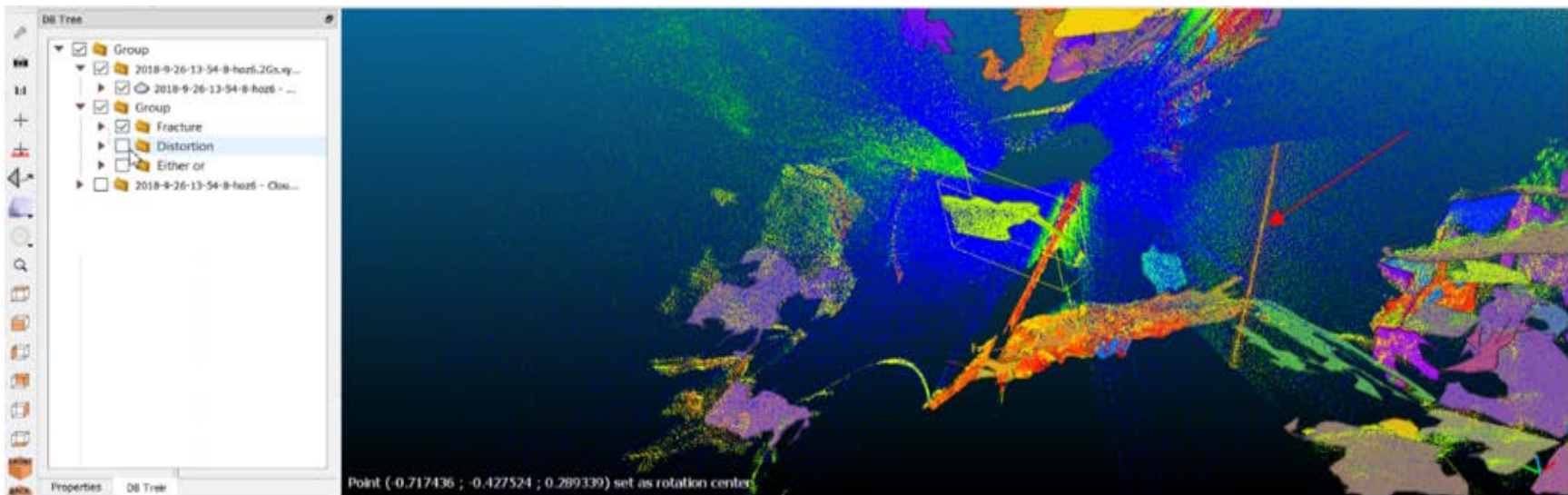


Figure 78. Rope ladder imaging shadow presenting an object-tied plane in the yellow box & fiber optic cable QB as a yellow-orange line marked with an arrow.

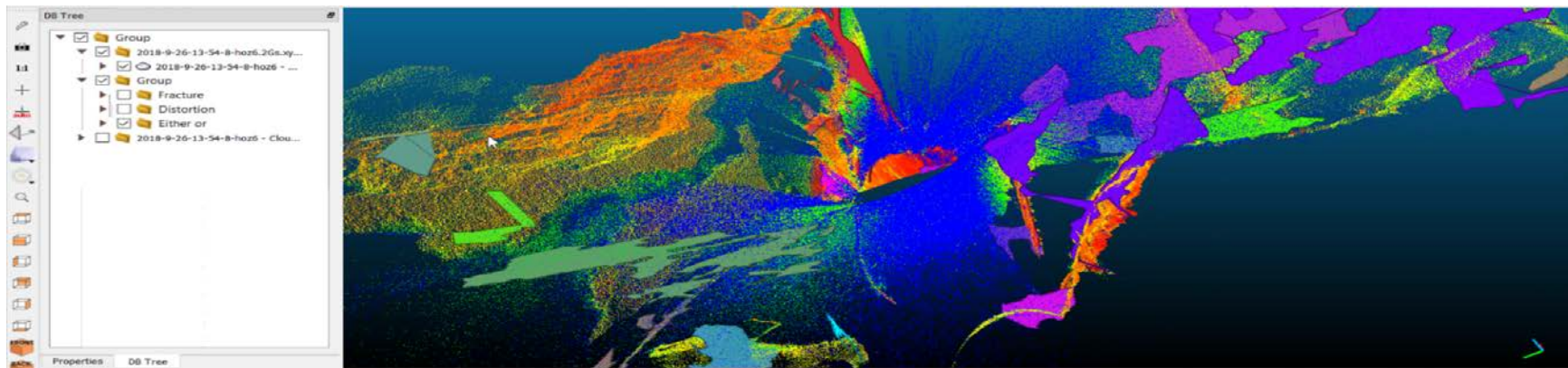


Figure 79. Kd plane extractions representing fractures or distortions requiring supervised classification related to PQV and KHI.

The datasets were stitched and analyzed within CloudCompare to identify fracture facets and non-linear optic ULS imaging artifacts and distortions for indexing. A regional scene coupled with the GDB, provides an immersive contextual setting for 3D spatial analysis, feature construction, and future ULS point cloud display. Shuttle radar topography mission level 2 (STRM-LVL2) datasets from the USGS provided content for development into 3D, z value polygon tube features that were submerged into the Yucatan karst platform relative to their 3D extracted elevation height. Surveyed Cenotes were added as blue dots and the AOI was marked with polygons at surface and depth into the platform. Figure 80 presents the extracted scene histogram for regional hemispheric tree canopy cover. IceSat laser altimeter datasets and areas of spatially correlated to cave system densities promote orbital to field RS karst survey (Denton et 2016; Stafford et al 2017; Healey et al 2014). Figure 81 displays the 3D regional scene heat map of cenote hotspots based on stream stem number and tree canopy density. This provides PSTAR exploration comparatives in unexplored cave systems for future ULS SWORT ORT.

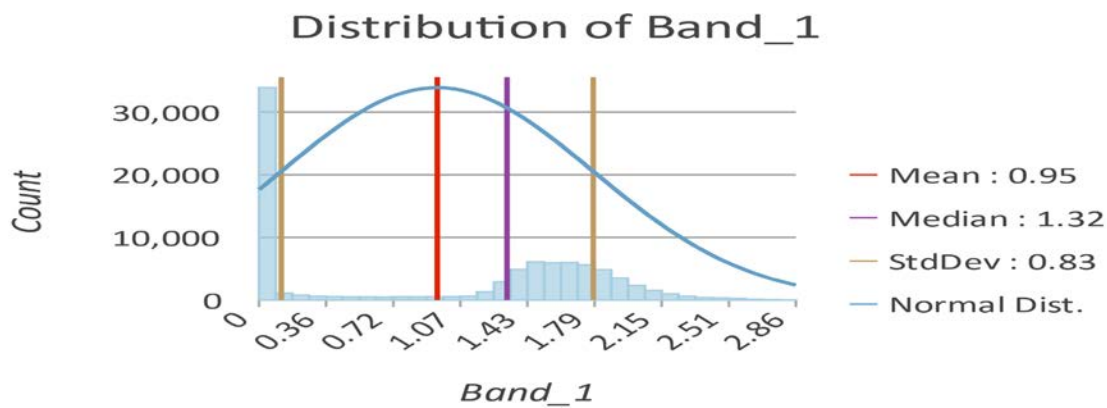


Figure 80. NDI Histogram of cenote density to synthetic streams, which correlate to continually winter tree canopy cover from IceSat datasets indicating cave presence.

Yucatan Peninsula 3D Cave Exploration Heat Map

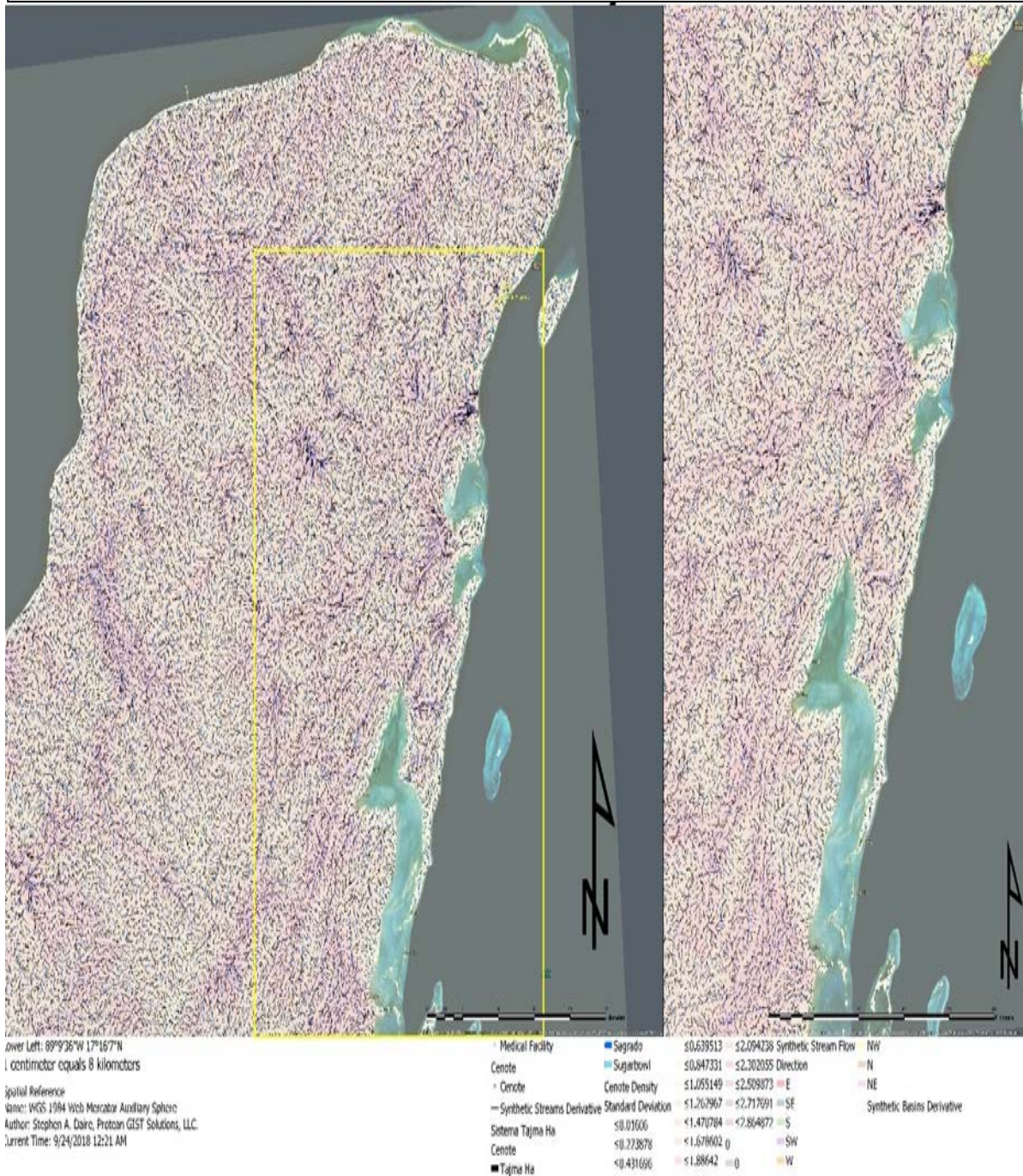


Figure 81. Cave-ins and exploration planning heat map correlated to STRM synthetic stream-NDVI IceSat datasets with high cave-in potential in darkest regions of red, the inset map represents unsurveyed regions, South towards Belize, for future research.

ULS point cloud data was not able to be uploaded into Esri City Engine due to processing and access problems with ArcGIS Pro. The datasets are ready for development into a contiguous stereoscopic, 3D, and VRL products and environments for future research, education, and outreach. The data is able to be visualized within CloudCompare and other software but requires ArcGIS and City Engine for a realistic isometric VRL with 3D GIS products for training and research simulations.

These surveys begin to provide insight into future ULS testing and PSTAR underwater mission planning and operation within cave-diving and astronautics extravehicular sorties for human factors research in remote sensing in extraterrestrial environments through VRL simulation. PSTAR analog operations through cave diving survey promote developments in equipment failure detection, integrative utilities, robust safeties, and adaptive ergonomics through VRL simulators for research and engineering in GIST.

4.2. Facts

The more we learn from underwater cave exploration and research the more we can develop and parallel testing in other application domains. Figure 82 through 86 present diagrams of planetary science knowledge areas where we know too little about our own environment. Figure 82 presents the areas of orbital exploration of new environments which can be dangerous and requires proper tools and techniques for safe and successful operations. Planetary sciences research provides new information and responses to limitations and obstacles related to climate change response, human evolution, and exoplanet points of interest and environmental obstacles for continued astronautic mission planning in human survival and robotic explorations.

REGIONS OF THE ATMOSPHERE

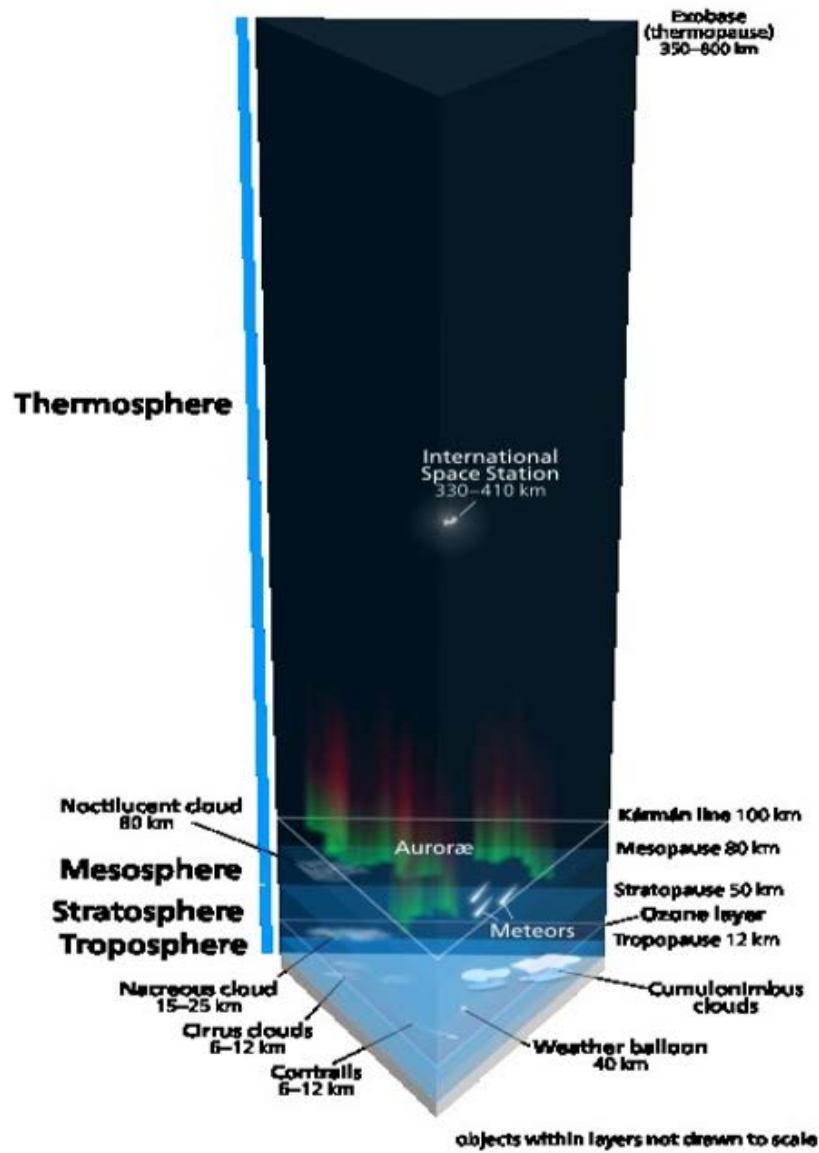


Figure 82. Earth Atmosphere model (Reimuller et al 2015).

Analogies between dissolution dynamics in underwater caves and polar MC turbulence assists climatological modeling error reduction. Figure 83 presents atmospheric carbon abundance estimates which effect existing speleogenetic and paleoenvironmental models and require updates relative to dissolution parameters, seasonal compression and rebound, as well as

saturation overloading increased from carbonic acid rain. These models benefits mission architecture for orbital vehicle launch and landing windows, informs potential sites for astronautic habitat development, and prompts geohazard risk classification on Earth and for other celestial bodies. Figure 84 presents limitations of RS systems and phenomenological errors that inhibit point per line (PPL) resolution for *in situ scans* and effect final products in model construction including occlusions, intersections, and other misalignments that effect VRLs geographic information communication capacity and utility.



Mesosphere In-Situ Atmospheric Sampler CO₂ abundance above 80 km

- CO₂ radiates infrared energy, heating the lower atmosphere and cooling the upper atmosphere
- The majority of *in situ* CO₂ abundance measurements of the mesosphere and lower thermosphere took place **before 1976**
 - 20-30% errors
 - Remote sensing errors are up to 50% and agree poorly with *in situ*

- CO₂ abundance in the troposphere has increased 21%
- The thermosphere is changing in response to climate change

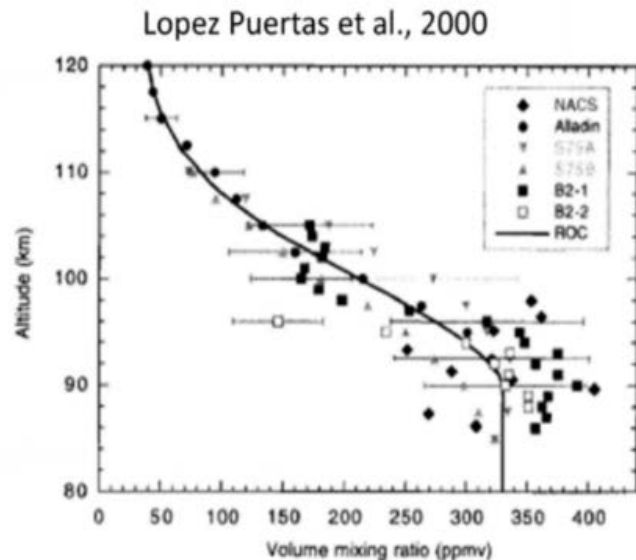


Figure 83. Earth Atmospheric Carbon Density (Reimuller et al 2015).

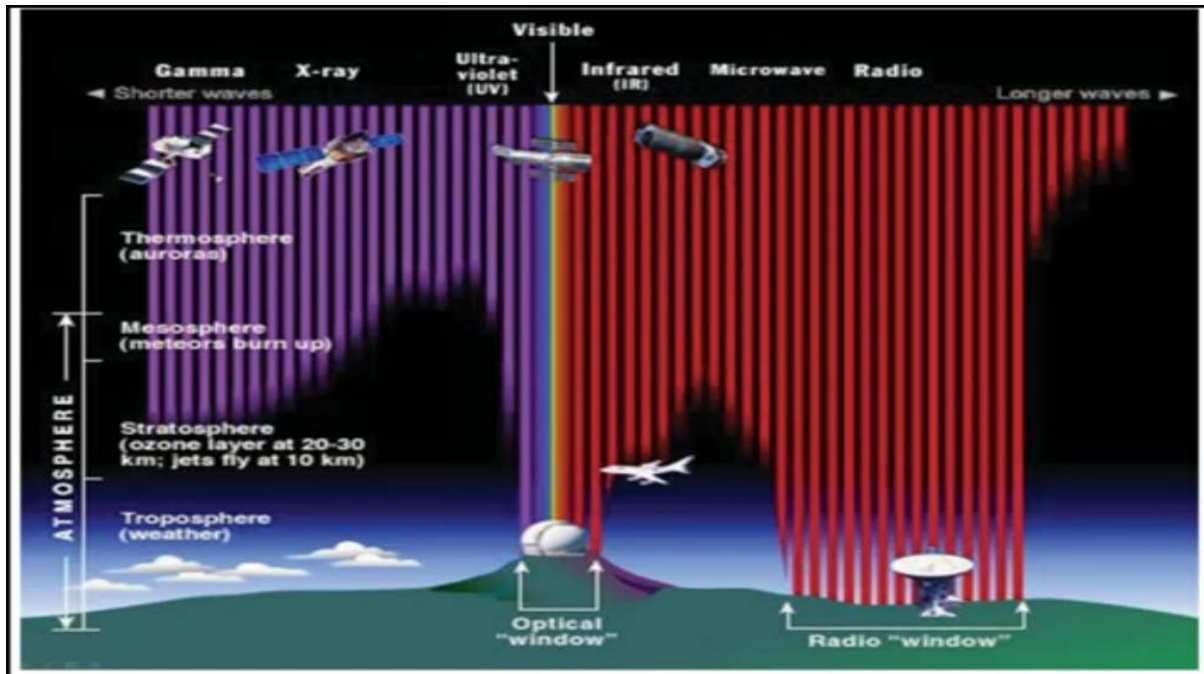


Figure 84. Remote Sensing range and environmental interference (Reimuller et al 2015).

Measurement of number-phase uncertainty relations of optical fields and PQV relates to geospatial sensor uncertainty in ecological and geohydrological studies. ULS and karst scanning benefit from habitual fractal-dimensional analysis within mapping relates to reducing particle-wave uncertainty in gated and non-gated quantum non-linear optics. Evaluations of cave model generation against the modified BCRA survey grades, with analogous suborbital survey represents progressions in GIST, LiDAR improvements, and new applications.

ULS propagated dynamics included PQV, with lemniscate and torus QTK that are visibly present in the video and photographic evidence collected by Natalie Gibbs and Marcelin Nebenhaus, Under the Jungle dive shop owner and cave exploration crew members. Figure 85 presents polar MC Kelvin-Helmholtz Instability (KHI) turbulence modeling. The ULS collected point cloud datasets on fluid dynamics related to KHI occurring within and along the cave halocline via HSF mediated GHR. Figure 86 shows comparative topographic complexity that

defines the contextual setting for the symplectic KHI dynamics that occur between the cave ceilings, walls, and floors of the cave that parallel MC structures.

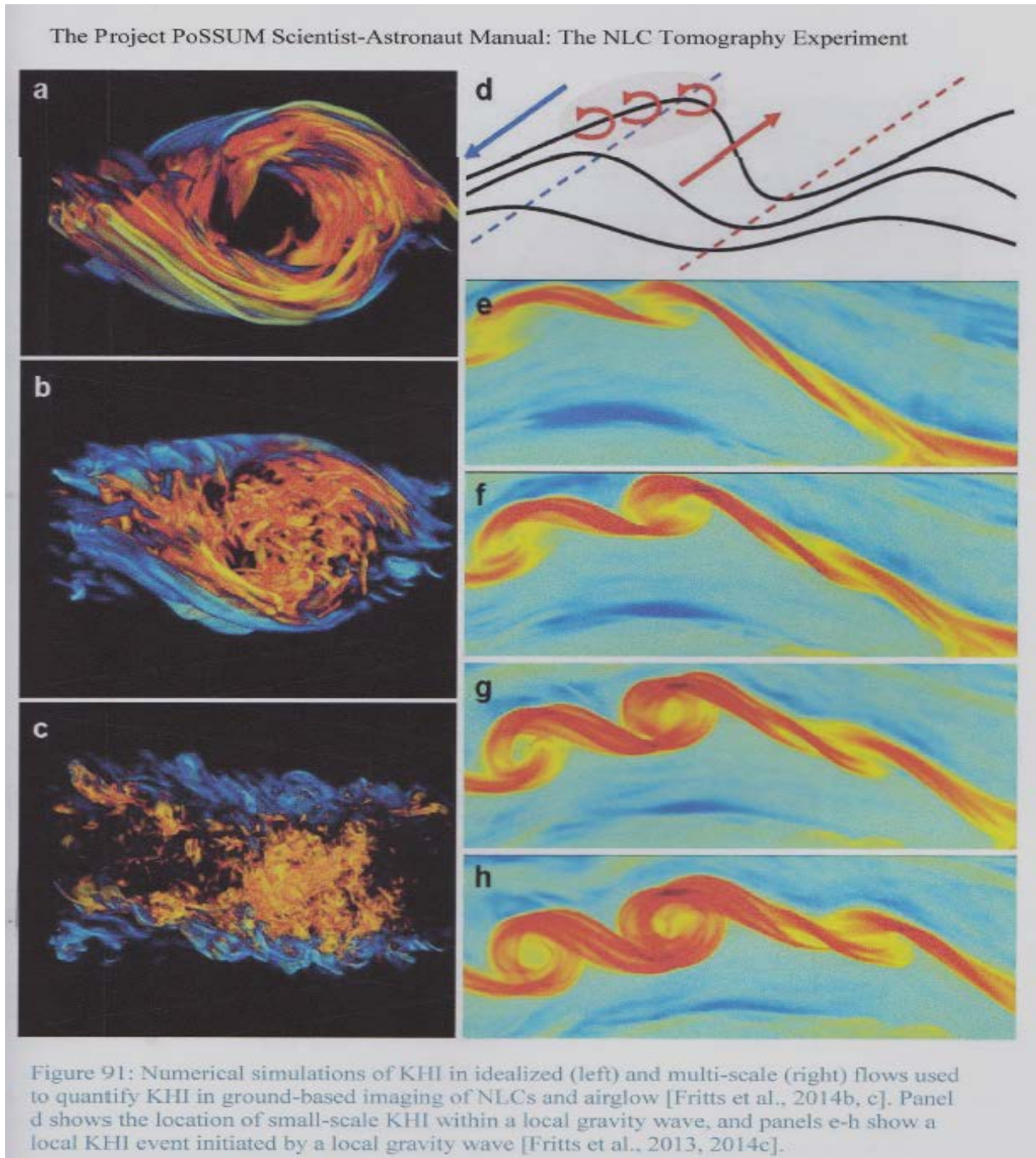


Figure 85. Polar mesospheric cloud simulations of turbulence dynamics (Reimuller et al 2015).

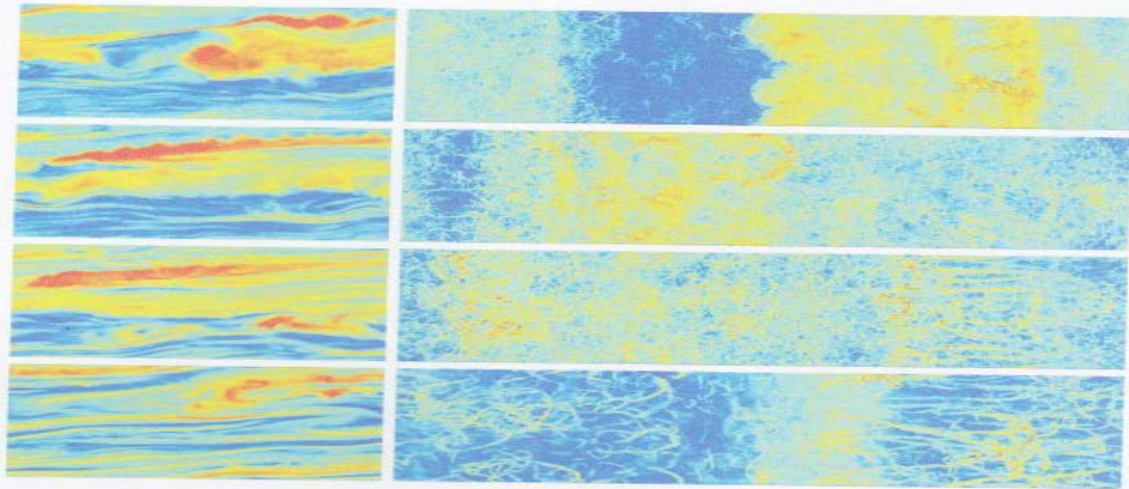


Figure 92: Vertical cross sections (left) and 3D views from above (right) showing various dynamics in a numerically-modeled flow described by Fritts et al. [2015b].

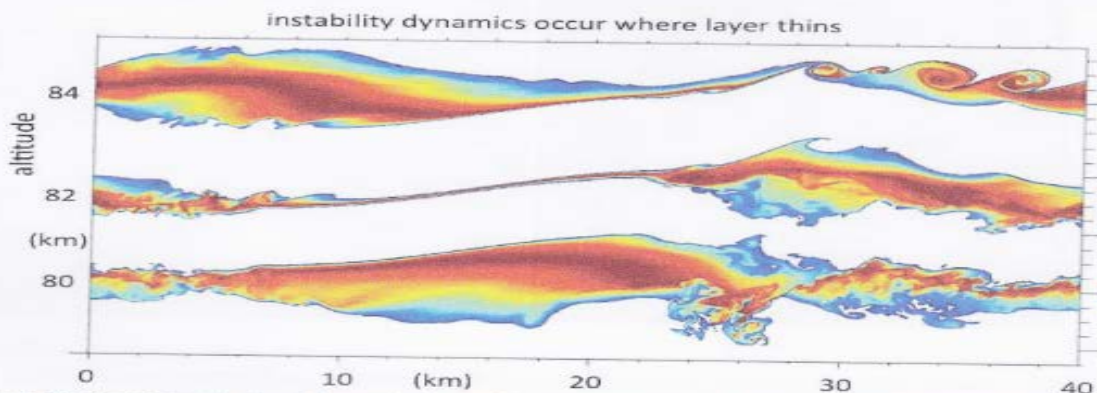


Figure 93: Noctilucent cloud dynamical models constructed by PoSSUM team researchers that will be improved by imagery obtained through PoSSUM flights (credit: GATS)

Figure 86. Polar mesospheric cloud simulations of Density-shear Kelvin-Helmholtz instabilities diagram (Reimuller, J. D. 2015).

ULS collects datasets of μm accuracy including hydrogeologic, biological, and quantum dynamic features at ranges of .015cm to 25m, Table 3. These datasets can be physically transliterated, and remotely simulated in VRL, from subaquatic and terrestrial environments to extraterrestrial exploration in terms of analytic methods, survey techniques, environmental stressors, operations procedures, accident response, and risk reduction.

Table 3. ULS-200 Survey Resolution Chart*ULS-200 Step Size to Radius Measurement Resolution for .6mm scans every 5 minutes
(0.144° per step)*

Radius or distance (250 to 2500) (mm)	Step Size (steps)	Step Size (degrees)	Line Coverage (mm)	Vertical Resolution (mm)	Rotational Resolution (mm)
2500	10	0.18	2331.5383	4.8574	7.8540
2450	10	0.18	2284.9075	4.7602	7.6969
2400	10	0.18	2238.2768	4.6631	7.5398
2350	10	0.18	2191.6460	4.5659	7.3827
2300	10	0.18	2145.0152	4.4688	7.2257
2250	10	0.18	2098.3845	4.3716	7.0686
2200	10	0.18	2051.7537	4.2745	6.9115
2150	10	0.18	2005.1229	4.1773	6.7544
2100	10	0.18	1958.4922	4.0802	6.5973
2050	10	0.18	1911.8614	3.9830	6.4403
2000	10	0.18	1865.2306	3.8859	6.2832
1950	10	0.18	1818.5999	3.7887	6.1261
1900	10	0.18	1771.9691	3.6916	5.9690
1850	10	0.18	1725.3383	3.5945	5.8120
1800	10	0.18	1678.7076	3.4973	5.6549
1750	10	0.18	1632.0768	3.4002	5.4978
1700	10	0.18	1585.4460	3.3030	5.3407
1650	10	0.18	1538.8153	3.2059	5.1836
1600	10	0.18	1492.1845	3.1087	5.0266
1550	10	0.18	1445.5537	3.0116	4.8695
1500	10	0.18	1398.9230	2.9144	4.7124
1450	10	0.18	1352.2922	2.8173	4.5553
1400	10	0.18	1305.6614	2.7201	4.3982
1350	10	0.18	1259.0307	2.6230	4.2412
1300	10	0.18	1212.3999	2.5258	4.0841
1250	10	0.18	1165.7691	2.4287	3.9270
1200	10	0.18	1119.1384	2.3315	3.7699
1150	10	0.18	1072.5076	2.2344	3.6128
1100	10	0.18	1025.8768	2.1372	3.4558
1050	10	0.18	979.2461	2.0401	3.2987
1000	10	0.18	932.6153	1.9429	3.1416
950	10	0.18	885.9846	1.8458	2.9845
900	10	0.18	839.3538	1.7487	2.8274
850	10	0.18	792.7230	1.6515	2.6704
800	10	0.18	746.0923	1.5544	2.5133
750	10	0.18	699.4615	1.4572	2.3562

700	10	0.18	652.8307	1.3601	2.1991
650	10	0.18	606.2000	1.2629	2.0420
600	10	0.18	559.5692	1.1658	1.8850
550	10	0.18	512.9384	1.0686	1.7279
500	10	0.18	466.3077	0.9715	1.5708
450	10	0.18	419.6769	0.8743	1.4137
400	10	0.18	373.0461	0.7772	1.2566
350	10	0.18	326.4154	0.6800	1.0996
300	10	0.18	279.7846	0.5829	0.9425
250	10	0.18	233.1538	0.4857	0.7854
200	10	0.18	186.5231	0.3886	0.6283
150	10	0.18	139.8923	0.2914	0.4712
100	10	0.18	93.2615	0.1943	0.3142
50	10	0.18	46.6308	0.0971	0.1571
0	10	0.18	0.0000	0.0000	0.0000

QB obfuscates ULS survey collection as it prevents specific measurement of universal entropy in datasets, providing only parameterized evaluations of 2nd Law thermodynamic decay (Hod 2011). As the ULS pulse samples datasets the beam floats up along the opposing side of the scanned FOI. Lack of specific entropy due to QB, PQVS induced QTK, and peripheral ablation RS artifacts exists within all LiDAR operations with solutions present in seifertometric studies, phononic harmonization, multiphasic pulsing, modulation columniation, and hyperspatial trimetric fractal marker V&V (Borkovec et al 1993; Pardo-Igúzquiza et al 2015; Mandelbrot, 1983; Feng et al 2017). Lack of extant calibration metrics and indices prevent subaquatic LiDAR survey in several ways and poses potentials for laser pulse amplification which may pose a potential eye hazard to divers, Figure 87 and Appendix N.



Figure 87. Laser goggles attached to cave-diving helmet for eye-safety.

Helmet bound laser safety goggles serve to prevent possible ocular damage from unexpected reflection, refraction, density shear, or amplification (Laser Safety Facts 2010). Divers chose to don and doff safety goggles prior to and after each scan, storing them in equipment pouches intermittently. CRSI arrays prevent these imaging knowledge gaps from effecting datasets sets via congruent survey, yet CSRI arrays do not provide responses or testing frameworks for comprehension and calibration for QB in ULS, which inhibits topobathic lidar surveys (Freire et al 2017). Figures 88 and 89 display GIST and VR datasets as they are promoting numerous innovations over various fields and providing solutions over numerous, traditional problem areas including karst hydrological network fractal analysis. Fractal markers act as versatile geospatial survey tools for use in scanning assessments in numerous conditions and promote 3D GIS and VR RS reconstruction (Pardo-Igúzquiza et al 2015; Mandelbrot, 1983; Feng et al 2017).

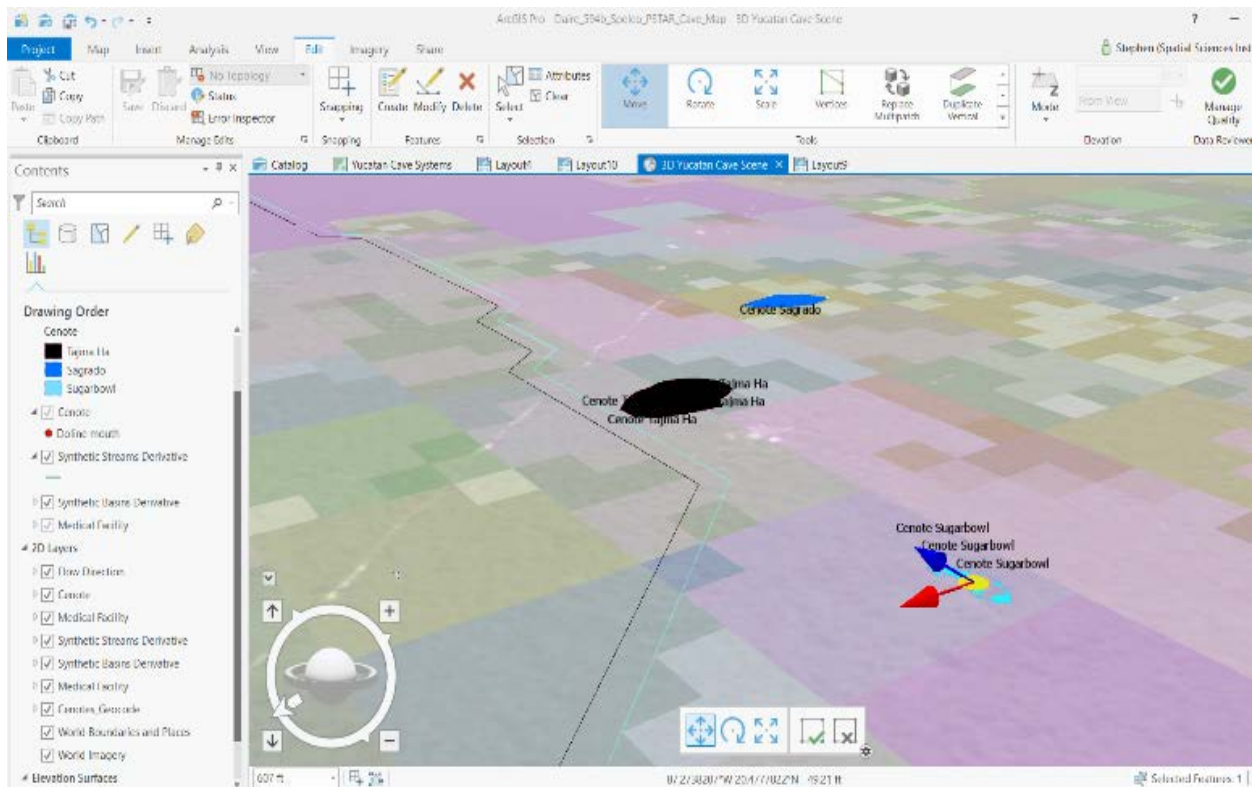


Figure 88. ArcGIS Pro 3D polygon development of surveyed cenote entrances related to synthetic stream locations and heat density mapping.

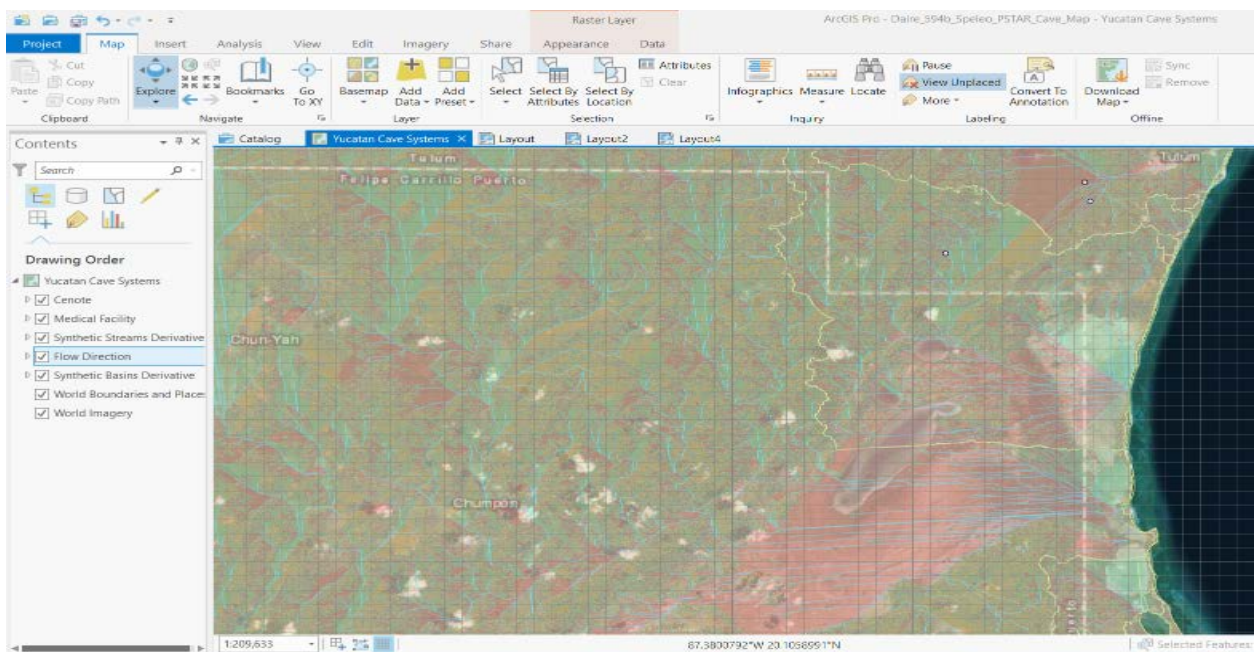


Figure 89. ArcGIS Pro map development of unsurveyed cenotes in region of future exploration interest towards the border of Belize.

In terms of subaquatic research, these are reflective, incompressible, spectrometrically cataloged material that are rapidly deployable, negatively buoyant, and can be fixed in substrates of interest or along a cave-line as necessary for measurement. The markers might serve to function as cave rescue tools serving as orange reflective bread crumbs for preventive and reactive teammate communication in lost diver situations where there is not a line present for self-rescue TRN and CIRMSS response time improvements.

Mandelbrot & Sierpinski functions act as a transitory tool away from analog survey equipment (tape measures, plumb-bob, etc) by resolving *in situ* methods of assessing spatial accuracy measurements via resultant surface areas of multiple targets, with concurrent vectorized color mapping, backscatter lidar contrast assessment, and chemometric calibration assessments. Figure 107 displays trimetric fractal survey markers in parallel projection as they are a novel and unrepresented RS survey tool and potential cave diving rescue tool.

Trimetrogon fractal marker deployment (fractal marbles, fractal bobs, fractal color scales) in FOI ULS CRSI arrays improve modeling survey accuracy and as serve as a potential cave diving rescue utility via scalability through 3D printer applications and parallel projection. CRSI also promote 3D printed cave maps for use in mission planning as well as for search, rescue, and recovery coverage assessments. 3D GIS references facilitate cadastral evaluations of public and private infrastructure compared to geohazard potential, structural loading effects on karst rheology, and dissolutions modification via urbanization in Figure 90. Accuracy improvements for RS and 3D GIS assists geohazard identification and mitigation.

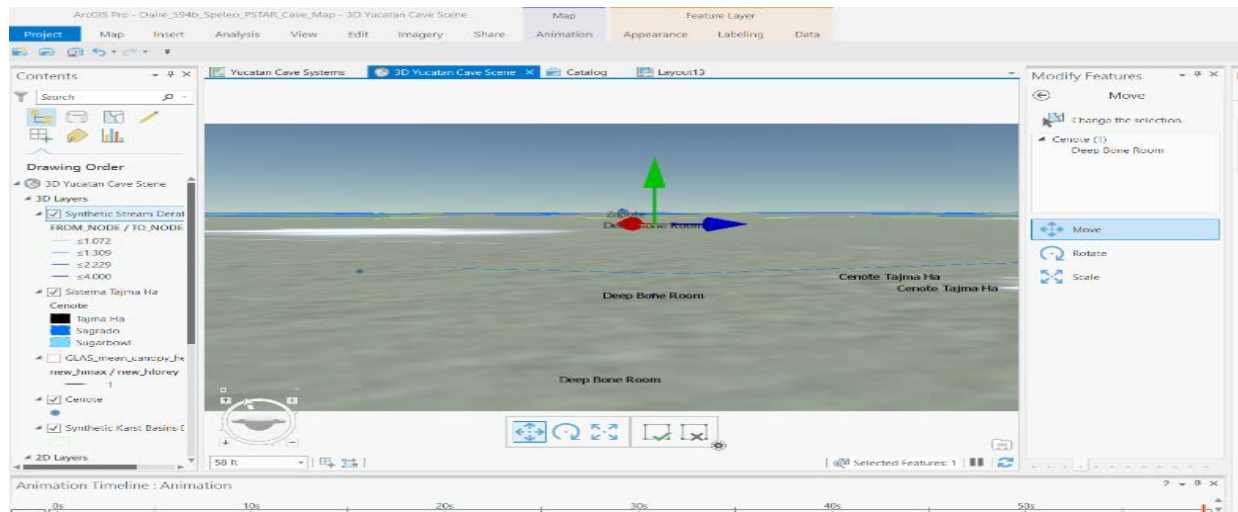


Figure 90. ArcGIS Pro 3D polygon development of surveyed cenote entrances related to surveyed depth of the water table and cadastral data.

Extended CRSI array FOI survey utilizing more than three separate remote sensing metrics (LiDAR, PhoDAR, SoNAR, and water quality, etc) employing fractal trimetrogon (spatio-spectra-volume metric) facilitate surface area survey with 1:1 PPL self-similarity TPU assessment scales at μm geospatial accuracy. Red, green, blue, contrast, and sharpness (RGB-CS) fractal markers provide geovisual reconstruction metrics in surveyed AOIs. These karst structural surveys coupled with a digital color estimate of extant phenomena for future photorealistic vector cloud and voxel (volumated pixel) texture modeling improvements for sub- μm accuracy 3D modeling and mapping with reference coding in Appendix K.

TIN PhoDAR reconstruction is promoted via fractal trimetric marker deployment during ULS survey. Trimetric marker enabled rapid tie point, surface area, and vector color extraction promote texture mapping for 3D GIS and VR development. Placement of the markers along the survey line at object of interest provides true-color and spatial modeling assessment advantages of assessing, developing, and producing 3D features within 3D GIS and VRL environments for geospatial survey deployments and education.

Texture edge-detection improvements directly benefit from high quality $>.5$ fractal marker PhoDAR optic quality by preventing object collision, promoting edge identification, and reducing backscatter. Is particularly important between areas of environmental stratification and mixing like Figures 13, 14, 31, 32, 33, and 34 (thermocline, halocline, density-cline, pressure-cline, sulfa-cline, etc) present during ULS scanning. Figure 91 presents a ULS pulse scan highlighting these issues as they all require continuing interdisciplinary research for lidar scanning improvements, and immediately benefit from fractal scale imaging and environmental assessment calibrations.

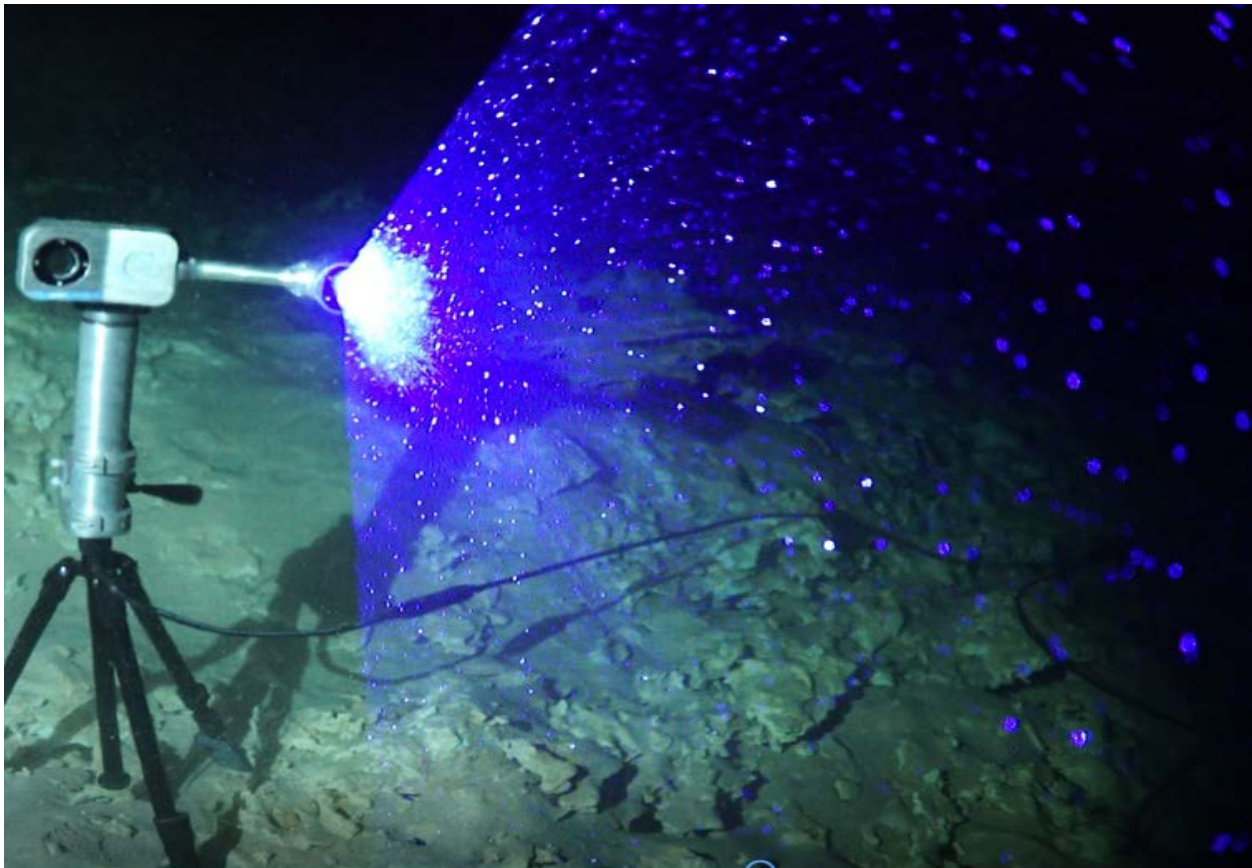


Figure 91. 2G Robotics Inc. ULS-200 scanning ceiling percolate manifold backscatter influencing scan accuracy by producing imaging artifacts from sensor ablation noise.

Mitigation of optic boresight pulse radiance disruption within the aquatically or meteorologically stratified region, dissolutions products, and off-gassing by dive teams/craft are all developmental topics within speleology and GIST research that require continued studies for accuracy calibration and novel dataset collection and assessment in aquatic and mesospheric NC CRSI settings. Mesospheric NC survey and cave diving promote CRSI emission and reception accuracy, quantum gating for forecasted sensor system settings, and analogs for shearing and instabilities in aeronomy, climatology, and speleology for interfacing dynamic systems in planetary sciences research.

4.3. Evidence

Figures 92, 93, and Table 4 display the water quality results report potable water conditions in all categories aside from Ca⁺ hardness in 24 grain 400ppm range and a basic 7.4-8 pH across the freshwater lens and saltwater basin. The differential ionization of the fluid admixture to rock, coupled with the Hele-Shaw continuous viscous matrix flow, causes density differential driven KHI turbulent dissolution. This comodulating HSF-KHI dynamics allow an overloaded volume to continuously manifold in discontinuous erosion upon angular lengths and densities of the crystalline karst structure. This erosive flow within an average 300L³ conduit allows for flows of approximately 300,000L/hr to conduct a natural cyclotronic dissolution field within the caves between the ionic differential of the matrix relative to the viscous flow (Kimmel Kirilyuk, & Rasing 2007). When firing the ULS-200 the laser agitated this electronically charged fluid media inducing emergent dynamic phenomena.

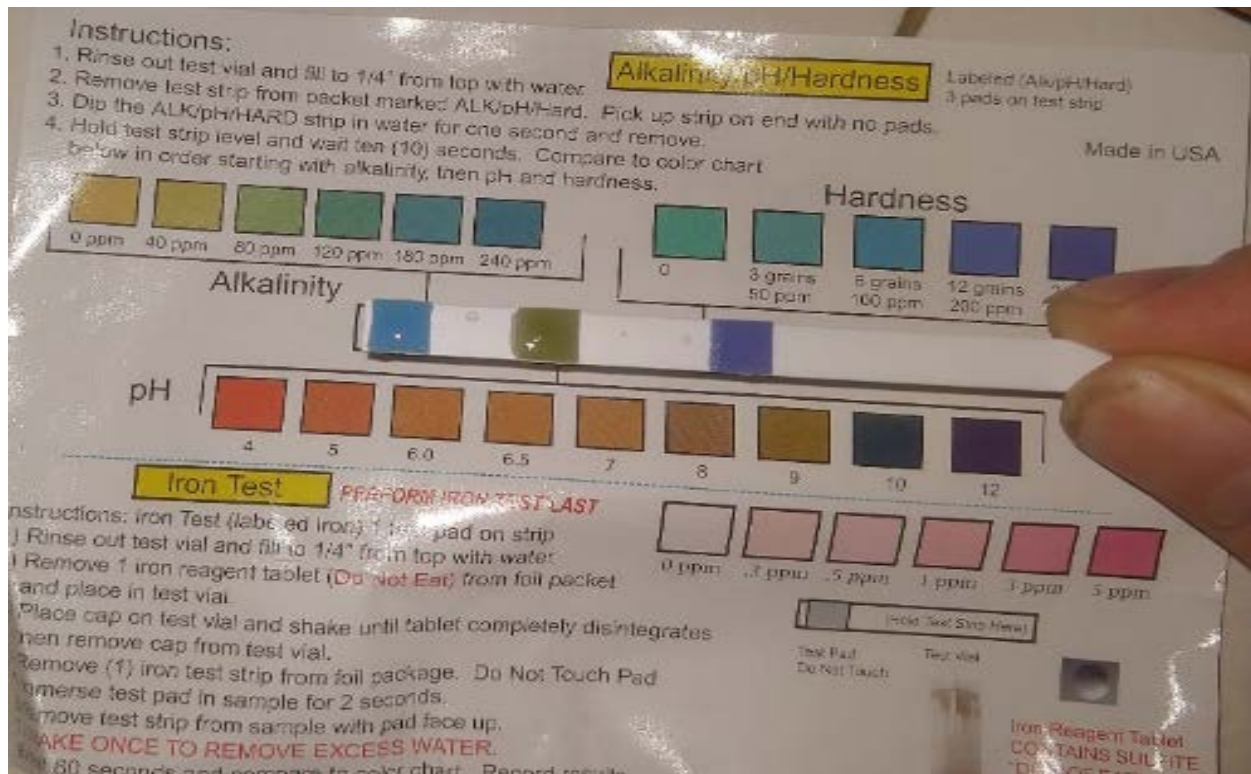


Figure 92. Salt water sample analysis for alkalinity, hardness, and pH from the Deep Bone Room.

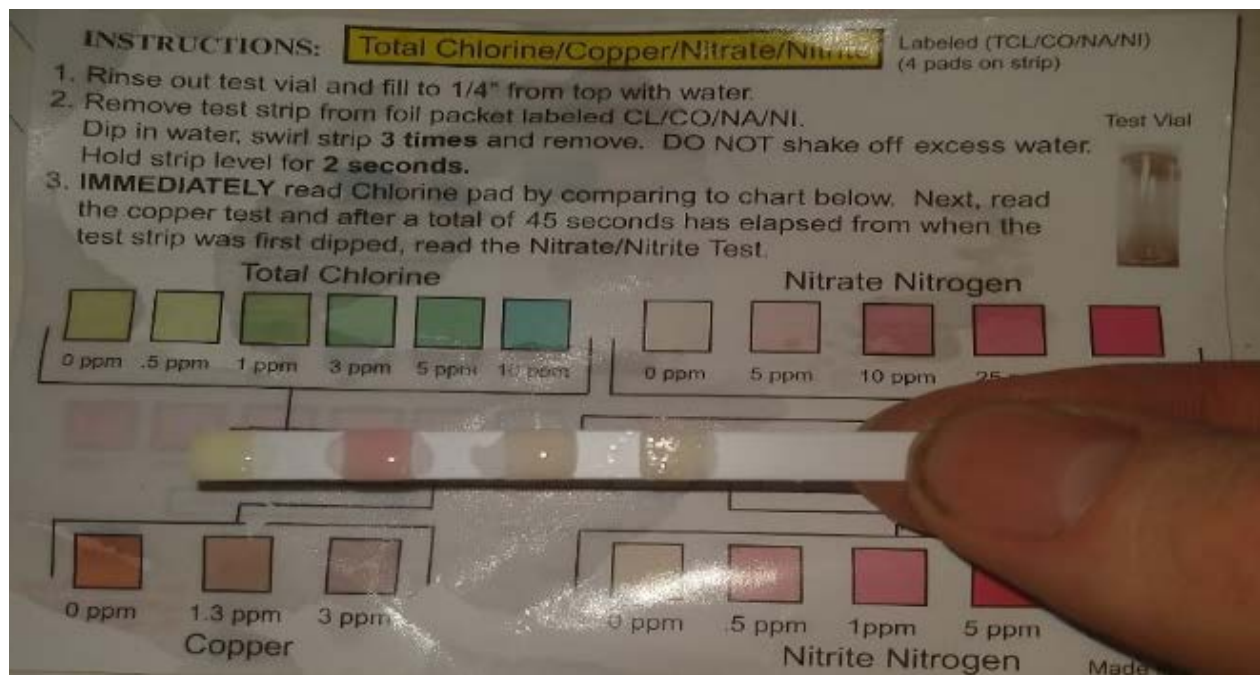


Figure 93. Salt water sample analysis for chlorine, copper, nitrates, and nitrites.

Table 4: Sistema Tajma Hal Water Quality Assessment for Cenotes Tajma Hal, Sugarbowl, & Sagrado in ppm					
Site ID	1	2	3	4	5
Date	18/09/2018	24/09/2018	26/09/2018	22/09/2019	21/09/2018
Location	Tajma Ha	Sagrado	Sugarbowl	GHR conduit halocline	Deep Bone Room
Altitude in Z m	-5	-5	-6	-4	-27
Latitude (N)	20.8408	20.4822	20.48412	20.484014	20.483559
Longitude (W)	87.27804	87.27546	87.27805	87.277964	87.278122
Watertable Depth in – Z m	-3	-4	-6	-17	-27
Temperature in C	23	23	22	23	24
pH	7.2	7	7	7.4	9
Cl	No Data	0.5	No Data	No Data	No Data
Na	No Data	0	No Data	No Data	No Data
Cu	No Data	1.3	No Data	No Data	No Data
Fe	No Data	0	No Data	No Data	0
Ca	40	40	40	40	40
Ca	24	24	24	24	24
NO₃	<5	<5	<5	<5	<5
NO₂	<0.5	<0.5	<0.5	<0.5	<0.5
Pb	No Data	No Data	No Data	No Data	No Data
Alkalinity	No Data	80	No Data	No Data	80
Bacteria	Negative	No Data	No Data	No Data	Null
Pesticide	No Data	No Data	No Data	No Data	No Data

Survey evidence collected in videos produced photos on recorded laser firing. Figure 94 presents the HSF induced KHI propagating along the GHR as an electromagnetic gradient of the calcinated water and the carbonated silicates producing a naturally occurring cyclotronic dynamo in the cave conduits mid- scan. ULS plasma caused fractal symmetric ionized particle alignments during scanning related to a vertex and edge transitive fluctuating orbifold space of radiation. This relates to ULS PQV, QTK, and QCED environmental interactions at the sampling instant.

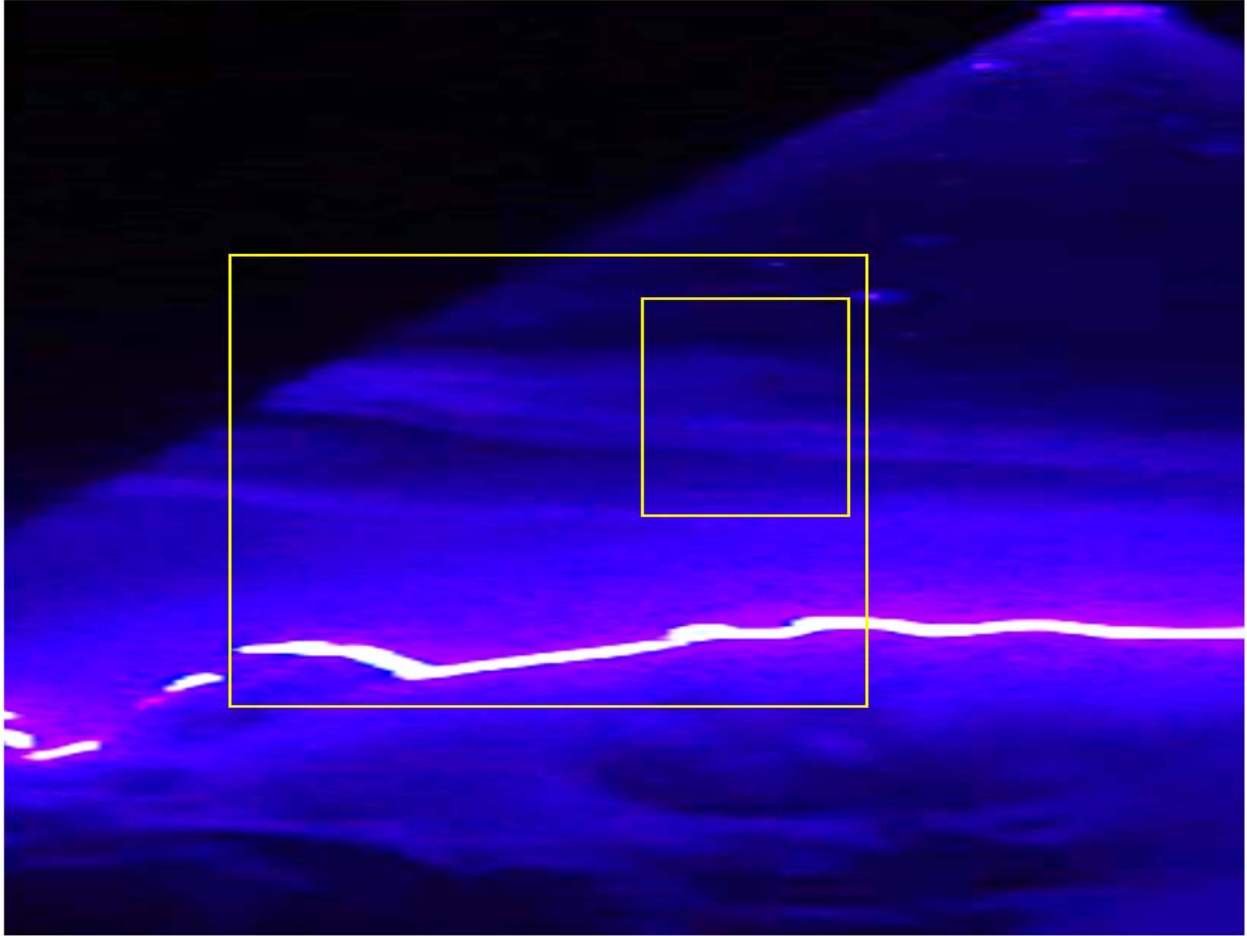


Figure 94. ULS vertically orientation presenting transverse scan of Kelvin-Helmholtz Instability, inner-square, related to karst topographic profile and halocline, outer-square, flow direction left to right (Gibbs 2018).

Extrapolation and assessment of quantum dynamics via the natural system dissolution dynamic manifolds within the datasets collected provided new perspectives which prove fruitful in continuing applied physics, chemistry, geospatial, and topological research settings via an underwater lidar imaging indexing. ULS PQV assessed from a boresight and an oblique offset perspective by an underwater camera collected spectral data and served as a pseudo-quantum gate. Modeling pulse dynamics provided unanticipated results in the form of an informal multiphase, multiresolution photonic and phononic harmonized optics index orbifold (spherical manifold) extending Figure 15 with field data evidence. Figures 95 through 130 display the

observed LiDAR plasma dynamics included PQV slipstream (PQVS) modulations, QTK, and a Gaussian beam carrying the laser collection pulse. Figure 95 presents a plot of an instantaneous intensity Gaussian beam as a function of r , intensity, and x , around an instant of time, showing two intensities for each multiphasic wavefront (Tombs 2011). This beam propagates QCED harmonic waves: frequency, period, wavelength, angular frequency, and wavenumber within Figure 15. Figure 96 diagram displays quantitative wavefunction relationships and properties for LiDAR calibration. Properties are organized on three axes: linear properties, left; angular equivalent, right; frequency properties, top; periodic reciprocals, bottom; temporal properties, front; and spatial equivalents, back (Waldir 2016). A cross-section of matrix wall and roof collapse, HSF inducing GHR KHI Turbulence with the primary dynamics of dissolution occur as density, temperature, geochemistry, and flow speed differential intersections causing ULS facet-phenomena detection as geometrically tied optical density distortions is presented Figure 97. Kd-tree facets extract these data sets as individually colored polygons at 90° cross-sections. The thermodynamics of dissolution occur as density, temperature, geochemistry, flow, & speed at differential intersections causing ULS geometrically tied facet-phenomena optics distortions. Figure 98 depicts ULS non-linear optics raw data in Cenote Sugarbowl openwater entrance bearing QB. QB propagated LiDAR points up along linear objects after impacting the objects. PQV induced a (PQVS) series, which provided datasets on in-situ quantum dynamics from the aphotic underwater environment for time slicing analysis. The time slice was hand mapped due to storm induced power failure. A ULS boresight perspective PQVS induced QTK hypergeometric-Gaussian pulse bearing a tri-modulating spiral vertex at the speed of light for time slicing in Figure 99. Figures 100 through 103 display PQVS, QTK, and QCED pulse dynamics including propagation, ablation, knotting, and dissipation. Figure 100 shows rear offset

perspective camera with variations to contrast and brightness highlighting visible PQVS-QTK interference peaks. Figure 101 provides rear offset perspective PQVS beam troughs preceding QTKs. Variations to contrast and brightness highlighting visible PQVS beam decay in Figure 102. Figure 103 displays a rear offset perspective camera with 4 variations to contrast and brightness highlighting visible PQVS beam QED dynamics. Figure 104 ULS non-linear optics distortions of fluid dynamics from sunlight, flow, PQV, ULS scan rotation, and suspended sediments presenting backscatter and imaging noise extracted as Kd-tiles. Figure 105 presents planarized facet of naturally occurring photonic quantum vortex from sunlight. Figures 106 through 111 One of sixteen imaging perspective orientations of 16 holographic points of inverted reflections bearing accurate volumetric holonomies from a homothetic core at 1-1.5m resolution. Surveyors outlines in yellow box with QRSS Surveyors Rory OKeefe, in grey, and Stephen Daire, in blue. Body silhouettes collected and presented in red by the ULS-200-point cloud from infrared (IR) body heat in Cloudcompare viewer. ULS PQVS introduce antanaklastic (Borrowed from rhetoric meaning Greek anta - anti, ana – up, klasis - breaking) holomorphic phase singularities.

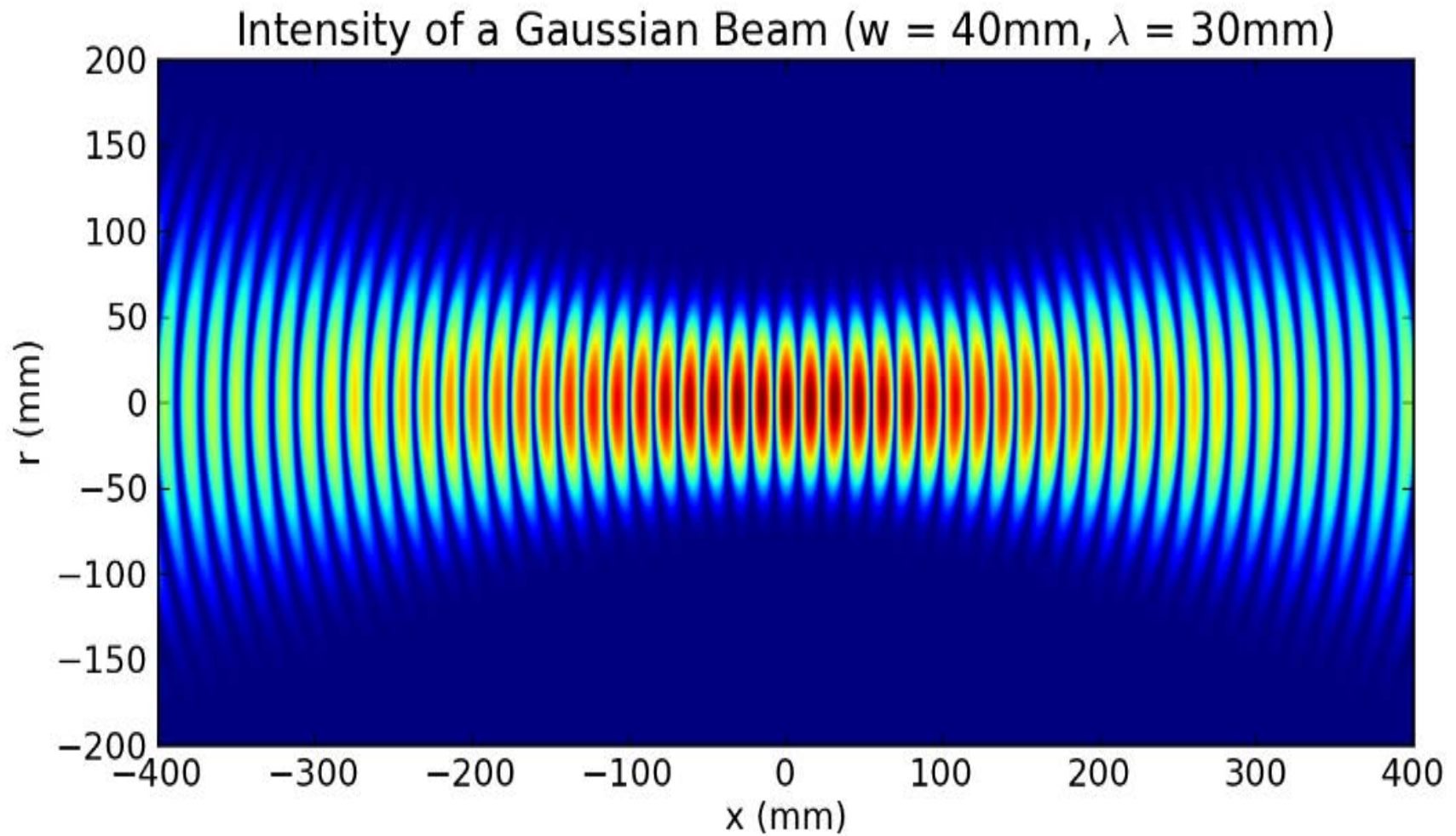
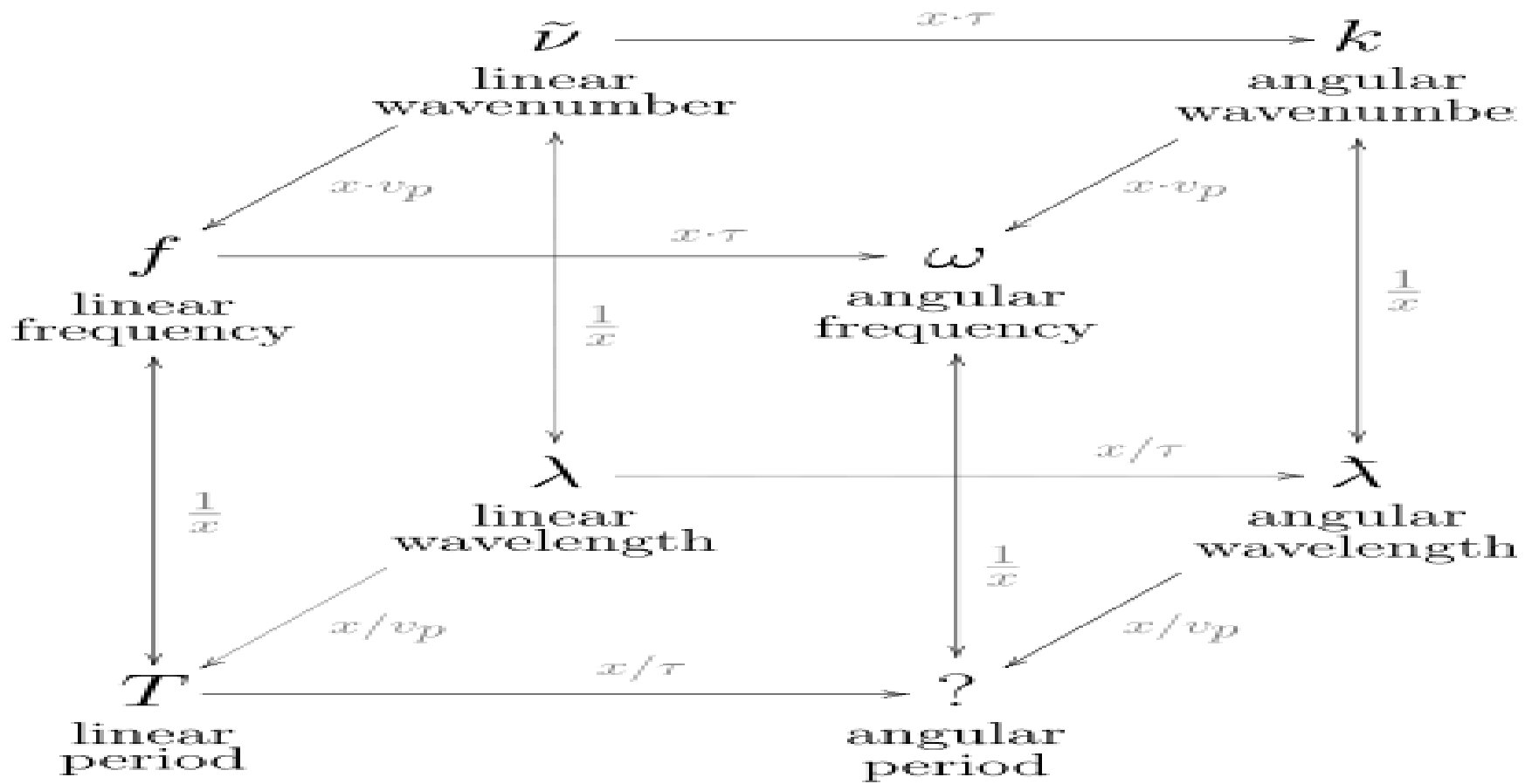


Figure 95. A plot of an instantaneous intensity Gaussian beam as a function of r and x , simulated intensity around a focused instant of time, showing two intensity for each wavefront (Tombs, Eric. 2011).



$v_p = \text{wave speed (phase velocity)}$
 $\tau = 2\pi$

Figure 96. Harmonic wave property-relationship diagram of frequency, period, wavelength, angular frequency, & wavenumber. 3 axes organize the properties: linear, left; angular, right; frequency, top; periodic, bottom; temporal, front; and spatial, back. (Waldir 2016).

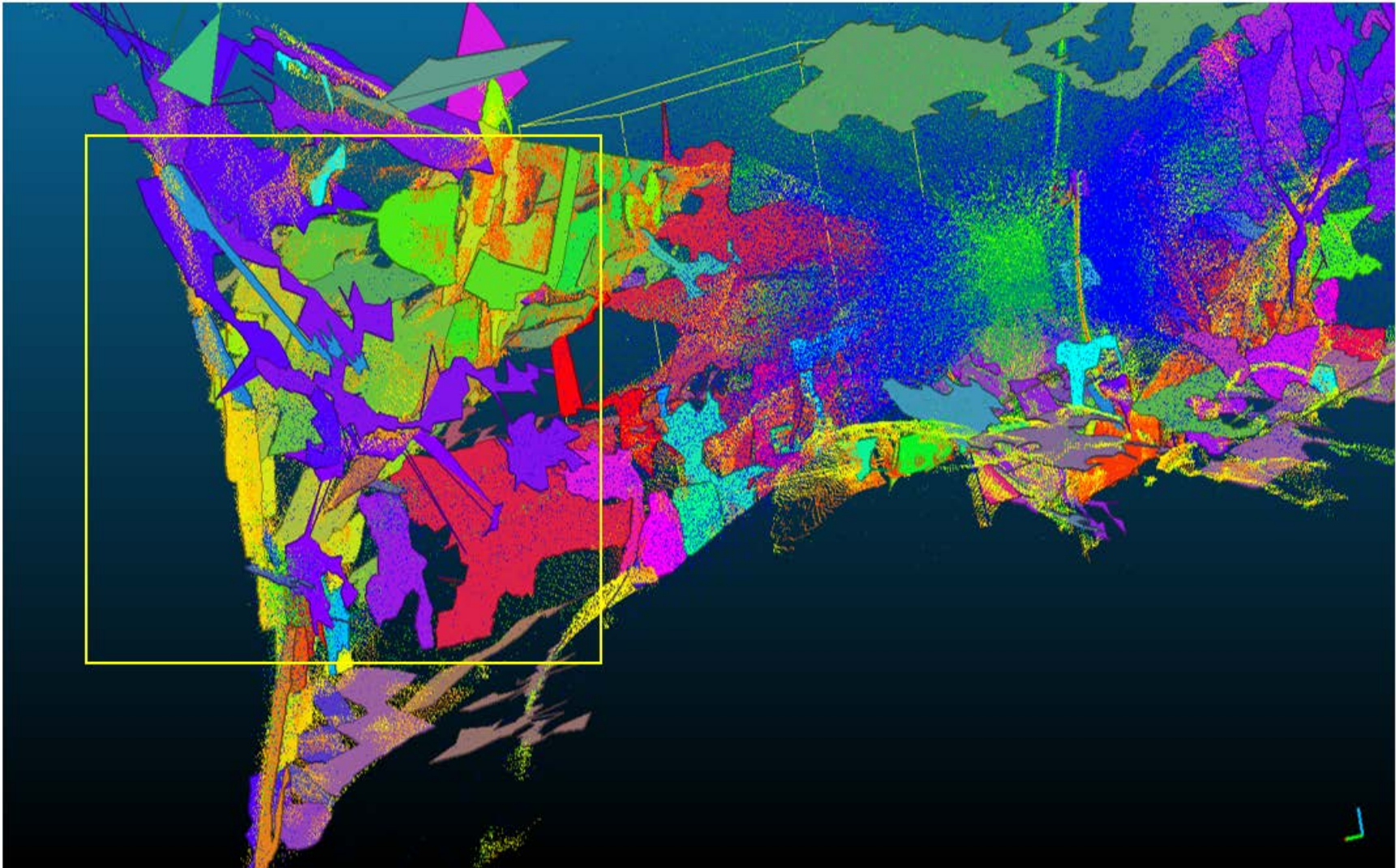


Figure 97. Cross-section of matrix wall & collapse, HSF inducing KHI, represented as the purple polygon in the yellow box, tied to the ceiling, wall, & floor.

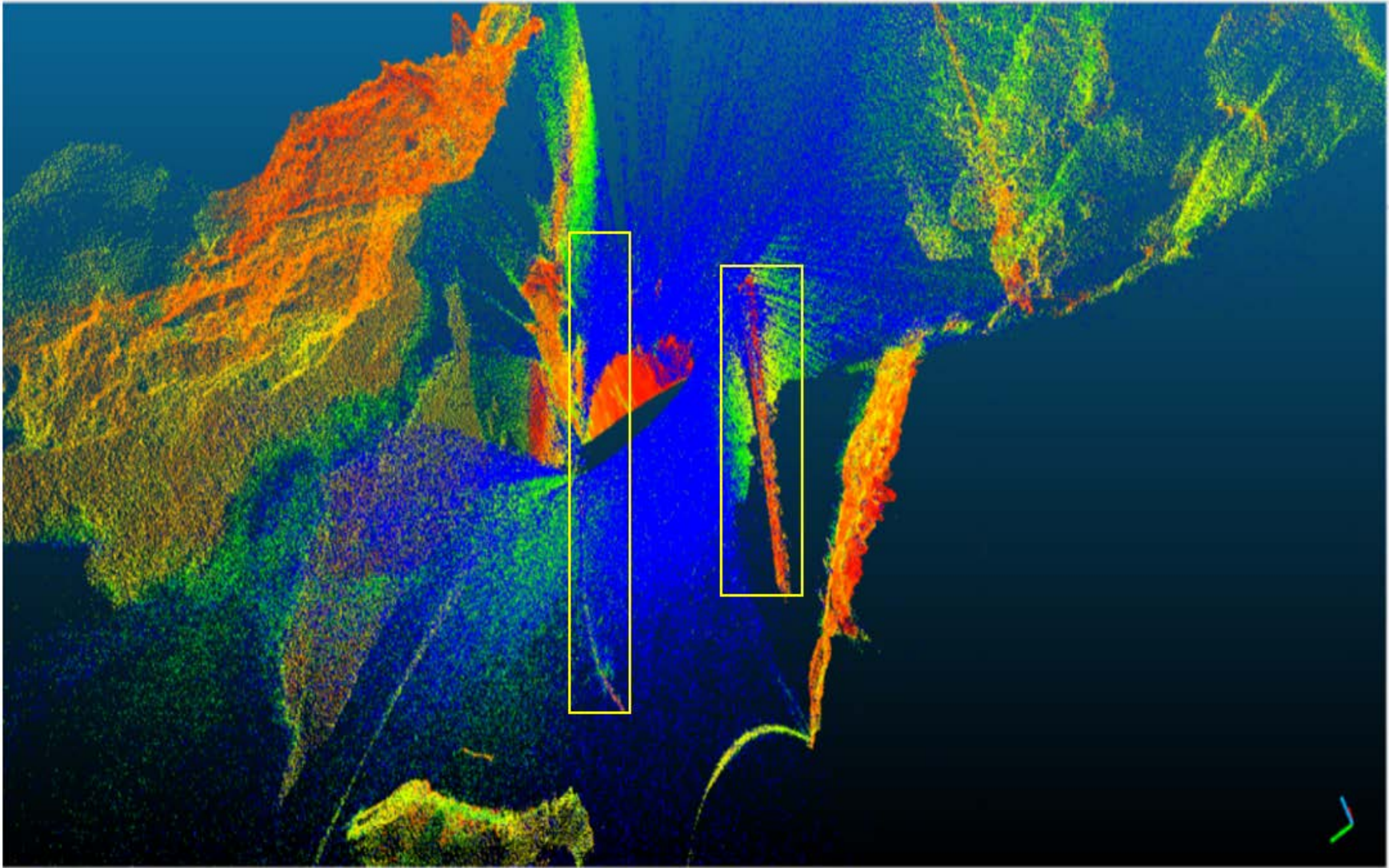


Figure 98. ULS non-linear optics raw data in Cenote Sugarbowl openwater entrance bearing quantum buoyancy as point clouds paths, yellow points, drift up behind linear objects like the fiberoptics and rope ladder anchor, red polylines.



Figure 99. Boresight perspective PQV induced QTK in ULS pulse bearing hypergeometric-Gaussian mode and modulating spiral vertexes nearly instantaneously.



Figure 100. Rear offset perspective camera with 4 variations to contrast and brightness highlighting visible PQVS topological knotting interference peaks at red arrows with +40% brightness and -40% contrast of the original.

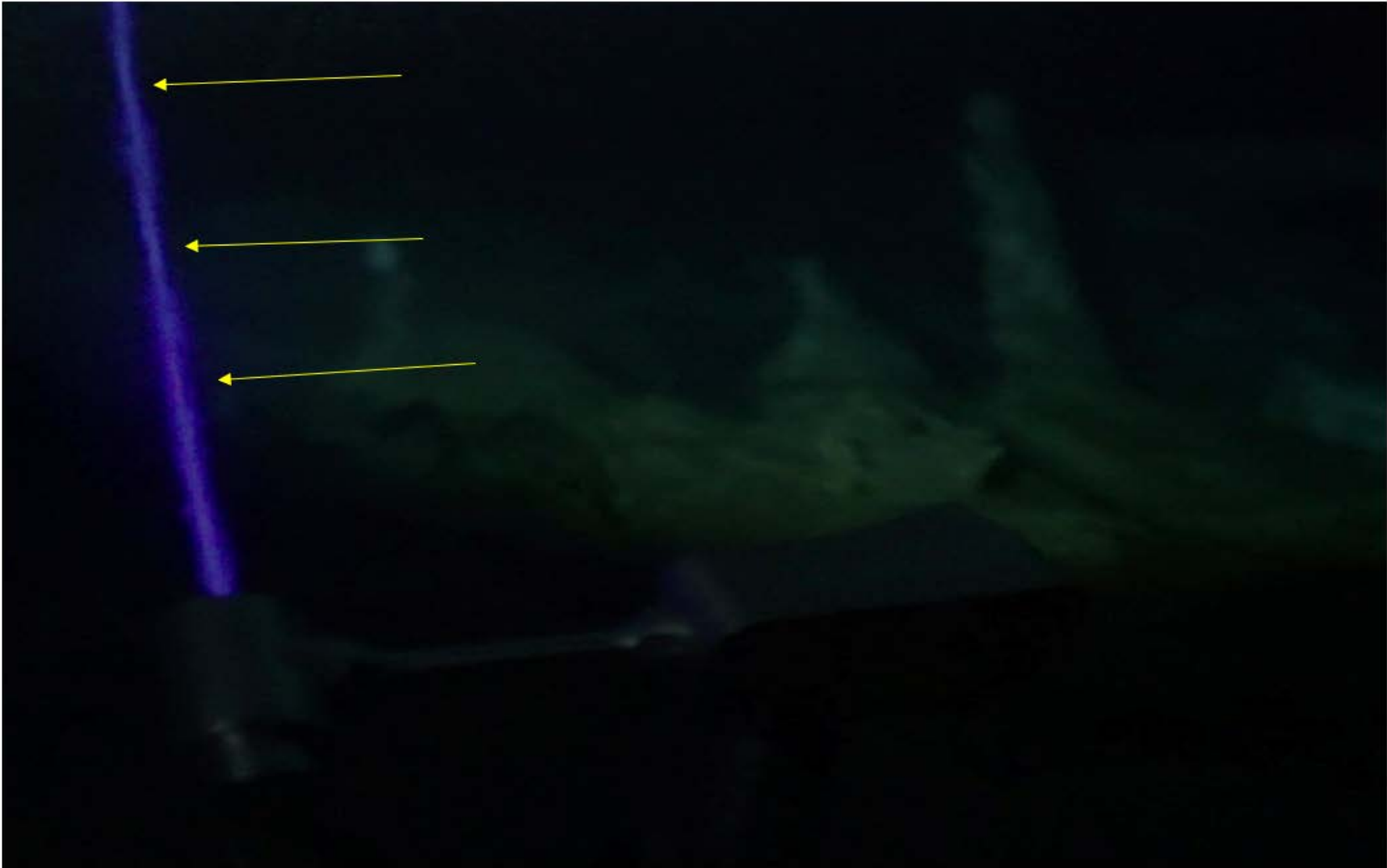


Figure 101. Rear offset perspective camera with 4 variations to contrast and brightness highlighting visible PQVS beam troughs preceding topological knotting at yellow arrows with -40% brightness and -40% contrast of the original image.

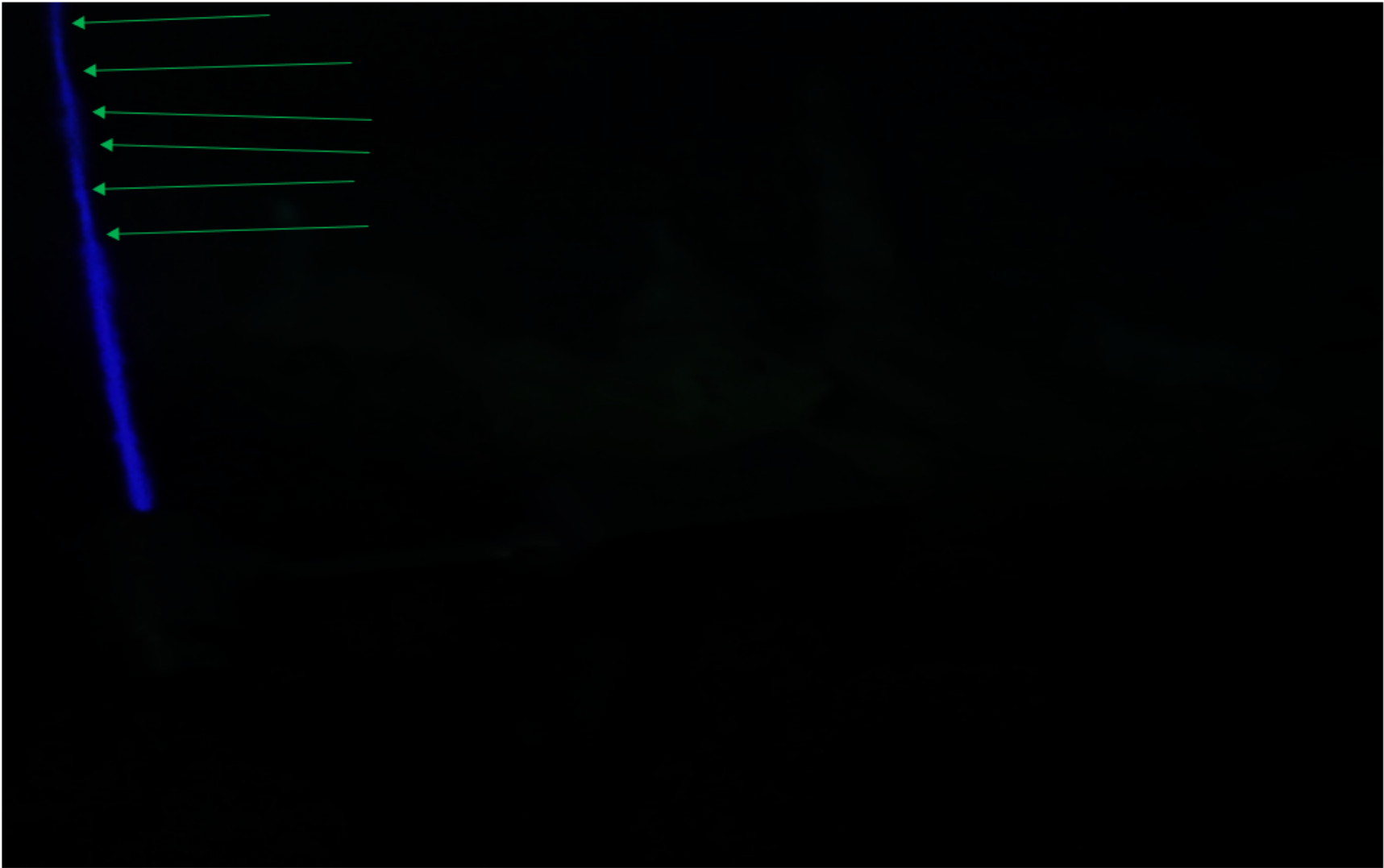


Figure 102. Rear offset perspective camera with 4 variations to contrast and brightness highlighting visible PQVS beam decay at green arrows with -40% brightness and +40% contrast of the original image.



Figure 103. Rear offset perspective camera with 4 variations to contrast and brightness highlighting visible PQVS beam QED dynamics at yellow arrows with +40% brightness and +40% contrast of the original image.

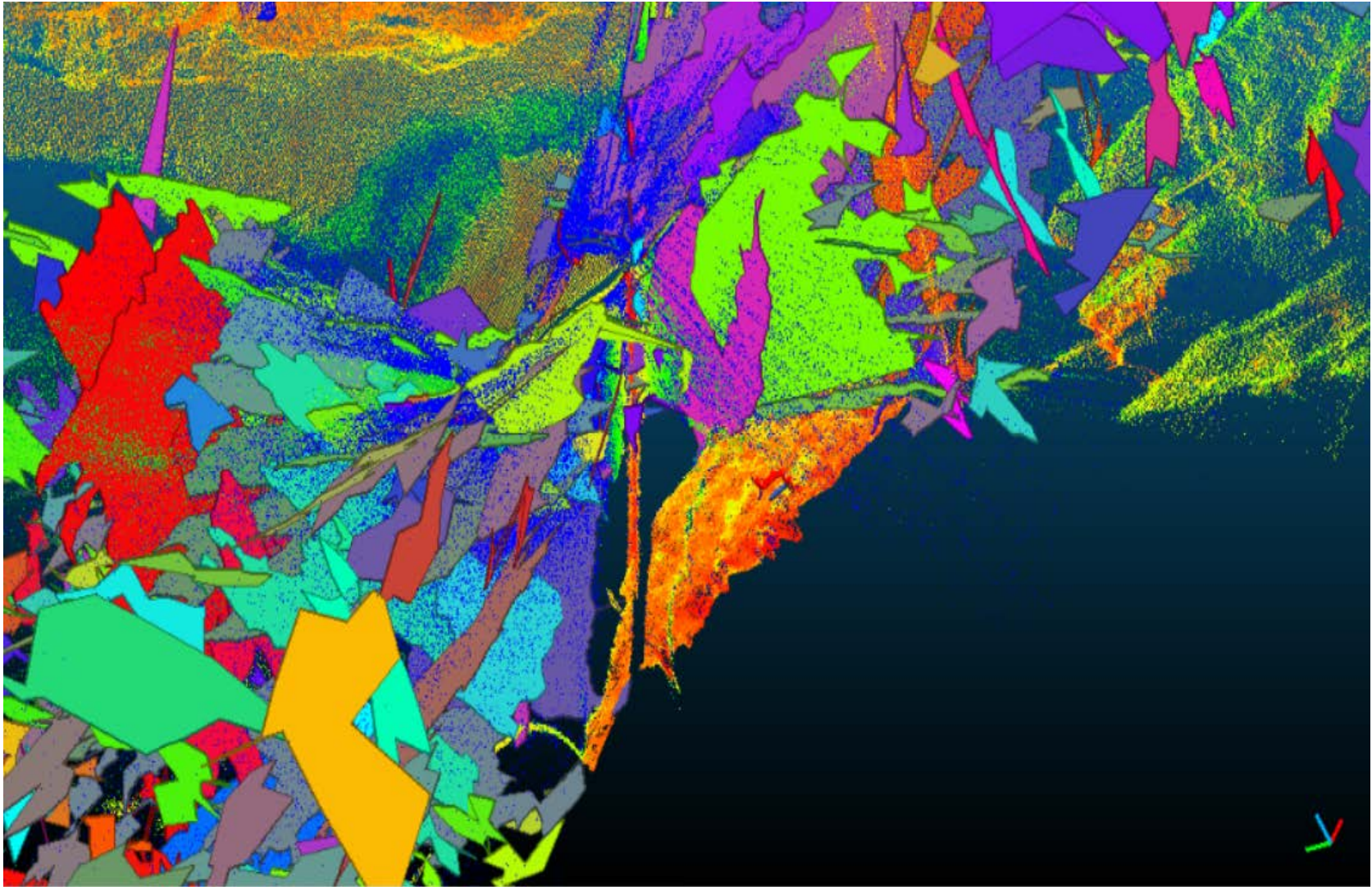


Figure 104. ULS of fluid dynamics from sunlight, flow, PQV, robotic rotation, and suspended sediments presenting imaging backscatter and noise extracted as Kd-tiles.

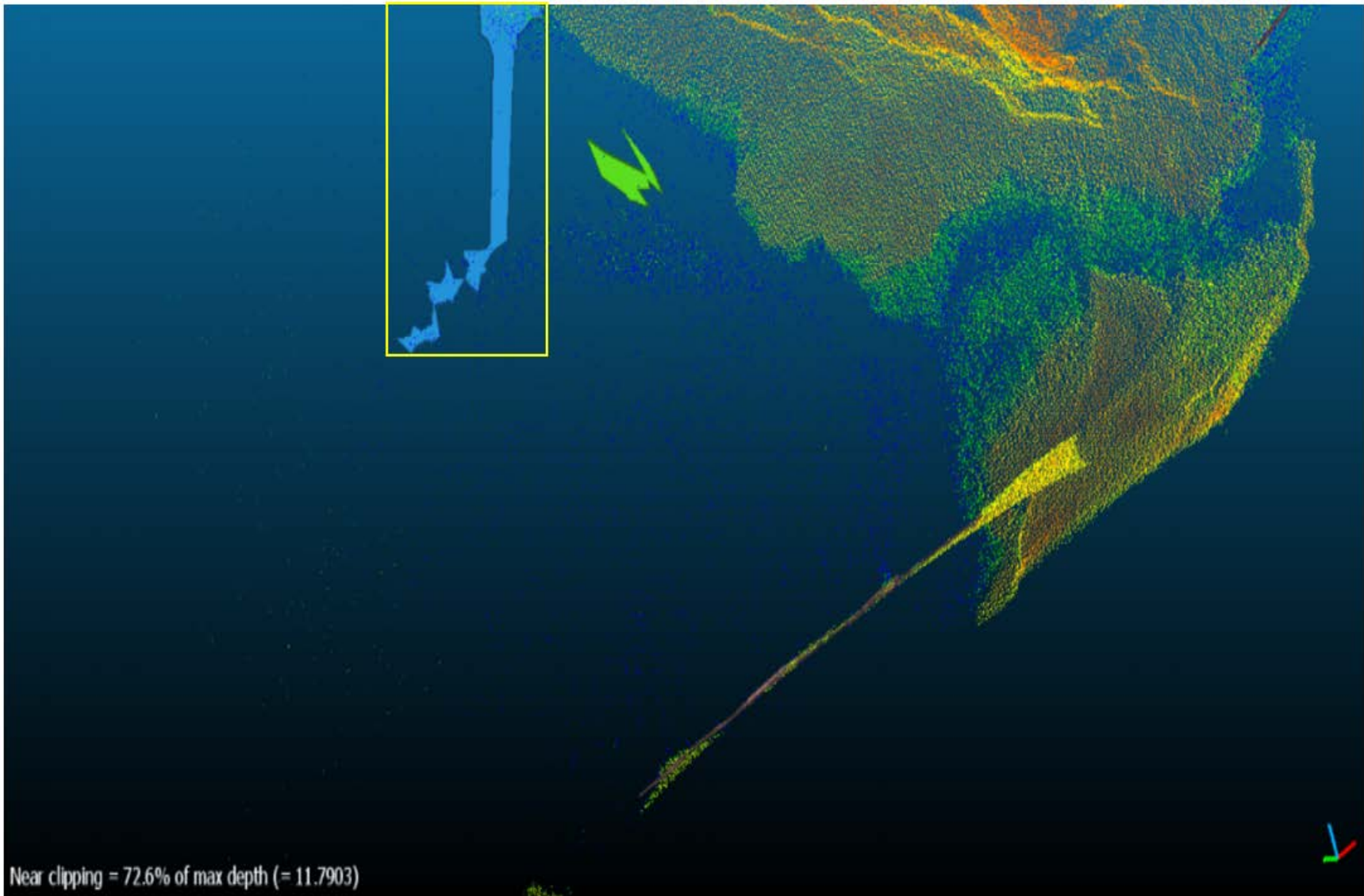


Figure 105. Yellow box presenting planarized facet of naturally occurring photonic quantum vortex from sunlight.

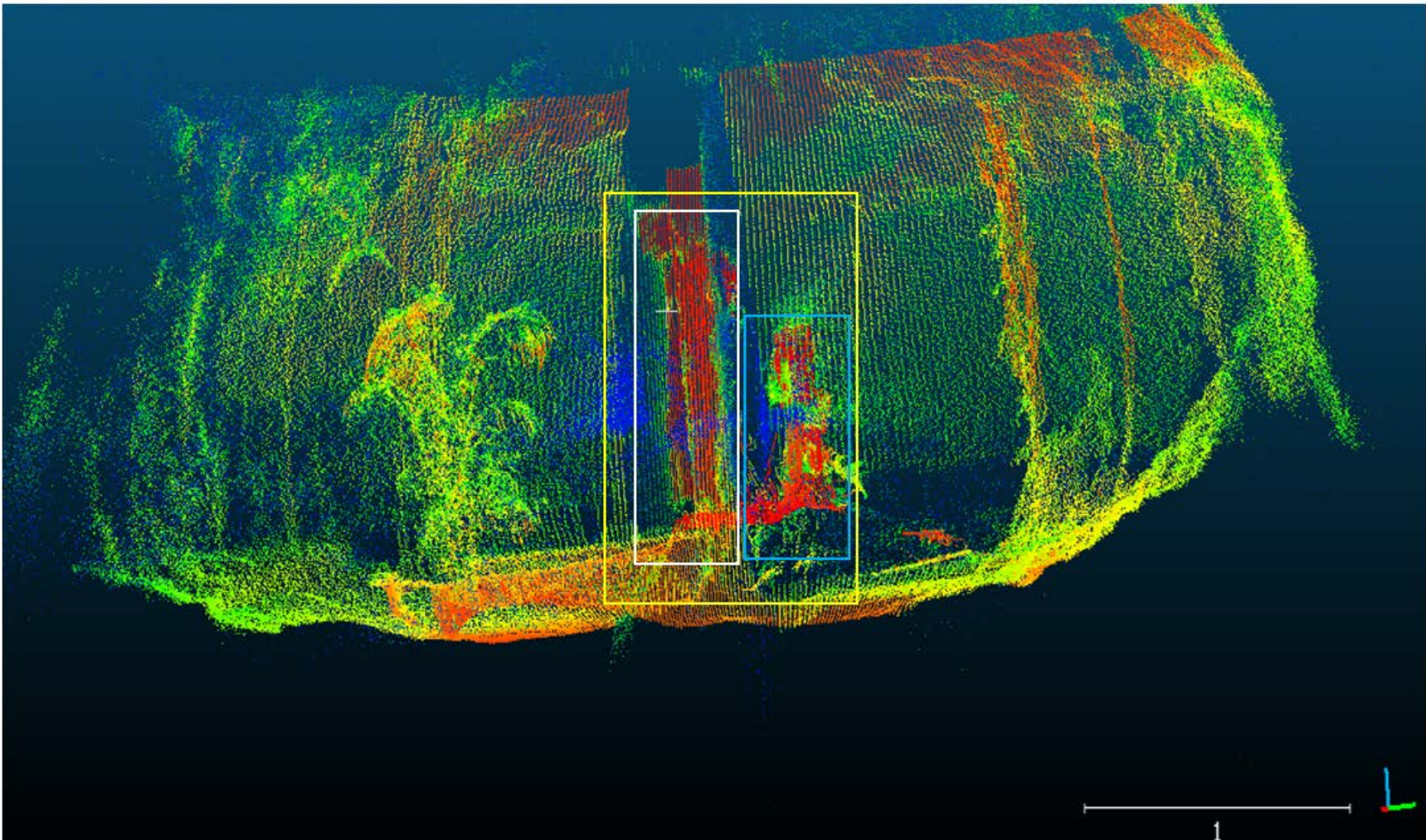


Figure 106. One-of-sixteen imaging perspectives of 16 inverted reflections points, bearing accurate volumetric holonomies from a homothetic core at 1-1.5m resolution. Surveyors silhouettes are located within the in yellow box with QRSS Surveyors Rory OKeefe, standing in the white box, and Stephen Daire sitting in the cyan box. Body silhouettes were collected by the ULS-200 and presented in red points from IR body heat in Cloudcompare viewer.

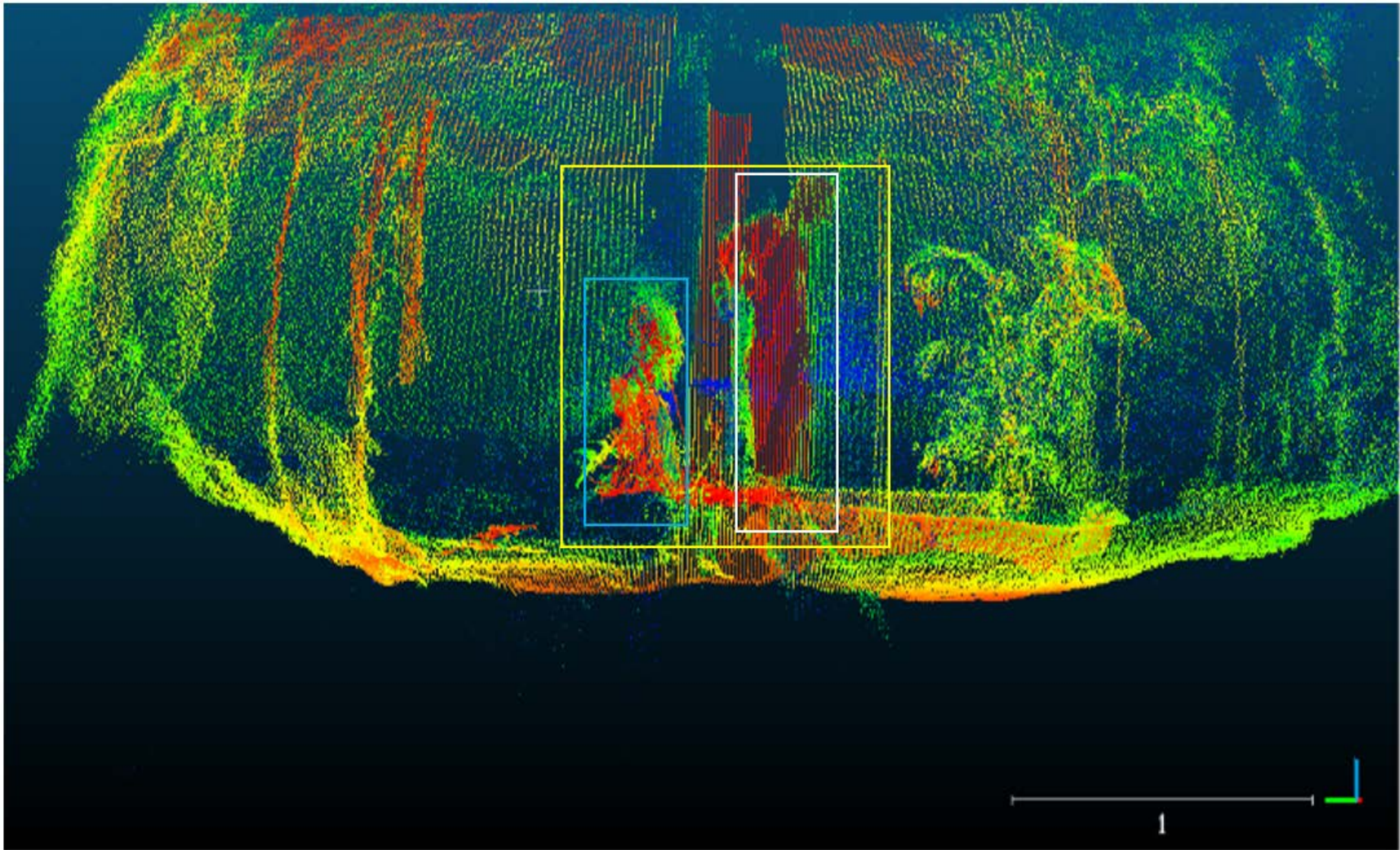


Figure 107. Two of sixteen imaging perspective orientations of 16 holographic points of inverted reflections bearing accurate volumetric holonomies from a homothetic core at 1-1.5m resolution. Surveyors silhouettes are located within the in yellow box with QRSS Surveyors Rory OKeefe, standing in the white box, and Stephen Daire sitting in the cyan box.

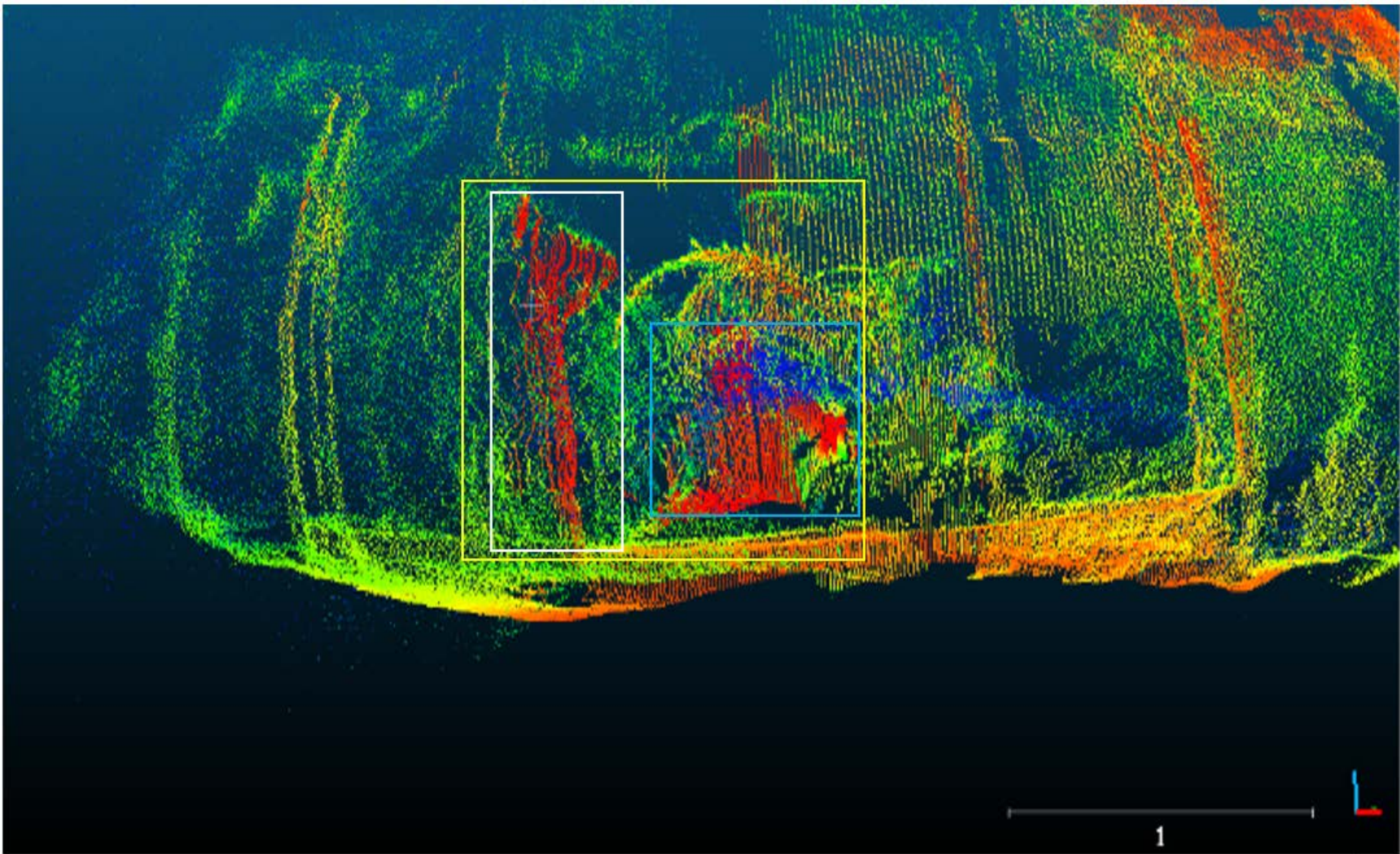


Figure 108. Three of Sixteen imaging perspective orientations of 16 holographic points of inverted reflections bearing accurate volumetric holonomies from a homothetic core at 1-1.5m resolution. Surveyors silhouettes are located within the in yellow box with QRSS Surveyors Rory OKeefe, standing in the white box, and Stephen Daire sitting in the cyan box.

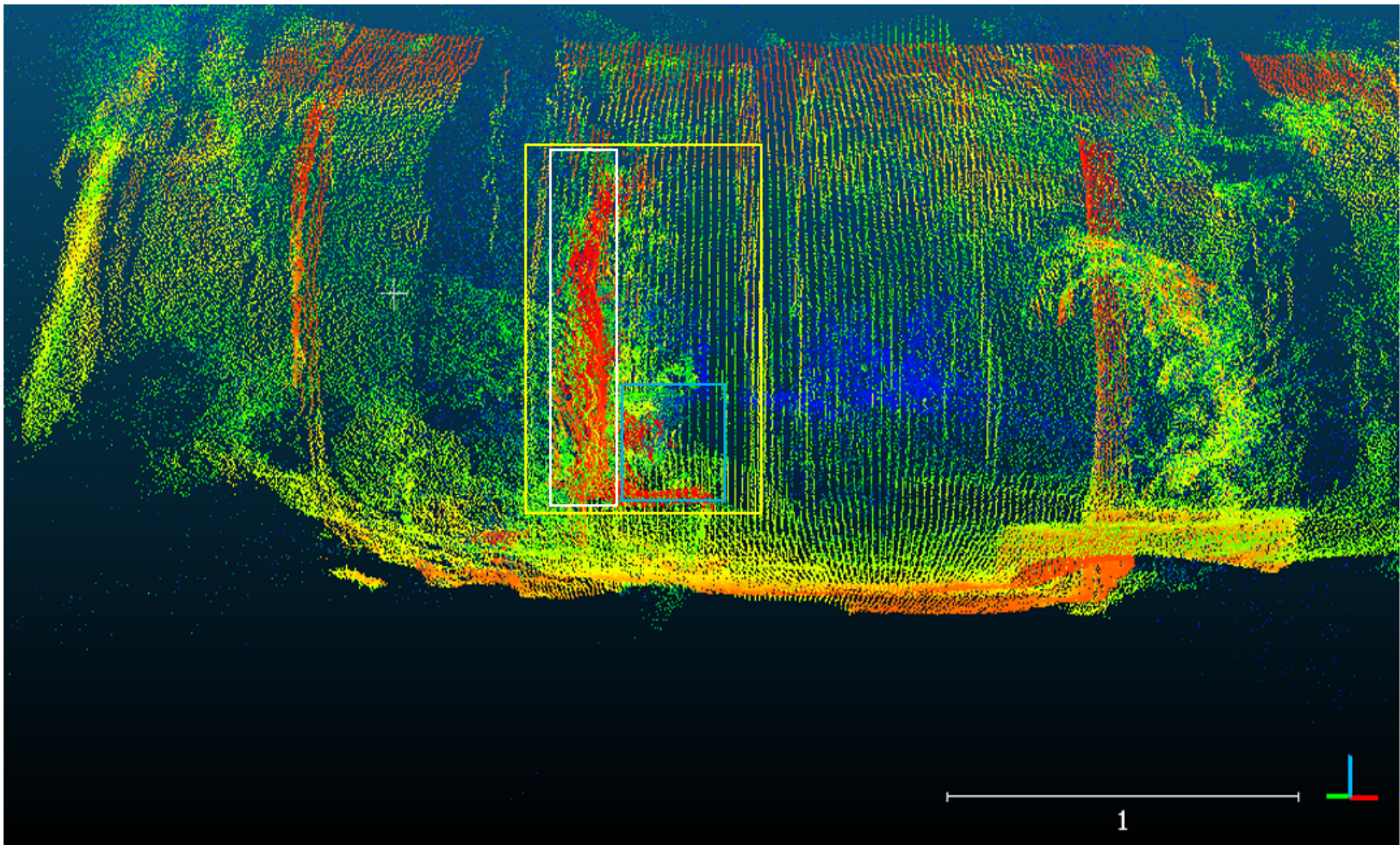


Figure 109. Four of Sixteen imaging perspective orientations of 16 holographic points of inverted reflections bearing accurate volumetric holonomies from a homothetic core at 1-1.5m resolution. Surveyors silhouettes are located within the in yellow box with QRSS Surveyors Rory OKeefe, standing in the white box, and Stephen Daire sitting in the cyan box.

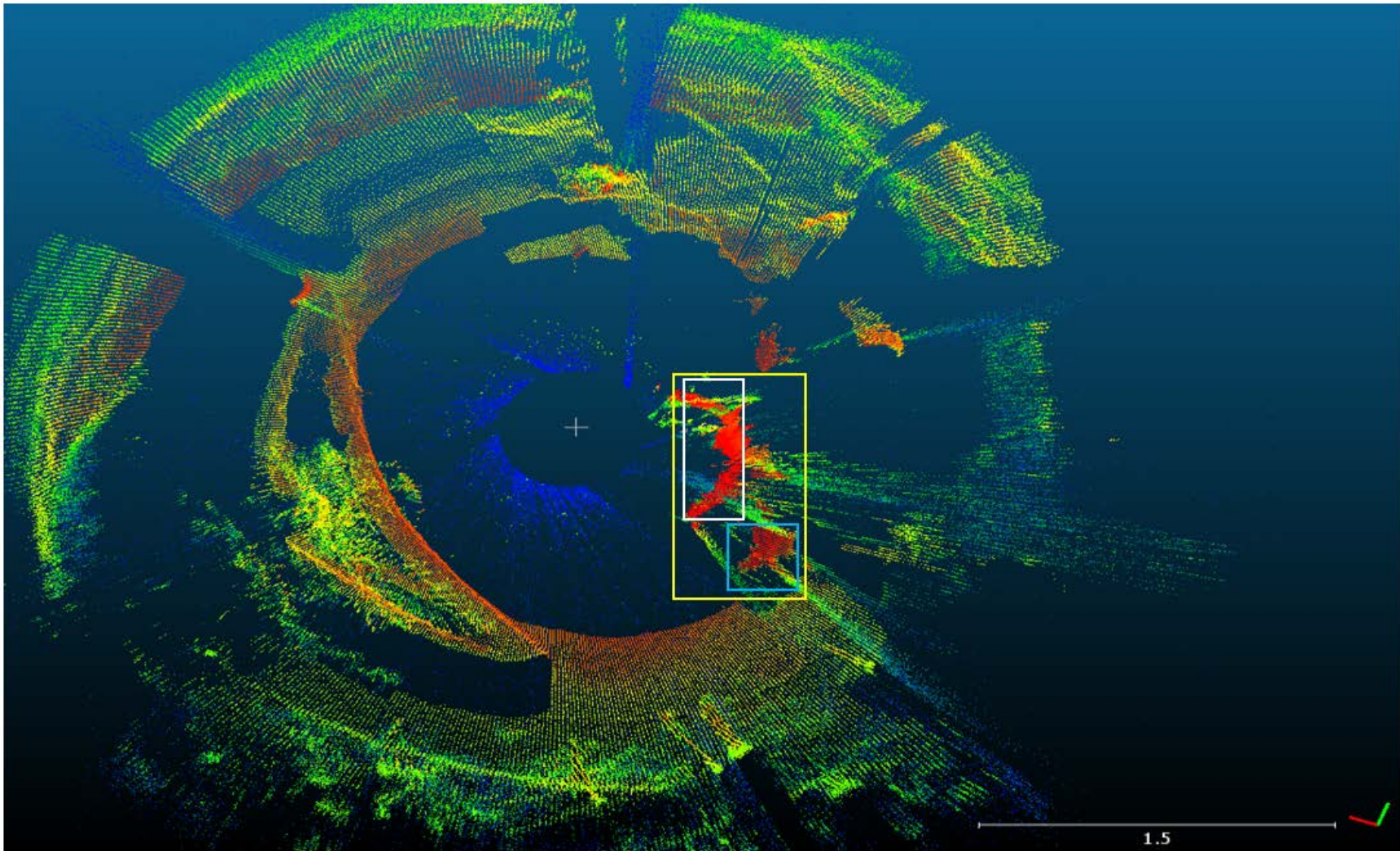


Figure 110. Five of Sixteen imaging perspective orientations of 16 holographic points of inverted reflections bearing accurate volumetric holonomies from a homothetic core at 1-1.5m resolution. Surveyors silhouettes are located within the in yellow box with QRSS Surveyors Rory OKeefe, standing in the white box, and Stephen Daire sitting in the cyan box.

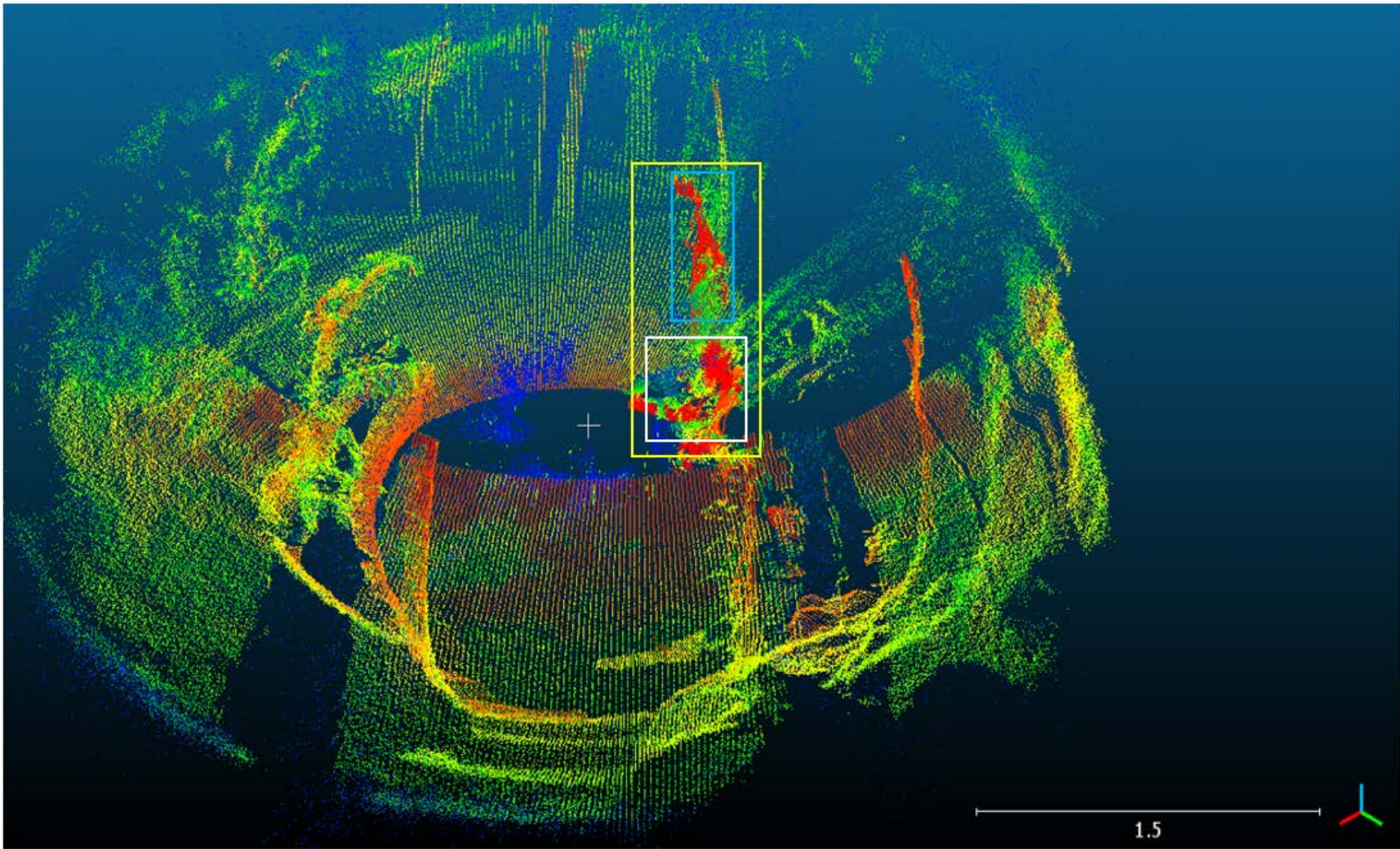


Figure 111. Six of Sixteen imaging perspective orientations of 16 holographic points of inverted reflections bearing accurate volumetric holonomies from a homothetic core at 1-1.5m resolution. Surveyors silhouettes are located within the in yellow box with QRSS Surveyors Rory OKeefe, standing in the white box, and Stephen Daire sitting in the cyan box.

Antanaklasic singularities within holographic models act as 16D reflexive axes on a Mandelbrot set. These facilitate LiDAR omni-angular parallax sampling of object in special orthogonal $SO(n)$ symplectic group $Sp(2n, \mathbb{C})$ of an infinite dimensional Lie $O(\infty)SU(\infty)Sp(\infty)$ group (Seiberg & Witten 1994). Photons are a quasicrystal presenting a vertex-edge starting point while maintaining fractal similarity across a stretched A to Z in a wave-spin function. Dissimilar points disassociate, maintaining RMT fibrational axioms of choice from semiprime A' to Z' on alternative orbifold wavefields, Figure 112. PQVS harmonized viscous fibrational BQP multiphasic topological index orbifold. Centimeter hashmarks represent one-time scale, while 1/16-inch dots represent imaginary time, cotangent linear geodesics present quantum gravitational lensing as convergent fore-scattering and divergent backscattering based on insignificant mass bearing momentum at the speed of light. ULS presents a perfectly inverted reflection of all the scanned area allowing users to phase shift from one opposing mode edge to the other while maintaining volumetric spatial dataset accuracy through a photonic quasiperiodic crystal vacuum orbifold (Shechtman 1988; Cahn, Schechtman, and Gratias 1986; Levine & Steinhardt 1984; Mackay 1982). Holonomic imaging points are reflexively transliterative axes that maintain relative positions in motion, from an extruded homothetic centroid. ULS geometric volumetric imaging via photonic-phononic spin-wave function maintains transformation accuracy of the contextual setting, while providing dynamic edge detection. In another perspective, LiDAR photons are akin to water balloons with a (photonic quasicrystal) balloon extending, twisting, bending, colliding, ricocheting, overtaking, and crystallizing within a (vacuum space orbifold). Both orbifolds sustain orientation through reflections of one another based on the space-filling central photonic balloon allowing for topological folding of the vacuum with dynamic DTFE quasitriangulation at a given timespace slice providing QCED

metrics. Automorphic reflections viewed away from the central vacuum orbifold mirror, allowing the model to shift through inverted reflections of poles to the other side of the model. These datasets prompted a hand drawn informal calibration model, due a power outage, which relates to Figures 15, 99, 112 and through 117, and the Hadwiger Conjecture.

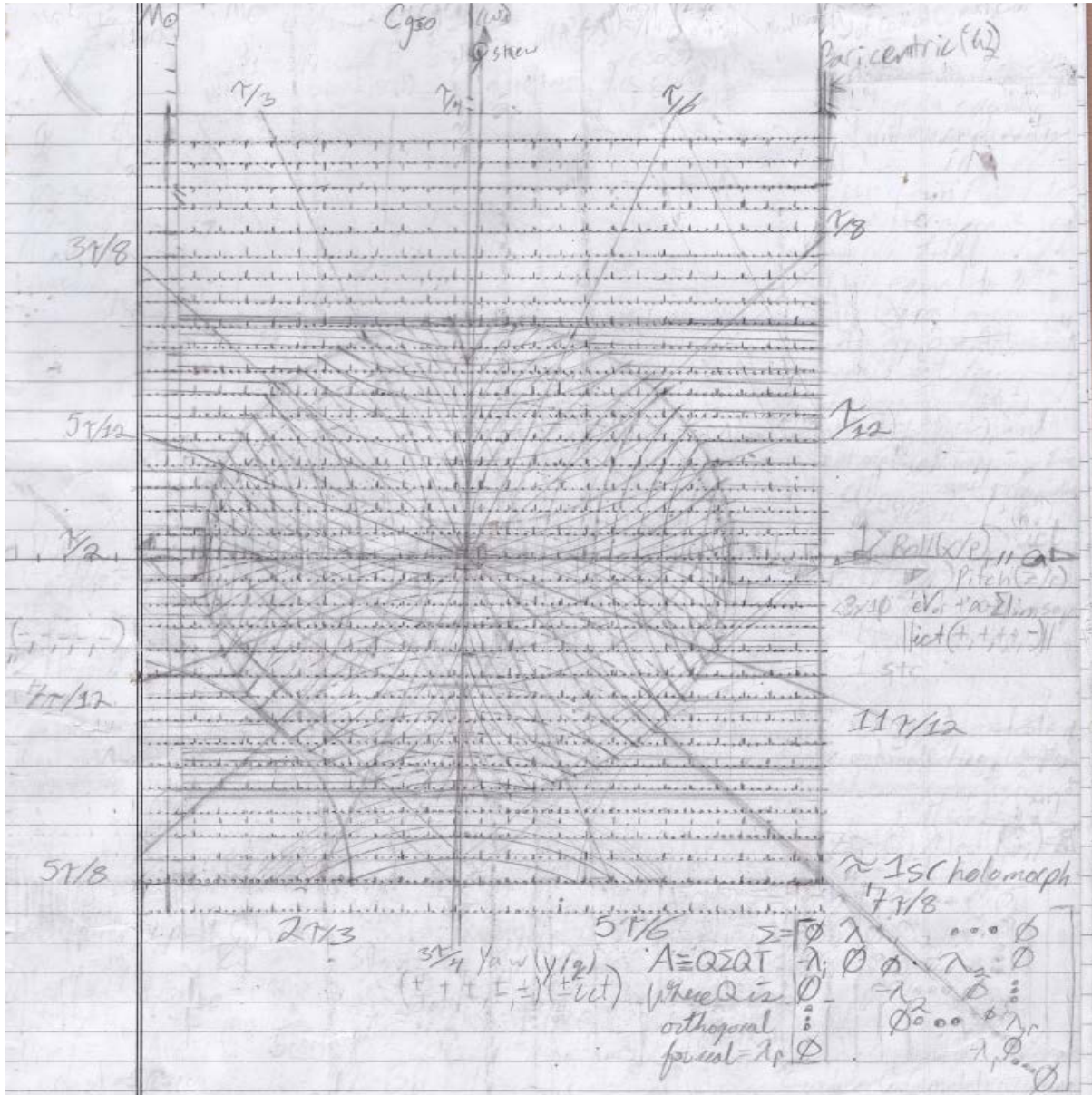


Figure 112. Informal hand drawn fieldnotes diagram, due power outage, of an 16D omni-angular parallax of a photonic quasiperiodic crystal in a Moduli Fields of Vacua Orbifold.

The Hadwiger Conjecture is a paradox in the number of strictly smaller homothetic copies of a convex body that may be needed to cover it, beyond a 2D spatial topology. A photonic quasicrystal with a homothetic center, center of similarity, is a geometric point from which at least two similar figures can be seen as a dilations or contractions of one another (Shechtman 1988). If the center is external, the two figures are directly similar to one another with similar angular rotational perspectives, if the center is internal, the two figures are scaled mirror images of one another with opposite perspective angles. Angular similarity in terms of holonomy is a curvilinear connection on a smooth manifold measuring a failed topological parallel transport around closed loops, if the center is internal. In terms of illumination the conjecture can be described as, a body is only illuminated if, and only if, for every single body boundary point there is at least one absorbing black or illuminating white radiating body separated from the body of interest by all intersecting tangential planes at that point (Jenkins 1997; Fetter & Walecka 2003; Mattuck 1976). Therefore, a facet can be illuminated by a minimum of two bodies, with edges and vertices requiring illumination or absorption for full effectiveness as the positive and contrapositive arguments.

4.4. Findings & Claims

Considering the positive Hadwiger as a harmonically rotating black body, and the contrapositive for a white body, both would require an equal number of smaller copies of the body to be totally illuminated or obfuscated, relating to the color sphere model presented in Figures 15 and 112. Figure 113 is the culmination of figures 15 and 112 in as a harmonically smoothed, multiresolution, multiphasic quantum non-linear optic index stemmed from observations of viscous fluid dynamics in the cave conduits by slow-motion video. The flow of

water through the caves bears a piezoelectric electric current between the fluid and surface, causing a natural cyclotron dynamo. The natural aphotic, overloaded porous, viscous fluid cave environment presents oscillating cyclotronic field radiation in a closed space leading to computationally complex harmonized combinatorial geometric interactions with quantum dynamics. These dynamics observed in slow-motion video operate in terms of non-uniform hyperspatial orbifold center (omnisnub icosahedral honeycomb) operating coherently in a clopen (closed-open set) spatially fibrational manifold with types I, II, and III presenting symmetric products from an asymmetric body presenting invariance, entanglement, and an axiom of choice.

This conclusion was developed from observations of expected ULS induced optic PQV Slipstream (PQVS) derived torus and leminscate ULS PQVS and QTK from a novel perspective. Figure 113 presents a conceptual viscous manifold with a photonic quasicrystal presenting a LiDAR pulse. The informal and semiformal models present novel theoretical insights, that begin to rectify and enunciate disparities and gaps within, between, and among quantum and relativistic physics particle-wave duality which related to RMT, OTK, TPU, and PQVS (Andreev et al 1996). This extended Poincare spheroid and extended Hilbert space provides possible explanations and new questions for scientific development in spatial sciences and topological mathematics as scale increases and decreases incrementally amplify in resultant eight set of triplet hexadecimals that relate to dodecaphonic serialism in 2nd harmonic microscopy and ULS spectrometry while utilizing the index.

Dodecaphonic serialism was first composed and performed by Arnold Schoenberg in 18744 – 1951 in the 2nd Viennese School and utilizes continuous 12 note chromatic scales, with no preferential key or note. Dodecaphonic Serialized Harmonic – I, II, III alto, treble, bass (likely extending to contra bass etc.) - seems to be related to a overtone harmonization field for LiDAR

indexing as it transliterates wave-spin function energy through selectively varying tonal phase range in polynomial instrument arrangements with each instrument playing at a different time or tempo. This model permits useful operands in photonic and phononic applied and theoretical research in aphotic aquatic remote sensing environments. 16 harmonically relative, inversely codominant rotational and fibrational axes of 1: 0 – 360, ... 16: 0 – 360° occur along each of τ pole along the surface of the orbifolds with each maintaining differential holonomic translations from a homothetic centroid over various changes and transitions calculable via Euler angles and DTFE. Table 6 presents the 16 and the potential LiDAR dynamics related to them. The 16 axes related to axis 1) = τ = Roll - speed of light, axis 2) as $\tau/12$ = Time - $\pm i$, axis 3) as $\tau/8$ = Lift, axis 4) as $\tau/6$ = Skew, axis 5) as $\tau/4$ = Polarity, axis 6) as $\tau/3$ = Shear, axis 7) as $3\tau/8$ = Torque borne torsion, axis 8) as $5\tau/12$ = Devil's Stair Case Fractal Chaos, axis 9) as $\tau/2$ = Harmonic Oscillation, axis 10) as $7\tau/12$ = Density – 4D volumetric center of gravity mass, axis 11) as $5\tau/8$ = Center of Gravity, axis 12) as $2\tau/3$ = Helicity or Chirality, axis 13) as $3\tau/4$ = Yaw, axis 14) as $5\tau/6$ = Gravity Solar Mass, axis 15) as $7\tau/8$ = Angular Fractal wavenumber, and axis 16) as $11\tau/12$ = Pitch.

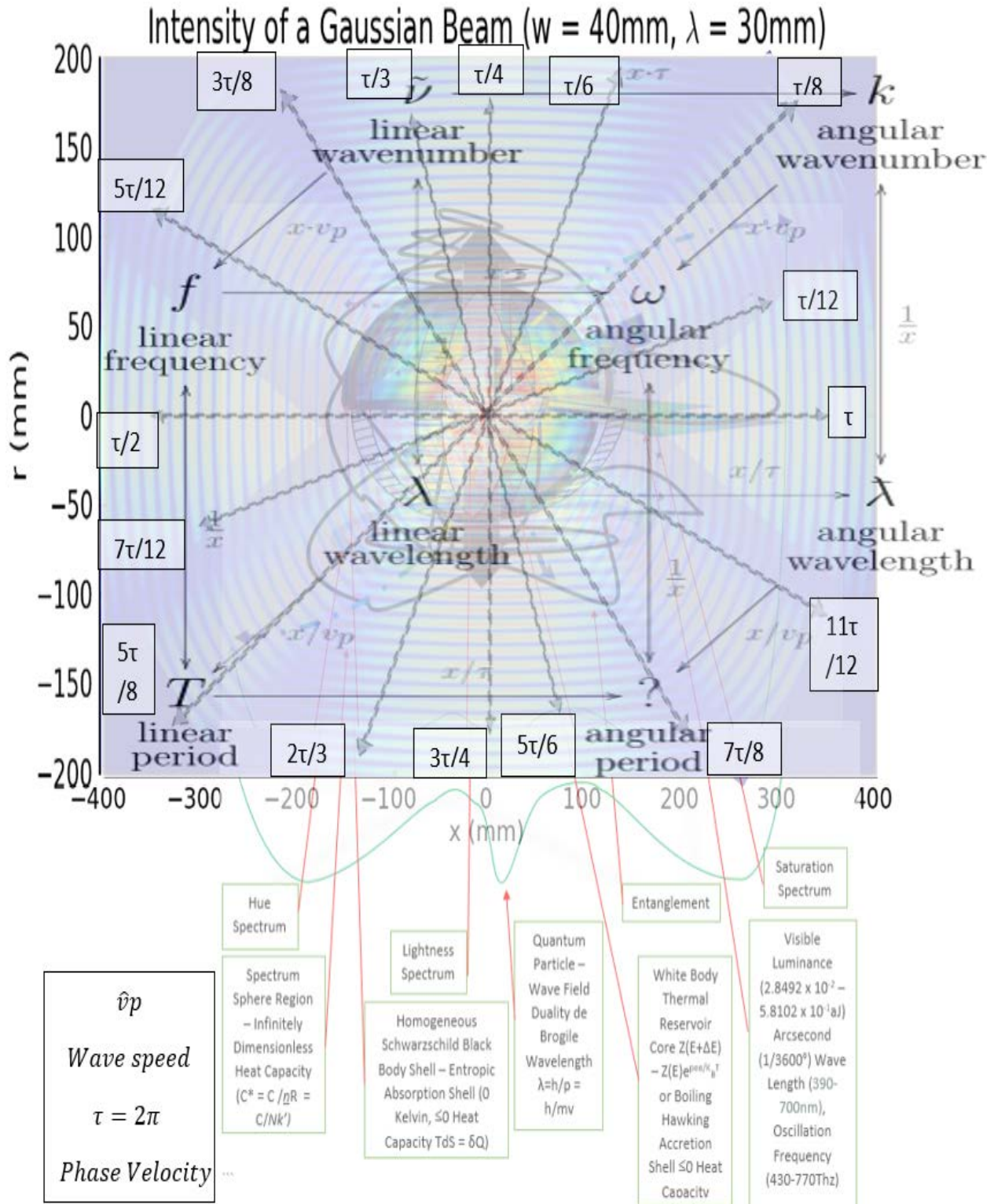


Figure 113. Semiformal Multiresolution-Multiphasic QCED Quasicrystal-Moduli Fields of Vacua LiDAR Indicatrix

Table 5: Photonic Quasicrystal - Vacua Unit Orbifold QCED LiDAR Calibration & DTFE Quasi-Triangulation Reference					
16, 0-360° 0 Rotation Axes	Reference Pole	Variable Dynamics	Force Equation & Details	Elementary & Subatomic Particles	Emergent Phenomena
1	τ or 0	Velocity	$\Delta n \Delta \phi > 1$ or $E = hv$ at velocity = (c^2) with frequency independent spin angular momentum vector p , wave vector k ($k = k = \tau/\lambda$) as $p = \hbar k = \frac{hv}{c} = h/\lambda$	Photon-Antiphoton	Combinatorial Quasicrystal Space Filling induced RMT
2	$\tau/12$	Infinite Eigen-Value Imaginary Time	Observer projected objective normalization: $ \pm it $	Sterile Neutrino	Indistinguishable Unreactive Quasiparticle or Collective Excitation
3	$\tau/8$	Curvilinear Lift over Plank Length, transporting energy not electric charge	$E_p = \hbar \sqrt{ne^2/me_0} = \hbar \omega_k$	Plasmon	Collective Excitation
4	$\tau/6$	QCD Gauge Symmetric Special Unitary Group SU(3) Surface Ablation Skewing	Color charge & Super Position: $(r\bar{b} + b\bar{r})/\sqrt{2}$ Color Singlet States: $(r\bar{r} + b\bar{b} + g\bar{g})/\sqrt{3}$ Gell-Mann Matrix Gluon Color Octet: $(r\bar{b} + b\bar{r})/\sqrt{2}$ - $i(r\bar{b} - b\bar{r})/\sqrt{2}$ $(r\bar{g} + g\bar{r})/\sqrt{2}$ - $i(r\bar{g} - g\bar{r})/\sqrt{2}$	Gluon	Asymptotic Freedom as quark distances increase their binding force increases, as distances reduce their binding forces reduces.

			$(b\bar{g} + g\bar{b})/\sqrt{2}$ - $i(b\bar{g} + g\bar{b})/\sqrt{2}$ $(r\bar{r} - b\bar{b})/\sqrt{2}$ $(r\bar{r} + b\bar{b} - 2g\bar{g})/\sqrt{6}$		
5	$\tau/4$	Polarity bearing a lattice momentum with defined energy.	$M(T) = M_0 [1 - (T/T_C)^{3/2}]$	Magnon	Collective Excitation electron quasiparticle quantized wave.
6	$\tau/3$	Shearing QED Synchrotronic Deceleration Emissivity	<p>Non-Relativistic Accelerated Power Radiation:</p> $a = \frac{1}{m} \frac{dp}{d\tau} = \frac{1}{m} \gamma \frac{d(\gamma m v)}{dt}$ $= \gamma^2 \frac{dv}{dt} = \gamma^2 \frac{v^2}{r}$ <p>Non-Relativistic Reimann Radiative Power Deceleration:</p> $\gamma = \sum_{m=2}^{\infty} (-1)^m \frac{\zeta(m)}{m} =$ $\ln\left(\frac{4}{\pi}\right) + \sum_{m=2}^{\infty} (-1)^m \frac{\zeta(m)}{2^{m-1}m}$	Electrons	Non-Thermal Dynamic Photoelastic Synchrotronic Radiation extending translations of the Euler-Mascheroni Constant from Brillouin-Wigner Scattering providing Delaunay tessellation field estimator (DTFE) operands.
7	$3\tau/8$	Phononic Cloud Dielectric Crystalline Torque	$\Gamma(\Omega)$ $\propto -Im \frac{Im\Sigma(\Omega)}{[\Omega - \omega_c - Re\Sigma(\Omega)]^2 + [Im\Sigma(\Omega)]^2}$	Polaron	Quasiparticle electronic mobility via phonon cloud

					induced atomic dielectric crystalline disequilibria increasing donor electron effective mass preventing acceptor absorption.
8	$5\tau/12$	Fractalized Productive - Destructive Chaos	Mode Locking Devil's Staircase: $\theta_{n+1} = \theta_n + \Omega - \frac{K}{\tau} \sin(\tau\theta_n)$	Anyon	Observable Indistinguishable 2D phase shifting Quasiparticle or Collective Excitation classified as abelian or non-abelian. Observations on abelian anyons show they play a role in fractional quantum Hall effect, non-abelian have not be detected.
9	$\tau/2$	Serialized Quantum Harmonic Oscillation	Zero-point energy quantum harmonic oscillator: $E_n = \left(\frac{1}{2} + n\right) \hbar\omega_k$;	Phonon	Combinatorial Harmonic Quasicrystal Excitation induced by

			<p>Quantum harmonic oscillator energy levels: $\left(\frac{1}{2}\right) \bar{h}\omega_k, \left(\frac{3}{2}\right) \bar{h}\omega_k, \left(\frac{5}{2}\right) \bar{h}\omega_k$ Crystal Momentum: $K = 2n\pi/a$ Thermodynamics: $n(\omega_{k,s}) = \frac{1}{\exp\left(\frac{\bar{h}\omega_{k,s}}{k_B T}\right) - 1}$</p>		<p>sound amplification by stimulated emission of radiation (SASER) phonoelastic energy transfer and RMT automorphy.</p>
10	$7\tau/12$	Density Time Slice	<p>Electromagnetic Dipole Moment: $\mu = g \frac{Q\bar{h}}{4m}$ Lepton Universality: $\frac{\tau_\tau/\tau_\mu}{\Gamma(\mu^- e^- + \bar{\nu}_e + \nu_\mu)} (m_\tau / m_\tau)^5$</p>	Leptons	<p>Lepton Universality Flavor Independence from committed boson interaction.</p>
11	$5\tau/8$	Radiationless QCED Exciton Well Confinement Yaw	<p>Förster/fluorescence resonance energy transfer (FRET) QCED yield: $E = 1 - \tau'_D/\tau_D$ Photobleaching Donor-Acceptor Coupling Decay Constants: $E = 1 - \tau_{pb}/\tau'_{pb}$</p>	Wannier-Mott Charge Transfer Excitons	<p>Electrically Neutral electronic energy transfer from a Combinatorial Quasiprinciple Bound molecular State of an electron and electron hole.</p>
12	$2\tau/3$	4D Tensor Scalar-Vector Baryogenic Gravitational Mass	Gell-Mann-Nishijima Quark Content Charge Expression Formula:	Baryon-antibaryon	Composite Fermionic Quasiparticle

			$Q = \frac{2}{3} [(n_u - n_{\bar{u}}) + (n_c - n_{\bar{c}}) + (n_t - n_{\bar{t}})] - 1/3 [(n_d - n_{\bar{d}}) + (n_s - n_{\bar{s}}) + (n_b - n_{\bar{b}})]$ <p>Parity Conservation (<i>P</i>-Symmetry): $P = (-1)^L$, Quantum Flavors: Strangeness: $S = -(n_s - n_{\bar{s}})$, Charm: $C = +(n_c - n_{\bar{c}})$, Bottomness: $B' = -(n_b - n_{\bar{b}})$, Topness: $T = +(n_t - n_{\bar{t}})$,</p>		with an odd valence number of quarks >3.
13	3τ/4	Chirality or Handedness	Higgs Gauge Elementary Particle Chirality Reduction: $(1, 3, 1)_2 \oplus (1, 1, 3)_2$	Higgs Boson	Collective Excitation
14	5τ/6	Seiberg-Witten Active Holomorphic Curvature Dielectric Gravitational Instantons	Seiberg-Witten QCED Significant Prepotential (Metric of the Moduli Space Vacua) Instanton Estimation & Counting: $Z(a; \varepsilon_1, \varepsilon_2, \Lambda)$ $= \exp(-1 / \varepsilon_1 \varepsilon_2 (\mathcal{F}(a; \Lambda) + \mathcal{O}(\varepsilon_1, \varepsilon_2)))$	Viscous Graviton	A hypothetical elementary particle mediating gravitomagnetic massless, vibrating, viscous, string state that leaves QTF incomplete due to

					mathematical limitations on general relativity renormalization.
15	$7\tau/8$	Cacophonous Induced Self-organized criticality (SOC) (e. g. attractor) Angular Wave Number	Double-QED-Well Tunneling Potential Energy of 0: $\phi_c(\tau) = \frac{m}{g} \tanh[m(\tau - \tau_0)]$ Euclidean Time, $\tau = it'$ Explicit Asymptotically Degenerate Harmonized Double-QCED-Well Potentials: $\frac{d^2y(z)}{dz^2} [E - V(z)]y(z) = 0$	Instanton	Supersymmetric Quantum field theorem (QTF) finite, non-zero action Pseudoparticle facilitating quantum tunneling in Yang-ills Theory, Einstein-Rosen Brides, and Penrose time-like wormholes PQVS phase transition.
16	$11\tau/12$	Dipole or Monopole Pitch	Mass: $\frac{m^*}{m} \approx 1 + \frac{\alpha}{6} + 0.0236\alpha^2,$ Weak Coupling: $\frac{\Delta E}{\hbar\omega} \approx -\alpha - 0.015919622\alpha^2$	Polariton	Combinatorial Quasiparticle of Photon and Exciton

The viscous Vacua Orbit-Fields- 3D Apollonian Gasket model presented in Figure 114 and its DTFE quasi-triangulation dynamics fits a n-th dimensional polynomial packing continuum with a serialized dodecaphonically harmonic continuous fluctuating bridle point at radius of infinity. This presents an inverse, or contrapositive, solution to the Hadwiger conjecture on combinatorial geometry and graph theory. Figure 114 promotes a thought experiment on the Hadwiger conjecture through an extension to Kepler's Dodecahedral conjecture by considering a rolling, spinning, malleable photonic quasicrystal on a photonically consumptive interfacing viscous fluid surface illuminating all surface areas completely via a rationally based quasiperiodic crystalline lattice projecting an optimal photon-phonon equilibrium on edges and surfaces (Weisstein a, b, c, d, e; Borkovec et al. 1993; Conway & Sloane 1999; Fetter and Walecka 1971). This Orbifold Vacua – Apollonian Gasket model relates to Figure 15, 113, and 114 for determining QCED entanglement, radiative facets, and chromatic edges in physical sciences based on objective TRN on the sphere and perspective deformational edge effects via environmentally emergent factors.

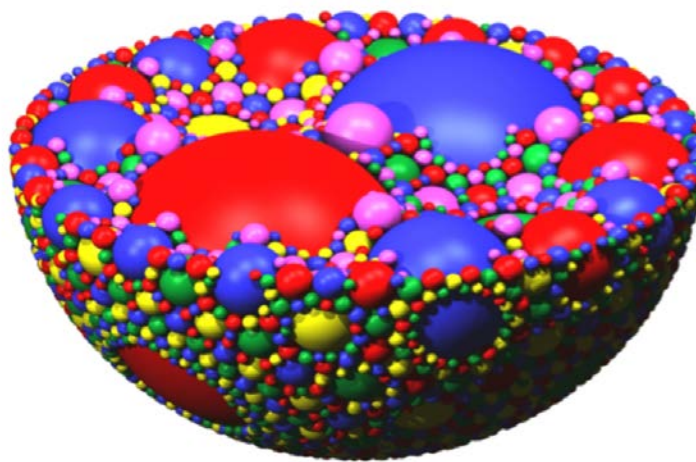


Figure 114. 3D Apollonian Sphere Packing (Borkovec et al. 1993).

Figure 115 presents a geometric snark-bridge diagram of the quasicrystal core which is a non-uniform, vertex transitive order 3 tetrahedrally semi-partial diminishing $\text{spd}\{3, 5, 3\}$ omnibus icosahedral honeycomb (Andrews and Bradshaw 2004). Figure 113 shell is a consumptive vacuum series space, the vacuum space is completely filled with subatomic particles extending from an antiphotonic-photonic quasicrystal akin to Figure 115 (Swartzendruber, L.; Shechtman, D.; Bendersky 1985).

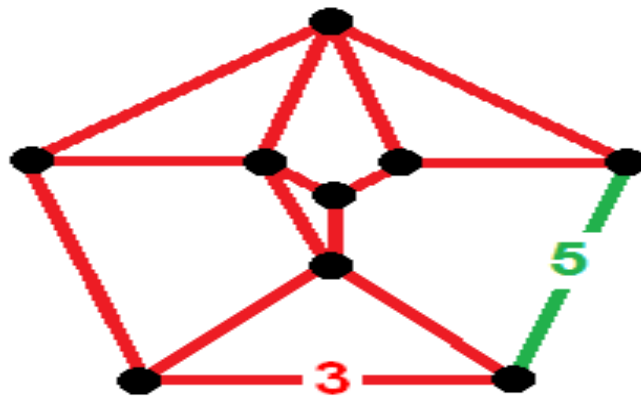


Figure 115. Snark graph of a vertex transitive $\text{spd}\{3, 5, 3\}$ with snub dodecahedron, octahedron, and tetrahedron that cannot be produced via uniformity (Ruen, Tom. 2013).

Figure 116 diagrams exterior of Figure 115 these model dynamics via a quasi-triangulable Poincare Sphere which correlates it as a photonic indicatrix with a harmonized general relativistic, quantum loop, Kaluza-Klien, and M-theory in a contextual setting related to Figures 15, 113, and 114. Operations of space, time, gravity, energy, spin, resistance, and inversion can each to be selected for the focus of a study with transition of the infinity bridle point at the omnibus central vertex to any set variable of interest for DTFE assessment of each subsequent sphere for topological accuracy assessments in lidar, spatial sciences, and other applications. This quasicrystal produces a deterministic affine holonomy with an axiom of choice

as an extended Hilbert Einstein-Podolsky-Rosen (EPR) probabilistic space $SO(48) \times E_{tp} \times E_{p \pm I}$ with $\pm i\tau$, standing for the Reimaniann zeta function. This $sp\{3, 5, 3\}$ omnibus icosahedral honeycomb is a face-centered, semi-symmetric, hexagonally clopen face-packed, holonomic photonic quasicrystal related to a homothetic center. The photonic quasicrystal centroid presents a recursive symmetric, asymmetrical inversion, oscillation, and recursions related to resonant QCED and Random (RMT based on quasiperiodic lattice growth, destruction, and deformation). As the photonic quasiperiodic crystal rolls along time at the speed of light on a $43/\tau = \pi$ radius sphere, an imaginary time-like infinity sphere provides ordered and chaotic systems to form fibrational continuity along quasiperiodic RMT resonance. The quasicrystal presents 16D kissing surfaces in sphered packed viscous space.

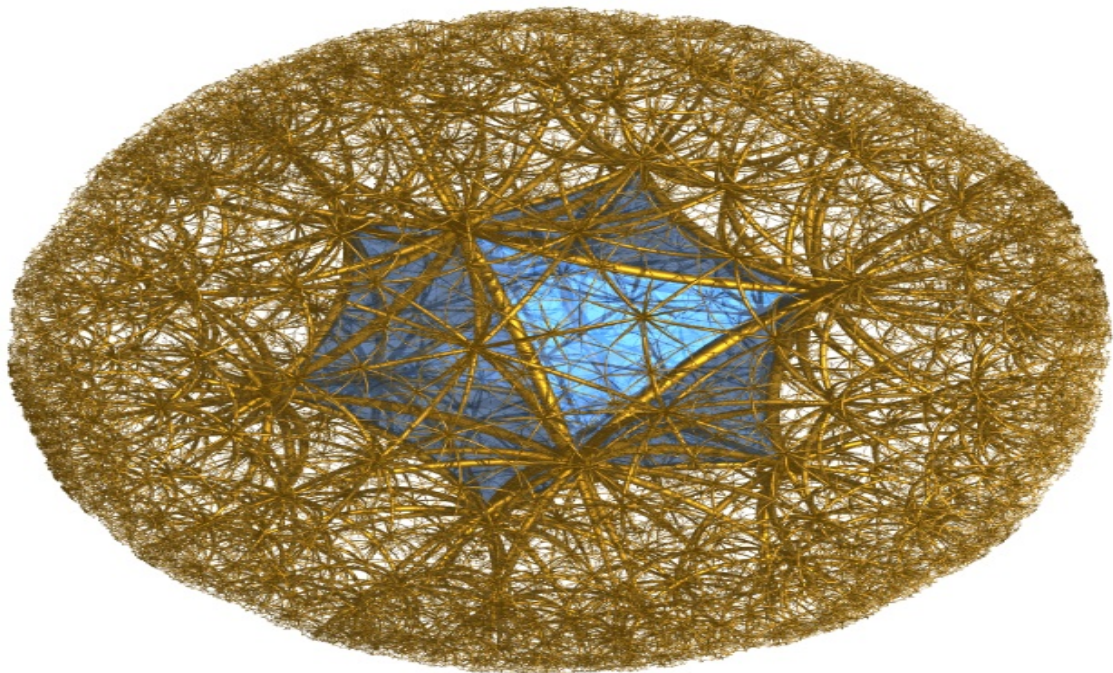


Figure 116. Hyperbolic Poincaré antiphotonic-photonic quasicrystal lattice spheroid with a $sp\{3, 5, 3\}$ centroid facilitating the orbifold indicatrix QCED DTFE & RMT (Rocchini, 2007).

As the quasiperiodic photonic crystal rolls or transits spacetime at light speed, 2π or τ steradian $\approx \theta = 2\pi rh$ spins propagate positive and negative eigen value QED emissions spherically with ejecta extending from all relative 45° angles related to PT symmetry, Brillouin Scattering, and Brillouin Zones (Znojil, M. 2001). $43 / 2\pi = \pi$ rotations of the Semiformal index or roughly equates as extending $43 / \tau = \tau/2 \approx 1$ spat $\sim 1.057 \times 10^{-4}$ light years from the subtended photonic quasicrystal homothetic center LiDAR system or the Sun . This produces a quasi-symmetric (symmetric-asymmetric), positive, and contrapositive holonomic transformation along the orbifolds 8-dimensions, with 16 poles of Ehresmann bridgeless fibrational turbulence harmonized in 4-dimensions within RMT, nth-dimensional sphere-packed Apollonian gasket. ULS pulse detections in space, time, and (tensor, scalar, vector) gravity related to hypergeometry and QED that the sphere models require helicity, attraction, repulsion, reflection, inversion, and ricochet calibrations.

This viscous space relates to an extended Fundamental Domain Voronoi Tessellation Diagram (VTD) presenting the sixteen seed force dynamics effecting the photonic quasicrystal transit through spacetime along an Einstein-Rosen Bridge in a Penrose diagram for time-like wormholes. Quantum wells in the time-like past and future prevent non-light speed information transfer with quasicrystal ricochet propagating curvilinear timespace. Figure 117 presents a Penrose 2D diagram which represents causal relations between different vectors in spacetime. It is an extension of a Minkowski diagram, time is represented in a vertical dimension, a horizontal spatial dimension, and quantum rays as slanted lines at *PT-symmetric* angle of 45° .

The Penrose diagram metric is equivalent to the actual metric in spacetime via a conformal factor chosen such that infinite spacetime is transformed into a finite size. Spherically symmetric spacetimes correspond to 2-dimensional diagrams at every point of the sphere and are

presented as extended dimensions in the QCED conceptual model. Figure 113 coupled with diagrams 116 and 117 each photon as it follows the first in a fractal curvilinear wavelet inducing QED dynamics between the wave peaks and trough via a potentially excessively dense photonic sterile neutrino, an Einstein-Rosen bridge into positive resonant voxelgraphic (volumized pixel fluid-like tensor-scalar-vector gravity) Hawking radiated space through a negative imaginary time. A reciprocally inverse dissonant chaotic firewall exists at the Penrose-Kruskal Transition Point presenting a LiDAR RS obstacle related to charge or rotational of gravity turbulence.

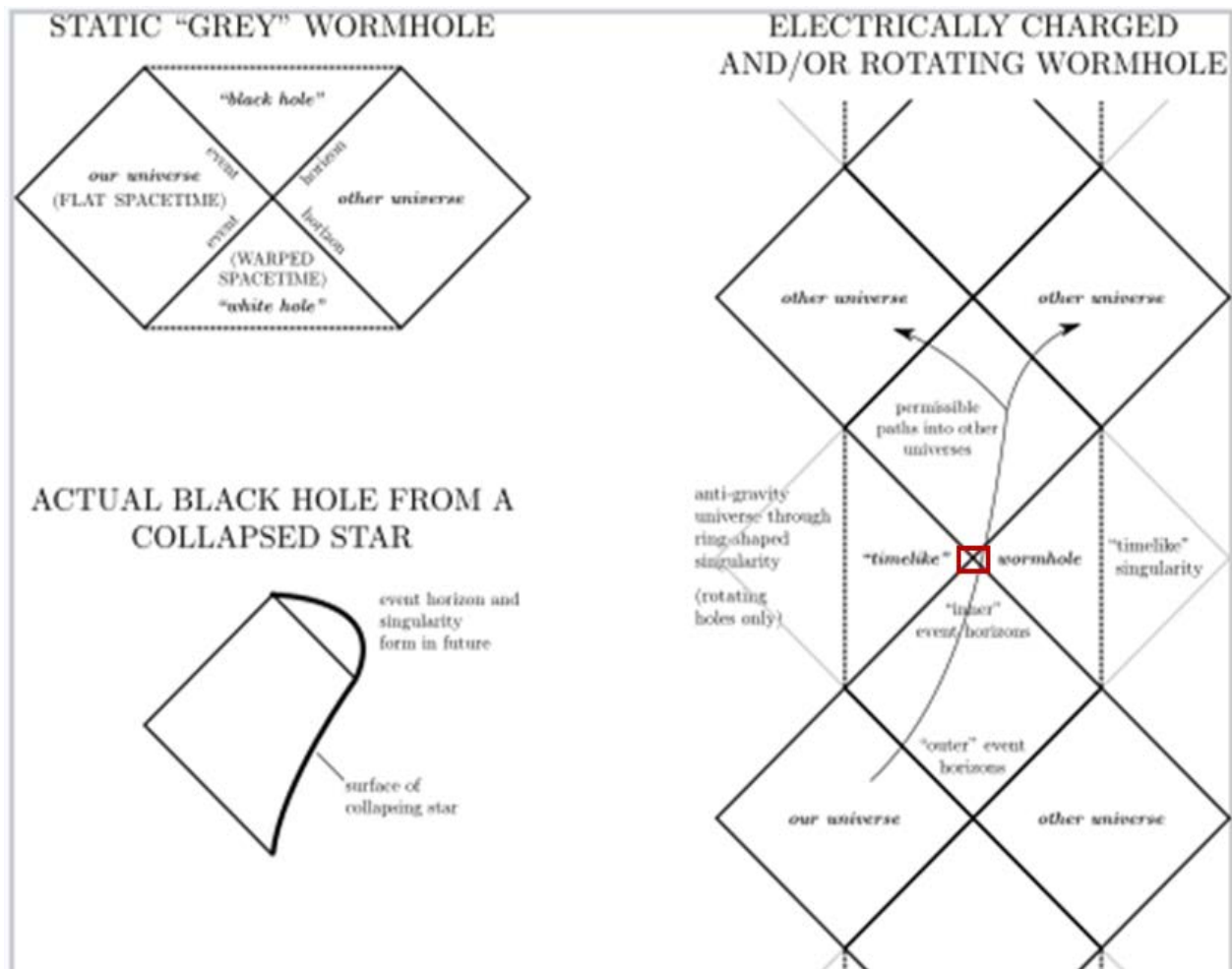


Figure 117. Penrose Diagrams of black hole solutions for flat timespace and time-like wormholes PQVS singularity present time at transition point in red (AkanoToE 2018; Penrose 2005).

ULS cave scanning collects and presents precise fluid dynamics of dissolution datasets in a series of three geometric vacuum manifolds. These manifolds related to PQVS and automorphically dynamic RMT turbulence of a cave silt storm. Scan time slice type I presents a Pseudo-Reimannian manifold, a Calabi-Yau manifold is present at time slice type II, and a Hofstadter's Butterfly exists at time slice type III within the video evidence of the silt storm. These observations compared to developed QCED LiDAR index related to a harmoniously, oscillating, fibrational (vibrating) complementarity perspective of quantum theory that correlates to bipartite quantum glitch at the Penrose-Kruskal diagram transition point and Hawking Radiation in a parsimonious manner on a Nth-Dimensional modulating viscous sphere-packed Apollonian Gasket in moduli vacuum space (Jost 2002). In terms of the number of smaller self-similar shapes required to cover a shape (e. g. Hadwiger and Keppler Conjectures) paralleled in ULS cave survey, is the problem of illuminating of an opaque convex surface in combinatorial geometry. Operating approaches filling a voided space with light for a fractal assessment of the survey space would require a near infinite number of laser lines for a perfect 1:1 scale. As well as for non-proximate color placement of cells, paralleled to quantum entanglement and invariance.

Photonic quasicrystals utilize plasma dynamics via fractalized wavelet mass/velocity transformations from photonic ricocheting and multiphasic inter-intra photonic singularities. Momentum and velocity are quanta mediated impact, pull, or slipstream along the pulsating beam. Quantum ricochets, or RMT harmonic flows, occur via PQV induced slipstream mechanic where the most parsimonious path of least resistance propagates a hyper gaussian beam. These phenomena are occurring within an extended Hilbert-Einstein-Podolsky-Rosen $So(48)$ hypergeometric manifold as a computationally complex Turing computer operating in bounded-

error quantum polynomial time (BQP) which presents an indicatrix sphere model for LiDAR calibration for power, intensity, and ranging. The index orbifold and spatially continuous and discrete non-monotonic fractilinear wavelet transforms, transmit via a complexified, coordinate free, quasi-symmetric $L_2(\mathbb{R}^n)$ 48D Hilbert Space maintaining a skew non-Hermitian spectral real (PT) symmetry via a Reimannian Zeta function of $z = \pm ic^2$ with observer projected objective normalization $\|\pm ic^2\|$ upon real eigenvalues. Paralleled or inverted values at imaginary or negative observation perspective eigenvalues without a normalization occur via and possibly induce entanglement. This orbifold presents a hyper-gaussian-hyperspatial series possessing non-random, natural asymmetrical fractal topological structures within harmonic resonance that produce, reflect, and respond to PQVS as an extension to the Penrose-Kruskal Diagram serving to visualize distortions of time, space, gravity, and quantum electrodynamics.

Figure 113 diagrams the index white body nested within a wave number-harmonic wave relationship diagram, represents an inverse solution to the Hadwiger Conjecture with space represented as black body radiation and white body radiation extending and ricocheting off a Gaussian beam. The index sits at a confluence of n-dimensional tensor hypergeometry, extends Mal'tsev Lie algebra and sphere geometry, transverses a Hilbert Space via concomitant de Broglie fractal wavelets with quantum electrodynamics transfer from photonic harmonization, and possibly promotes extensions of the Feynman diagrams for research in oscillation, collision, and fractalized compression and decompression in space, time, and gravity related to virtual particles and vacuum space.

Figures 118 and 119 display conceptual models of the exterior and interior of photons allowing for the development of a non-Euclidean 16D Hyperspatial Poincare orbifold Apollonian packed clopen (closed-open) set that produces triplet-octets (e. g. triplets in eight sets) resultants via dodecahedral harmonic variation internally and externally holding tied durations. This 16D spheroid fits numerous unit sphere and circle equations within the RMT index orbifold $N > 2$ Yang-Mills supersymmetry (Seiberg and Witten 1994).

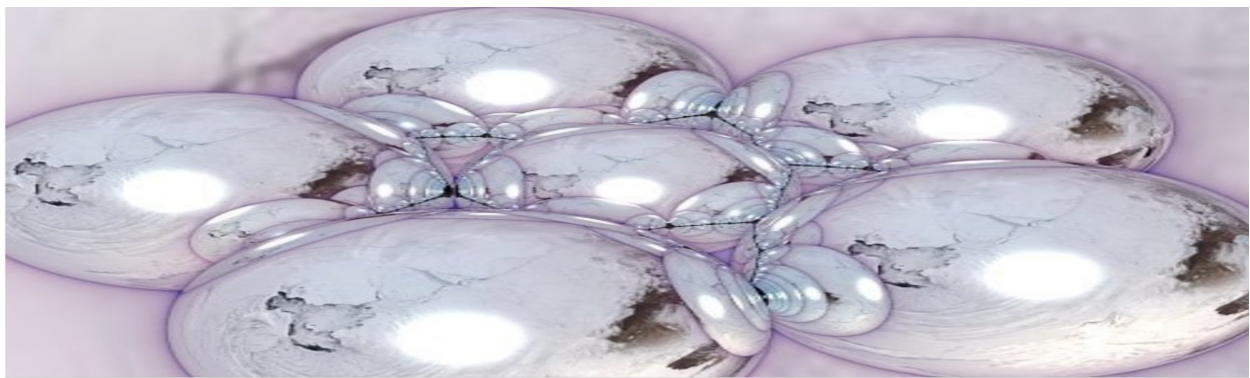


Figure 118. Wadabasin Mandelbub 3D generated representation of antanaklastic singularity developed for 6, 16D reflective holonomic inverse transliterations of a homothetic center.

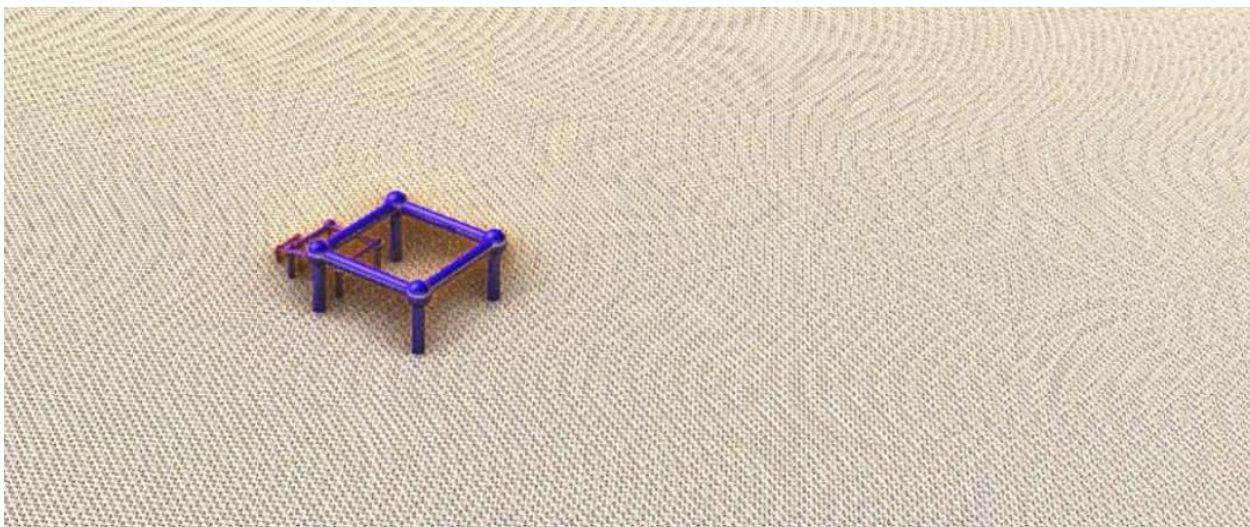


Figure 119. Mandelbub 3D generated conceptual model where TPU relates to cubes series volumetric measurement accuracy as each cube internally or externally distorts the subsequent.

QCED, space, time, and potentially gravity, seem to harmonically resonate from a commutating entropic Devil's Staircase fractal chaotic dissonance pattern via parallelepiped collineation of density, mass, energy, oscillation, polarity, helicity, and phase out of a homothetic center, evolving multiphasic holonomic transliterations via an antanaklastic holomorphic photonic quasicrystal singularity series which related to TPU. A BQP Turing Computer bears a bounded error of 1/3 of all instances of computations within a quantum algorithm, that can also solve 2/3 of calculations within polynomial time at a high probability. Meaning that as the BQP PQVS is occurring along a pulse each individual photon continuous utilization of the wave-spin function peak or trough flows of least resistance 2/3 of time. 1/3 induce or incur pilot wave interference as TPU phonon clouds, photonic ricochet, electron shearing dissipation, or mode locking fractal chaos leading to CRSI noise, excitation, or dissipation modeling error (Portugal et al 2014; Larocque et al 2018; Selig et al 2010; Smithey et al 1993).

The hand-mapped PQVS phase singularity results from the photographic and slow-motion video evidence and correlates with a second harmonic grouping and QCED theories of black body and white body radiation, vacuum space, and the hypergeometric-hyperspatial topological structural ordering. The representative photon acts in an oscillating wave-spin-particle function as a viscous orbifold in multiphasic serialized time, with potential for variance. The evidence suggest photons are operating as extended quantum Turing machines within BQP time producing computationally complex derivatives in 8 sets of tuples with harmonic curve calibrations resultants in the range of 10^{216} to 10^{432} per nanosecond.

The photonic-phononic harmonics and frequency modulation sampled and modeled here are relative to a blue-purple laser pulse, which is utilized by the ULS-200. The viscous hyperspatial spheroid promotes 45° intra-angular Boltzmann and non-Boltzmann energy

transmission via chaotically commutative 2nd harmonic Archimedes' spirals, on comodulating Ricci tensor off of photonic cell ejecta from the homothetic centroid as a circumference-based triquetra simultaneously, fitting PT symmetry skew non-Hermitian spectral theory matrixes as a γ from a non-solid omniscube icosahedral honeycomb (Znojil. 2001; Borkovec et al. 1993). This skew non-Hermitian matrix extension provides a mechanics for fractalized compressions and distortions within, space, infinitely weak gravity, and imaginary time in a positive, negative, and normalized extension Hilbert virtual-empty-real space providing for naturally occurring evenly distributed oscillations between a Calabi-Yau, Pseudo-Riemannian, and Hofstrader's Butterfly as inverse reciprocals, to a quantized HSF viscous fluid dynamo, with KHI mediated turbulent dissolution occurring around regions of karst matrix electromagnetic-density gradients in a +5D viscous manifold. A >3d fractional quantum Hall effect interacts along a 16D generator VTD serving to represent a dynamically harmonized vicious moduli fields of vacua gauge for LiDAR. Quantum chromoelectrodynamics (QCED) concentrates via Brillouin scattering with quantum entanglement preventing extrapolation of information beyond a Brillouin zone 1 firewall. The presented hypergeometric orbifold and $N \geq 2$ supersymmetric viscous vacuum space relate to fractional quantum Hall commutator, RTM chaos, and PQSV vacuum-edge dynamics. RMT related Brillouin-Wigner and Rayleigh-Schrödinger perturbations within a viscous vector-tensor-scalar gravitational HSF, photonic quasicrystal quantum chromodynamics (QCD) from Apollonian packed-sphere rolling propagated KHIs, and emergent phenomena through collective excitation, quasicrystals, and combinatorial quasiparticles along the 16D anyonic fractional quantum Hall commuting unit orbifold (Mattuck 1976). Datasets were assessed relative to oscillation harmonics and fractilinear reference objects for a blue laser with theoretical

extrapolations based on multiresolution QCED fractal wavelet transliterations occurring within, between, among, and separately from photon within the PQVS.

The PQVS relates to or stems from a quantum glitch, defined here as Occam's Ratchet, with the initial parsimoniously logical, photonic-dodecaphonic wave-spin-particle function producing a curvilinear least cost parsimonious action relative to the highest density-resistance as a reductive field, inducing individually sequential parsimonious flow in continually extending progeny waves which in turn propagate an inverse resistance dynamic preserving Newton's 1st, 2nd, and 3rd Laws of Thermodynamics. This occurs within a virtual-interspace with QCED carrying energy from photonic ricocheting or photonic envelopment via homothetic entanglement and holonomic transliteration correlating to a *PT*-symmetric spectral theory matrix space. Continuing remote sensing studies evaluating this index will promote ULS dataset accuracy and precision improvements. These improvements add to 3D GIS modeling accuracy and extend to PSTAR analogs for astronautics CRSI developments in simulations for survey training. NC and cave haloclines present analogous natural interface systems with shearing, instabilities, and other phenomena that are related to climatological systems and long-term trends and patterns in humanities history of interest to LiDAR, GIST, and PSTAR research.

Underwater and interorbital survey both present analogous novel phenomena, navigational principles, oppressive environmental stressors, microgravity equipment simulation training, survival techniques, extended LSS, and robust IVA exoskeletons needs and potentials for GIST research in VRLs. Figure 120 depicts a pool simulation with a PSTAR RS operator experiences similar needs in microgravity synesthesia during a spacewalk. Benefits from GIST ULS analogous solution formation leading to developments in STEAM knowledgebases and skills sets for future educational references for scientific and public interests via VRLs, 3D maps,

and interactively immersive educational experiences. Figure 121 presents a NC tomography scan full simulation for RS operator training in space suit ergonomics, flight procedures, CRM communication and scientific objectives synchronization.



Figure 120. PoSSUM Astronaut-Scientist Candidate immersed in a Ballast! underwater VRL HUD simulating an ISS spacewalk with ULS-200 scanning distortions from turbulent waves.



Figure 121. PMS tomography full simulation with Astronaut-Scientist operating RS equipment, and Embry-Riddle Astronaut-Pilot controlling spacecraft trajectory.

VRLs produced by speleonor and astronaut exploration promote engineering next-generation apparatus, soft robotics, and craft development as novel environmental conditions are encountered. VRLs promote STEAM education and access to individuals, public schools, universities, museums, governments, and non-governmental organizations. Figure 122 presents H-R C⁵I² GIST survey systems for adaptive CRSI modeling applications in synchronous and asynchronous operations to enhance public access to PSTAR and cave research. H -R surveys promote VRL development for karst and PSTAR education, research, and simulations for training simulations in pools for orbital and cave operations in microgravity.



Figure 122. Underwater drones promote research projects in numerous ways by operating as black boxes in accident analysis, CIRMMS response, and RS H-R toolkits for PSTAR surveys.

Figure 123 presents a GIST PSTAR survey research map which provides fields benefit from first hand *in situ* DTM development from their surveys, field report comparisons, evidence samples, and PTAs. Remote sensing survey and dataset accuracy and precision benefit from technological developments with ULS reliability and novel point cloud training data.

Yucatan Peninsula 3D Cave-In Geohazard Heat Map

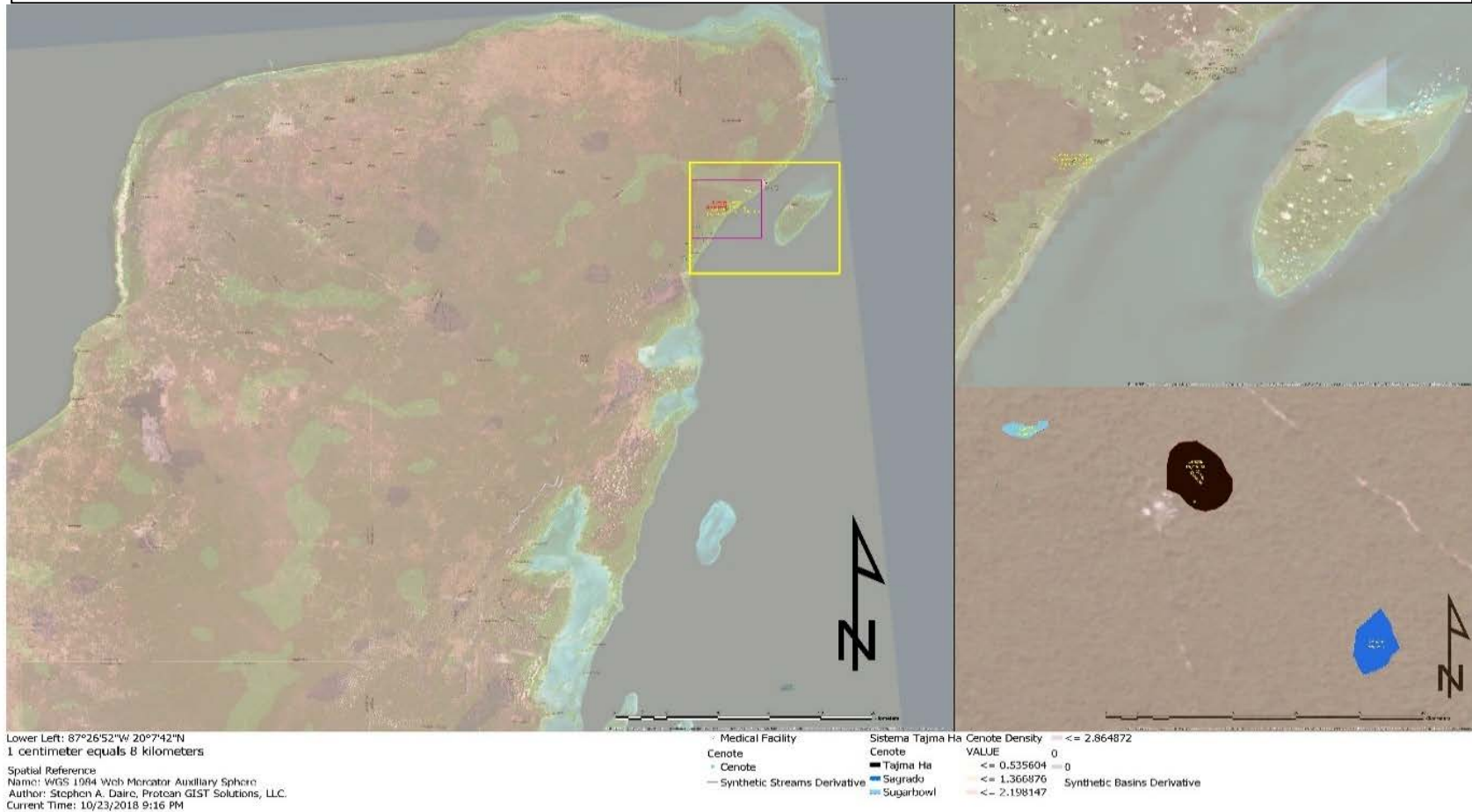


Figure 123. Yucatan Peninsula 3D Cave Density Heat Map. Dark red representing areas of more than three synthetic streams per 5mx5m areas with focus on the survey cenotes in Sistema Tajma Hal on the bottom right as polygons with Tajma Hal in black, Sugarbowl in light blue, and Sagrado in dark blue.

4.5. Outcomes

The outcomes of this project related to the objectives, were conducted effectively and provided useful products for research inferences. Parallel projection imaging assessment of the 15cm³, 15000L Red, green, black, blue, orange, and white targets from all viewing angles, in theory should produce a 100% filled square. Deviations from 100% vector fill are representative of voids, quantum distortions, fluid turbulence, and RS operator error within the model. Voiding, imaging artifacts, orthometric texture, geospatial accuracy, and geovisual precision compared to the modified BRCA grades provide QAQC related to >5x modified BRCA grade photoplethysmograms.

ULS presents next generation cave mapping techniques for IR photoelasticity analysis to designate regions of fracture, stress, and matrix loading for geohazard classification, Figures 98 and 137. As atmospheric CO₂ continues to build in abundance it promotes cave formation, thereby increasing structural instabilities corresponding to anthropogenic induced cavity development. Mesospheric developments in in situ measurements above the Armstrong line promote understanding of our atmosphere in non-traditional settings, and parallels to Martian environment dynamics for PSTAR.

The index informal and semiformal models can be developed and assessed with .svg analytic program as an underwater lidar calibration and topobathic lidar range extender. It relates to photonic quasicrystals quantum and aeronautic dynamic analysis. The photonic quasicrystal is a vertex and edge transitive omniscub icosahedral honeycomb $s\{3, 5, 3\}$ with a Poincare Sphere lattice figure with snub dodecahedron, octahedron, and tetrahedron cells that cannot be produced via uniformity. The orbifold also induces automorphic RMT via Brillouin-Wigner (BW)

Perturbation Theory. Using $\tau = 2\pi$ as circumference to diameter ratio of a unit circle within a n th dimensional harmonized orbifold-spheroid, in place of π radius to diameter perspective, which promotes simplification of calculations and facilitates visualization of phenomena from spherical axes for objective and disassociated perspectives for topological assessments in terms of nonlinear optics and TPU. The rolling photonic quasicrystal exists within an extended Hilbert Space that is relatively comparable to hyperbolic Euclidean Space with vertex and edge transitive elements. In layman's terms, a light producing crystal can fill an entire room with illumination as it harmonically and chaotically rolls within and upon a viscous gravity medium. Figure 138 displays artistic representations of the omni-angular parallax utilized by ULS for survey data collection. Figure 139 is an artistic diagram of TPU effects on 3D measurement accuracy

Chapter 5 Discussion & Conclusions

ULS point cloud assessment, classification, characterization, and representation are highly effective tools for PSTAR and underwater cave mapping. ULS require background knowledge of the active imaging systems and potential effects of those systems on survey datasets and deployment environments, as well as the effect of those environments on the LiDAR systems and the RS operator. PSTAR efforts represent new frontiers in the field of science and exploration for GIST, speleology, aquanautics, and astronautics. Prior citizen scientist efforts have promoted these fields and stand to extend anthropoid activity, interaction, and evolution across ever expanding horizons via visible and unforeseen agencies. Comparative orbital and phreatic karst lidar surveys inform quantum optics seifertometry, LiDAR spectrometric plasma density, and volumetric measurement calibration. PSTAR analogs highlight C⁵I² procedural incorporations for human-computer-robotic interfacing, LSS equipment limitations, and LSS bioendurance equipment integrated CRSI modular systems extensions. They present analog potentials in halocline-NC cross-section analysis, ergonomic interoperational suit (ExOS) design for precision apparatus operation, rebreather integration for suborbital craft hypoxia mitigation and other factors.

This work informs PSTAR and public stakeholders via cave diving training and exploratory survey methods development for remote sensing scientists and engineers and cartographers in caves, as well as for EVA operations and toolset engineering (Spidle et al 2013; Morwood 2005; Wheelock & LaFleur 2000; Diaz-Bolio 1975; Weidner 2016; Vassiliou 2007 Jones & Christal 2002; NMAI. 2017; VRARA. 2018; UNESCO 2002; National Park Service,

2017; Virrantaus et al 2009; Denson 2016; Boston et al 2008; Domagal-Goldman et al. 2011; Charles 2013; Vakoch 2014; Orosei et al 2018; Federal Grant: NASA ROSES PSTAR 2018).

Progressions in understanding of cave dissolution dynamics *in situ* promote climatological projections and calibration along with geohazard identification and urban planning foresight by avoiding dense areas of cave confluence and potential collapse. New modalities of understanding in aeronomy, QED, paleoclimatology, and speleology promote synergistic analog research in phreatic caves in terms of halocline dissolution CRSI examinations. Planetary sciences benefit from ULS integrated CRSI surveys in terms of geohazard avoidance, watershed forecasting, and environmental impacts with high accuracy maps (Benson & Yuhr 2016). The planetary science surveys benefits of ULS exploration exist in terms of novel dataset access and are increasing RS and LSS equipment improvements (Raggett & Jacobs 2018; Pronk et al 2009; Perrin & Andreassian 2001; Scanlon et al 2003).

Camera calibrations for PhoDAR act as representative voided sections (open cave) that match the natural environment for orthometric model developments with utilitarian accuracy. ULS allow for μm point cloud generation in several minutes time, reducing work time, cost, inefficiency, and survey crew safety, promoting survey beyond BCRA grade 3x surveys. Real-time geospatial survey and modeling via speleonator CRSI integrated ULS surveys promote engineering grade underwater survey with numerous geospatial applications. In terms of fractal analysis, when deployed in unison with trimetric fractal marker CRSI array survey within an AOI and proximate to FOIs benefits imaging production, comparison to the Fort Station Cave Study Project VRL, this survey and site reconstruction presents marked technological progression in terms of GIST for karst survey, modeling, and communication. ULS represents numerous improvements in analysis, providing new potentials for GIST and PSTAR.

5.1. GIST, QCED, Moduli Fields of Vacua, & Quasicrystals

LiDAR and PhoDAR parallel projections serve to referentially identify and develop 3D modeling for karst matrix surveys with fractal analysis methods for edge-detection. A superficial Delaunay tessellation field estimator (DTFE) promotes fractal-wavelet analysis of phononic-photonics quasicrystal lattices which provides measurement tools to improve plasmon detection and QCED indexes for LiDAR fixed point mapping and Brillouin Zone LiDAR pulse wave-function synchronizations (De Loera, Rambau, and Santos 2001; Cautun & van de Weygaert 2011; Aichholzer et al 2013). Linear and non-linear σ modeling, random matrix theory (RMT), TPU, and quantum chaotic dynamics stand to be understood via the 16D kissing surface Poincare orbifold presented in Figure 142.

The partially diminishing order 3 hyperbolic omniscub icosahedral honeycomb centroid provides QED and RMT tessellation references related to BQP. The chiral curvilinear Coxeter $\{3, 5, 3\}$ vertex figure produces a QCED manifolds with Brillouin-Wigner (BW) and Rayleigh-Schrodinger scattering, perturbation, and turbulence projections. The QCED model presents to an edge and vertex transitive, Coxeter $pd\{3, 5, 3\}$ omniscub icosahedral honeycomb orbifold operating as a harmonized rolling 16D quasiperiodic crystal τ unit sphere in dense flow. Crystal lattice structure presenting 8 rotation poles provide calculations for LiDAR plasma PQVS metrics and calibrations via topologic hypergeometric analysis into a consumptive $N > 2$ supersymmetric vacuum manifold with asymmetric reflected flavor independence, asymptotic freedom, and RMT automorphic elements.

Quasi-triangulation and Delaunay Triangulation on the orbifold and its quasicrystal centroid provide versatile tool for complex matrix analysis for quantum systems, fluid space, and holographic LAMIS reconstruction (De Loera, Rambau, and Santos 2010). The internal orbifold

lattice relates to a photonic quasicrystal completely filling a 4D, 16 VTD seeds randomly and systematically (Guibas & Stolfi 1985). Each of the Apollonian sphere kissing surface relates to a reference variable effecting LiDAR pulse propagation, ablation, detection, and degradation in terms of . Presenting the VTD cells as a viscous 3D Apollonian sphere-packing extends the conceptual model to permit imaginary time along an infinite radius sphere with photonic Coxeter {3, 5, 3} omniscub icosahedral honeycomb quasicrystals rolling, vibrating, and flowing on a fluid surface PQVS inducing RMT quantum entanglement between time-like kissing surfaces that translate to fractalized space and viscous gravity (tensor, vector, scalar) that induce TPU and QED in a Many-Body Problem.

5.1.1. Limitations of Accomplishments

Coupled with these benefits, ULS survey is inhibited by a series of factors, as well as by Murphy's Law. The fiberoptic surface tether, power consumption relative to battery size, lack of an underwater computer for dive crew scan touch ups, and the lack of an *in situ* ULS calibration index for dataset collection all negatively impact datasets processing, image analysis, artifact characterization, facet extraction, and model development. Human factors in ULS use and deployment can inhibit accuracy with laser misfires, poor ULS scan placement, water turbidity, as well as environmental complications, physiological limits, and other stressors.

Exploration of exotic environments underwater and out of Earth's orbit induce massive evolutionary stressors upon human anatomy and physiology. Open circuit scuba systems allow crews to survey flooded caves with redundantly separated air tanks or rebreathers, and limit survey distance and time relative to diver physiological conditioning, environmental stressors, and breathing gas volume. Closed circuit rebreathers allow for extended duration dives and use in orbital EVA research missions, delicate internal parts require meticulous care or robusticity

improvements for safety. Breathing air under high or low pressure, with depth or altitude fluctuation, causes the body to uptake or off gas nitrogen loading of the blood, respectively. Cave divers and astronauts mechanically offset environmental stressors by utilizing or manipulating spatial position, physics, and organic chemistry within survivable limits to provide breathing gas mixtures to work in exotic environments. Connection to, and function of, LSS restrict mission scope, operational parameters, and expose failure points which must be prepared for and responded to ensure mission safety and success.

The data was not able to be uploaded into ArcGIS for development of a contiguous DEM to 3D subsurface map for use in a VRL due to data and image processing constraints extending from a limited 30-day free trial of CityEngine and hardware (H/W) limitations from an Acer Predator with a Nvidia GeForce 1060 graphics card was not able to process the data within ArcGIS for a complete .xml and .mxd export. Figure 124 presents the datasets and product materials that were able to be developed into a full stereoscopic system map in Cloudcompare from LiDAR and PhoDAR point cloud overlays, these materials can be exported into mapping files for full display in CityEngine. A robust system server can produce a complete real-time model without calibration correction in the future for the data collected without resources limitations of this research project.

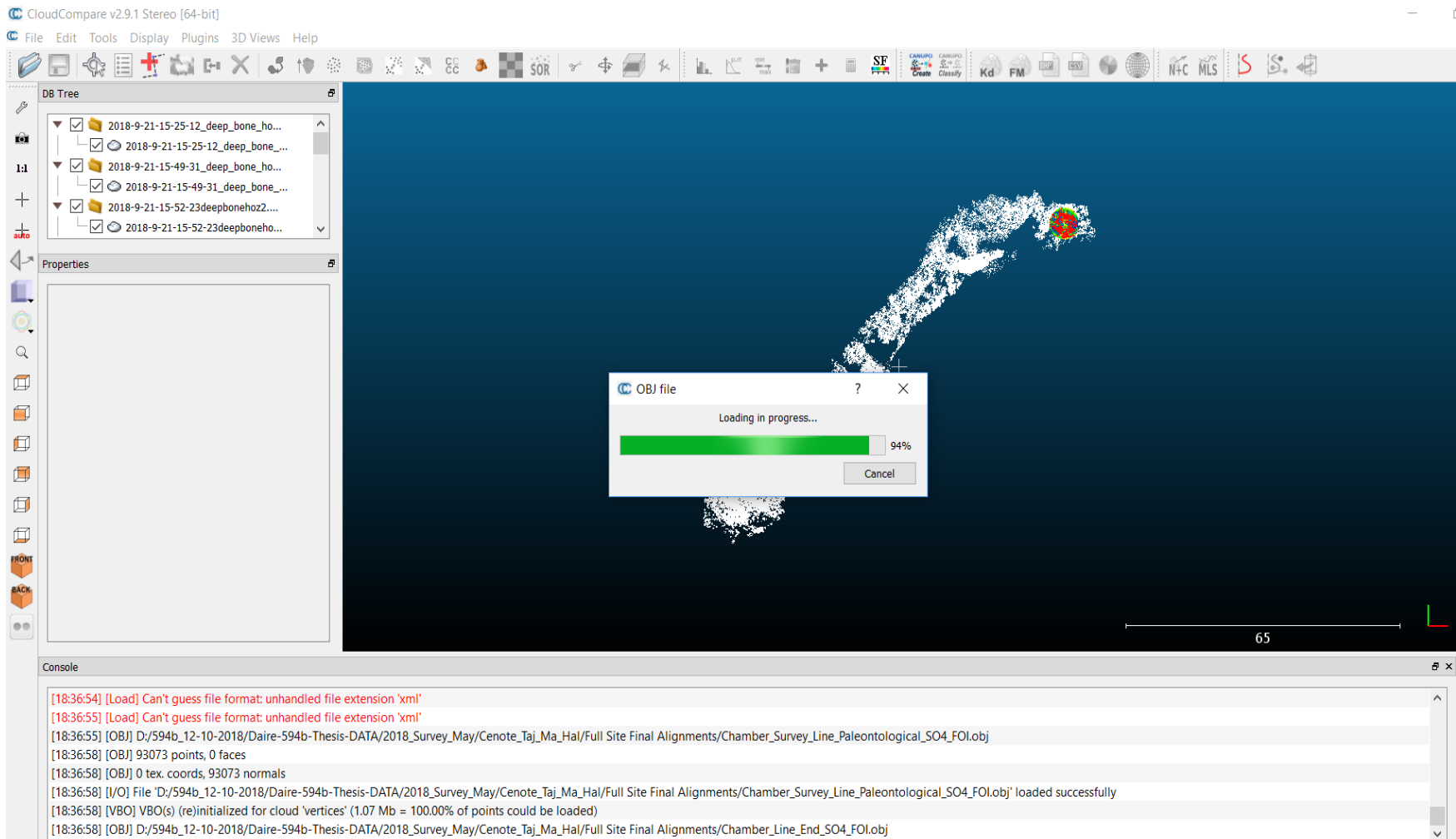


Figure 124. Full stereoscopic Taj Mahal system photoplethysmogram at 65m linear scale in Cloudcompare from LiDAR and PhoDAR point cloud overlays, these materials can be exported into mapping files for full display in CityEngine, magnetic North is toward screen bottom.

ULS dataset processing and imaging characterization limitations stem from the field methods, ULS scanning rotation, and QB obfuscation of the total free energy and entropy of the environmental system and its total effect on ULS pulse dynamics related to propagation, degradation, interference, and detection. Density shearing and QB poses problems within CRSI ULS systems due to the capacity of environmental pulse interactions to cause false detections, overshoot, or over ablated points causing variability in estimates of molecular PCA distance and TPU within topobathic lidar. ULS power input for effective system operation is also a concern with need for a consistent charge and effective battery charge to be maintained via a generator, car battery, or portable battery. Lack of modular, submersible power systems and data storage coupled with quantum information transmission fidelity (Qi-Fi) inhibit dive team maneuverability and deter full site scans limiting them based on effective fiberoptic cable length of 150m. Cables also deter linear survey penetration as laser baud rates decay in cables longer than 150m. Laser sizes of greater than 1m in length prevent access to confined portions of cave that require future scale reductions to systems. Power requirements deter solar cell options within restrictive doline entrances and overcast tropical storm settings, which require vehicle integration or several series of batteries to prevent scan interruption.

Lack of established *in situ* remote sensing halocline dynamics modeling, definitive TPU reductions for topobathic lidar, and physiological stressors prevent ready verification of phreatic cave dynamics by the general scientific community. This has had an inhibiting effect on geospatial communication of complex natural features and a transitory physical-virtual experience that can be made accessible to the public.

5.2. Future Research

The research objectives were all completed safely with varying degrees of effectiveness relative to time, cost, environmental, and physiological constraints. ULS phreatic cave surveys promote mapping and modeling and provide analogs for PSTAR research objectives in relation to integrative human-robotic space operations conducting numerous PSTAR GIST tasks. Four days of survey with approximately four hours of diving and scanning per day completed a 50m length of cross-sections collected along 5m increments with <.17mm measurement accuracy average, with areas of higher accuracy in most models related to ULS holographic omni-angular dataset collection parallaxes. These levels of cave survey accuracy are previously undocumented and stand as a preliminary assessment for next-generation ULS and GIST field improvements.

The ULS point cloud data was prepared in AgiSoft photoscan for input into GIS and CityEngine with conjoining photogrammetric data for development of the contiguous 3D model. PSTAR GIST survey dataset accuracy and precision benefit from ULS reliability, novel point cloud training data, and crew risk reduction. New technologies are contending with traditional deficits and are prompting novel access and imaging of previously unreported phenomena in atmospheric, hydrogeological, and speleological surveys. ULS, suborbital spacecraft, and rebreathers are pushing human evolution and understanding into the next generations of technological development and exploratory inquiries as manipulations of human biochemistry allow for extended niche explorations. These access points allow for new perspectives, literally and metaphorically, to be added to humanities understanding of itself, its environments, and the dynamic extensions of our effects on those niches that we explore via EES (Laland et al 2015).

Various deployments of various laser types and grades will be required for future research relative to karst cavity and conduit sizes along with calibration assessments. Laser size,

cables, and power access are concerns and require prior planning to promote access to confined conduits, cables present novel concern in diver and environmental safeties, and continuous power must be provided without modulation to prevent laser pulse energy fluctuations. Developments in underwater batteries and IT for connection and deployment stand to promote increased survey ranges and scientific mapping.

Direct correlation of CRSI via trimetric fractal markers compensate for inter-swath displacement. CRSI borne ULS survey promotes comparative planetology, reduces data collection volume, and deducts time lost for root mean square error estimation in real-time modeling for GIST human and robotic applications and deployments in research studies. Potential areas of development reside in AR/MR holographic heads up displays (HUDs), integrated intra-vehicular activity (IVA) and intraorbital planetary (IoP) LSS suit design, CRSI integrated rebreather helmets, and crew and individual resource management (CIRM) geospatial and LSS monitors, which will benefit mission architecture and systems information for speleonauts and astronauts during field campaigns and research sorties.

Halocline density differential and shearing cause reflection of ULS pulse off the linear measurements that produce ghost points as imaging artifacts that deter analysis and require continued study during field deployments. Lack of detailed halocline and NC tomography scanning and *in situ* CRSI chemistry assessments prevent detailed metrological model calibration and prevent synergistic research on diverse hydrological and atmospheric systems on varying scales (Law & Rennie, 2015; Hod 2011; Larocque et al 2018; Reimuller et al 2015).

Halocline and mesopause possess and provide analog research in RS imaging, calibration, and training for extra-orbital IVA surveys from transiting Martian Low Xenoplanetary Orbit (LXO) CRSI missions, to CRSI atmospheric and hydrogeological swaths

for climate modeling uncertainty calibration which prompt higher quality subsurface cave exploration and modeling. These analog hydrogeological datasets aid mission planners on nominal landing sites in terms of atmospheric and hydrogeologic features of interest and avoidance for Martian missions, as well as geohazard avoidance for infrastructure on Earth. These datasets increase future landing procedural success for international Mars and Lunar missions with atmospheric comparatives of MC on Earth and Mars. Kelvin-Helmholtz instability and shearing structures of turbulence in understudied karst halopause (freshwater-halocline-saltwater interface) and mesopause environments promote karst model development via fractal geometric analysis, fractal marker, and congruent synchronous and asynchronous CRSI ULS array surveys. PSTAR ULS surveys promote rapid real-time point cloud detection and production, affording static and dynamic scanning for various novel geospatial, biogeographic, and environmental analyses.

In terms of planetary sciences, speleogenetic processes, and interrelations of atmospheric and hydrogeological cycle dynamics assessed via LiDAR, SoNAR, and PhoDAR in karst survey produce various GIST phenomenological datasets that are correlative and comparative for PSTAR in ULS cave surveys. Understanding naturally occurring analogous dynamic fluid interfaces through fractal wavelet dimensions promotes research in forecasting of climate change, quantum biology, mesospheric aeronomy, fluid dynamics, dissolution chemistry, bioastronautics, and GIST (Yoshizawa and Jeffery 2008; Lambert et al. 2013).

ULS datasets present dissolution dynamics as faster moving fresh water on top of denser salt water is one of the primary dissolution mechanisms along the karst aquifer freshwater lens relating to its seasonal relative rise and fall, and chemistry changes which may parallel polar mesospheric formation. Kelvin-Helmholtz Instability in the halocline likely produces jagged

pockmarked features of the conduit walls along the halocline mixing zone at 13-17m deep. Kelvin-Helmholtz instabilities in halopause likely possess internal and external seasonal variations with spatially homogenous and heterogenous features relative to superficial and subterranean topographic formations, proximate anthropogenic disturbance, karst matrix density, magnetized crystalline formations, bioperturbation, and climate change regime modifications are all areas of PSTAR survey interest.

Cave surveys with habitation and exploration lasting a week or longer parallel necessary PSTAR training, equipment, operations, testing, and crew development in subterranean basecamp and subaquatic subterranean survey environments which translate to extraterrestrial habitat dynamics and experiential EVA crew stressors. The crew members possess years of cave diving, surveying, and survival experience in the Yucatan karst region, regional knowledge of specific cave system features and risks in other regions stand to provide other novel ULS datasets. Crew awareness and effectiveness benefit from volatile organic chemical situational awareness, LSS gas toxicity situational awareness, operational LSS gas toxicity symptoms simulations, and environmental data collation in turbulence and differential gravity. Hyperbaric and space medicine, field bioendurance technologies & sensing techniques, CIRM communication flows, operational CIRMSS considerations, proactive CIRMSS PP-CR, human evolution in solitary confined environments, and other integrated space services areas stand to benefit from this intersection of multidisciplinary research. Microbial & human coevolution research in undisturbed caves and artificial environments informs LSS system design and artificial ecological habitat construction through the lens of niche construction theory. Speleological and astronautical long-term/low-input permaculture habitat development, RS apparatus improvements, and crew effectiveness in exotic environments extend from problem-

tree analysis and continued experiential field settings on Earth. These developments prompt research in proteomics research in microbiological and synthetic coevolutionary biomedical responses to spaceborne anatomic and physiological degradation, along with novel microbiological field identification and modeling.

PSTAR ULS cave surveys improve GIST and RS techniques and toolsets in exotic, extremophile, astrobiological, epigenetic, bioastronautic, viscous-thermodynamics (water-sodium-methane-temperature-helium-etc), proteomics, and other areas of study. Proteomics is the study of proteomes, the set of proteins produced in an organism, system, or biological contexts on microscopic scales. Proteomic responses potentially serve to provide synthetic protein modification countermeasures for PSTAR crews to off-set long-term negative impacts from microgravity operations. These impacts are related to subaquatic and orbital environments producing long-term novel volatile chemical exposure, variable radiation, microgravity muscle degradation, and isolation in extreme environment exploration on biologic protein production and topological folding, as well as for real-time identification of novel microbiological protein structures may contend with physical stressors during astronautic missions. Figure 125 presents actin, myosin, and collagen proteins that are affected by various lifestyle and environmental differences for speleonator and astronautic settings which provide analogs for comparative proteomic studies in anatomical and behavioral systems fluctuation.

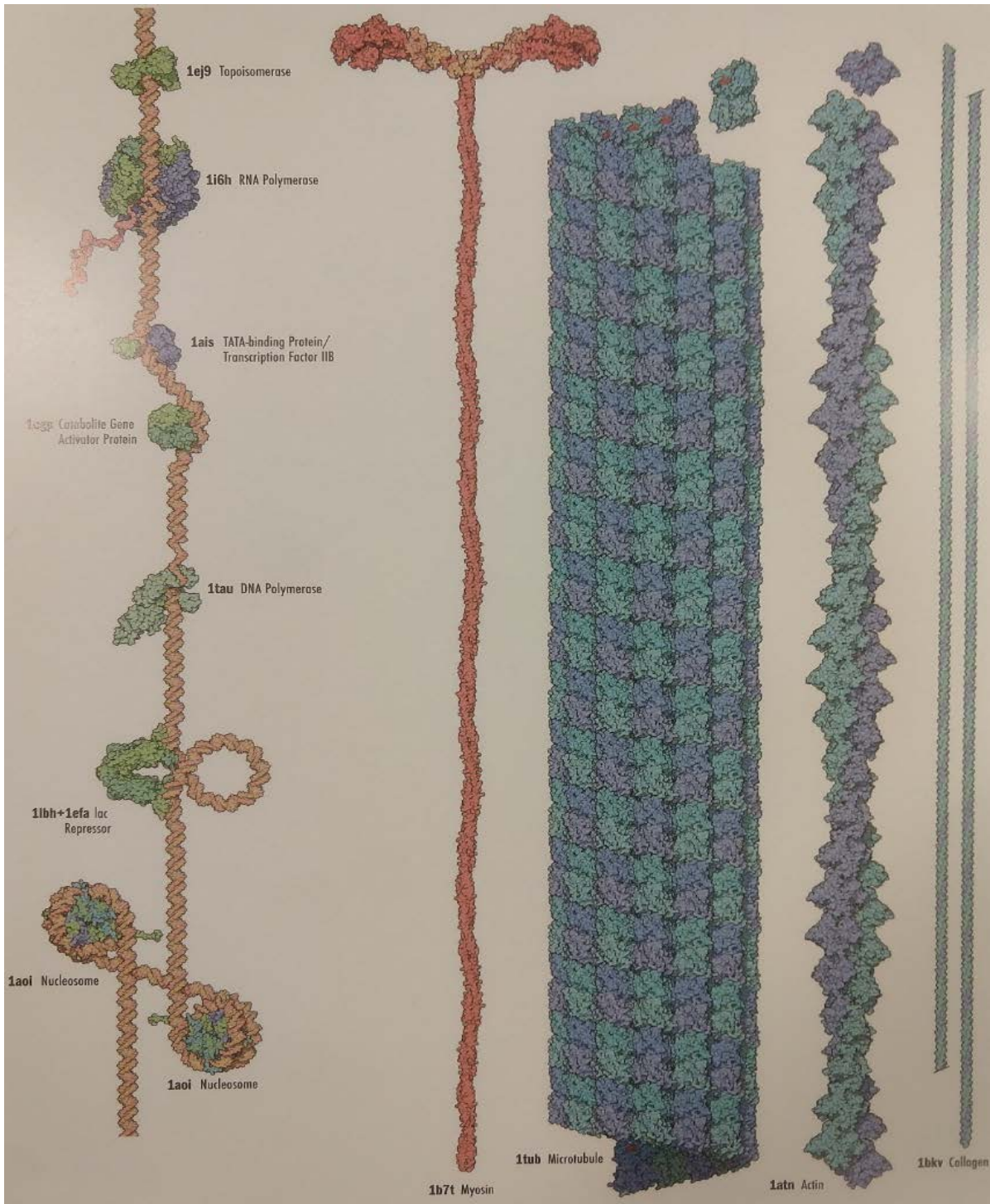


Figure 125. Protein Databank proteomic models of human muscle proteins that degrade during astronautics missions and require countermeasures for future space environment anatomical and physiological stress mitigation for Myosin, Actin, and Collagen (Protein Databank 2018).

ULS spectrometry provides real-time mapping as CRSI survey provides rapid detection and ranging for emergency planning, solutions, and response in geohazard, cave diving, aerospace, and astronautics accidents or crises with multiple corroborating datasets for PSTAR. Continued operations and explorations within these areas of science prompt developments and responses with new definitions of personnel functions and roles (Langston & Pell 2015). Planetary protections promote mediated anthropogenic environmental interactions in terms of Outer Space Treaty (1967) etiquette and increasing intraorbital operations with stipulations to assist damaged craft and conduct all operations at all junctures.

ULS cave surveys provide inferences and possibilities for laboratory and pool nitrogen narcosis/hypoxia simulations, wilderness medicine for underwater and space environments, operations in delicate microgravity environments, chain-of-command, emergency response, duty delegation, injured, missing, or gas toxified crew member contingencies for safe and successful operations. 3DGIS and PSTAR VRL simulators provide stakeholders remote access to remote regions in novel ways for acknowledgement, cessation, reflection, consideration, solution-problem response, and reporting in cave survey, astronautics missions, and citizen-science.

5.3. Summary of GIST Contributions

Chicxulub impact crater on the Yucatan karst platform is a natural laboratory for investigations on cave formation processes, effects of near-Earth object impact, gravitational anomalies, ecological-biogeographic response to catastrophe, CRSI testing, and PSTAR analogs in astronautics operations training through cave diving survey. The impact point marks the Cretaceous/Paleogene (K/Pg) boundary at 65Ma (millions of years ago) with an object 15 km wide with a velocity of 20 km/s, forming a 25-30 km deep, 100-200 km diameter crater ejecting

a global iridium-clay mushroom cloud with a geodesic center at Chicxulub Puerto, Mexico in picoseconds (Ps) (one/trillionth of a second). Differential compaction and fracturing produced rings of cenotes and cave-networks propagated from the vaporized shallow sea, coral reef, and half of the near-Earth object (NEO) asteroid on impact. As Earth reverberated with seismic waves, the ablated reef crystallized under rheological processes of heating, compression, and compaction as the sea vaporized and the second half of the NEO lodged into the exposed seafloor. Portions of cave systems then began to form by matrix overload dissolution of rain cycles, structural collapsing, and oceanic erosion over millions of years with various species utilizing them for habitat and adapting to their homes during this period for hundreds of thousands of years. Humans began occupying the regional caves roughly 20-15Ka, modifying chambers for subterranean life with firepits and ambush hunting sites. These cave dwellers left their graves and hunted llama remains as evidence of their explorations, and their ancestors developed into the Maya cultural groups of the following millennia.

Modeling underground karst structures with unprecedented details promotes understanding in analog structural typological classification, halocline analog mesopause dynamics, hydrogeological stratigraphy, rheological behavior under a single-cleavage celestial body impact, quantum mechanics, and paleoclimatology studies analogous to conditions that have occurred from an asteroid impact on Mars and the Moon. Chicxulub is one of three documented multi-ring craters in the terrestrial geological record producing instantaneous climatic change and mass extinction.

The geologically inactive Yucatan Platform presents neither volcanoes nor mountains, with sedimentation acting solely through cave formation or human activity. The peninsula serves as a global isotopic-stratigraphic correlation point. Regional remote sensing in terrestrial, karst,

submarine, and aerial geophysical environments benefit from high resolution imagery feature analysis of the peninsula. This work resides within the interdisciplinary intersections of several themes, topic areas, and research domains via planetary sciences, exotic environment survey, and remote sensing engineering. GIST and PSTAR developments promote mesospheric and speleogenetic research, which in turn benefit public health, climate change response, next-generation aerospace engineering development, salient flight procedures, RS techniques, calibration procedure, and new perspectives in environment-human-machine interactions.

These technological and methodological developments benefit geoheritage preservation, evolutionary biology, cave rescue, urban planning, PSTAR comparatives, and quantum non-linear optics research. This research analog allows for strengths, weaknesses, risks, and opportunities to be referenced from underwater caves contexts onto extraterrestrial and astronautic environments equipment and craft planning for continued technological innovation, crew vigilance, and mission architecture improvements. These topics flow from aeronomy, paleobiogeography, paleohydrogeology, paleospeleology, and paleoecology via ULS applied linear and quantum optics in cave survey into a GIST and PSTAR comparative. This work provides notations on analog field experience for extrapolation and adds to discussions in underwater speleology, astronautics, quantum dynamics, condensed matter physics, and applications in topological geometry in spatial sciences. Continuations of such analogs promotes GIST and planetary sciences in terms of classical and quantum physics, and human factors dynamics in PSTAR GIST applications and research.

References

- 2G Robotics, Inc. 2015. *ULS-100/200 User's Manual*. Waterloo, ON, Canada: 2G Robotics, Inc.
- Abbott, M. B. and Refsgaard, J.C. 2013. "Distributed hydrological modelling." In: Abbott MB, Refsgaard JC (ed) *Kluwer Academic Publishers*, Dordrecht 1996 Redistribution. Springer-Verlag.
- AgiSoft Inc. 2013. *Agisoft Photoscan User Manual Version 1.1*. St. Petersburg, Russia: AgiSoft, Inc.
- Aichholzer, O. Fabila-Monroy, R. Hackl, T. van Kreveld, M. Pilz, A. Ramos, P. and Vogtenhuber, B. "Blocking Delaunay Triangulations." *Computational Geometry: Theory and Applications* 46, no. 2 (February 2013): 154–159.
- Alberts, D.S, Nissen, M.E., and Naval Postgraduate School Monterey Ca.2009. "Toward Harmonizing Command and Control with Organization and Management Theory." *The International C2 Journal*, Volume 3, Number 2, 2009. <http://handle.dtic.mil/100.2/ADA508759>.
- Alcocer, J. Lugo, A. Marín, L.E. and Escobar, E. 1998. "Hydrochemistry of Waters from Five Cenotes and Evaluation of Their Suitability for Drinking-Water Supplies, Northeastern Yucatan, Mexico." *Hydrogeology Journal* 6, no. 2 (August 1998): 293–301.
- Alvey, D.C. K. Morton., R. S. Harmon, Gottfried, J. L., Remus, J. J., Collins, L. M. and Wise, M. A. 2010. "Laser-Induced Breakdown Spectroscopy-Based Geochemical Fingerprinting for the Rapid Analysis and Discrimination of Minerals: The Example of Garnet." *Applied Optics* 49, no. 13 (2010): C168–C180.
- Andreev, A. Simons, A. and Andreev, A. "Quantum Chaos, Irreversible Classical Dynamics, and Random Matrix Theory." *Physical review letters* 76, no. 21 (May 20, 1996): 3947–3950. <http://search.proquest.com/docview/1859256948/>.
- Andreo, B. Carrasco, F. Durán, J. J. Jiménez, P. and LaMoreaux, J. W. 2015. *Hydrogeological and Environmental Investigations in Karst Systems*. Berlin, Heidelberg: Springer Berlin Heidelberg.
- Angelo, M. 2017. "We Are Stronger Than Me. The Underwater Cave Archiving Project: An Update." *Underwater Speleology: Journal of the Cave Diving Section of the National Speleological Society*.
- Anita, K. P. Przemyslaw, K. Rafal, K. Lukasz, O. and Tomasz, O. 2013. "The Possibility of Using Remote Sensing Techniques in Geometric Surveying of Caves." *International Multidisciplinary Scientific GeoConference Surveying Geology and Mining Ecology Management, SGEM*, 2:479–486. International Multidisciplinary Scientific Geoconference.

- Armstrong, B. (ed). 2017. "American Caving Accidents: Improving Safety Through 50 Years of Accident Reports and Analysis." *National Speleological Society – Cave Diving Section*. Fulton, Missouri: Ovid Bell Press, Inc.
- Ashley, G. M. Bunn, H. T. Delaney, J. S. Barboni, D. Domínguez-Rodrigo, M. Mabulla, A. Z. P. Gurtov, A. N. Baluyot, R. Beverly, E. J., and Baquedano, E. "Paleoclimatic and Paleoenvironmental Framework of FLK North Archaeological Site, Olduvai Gorge, Tanzania." *Quaternary International* 322-323 (February 16, 2014): 54–65.
- Batty, M., Hudson-Smith, A. Milton, R. and Crooks, A. 2010. "Map Mashups, Web 2.0 and the GIS Revolution." *Annals of GIS* 16, no. 1 (April 22, 2010): 1–13.
- Baldini, J. U. L. Mcdermott, F. and Fairchild, I.J. 2006. "Spatial Variability in Cave Drip Water Hydrochemistry: Implications for Stalagmite Paleoclimate Records." *Chemical Geology* 235, no. 3 (2006): 390–404.
- Bartos, K. Pukanská K., Sabová, J. and Weiss, G. 2014. "Analysis of low-cost photogrammetric procedures in the process of historical objects survey." *International Journal of Science Commerce and Humanities*. Vol 3(2).
- Bauer-Gottwein, P., Gondwe, B. Charvet, G. Marín, L. Rebolledo-Vieyra, Mario, M. and Merediz-Alonso, G. 2011. "Review: The Yucatán Peninsula Karst Aquifer, Mexico." *Hydrogeology Journal* 19, no. 3 (May 2011): 507–524.
- Bhattacharya, S. and Shankaranarayanan, S.. 2017. "Negative Specific Heat of Black-holes from Fluid-gravity Correspondence." *Classical and Quantum Gravity* 34, no. 7 (April, 6, 2017): 14.
- Blamey, N. Boston, P. and Rosales-Lagarde, L. 2016. "High-Resolution Signatures of Oxygenation and Microbiological Activity in Speleothem Fluid Inclusions." *International Journal of Speleology* 45, no. 3 (September 1, 2016): 231–241. <http://search.proquest.com/docview/1855305008/>.
- Blaser, M. 2015. Opportunities of an Interpretive Application for Self-Guided Tourism within the National Park System. Professional Project. University of Nebraska-Lincoln.
- Benson, R. C. and Yuhr, L. B. 2016. "Site Characterization in Karst and Pseudokarst Terraines." *Practical Strategies and Technology for Practicing Engineers, Hydrologists and Geologists* 1st ed. Dordrecht, Netherlands: Springer.
- Bonet, F. and J. Butterlin, J. 1962. "Stratigraphy of the Northern Part of the Yucatan Peninsula". *Guidebook - Field Trip to Peninsula of Yucatan*. New Orleans: New Orleans Geological Society.
- Borkovec, M, W. De Paris, and R. Peikert. 1994. "The Fractal Dimension of the Apollonian Sphere Packing." *Fractals* 2, no. 4 (December 1994): 521–526.

- Boştenaru, D. M. Armas, I. and Goretti, A. 2014. *Earthquake Hazard Impact and Urban Planning*. Dordrecht: Springer Netherlands.
- Boston, P., M. N. Spilde, D. E. Northup, A. Dichosa, A. D. Anbar, and E. K. DeVore. 2008. "Biogenic Fe/Mn Oxides in Caves and Surface Desert Varnish; Potential Biosignatures for Earth and Mars." *Astrobiology*. Larchmont, NY: Mary Ann Liebert, Inc.
- Bowens, A. 2009. *Underwater Archaeology: The NAS Guide to Principles and Practice*, 2nd Edition. Blackwell Publishing Ltd.
- Cahn, J, Shechtman, D, Gratias, D, and Cahn, J. "Indexing of Icosahedral Quasiperiodic Crystals." *J. Mater. Res* 1, no. 1 (January 1, 1986): 13–26.
<http://search.proquest.com/docview/24134794/>.
- Campbell, J. B. and Wynne R. H. 2011. *Introduction to Remote Sensing*. 5th ed. New York: Guilford Press.
- Carney, B. Bissett, D. Bruning, J. Harrison, S. Phillips, S. Piskula, M. Pulley, D. and Drecher, R. 2013. "Diving in Overhead Environments: Your Completed Guide to Cavern and Cave Diving." *International Training*. ISBN: 1-931451-71-0
- Cautun, M, C. and van de Weygaert, R. 2011 "The DTFE Public Software - The Delaunay Tessellation Field Estimator Code" (May 2, 2011).
- Çengel, Y. A., and Boles. M. A. 2002. *Thermodynamics: An Engineering Approach*. 4th ed. McGraw-Hill Series in Mechanical Engineering. Boston: McGraw-Hill.
- Charles, J. 2013. *Origins and Early History of Underwater Neutral Buoyancy Simulation of Weightlessness for EVA Procedures Development and Training*. Hampton: NASA/Langley Research Center. <http://search.proquest.com/docview/2128139847/>.
- Chica-Olmo M. and Luque-Espinar, J.A.. 2003. "Creación de mapas de calidad de aguas subterráneas mediante métodos de Krigeaje." *Boletín geológico y minero* 114(3):299–310
- Clark, G. 2000. *Introduction to Human Ecology*. Kendall-Hunt Publishing Company.
- Cohen, K. M., S. Finney, and P. L. Gibbard, P. L. 2012. International Chronostratigraphic Chart: International Commission on Stratigraphy, www.stratigraphy.org (last accessed July 2018). (Chart reproduced for the 34th International Geological Congress, Brisbane, Australia, 5–10 August 2012.)
- Conway, J. H. and Sloane, N. J. A. *Sphere Packings, Lattices, and Groups* New York: Springer-Verlag, 1988.
- Corcovilos, T. A. 2018. "A Simple Game Simulating Quantum Measurements of Qubits." *American Journal of Physics* 86, no. 7 (2018): 510-517.

- Cristoforetti, G. Tiberi, M. Simonelli, A. Marsili, P. and Giammanco, F. 2012. "Toward the Optimization of Double-pulse LIBS Underwater: Effects of Experimental Parameters on the Reproducibility and Dynamics of Laser-induced Cavitation Bubble." *Applied Optics* 51, no. 7 (2012): B30-B41.
- Cruz, J.A. J. Martín-Chivelet, A. Marín-Roldán, M. J. Turrero, R. L. Edwards, A. I. Ortega, and J. O. Cáceres. 2015. "Trace Elements in Speleothems as Indicators of Past Climate and Karst Hydrochemistry: A Case Study from Kaite Cave (N Spain)." *Environmental Earth Sciences* 1 (2015): 569–577.
- Daire, S. A. Lee, T. O. Nolasco, E. Loew, C. Aviles, J. Gerdes, R. "A Formative Speleological Database for Quintana Roo, Mexico: Cenote Paleontological Site Suitability Analysis for Remains." *Fourth International Congress on Underwater Cultural Heritage and New Technologie.- Instituto Nacional de Antropología e Historia de o.* 2017 Abstract.
- Daire, S. A. 2018. "Martian Karst of Noctis Labyrinthus and Unmanned System Survey Geohazards" University of Southern California Spatial Sciences Insitute – Cartography and Geovisualization.
- Andrews, D. L. 2004 "Virtual Photons, Dipole Fields and Energy Transfer: a Quantum Electrodynamical Approach." *European Journal of Physics* 25, no. 6 (November 1, 2004): 845–858.
- Davis, E. 2010. *Nomad Codes: Adventures in Modern Esoterica*. Verse Chorus Press. ISBN-13: 978-1891241543
- Day, A. 2002. *Cave Surveying Grades [Cave Studies Series 11]*. 40pp, A5, with diagrams and photos. Buxton, England: British Cave Research Association.
- De Loera, J. A. Rambau, J. and Santos, F. *Triangulations Structures for Algorithms and Applications* Heidelberg. Springer, 2010.
- Diaz-Bolio, J. ed. 1975 [Zavala, M. y Medina, A. Vocabulario Español-Maya *Imprenta De La Ermita*]. *Area Maya*. Facsimile. 1898.
- Denson, T. J. "Majestic Yosemite Hotel Virtual Tour Application and Indoor Model". *University of Southern California Digital Library (USC.DL)*, November 30, 2016.
- Denton, R. K. A. Hogan, and R. D. Thomas. 2016. "The Integration of Data Review, Remote Sensing and Ground Survey for a Regional-Level Karst Assessment." *Environmental and Engineering Geoscience* 22, no. 1 (February 1, 2016): 81–92.
- Dixon, B. 2018. "The Technology Behind the Thailand Cave Rescue." *Esri blog*, July 18. 2018 Accessed July 28, 2018. <https://www.esri.com/about/newsroom/blog/technology-behind-thailand-cave-rescue/>

- Domagal-Goldman, S. D. V. S. Meadows, M. W. Claire, and J. F. Kasting. 2011. "Using Biogenic Sulfur Gases as Remotely Detectable Biosignatures on Anoxic Planets." *Astrobiology* 11, no. 5 (June 1, 2011): 419–441.
- Dyson, F. J. "General Theory of Spin-Wave Interactions." *Physical Review* 102, no. 5 (1956): 1217–1230.
- Exley, S. 1986. *Basic Cave Diving: A Blueprint for Survival 5th Ed.* National Speleological Society.
- Fabrocini, A. Fantoni, S. and Krotscheck, E. Introduction to *Modern Methods of Quantum Many-Body Theory and Their Applications*. River Edge, NJ: World Scientific, 2002.
- Fairchild, I. J. G. W. Tuckwell, A. Baker, and A. F. Tooth. 2006. "Modelling of Dripwater Hydrology and Hydrogeochemistry in a Weakly Karstified Aquifer (Bath, UK): Implications for Climate Change Studies." *Journal of Hydrology* 321, no. 1 (2006): 213–231.
- Federal Grant: ROSES 2018: Planetary Science and Technology Through Analog Research." *US Fed News Service* (Washington, D.C.), February 20, 2018.
- Fetter, A. L. and Walecka, J. D. *Quantum Theory of Many-Particle Systems*. San Francisco: McGraw-Hill, 1971.
- Feng, J. C. 2017. *The Poor Man's Introduction to Tensors*. The University of Texas: Physics Department Austin (December, 2017)
- Feng, G. Ming, D. Wang, M. and Yang, J. 2017. "Connotations of Pixel-Based Scale Effect in Remote Sensing and the Modified Fractal-Based Analysis Method." *Computers and Geosciences* 103 (June 2017): 183–190.
- Flannery, M. C. 2005. "Goethe and the Molecular Aesthetic." *Janus Head* 1: 273-289.
- Fleury, P. B. Ladouche, Y. Conroux, H. Jourde, and N Dörfliger. 2009. "Modelling the Hydrologic Functions of a Karst Aquifer Under Active Water Management – The Lez Spring." *Journal of Hydrology* 365, no. 3 (2009): 235–243.
- Ford, D. and Williams P. W.. 2007. *Karst Hydrogeology and Geomorphology*. ed. Chichester, England: John Wiley & Sons.
- Fortes, F. J. Moros, J. Lucena, P. Cabalín, Luisa M, Laserna, J J. and Fortes, F. J. "Laser-Induced Breakdown Spectroscopy." *Analytical Chemistry* 85, no. 2 (January 15, 2013): 640–669. <http://search.proquest.com/docview/1273555880/>.
- Freire, R., Pe'eri, S., Alexander, L. Lippmann, T. Parrish, C. and Rzhhanov, Y. "Evaluating Satellite Derived Bathymetry in Regard to Total Propagated Uncertainty, Multi-Temporal

- Change Detection, and Multiple Non-Linear Estimation”. ProQuest Dissertations Publishing, 2017. <http://search.proquest.com/docview/1981372078/>.
- Gale Group. *Encyclopedia of Emerging Industries*. 6th ed. Gale Virtual Reference Library. Detroit, Mich.: Gale, 2011.
- Goldscheider, N. and Drew, D. Editor: Dr. Robins, N. S. *Methods in karst hydrogeology*. Taylor and Francis, London. 2007.
- Graniel E, P. A, Coronado V. Origen de los sulfatos en el agua subterránea del Sur de la Sierrita de Ticul, Yucatán. *Ing Rev Acad FI-UADY* 13(1):49–58. (2009) ISSN:1665-529X
- Gray, J. M. *Geodiversity Valuing and Conserving Abiotic Nature* 2nd ed. Chichester, West Sussex, UK: John Wiley & Sons Inc., 2014.
- Guibas, L. and Stolfi, J. “Primitives for the Manipulation of General Subdivisions and the Computation of Voronoi.” *ACM Transactions on Graphics (TOG)* 4, no. 2 (April 1, 1985): 74–123.
- Harmand, S. Lewis, J. E. Feibel, C. S. Lepre, C. J. Prat, S. Lenoble, A. Boës, X. et al. “3.3-Million-Year-Old Stone Tools from Lomekwi 3, West Turkana, Kenya.” *Nature* 521, no. 7552 (May 20, 2015): 310–315K.
- Hartmann, A., Weiler, M. Wagener, T. Lange, J. Kralik, M. Humer, F. Mizyed, N. et al. “Process-Based Karst Modelling to Relate Hydrodynamic and Hydrochemical Characteristics to System Properties.” *Hydrology and Earth System Sciences* 17, no. 8 (August 1, 2013): 3305–3321. <http://search.proquest.com/docview/1431445980/>.
- Healey, S.P., M.W. Hernandez, D.P. Edwards, M.A. Lefsky, E. Freeman, P.L. Patterson, E.J. Lindquist, and A.J. Lister. *CMS: GLAS LiDAR-derived Global Estimates of Forest Canopy Height, 2004-2008*. ORNL DAAC, Oak Ridge, Tennessee, USA <https://doi.org/10.3334/ORNLDAAC/1271> 2014.
- Halligan, J. J. Waters, M. R. Perrotti, A. Owens, I. J. Feinberg, J. M. Bourne, M. D. Fenerty, B. et al. “Pre-Clovis Occupation 14,550 Years Ago at the Page-Ladson Site, Florida, and the Peopling of the Americas.” *Science Advances* 2, no. 5 (May 2016): e1600375.
- Holdaway, S. J. King, G. C. P. Douglass, M. Fanning, P. C. Human-environment interactions at regional scales: the complex topography hypothesis applied to surface archaeological records in Australia and North America. *Archaeology in Oceania*.50: 59-69. (2015)
- Hod, S. “Quantum Buoyancy, Generalized Second Law, and Higher-Dimensional Entropy Bounds.” *Journal of High Energy Physics* 2010, no. 12 (December 2010): 1–12.
- Hollingsworth, E. “Karst Regions of the World (KROW)—Populating Global Karst Datasets and Generating Maps to Advance the Understanding of Karst Occurrence and Protection of

- Karst Species and Habitats Worldwide”. ProQuest Dissertations Publishing, 2009. <http://search.proquest.com/docview/304847145/>.
- Hunsaker, C T. Spatial uncertainty in ecology : implications for remote sensing and GIS applications *New York: Springer*, 2001.
- Jacřková, K. and Romportl, D. The relationship between geodiversity and habitat richness in Šumava national park and Krřivoklátsko Pla (Czech Republic): a quantitative analysis approach. 2008 *Journal of Landscape Ecology* 1:23–38
- Jaubert, J. Verheyden, S. Genty, D. Soulier, M. Cheng, H. Blamart, D. Burlet, C. “Early Neanderthal constructions deep in Bruniquel Cave in southwestern France.” *Nature* 534, no. 7605 (n.d.): 111–114M.
- Joint Committee of American Society of Civil Engineering, American Congress on Surveying and Mapping, and American Society of Photogrammetric and Remote Sensing. (2011) Glossary of the Mapping Sciences. *American Congress on Surveying and Mapping, and American Society of Photogrammetric and Remote Sensing*.
- Jones, G. and Christal, M. “The Future of Virtual Museums: On-Line, Immersive, 3D Environments.” 2002 *Created Realities Group*. 2018 http://w.created-realities.com/pdf/Virtual_Museums.pdf
- Jost, J.. *Riemannian Geometry and Geometric Analysis*. 6th ed. Berlin: Springer, 2011.
- King, T F. *Cultural Resource Laws and Practice* Fourth edition. Lanham, Maryland: AltaMira Press, 2013.
- Kimel, A. V., Kirilyuk, A., and Rasing, T. “Femtosecond Opto-magnetism: Ultrafast Laser Manipulation of Magnetic Materials.” *Laser & Photonics Reviews* 1, no. 3 (December 14, 2007): 275–287.
- Klimchouck, A. B. Ford, D. C. Palmer, A. N. Dreybrodt, W. Speleogenesis: Evolution of Karst Aquifers. 2000 *National Speleological Society*. 2nd ed. ISBN-13 978-1879961098
- Laser Safety Facts. “Laser Classes Spread Sheet.” Accessed: 8/8/2010 <http://www.lasersafetyfacts.com/laserclasses.html>
- Langston, S. and Pell, S. J. “What Is in a Name? Perceived Identity, Classification, Philosophy, and Implied Duty of the ‘astronaut.’” *Acta Astronautica* 115, no. C (2015): 185–194.
- Larocque, H. Sugic, D. Mortimer, D. Taylor, A. J. Fickler, R. Boyd, R. W., Dennis, M. R. and Karimi, E. “Reconstructing the Topology of Optical Polarization Knots.” *Nature Physics* 14, no. 11 (November 1, 2018): 1079–1082.
- Law, J. & Rennie, R. Unruh effect. *A Dictionary of Physics*, 2015

- Laland, K. N, Uller, T. Feldman, M. W. Sterelny, K. Müller, G. B. Moczek, A. Jablonka, E. Odling-Smee, J. and Laland, K. N. “The Extended Evolutionary Synthesis: Its Structure, Assumptions and Predictions.” *Proceedings. Biological sciences* 282, no. 1813 (August 22, 2015): 20151019–20151019. <http://search.proquest.com/docview/1702659198/>.
- Levine, D. Steinhardt, P. and Levine, D. “Quasicrystals - A New Class of Ordered Structures.” *Physical Review Letters* 53 (December 24, 1984): 2477–2480. <http://search.proquest.com/docview/24364551/>.
- Mackay, A. L. “Crystallography and the Penrose Pattern.” *Physica A: Statistical Mechanics and its Applications* 114, no. 1 (1982): 609–613.
- Mandelbrot, B. B. “How Long Is the Coast of Britain? Statistical Self-Similarity and Fractional Dimension.” *Science (New York, N.Y.)* 156, no. 3775 (May 5, 1967): 636–638. <http://search.proquest.com/docview/733232575/>.
- Mandelbrot, B. B. *The Fractal Geometry of Nature* Updated and augmented. New York: W.H. Freeman, 1983.
- Martínez-Navarrete, C., Jiménez-Madrid, A., Sánchez-Navarro, I., Carrasco-Cantos, F., and Moreno-Merino, L. “Conceptual Framework for Protecting Groundwater Quality.” *International Journal of Water Resources Development* 27, no. 1 (March 1, 2011): 227–243.
- Massei, N., Dupont, J.P. Mahler, B. J. Laignel, B. Fournier, M. Valdes, D. and Ogier, S. “Investigating Transport Properties and Turbidity Dynamics of a Karst Aquifer Using Correlation, Spectral, and Wavelet Analyses.” *Journal of Hydrology* 329, no. 1 (2006): 244–257.
- Mattuck, R. D. *A Guide to Feynman Diagrams in the Many-Body Problem* 2d ed. New York: McGraw-Hill, 1976.
- Mayor, D. Mnemo Caveline Survey mapCSV/.svg files on cave mainline survey. *Quintana Roo Speleological Society* 2018
- Miller, H. J. “Tobler’s First Law and Spatial Analysis.” *Annals of the Association of American Geographers* 94, no. 2 (June 1, 2004): 284–289.
- Moore, C. H. and Wade, W. J. *Carbonate Reservoirs : Porosity and Diagenesis in a Sequence Stratigraphic Framework* 2nd ed. Amsterdam. Elsevier Science, 2013.
- National Park Service. 2012. “Sense of Place: Design Guidelines for Yosemite.” ISBN: 978-0-16-090412-7
- National Park Service. n.d.a. “Yosemite National Park: Your Safety - Special Protection for Special Places.” Accessed June 9th, 2017. Available at <https://www.nps.gov/yose/planyourvisit/safety.htm>

- Nebenhaus, M. Sistema Taj Mahal Survey: Xpu Ha, Quintana Roo, Mexico. UTM Coordinates 16Q East 471134 North 2265043. Total Surveyed Underwater Passage: 8226.2m. Maximum Survey Depth 23.78m. 2017 *Quintana Roo Speleological Society*.
- Lambert, N. Chen, Y. Cheng, Y. Li, C. Chen, G. and Nori, F. “Quantum Biology.” *Nature Physics* 9, no. 1 (December 9, 2012): 10–18.
- Neufeld, M. J. and Charles, J. B. “Practicing for Space Underwater: Inventing Neutral Buoyancy Training, 1963–1968.” *Endeavour* 39, no. 3-4 (2015): 147–159.
- Nielsen, A. B., and Shoom, A. A. “Conformal Killing Horizons and Their Thermodynamics.” *Classical and Quantum Gravity* 35, no. 10 (April 11, 2018): .
- NMAI. n.d. The 4D/NMAI Virtual Museums Project Story. 2017. *National Museum of American Indian* Available at http://www.nmai.si.edu/exhibitions/all_roads_are_good/VTStory.htm
- Noaa Diving Program (U.S.), and Joiner, J. T. *NOAA Diving Manual: Diving for Science and Technology*. National Oceanic and Atmospheric Administration, Office of Oceanic and Atmospheric Research, National Undersea Research Program, Office of Marine and Aviation Operations, NOAA Diving Program, 2001. <http://hdl.handle.net/2027/uiug.30112047045957>.
- Nunn, C. L. *The Comparative Approach in Evolutionary Anthropology and Biology*. Chicago ;; University of Chicago Press, 2011.
- Obermeyer, N. J., and Pinto, J. K. *Managing Geographic Information Systems* 2nd ed. New York: Guilford Press, 2008.
- Orosei, R. Lauro, S. E. Pettinelli, E. Cicchetti, A. Coradini, M. Cosciotti, B. Di Paolo, F. et al. “Radar Evidence of Subglacial Liquid Water on Mars.” *Science (New York, N.Y.)* 361, no. 6401 (August 3, 2018): 490–493. <http://search.proquest.com/docview/2076889082/>.
- “Outer Space Treaty.” *Britannica Online Academic Edition*, October 24, 2018. <http://academic.eb.com/levels/collegiate/article/57747>.
- Padilla, A., Pulido-Bosch, A., and Mangin, A. “Relative Importance of Baseflow and Quickflow from Hydrographs of Karst Spring.” *Ground Water* 32, no. 2 (March 1994): 267–277.
- Padilla, A. and Pulido-Bosch, A. “Study of Hydrographs of Karstic Aquifers by Means of Correlation and Cross-Spectral Analysis.” *Journal of Hydrology* 168, no. 1 (1995): 73–89.
- Pardo-Iguzquiza, E. Dowd, P. A., Xu, C. and Durán-Valsero, J. J. “Stochastic Simulation of Karst Conduit Networks.” *Advances in Water Resources* 35 (2011): 141–150.
- Pardo-Igúzquiza, E. Durán-Valsero, J. J. Dowd, P. A. Guardiola-Albert, C. Liñan-Baena, C. and Robledo-Ardila, P. A. “Estimation of Spatio-Temporal Recharge of Aquifers in

- Mountainous Karst Terrains: Application to Sierra de Las Nieves (Spain).” *Journal of Hydrology* 470-471 (November 12, 2012): 124–137.
- Pardo-Igúzquiza, E., Durán, J. J., Robledo-Ardila, P.A., and Paredes, C. “Fractal Modeling and Estimation of Karst Conduit Porosity.” *Environmental Earth Sciences* 1 (2015): 271–276.
- Parks, K. and Mulligan, M. “On the Relationship Between a Resource Based Measure of Geodiversity and Broad Scale Biodiversity Patterns.” *Biodiversity and Conservation* 19, no. 9 (August 2010): 2751–2766.
- Paschotta, R. *Encyclopedia of Laser Physics and Technology* Weinheim: Wiley-VCH, 2008.
- Penrose, R. *The Road to Reality : a Complete Guide to the Laws of the Universe* 1st American ed. New York: A.A. Knopf, 2005.
- Perrin, C. M. and Andréassian, V. “Does a Large Number of Parameters Enhance Model Performance? Comparative Assessment of Common Catchment Model Structures on 429 Catchments.” *Journal of Hydrology* 242, no. 3 (2001): 275–301.
- Perrin, J. A conceptual model of flow and transport in a karst aquifer based on spatial and temporal variations of natural tracers. PhD thesis. 2003 *University of Neuchâtel*
<https://core.ac.uk/download/pdf/20637364.pdf>
- Peterson, R. Terr, D. and Weisstein, E. W. 2019 "Fundamental Domain." From *MathWorld*--A Wolfram Web Resource. <http://mathworld.wolfram.com/FundamentalDomain.html>
- Pickering G. Bull J. M. Sanderson D. J Fault populations and their relationship to the scaling of surface roughness. *Journal of Geophysical Research* 1999 104(B2):2691–2701 276 E.
- Pike, R J. “Geomorphometry -Diversity in Quantitative Surface Analysis.” *Progress in Physical Geography* 24, no. 1 (March 2000): 1–20.
- Pořízka, P., Prochazka, D., Pilát, Z., Krajcarová, L., Kaiser, J., Malina, R., Novotný, J., et al. “Application of Laser-Induced Breakdown Spectroscopy to the Analysis of Algal Biomass for Industrial Biotechnology.” *Spectrochimica Acta - Part B Atomic Spectroscopy* 74-75, no. C (August 2012): 169–176.
- Portugal, S. Tatjana J. Hubel Y. Fritz, J. Heese, S. Trobe, D. Voelkl, B. Hailes, S. Wilson, A M. and Usherwood J. R.. “Upwash Exploitation and Downwash Avoidance by Flap Phasing in Ibis Formation Flight.” *Nature* 505, no. 7483 (January 15, 2014): 399–402.
- Pronk, M. Goldscheider, N. Zopfi, J. and Zwahlen, F. “Percolation and Particle Transport in the Unsaturated Zone of a Karst Aquifer.” *Ground Water* 47, no. 3 (May 2009): 361–369.
- “Project PoSSUM Inc.; PoSSUM Scientist-Astronaut Candidates Test Novel Space Suits and Biometric Monitoring Systems in Zero-G with the National Research Council of

- Canada.” *Defense & Aerospace Week*. Atlanta: NewsRx, December 19, 2018.
<http://search.proquest.com/docview/2155494307/>.
- Raggett, D. Le Hors, A. Jacobs, I. 2018 B. C. R. A. Survey Grades. Draft Date: 2018/04/05
 15:13:09 file:///C:/User/User/Downloads/B.C.R.A.%20survey%20grades.html
- Ratcliffe, M. A Century of Delineating a Changing Landscape: The Census Bureau’s Urban and Rural Classification, 1910 to 2010. Unpublished, 2014.
- redata.org. NIST Values of Fundamental Physical Constants; Values of Fundamental Physical Constants; NIST Reference on Constants, Units, and Uncertainty; The NIST Reference on Constants, Units, and Uncertainty. re3data.org - Registry of Research Data Repositories, 2014.
- Refsgaard J. C. van der Sluijsb J. P. Højberg A. L. Vanrolleghemc P. A. (2007) Uncertainty in the environmental modelling process—A framework and guidance. *Environ Model Softw* COST 65 (1995) Hydrogeological aspects of groundwater protection in karstic areas. Final report (COST action 65), Directorate-General for Science, Research Development; European Commission. *COST Action 65: Hydrogeological Aspects of Groundwater Protection in Karstic Areas*. Luxembourg: OPOCE, 1995. European Commission, Brussels, Luxembourg
- Reimuller, J. D. 2015 The Project PoSSUM Scientist-Astronaut Manual. *Project PoSSUM, Inc.* ISBN: 978-0578161426
- Rodríguez-Galiano V. Pardo-Igúzquiza E, Durán J. J. Chica-Olmo M, Luque-Espinar J. A. Guardiola-Albert C., Martos-Rosillo S. A. and Robledo-Ardila P. (2012) Cartografía del Epikarst integrando información de campo, geología e imágenes de satélite: caso de Sierra de las Nieves (Málaga). In: López-Geta JA, Ramos González G, Fernández Rubio R, Lorca Fernández D (eds) *El Agua en Andalucía. Retos y avances en el inicio del milenio*. Publicaciones del Instituto Geológico y Minero de España. Serie Hidrogeología y Aguas Subterráneas, vol 30, 2, pp 1611–1620
- Sakka, T. Tamura, A. Nakajima, T. Fukami, K. and Ogata, Y. H. “Synergetic Effects of Double Laser Pulses for the Formation of Mild Plasma in Water: Toward Non-Gated Underwater Laser-Induced Breakdown Spectroscopy.” *The Journal of Chemical Physics* 136, no. 17 (May 7, 2012): 174201.
- Scanlon, B. R. Mace, R. E. Barrett, M. E. and Smith, B. “Can We Simulate Regional Groundwater Flow in a Karst System Using Equivalent Porous Media Models? Case Study, Barton Springs Edwards Aquifer, USA.” *Journal of Hydrology* 276, no. 1 (2003): 137–158.
- Schiller, A., and Pfeiler, S. “A Laser Technique for Capturing Cross Sections in Dry and Underwater Caves.” *Environmental Earth Sciences* 1 (2015): 551–558.

- Seiberg, N., and Witten, E. “Electric-Magnetic Duality, Monopole Condensation, and Confinement in N=2 Supersymmetric Yang-Mills Theory.” *Nuclear Physics, Section B* 426, no. 1 (1994): 19–52.
- Selig, M. S. “Modeling Propeller Aerodynamics and Slipstream Effects on Small UAVs in Realtime.” In *AIAA Atmospheric Flight Mechanics Conference 2010*, 2010.
- Skanelect. n.d. “3D Scanning: Fast, Easy, and Low-Cost.” 2017. Available at <http://skanect.occipital.com/>
- Slocum, T. A. *Thematic Cartography and Geovisualization* 3rd ed. Upper Saddle River, NJ: Pearson Prentice Hall, 2009.
- Smithey, B, Cooper, R, and Smithey, B. “Measurement of Number-Phase Uncertainty Relations of Optical Fields.” *Physical review. A, Atomic, molecular, and optical physics* 48, no. 4 (October 1, 1993): 3159–3167. <http://search.proquest.com/docview/1859171047/>.
- Spilde, M, N. Melim, L. A., Northup, D. E., and Boston, P. J. “Anthropogenic Lead as a Tracer of Rock Varnish Growth: Implications for Rates of formation.(Author Abstract).” *Geology* 41, no. 2 (February 1, 2013): 263–266.
- Stafford, K. Brown, W. Ehrhart, J. Majzoub, A. and Woodard, J. “Evaporite Karst Geohazards in the Delaware Basin, Texas: Review of Traditional Karst Studies Coupled with Geophysical and Remote Sensing Characterization.” *International Journal of Speleology* 46, no. 2 (May 1, 2017): 169–180. <http://search.proquest.com/docview/1906353572/>.
- Staff Writers. “12 Scientist-Astronaut Candidates Graduate at Embry-Riddle Through Project PoSSUM.” *UPI Space Daily*. Washington: United Press International, May 1, 2017. <http://search.proquest.com/docview/1893469902/>.
- Stevanović, Z. *Karst Aquifers - Characterization and Engineering* Cham, [Germany: Springer, 2015.
- Stevanovic, Z. and Milanovic, P. “Engineering Challenges in Karst/Inženirski Izzivi V Krasu.” *Acta Carsologica* 44, no. 3 (September 1, 2015): 381–399. <http://search.proquest.com/docview/1768942982/>.
- Stinnesbeck, S. Frey, E. Olguín, J. Stinnesbeck, W. Zell, P. Mallison, H. González A. G. “Xibalbaonyx Oviceps , a New Megalonychid Ground Sloth (Folivora, Xenarthra) from the Late Pleistocene of the Yucatán Peninsula, Mexico, and Its Paleobiogeographic Significance.” *PalZ* 91, no. 2 (June 2017): 245–271.
- Stinnesbeck, W. Becker, J. Hering, F. Frey, E. Gonzalez, A. G. Fohlmeister, J. Stinnesbeck, S. et al. “The Earliest Settlers of Mesoamerica Date Back to the Late Pleistocene.(Research Article).” *PLoS ONE* 12, no. 8 (August 30, 2017): e0183345.

- Stinnesbeck, W. Frey, E. Zell, P. Avilés, J. Hering, F. Frank, N. Arps, J. et al. "Hells Bells – Unique Speleothems from the Yucatán Peninsula, Mexico, Generated Under Highly Specific Subaquatic Conditions." *Palaeogeography, Palaeoclimatology, Palaeoecology* 489 (January 1, 2018): 209–229.
- Suslick, K. S. "Synesthesia in Science and Technology: More Than Making the Unseen Visible." *Current Opinion in Chemical Biology* 16, no. 5-6 (December 2012): 557–563.
- Stuart, J. "The Pocket Oxford Latin Dictionary." *Reference Reviews* 9, no. 6 (August 20, 1995): 23–24. <http://search.proquest.com/docview/215218263/>.
- Takeuchi, S. "Unruh Effect in a Real Scalar Field with the Higgs Potential on a Dynamically Variable Background Space-Time." *The European Physical Journal C* 75, no. 9 (September 2015): 1–9.
- Vakoch, D. A. *Archaeology, Anthropology, and Interstellar Communication* Washington, DC: National Aeronautics and Space Administration, Office of Communications, History Program Office, 2014.
- Vassiliou, M.S. "The Virtual Research Laboratory: Taxonomy and Analysis." In *Aerospace Conference, 2007 IEEE*, 1–8. IEEE, 2007.
- Villasuso-Pino, M. Sanchez, I. J Y Pinto, E. Macario, G. B. Salazar, C, C. Cetina, R. C. Euan, J. S. Poot, P and Pech C. "Hydrology and Conceptual Model of the Karstic Coastal Aquifer in Norther Yucatan State, Mexico." *Tropical and Subtropical Agroecosystems* 13, no. 2 (April 1, 2011): 243–260. <https://doaj.org/article/f69aa3df4bf04dd49aa9bf4fa8de4015>.
- Vázquez-Domínguez, E. and Arita, H. T. "The Yucatan Peninsula: Biogeographical History 65 Million Years in the Making." *Ecography* 33, no. 2 (April 2010): 212–219.
- Virrantaus, K. Fairbairn, D. and Kraak, M. "ICA Research Agenda on Cartography and GIScience." *Cartography and Geographic Information Science* 36, no. 2 (January 1, 2009): 209–222.
- VRARA. "Top 10 Virtual Reality Best Practices." Virtual Reality/ Augmented Reality Association Stories & Audiences Committee. 2017.
- Weary, D. J. and Doctor, D. H. 2014, Karst in the United States: A digital map compilation and database: U.S. Geological Survey Open-File Report 2014–1156, 23 p., <https://dx.doi.org/10.3133/ofr20141156>. ISSN 2331-1258 (online)
- Weidner, N. Rekleitis, I. O’Kane, J. Valtorta, M. and Wang, S. "Underwater Cave Mapping and Reconstruction Using Stereo Vision". ProQuest Dissertations Publishing, 2017. <http://search.proquest.com/docview/2018329894/>.
- a) Weisstein, E. W. 2019 "Antiprism." From *MathWorld*--A Wolfram Web Resource. <http://mathworld.wolfram.com/Antiprism.html>

- b) Weisstein, E. W. 2019 "Dodecahedral Conjecture." From *MathWorld*--A Wolfram Web Resource. <http://mathworld.wolfram.com/DodecahedralConjecture.html>
- c) Weisstein, E. W. 2019 "Edge-Transitive Graph." From *MathWorld*--A Wolfram Web Resource. <http://mathworld.wolfram.com/Edge-TransitiveGraph.html>
- d) Weisstein, E. W. 2019 "Map Fixed Point." From *MathWorld*--A Wolfram Web Resource. <http://mathworld.wolfram.com/MapFixedPoint.html>
- e) Weisstein, E. W. 2019 "Snub Dodecahedral Graph." From *MathWorld*--A Wolfram Web Resource. <http://mathworld.wolfram.com/SnubDodecahedralGraph.html>
- White, W. B. "Conceptual Models for Carbonate Aquifers." *Ground Water* 50, no. 2 (March 2012): 180–186.
- Wheelock, F. M., LaFleur, R.A., and Wheelock, F.M. *Wheelock's Latin* 6th ed. New York, N.Y: HarperResource, 2000.
- Winder, I., King, G., Devès, M., and Bailey, G. "Complex Topography and Human Evolution: The Missing Link." *Antiquity* 87, no. 336 (June 1, 2013): 333–349. <http://search.proquest.com/docview/1372488360/>.
- World Heritage : Archaeological Sites and Urban Centres. 1st ed. Paris: Unesco, 2002.
- Xiong, Q., Zhu, Q., Du, Z., Zhu, X., Yeting, Z., Niu, L., Li, Y., and Zhou, Y. "A Dynamic Indoor Field Model for Emergency Evacuation Simulation." *ISPRS International Journal of Geo-Information* 6, no. 4 (2017)
- Yoshizawa, M. and Jeffery, W. R. "Shadow Response in the Blind Cavefish *Astyanax* Reveals Conservation of a Functional Pineal eye.(Author abstract)(Report)." *Journal of Experimental Biology* 211, no. 3 (February 1, 2008): 292–299.
- Znojil, M. "What is PT Symmetry?" Theory Group, Nuclear Physics Institute AS CR, CS 250 68 Režec, Czech Republic. *Journal of Physics*. (2001)

Appendices

Appendix A. Conceptual Periods in Speleogenetic Thinking

Conceptual Periods in Speleogenetic Thinking

<p><i>Protohominid Period – Jurassic to Pleistocene: 200Ma to 2.6Ma</i></p>	<p>Datasets from caves include speleothems, microbial colonies, giant sloths (<i>Xibalbaonyx oviceps</i>), saber tooth cats (<i>Simlodon fatalis</i>), mammoths, cave bears, human, and other paleontological and lithic remains. These present and provide direct and indirect evidence of troglolobiotic (cave flora and fauna) behavioral ecology. Paleokarst regions provide evidence of climatic formation stratigraphy, isotopic assay for global climate data calibration in temporally deep datasets, and climate prediction model TPU reduction.</p>
<p><i>Paleolithic Globalization Period - Pleistocene to Holocene: 2.6Ma – 10Ka</i></p>	<p>Human communities utilized caves since time in memoriam, emerging evidence from numerous global cave sites are revising the narrative of hominin globalization, complex topography hypothesis, and niche construction theory within human behavioral ecology. Human and faunal osteological samples are providing new understanding of geospatial phylogenetic timings, egression routes from Africa, bottlenecks, and refugia locations during glaciation cycles. Human remains from late Pleistocene stratigraphy are promoting cladistic arguments towards human species lumping, revisions to the savannah hypothesis, and new insight into behavioral ecology.</p> <p>≈2.6Ma - These arguments are representative of several factors stemming from survival needs and environmental fluctuations over evolutionary trajectories from cosmopolitan family to species scale. These factors are related to and include admixed Great Ape families making a rapid migration out of Africa before 2.1Ma.</p> <p>≈2.1Ma - with modern human ancestors emerging and coexisting several ancestors and admixing with others near exodus terminus. Activities by hominins eventually extend to nearly all biological niches, high cognitive functioning, creative exploration in terms of spatial cognition, and built environment development for survival all relate to and emerge from these factors.</p> <p>Global geoarchaeological evidence in terrestrial, karst, and subaquatic environments from South Africa, Kenya, Israel, Georgia, Spain, China, the United State of America, the United Kingdom Mexico, and other localities are diverse. They possess paleoclimatological, paleontological, lithic technology, behaviorally modified materials, and trace element in various forms, in various complex topographic landscapes. These include some of the oldest global environmental, faunal, and floral isotopic remains, burnt/cut (BRM) prey and human remains evidence, stone tool technologies, hollowed/compacted karst features, and residue of carbon monoxide and dioxide. New evidence is prompting an evaluation of caves in terms of humanities evolution as well as possibilities of unnecessary cladistic differentiation, as argued by Goethe.</p>
<p><i>Classical Period –</i></p>	<p>4th Century BCE (2468±25 calibrated BP) - The beginning of Western academic study of caves began in globalized Ancient Greek, Egyptian, or Sumerian traditions. Numerous etiological mythologies of various</p>

<p><i>Lower Holocene to Upper Holocene: 10ka to 0 CE</i></p>	<p>cultures, cults, and recordings intertwine with global caves with the births of gods, kings, and rivers. Aristotle noted the existence of caves and of rivers entering valleys with no outlets, flowing beneath mountains.</p> <p>250BCE (2268±10 cal. BP) - Archimedes of Syracuse authored <i>On Floating Bodies</i>, which stands as the formative, though poorly understood, conceptual, mathematical, and exploratory framework on buoyant forces, which are intricately linked with fluid dynamics and cave formation.</p> <p>63BCE (1984±5 cal. BP) - Records of Phoenicians and Strabo's description of fresh water collection in leather bags by boatmen offshore submarine springs had been known and utilized as a source of fresh, potable water, for 3000 years of maritime activity. The same technique can be seen used today in the Persian Gulf. The freshwater bubbles up giving a boiling impression representative of an offshore or submerged aquifer discharge.</p> <p>The following centuries saw the exploration of the concept in several areas between catastrophist and uniformitarian theories of geological processes. Speleogenesis formation processes of the subsequent centuries included human creation through mining, formation with contemporary rock, tectonic activity, rapid erosion, rapid dissolution, visible erosion cycles, and visible dissolution cycles.</p>
<p><i>Foundational Period - Upper Holocene: 1CE to 1900CE</i></p>	<p>Caves were used for food fermentation control, moonmilk collection for medicinal use, along with habitation or concealment by bandits and militaries, among other things over the centuries. Classical and renaissance theories that maintained scholarly discussions on caves began to distill in the Age of Enlightenment. These works promoted experimentation, as well as deductive and inductive reasoning to develop foundations of the larger concepts in physical sciences, understanding of planetary systems, and remote sensing.</p> <p>1708 – Lang described water draining from the surface through ground cracks, corroding them, off-gassing, and producing voids for underground lakes.</p> <p>1729 - Martyn considered that soft inclusions in rock could be removed by erosion</p> <p>1756 - Alexander Catcott found caves to result from water processes and produced the first karst interior cross-section illustrations of bedding plane midheight (now understood as formation while filled with water).</p> <p>Other events of the 1700s - involved and promoted new insights of scientific inquiry and experimentation. Prior to the American Revolution, Mohawk's of the Iroquois Confederacy utilized the limestone escarpments of Voorheesville, New York as a trail network, providing access to Henry Hudson's trading outpost. During the American Revolution a regional cave became named Tory Cave, serving as a hideout for Jacob Salisbury a British loyalist (Tory) while reporting and raiding on farmers and troops allied with patriots, Salisbury was eventually caught and hung when smoke was seen coming out of the cave. The site is preserved within Indian Ladder Trail of Thatcher State Park, Voorheesville, New York. The Indian Ladder trail represents karst topology of more than 20 caves within a few miles. After the war this area was subsequently examined and surveyed by Charles Lyell, Amos Eaton, James Hall, and Winifred Goldring.</p>

1788 - James Hutton, later popularized by Lyell, recognized fluvial erosion of surface geomorphology, noting 'the present is the key to the past'. Other authors began recognizing the possible hydrological processes in speleogenesis.

1817 & 1819 - Brongniart and Aubuisson de Voisins respectively noted salt (NaCl) inclusions could be deposited or removed by water and would lead to cave erosion formation.

1830 - Charles Lyell, proponent of Hutton and Father of Modern Geology, as well as Charles Edouard Thirria cited the activities of carbonic acid dissolution of limestone, concurrently and independently.

1858 - Lyell's recognition of deep-time, solution chemistry, and geographic evolution caused him to assist publishing Charles Darwin's and Alfred Russel Wallace's essays on biological evolution through natural selection in 1858.

1859 - Edouard Martel informed the speleological community of vadose zone solution activity and argued against phreatic speleogenesis until the 1890s.

1870 - Thirria's publication covered numerous caves related to aqueous carbonic acid formation in relation to mining studies. Franklen Evans' paper discovered most karst systems are formed via in phreatic groundwater dissolution below the ground water saturation zone.

1893 - Jovan Cvijic published on the topic of landform development sequence in Dinaric karst region. Thirria's publication was comprehensive, in comparison to Lyell's topical assessment of limestone dissolution in Principles of Geology. Ferencz Posepny, explained groundwater movement in speleogenesis as both lateral and horizontal motion. The papers presented by Thirria, Evans, and Posepny were all revolutionary in their comprehension of the speleogenetic process but were all equally unrecognized by contemporary mainstream counterparts. Speleogenetic discussions segmented and factionalized due to this oversight and progressed in several different camps. The Belgian Society of Geology, Paleontology, and Hydrology was the scene for a series of debates on formation modeling favoring phreatic dissolution or vadose erosion speleogenesis.

1896 - Armand Flamache argued for all-erosion, non-dissolution theory against Edouard Dupont speleogenesis concepts because of the observation that calcium carbonate saturated groundwater and that it promoted mechanical erosion in karst systems as on the surface. Finally, Edouard Dupont forwarded carbonic acid dissolution occluded above and below the water table with illustrations representing the effects of scouring and attrition of cave walls from hydrologic fluvial processes. Caves existing below the water table during the quaternary were intersected by surface valleys down cutting. This three-theory preface of speleogenesis: vadose zone activity by Martel, erosion-only by Flamache, and continuous phreatic dissolution by Dupont and Cvijic influenced the understanding of hydrogeologic processes in speleogenetic research through the 1900s.

<p><i>Early Modern Period – Upper Holocene: 1900 to 1930CE</i></p>	<p>Reconciliation by later generations of geomorphologists and geologists led to the unison of all three speleogenetic theories acting in a cohort process on a continuum in combination, collaboration, succession, proportion, and/or variation dependent upon the local environment evolutionary trajectory. Progression of exploration and publication on observations for model comparison prompted further discussion, debate, and model constructions that were fouled by regional biases and narrow views in formation potentials. Cvijic, Grund, Katzer, and Sanders further developed the concepts and misconceptions for this modern perspective of speleogenetic processes that guided the next half century.</p> <p>1903 - Alfred Grund proposed karst aquifers were divided into two zones above and below the water table at a regional extent. He added that the lower zone below the table was stagnant water, and above the zone, was circulating in open caves. Grund's stagnant groundwater fallacy persists reflecting the misconception of the effects of flood zone flux induction of speleoinception.</p> <p>1909 - Katzer was an extreme extension of the groundwater table argument. He proposed no zone of saturation existed and therefore no watertable was possible. Martel supported Katzer's argument of surface water downcutting along the most permeable bedding plane as well as the largest gauge fissures to bottom. This model viewpoint has benefits and deficits, the speleogenetic process described is important. It does not prove or imply relevance of origin, earliest development phases, and drainage patterns are restrictive to time scales in speleogenesis.</p> <p>Between 1893 & 1918 - Albrecht Penck, Cvijic's professor, and William Morris Davis took a group of students on a field survey of the Classic and Dinaric Karsts. These surveys were patriarchal for geomorphology. The conclusion and model impacts are still being felt due to attempts to fit reality into an unfit erosional cycle concept.</p> <p>1918 - Cvijic published a controversial second paper on the development of landforms to subsurface karst hydrology. He signified a descending dry, transitional, and saturated hydrographic zone order to caves. This stratification is still accepted today in more developed forms. Cvijic also proposed most groundwater flow, and the major focus of cave development, occurred proximate to the water table, above or below.</p> <p>1921 - Martel published again, in support of Katzer's argument, which provided him large experiential backing.</p>
<p><i>Golden Age – Upper Holocene: 1930 to 1942CE</i></p>	<p>This period saw a refinement of the existing works of by Thirria, Evans, and Posepny, and maintained central themes that were forming in karst research. These included the development of concepts of hydrodynamics, dissolution chemistry, drainage patters, and geomorphology. Davis, Swinnerton, Lehmann, Gardner, Malott, Laptev, Moneymaker, Rhoades, Sinacoria, and Bretz were among the primary authors of this</p>

period. Their work began synthesizing radiometric dating, palaeoecological records, dissolution chemistry, statistical flow modeling, and geometric considerations in network development.

1930 - Money maker worked for the Tennessee Valley River Authority and had extensive access to boring cores and open cut excavation sites developed to determine dam construction sites. He observed numerous dissolution cavities of diverse sizes that formed above and below the recognized watertable. He recognized a statistical link between cavity dimensions, density of cavities related to depth, and abundance in specific rocks. He finally noted after downcutting by surface streams, speleoinception initial dissolution occurs below the water table leading to cavity enlargement above the water table. Rhoades and Sinacoria were one of the first truly modern studies, was entirely theoretical, and utilized early mathematical modeling for groundwater flow. Their flow net model utilized Laplace's differential equation and Darcy's Flow Law. They solved numerous two-dimensional seepage problems by defining the flow lines and equipotential lines of the flow curve set to two. Their work proved that the Davis and Swinnerton modeling both occurred and could concurrently in the same area. Davis wrote his classic deductive essay, *The Origin of Limestone Caverns*, which has reception in karst geomorphology and hydrology, introducing the geologic timescale for the speleogenetic process. Davis' proposed speleogenesis originates as a multistage cycle below the watertable, in deep phreatic dissolution processes over tens to hundreds of millions of years and the shallow areas processes in shorter time spans. His work was critiqued for lack of detailed models of deep drainage, dissolution chemistry, and concepts in hydraulic pressure for groundwater flow at depth. Though some sections of his work were disproven, some remain up for confirmation, and some prompted further developments.

In 1932, Swinnerton and Lehmann both published their works, which represented some of the next integrative phases of karst science. Swinnerton was the first author to note significant cave tiers features formation in terms of karst hydrogeomorphology and chemical dissolution. His views, ahead of his peers, are now historic in terms of cave research from his lack of development of the concepts from both disciplines. Lehmann's work was very inductive based on extensive field survey experience, refuted hydrographic zones, supported cave river erosion, like Martel and Katzer, was published in German, and was later found to be partially correct. These represent the most widely received speleogenetic research papers of the period from Europe and the Americas. Swinnerton's work was comprehensive in consideration of Davis model, and argued a shallow processes series proximate to the watertable were critical in cave generation. Swinnerton postulated tiers represented recurring karst passages subhorizontally cut at parallel levels by sequential drainage of preferential conduits. He proposed tiers formed in a near vertical range via seasonality through erosion and dissolution of watertable by volume and high fluctuation. Swinnerton's model did not describe mechanisms for the needed watertable fluctuation in impermeable rock and the concentration increases in carbonic acid to dissolve the

matrix. His model built upon Cvijic's, Martel's, and Katzer's works; incorporating hydrographic zoning, groundwater flow down cutting along caves as a least cost path, and karst dissolution growth rate of deep phreatic zones lower than vadose zones in speleogenesis. Lehmann's work was very inductive based on extensive field survey experience, refuted hydrographic zones, supported cave river erosion like Martel and Katzer, was published in German, and was later found to be partially correct. He first described the dual function the estavalles mechanism for formation of skin holes and springs. Lehmann first noted karst hydrological contrast as the discrepancy of numerous input sink holes and sparse output conduits or springs. Hydrological contrast has since been revised with inclusion of conduits inactive in the dry season and active in the rainy season. It has also been discovered tectonic fissures, and bedding planes effect input and output potential and these vary with regional geology and landscape morphology.

In 1935, Gardner further developed Grund's work as he was seeking explanations for large cavern development. By questioning static groundwater down cutting promoting conduit preference and abandonment leading to karst levels and tiers; he promoted understanding of hydraulic forces effects on vadose modification as cross-formational piracy. Grund's model, prophetic asides on speleogenesis, and favor of Swinnerton's one-cycle model effected research profoundly, leaving several topics open to argument and study. Gardner was the first to incorporate stratigraphic modeling and bedding planes as carriers for groundwater flow from downcutting of valleys. His model lacked an explanation for conduit flow piracy by lower level strata in carrier bedding through impermeable rock. His work never concluded with an obvious limit and could have built on speleoception, multilevel karst, stratigraphic controls, ore deposition, sulfur water, and salt water.

Malott, in 1937, covered cavern development through invasion theory. Malott did not discuss cave origins but came the closest to producing a modern speleogenetic model. He highlighted early dissolution of caves occurs throughout the entire karst stratigraphy, without preference to saturation typology. Surface rivers down cut and enter existing aquifer inputs. Percolating groundwater follows the largest, oldest, least cost path fissure, or conduit to the watertable creating caves proximate to the watertable. Malott promoted that early uplift of caves from the watertable is three-dimensional and poorly integrated leading to stratigraphic and structural factors effecting sedimentation. His work is the first to propose that speleoception occurs in the phreatic zone. Geopolitical violence and power transition divides promoted redundant research to occur on both sides of the divide during the rest of the 1900s.

Laptev authored his work in 1939, but it was not recognized in Western Academia until 1964 due to the geopolitical and socioeconomic divides between the former Soviet Union. Laptev's work is the best representation of the echoing geopolitical complications this period caused in research. His work focused in detail on the equilibrium chemistry of calcite and the effects of mixture corrosion via water on carbonate rock, concrete,

	<p>and gypsum. Laptev discovered that as carbon dioxide built up in water the carbonic acid formed would weather the rock, and prompt positive feedback in more acidic dissolution solvent promoting further cave development. He particularly noted the likely genesis of caves in deep phreatic zones from dissolution. Laptev's work as well as later Russian scientists would promote bridges in research comprehension of karst formation across the Iron curtain but also denoted redundant research.</p> <p>In 1941 Moneymaker, as well as Rhoades and Sinacoria published their respective works. The works would greatly affect the next fifty years of research. Moneymaker's model was one of the most coherent, developed, and advanced in the understanding of speleogenesis of the time. Rhoades and Sinacoria redefined the conduit piracy proposed by Gardner and greatly promoted later modeling and understanding.</p> <p>1942 – Bretz marked the end of the Golden Age and had primarily studied caves in Cambrian to Permian geologic contexts. He supported and added to Davis' developments. Bretz became the first speleologist to name, describe, and classify hydrological and geomorphological features in terms of vadose and phreatic zones. He also described the infilling of caverns by stagnant water during re-uplift periods, though this has been proven to be accomplished by flowing water. Groundwater flow discussions continued to progress over the prevailing years and have promoted much of the modern basis for karst research.</p>
<p><i>Second World War Lag Period – Lower Anthropocene : 1943 to 1957CE</i></p>	<p>This period is marked by a karst research hiatus due to mobilization of national and global resources for war against fascism. Notable activities, in the hiatus of research, occurred in karst regions during the war in the European and Japanese theaters. The activities included uses by numerous groups based on varied considerations and applications for karst resource utilization. Jewish partisans also utilized the networks of European karst to evade capture by fascist forces, and stage ambushes. Austrian, Italian, and Yugoslavian partisans utilizing caves against Germany with ruthless effectiveness until the end of the war. Nazi development of the 24th Armed Cave/Mountain Division of the SS, <i>Waffen Schutzstaffel Karstjager</i>, from recommendation from karst regional researchers in Austria. It was one of the first recorded cave combat forces, reached 10000 men in total, and was unable to effectively respond to terranean knowledge advantages of partisans in caves.</p> <p>1943 - Quebec Agreement between the United Kingdom and the United States promoted coordinated research, development, and deployment of nuclear energies and weapons, and the subsequent arms race. The success of this agreement denotes the end of the Second World War in 1945 by the detonation of the uranium gun and plutonium implosion nuclear devices over Hiroshima and Nagasaki Japan, respectively. The agreement also signifies the beginning of the Cold War, and the Anthropocene Geologic Epoch in 1950, as the year represents the several geophysical and ecosystem factors.</p> <p>1950 - Is carbon isotope radiometric dating foundational year zero, with all years prior to January 1st, 1950 represented as BP (argued as meaning before present or before physics). Subsequent years are identified as CE</p>

	<p>(argued as common era or current era). It is represented as global datasets of irradiated geochemical microstrata, bioorganic matter, and atmospheric ionizations from incessant nuclear weapons testing, which with current technological means are irreversible in impact. These subsequently distort future radiometric dating efforts by alteration of naturally occurring carbon isotopes. This year also marks a relative delineation of the Former Soviet Union's, now the Russian Federation, 4-month entry into atomic energies and weapons development, testing, and mobilization.</p>
<p><i>Modern Period – Lower Anthropocene : 1958 to 1999CE</i></p>	<p>The beginning of this period marks the end of research lag in Western academia due to the cessation of the Second World War. It also marks the conceptual shift on from watertable dynamics to renewal of geological setting, speleogenesis preeminence in aquifer hydrogeology, and dynamics of chemical dissolution. Three perspectives formed: cave geology, karst hydrology, and chemistry and fluid mechanics. Developments in nuclear physics, technology, and analysis promoted karst studies in several ways. Uranium/thorium (U/Th) and Argon/Argon ($^{40}\text{Ar}/^{39}\text{Ar}$) mass spectrometry radioactive dating of speleothems allowed for minimum age identification, and paleomagnetism of pole reversals during sediment formation promoted dating of caves.</p> <p>1953 - The largest development noted by White's paper is the development of integrated theory for karst research by the International Congress on Speleology. This was the final the movement away from regionally based exploration and research methods to a common international conceptual framework. These led to appreciation of halocline, hydrothermal, and sulfuric acid activities and alternative speleogenetic processes. Research on underlying processes and mechanisms of speleogenesis have developed in concert since.</p> <p>1992 – Lowe covers the development of concepts in speleogenesis over the course of the 1900s. His coverage is thorough and recognizes cultural gaps causing research redundancy from lack of ability for global conferencing on current topics. His critical historical assessment sets the scene, characters, and concepts into a dialog that reflects and builds on the research tradition with current knowledge.</p> <p>1997 - White succinctly reiterated the developments of the past four decades of research to highlight major discoveries. He performed a topical assessment of karst research and notes three competing perspectives and directions for speleogenetic modeling. The three perspectives developed into cave geology, karst hydrology, as well as chemistry and fluid mechanics perspective in between the two. Geology focused upon morphology, sedimentation, and setting. Hydrology considered hydrodynamics solely effecting the evolution of karst aquifers. Consideration on relative dissolution rate as a function of fluid flow from experimental testing promoted understanding of dissolution-cut carbonate single conduit formation because of runaway dissolution. He notes Ford-Ewers model quelled arguments of cave formation relationship to the watertable based on fractures frequency. The Ford-Ewers conceptual framework for deep flow loop, horizontal conduit-stream networks, and</p>

	<p>deep shaft systems promoted developments in geochemical water quality testing equipment, spectrofluorimetry, hydrograph assessment, and flow tracer dye development.</p>
<p><i>Foundational Revolution – Middle Anthropocene : 2000BCE to Present</i></p>	<p>Recent technological developments from the fourth and fifth industrial revolutions have affected environmental, socioeconomic, and research communities immensely. Technologies in computer science, electronics, automation, biochemistry, geographic information science, and physical mensuration have continued to extend range and scope of possible observable phenomena.</p> <p>2000 (68AP, After Physics) – Klimchouck et al. represents the mark of the beginning of modern karst science in terms of speleogenetic, hydrogeologic, and landscape morphologic evolution; covering numerous topics of speleogenesis, including include historical perspectives of research, hydrogeologic controls of cave evolution, theoretical processes, setting variation in development of cavities & systems, morphology across microscopic to macroscopic scales, and implications of research.</p> <p>Developments range and scope promoted rapid progression of accuracy and precision of data collection in the past decade and a half. Speleology underwent a revolution in comprehension of the speleogenetic processes. Appreciation of paleokarst formation, speleothem calibration in geochronology and biological evolution, and an increased capacity for systems modeling and exploration are benefiting from remote sensing, robotics, and geodatabase development progress.</p>

Appendix B. Glossary

Analog – A situation, that has similarities to another environment; also, datasets collected with non-digital methods.

Anthropogeny – the study of the biogeographic and phylogenetic emergence and origins of humanity.

Astrobiology – A field of biological science focused on the topics of the universal origins of life, evolution, intergalactic supercluster distribution, & potential futures of first contact & coevolution between humans and exobiological organisms. Similar to exobiology.

Barycenter - the astrophysical center of mass of two or more co-orbiting bodies and the point about which those bodies orbit.

Boson – one of the two classes of Bose-Einstein statically obedient elementary particles, fermions being the other, that make up fundamental particles including: photons, gluons, Higgs, W, Z, force-carrying gauges, and potentially quantum dynamic gravitons.

Bounded-Error Quantum Polynomial Time – a class of solvable decision problems by a quantum computer in polynomial time, with an error probability of at most 1/3 for all instances in computational complexity theory.

Brillouin Scattering - a transparent materials index of refraction changes under deformation (compression-distension or shear-skewing) with the results of materials interactions and a 3D fractal quantum dynamics light-wave and carrier-deformation momentum translation in preferential photoelastic oscillatory diffraction grating directions.

Brillouin Zones – an identified minimum volume cell within a lattice space that has a single point of transitive symmetry in reciprocal 2 or 3-dimensional crystal space. The first zone is closer to the origin of the reciprocal lattice than to any other reciprocal lattice points and serves as a locus of points in reciprocal space. Subsequent vectors do not provide more information than the primary zone.

Brillouin-Wigner (BW) Perturbation Theory – utilized less than the Rayleigh-Schrodinger Perturbation Theory. First order in the perturbations for both theories are equivalent. BW extends to higher dimensional orders, avoiding separate treatment of degenerate and nondegenerate fields.

Clinometric – Measurement of the incident Angle of Slope.

Collective Excitation – a type of emergent phenomena that occurs when a microscopically complicated systems free spaces seems to operate as if it possesses weakly interacting forces.

Complementarity – a concept in physical sciences that contrasted theories, e. g. dualistic wave and particle theories of light, explain dualistic phenomenon, although each only individually account for some aspects of the whole phenomena.

Complex Topography Hypothesis – Conceptual framework within evolutionary biology superseding the Savannah Hypothesis of human evolution, placing emphasis on exploitation of rugged landscapes (mountains, caves, valleys, cliffs, etc.) for predation, protection from predators, and remote access to water sources leading to continued adaptive advantages extending from prior arboreal terminal branch omnivores in terms of binocular vision, opposable thumbs, geospatial cognition, and etc.

Coxeter Group – an abstract mathematical set admitting definitions by presentation in of kaleidoscopes and reflections.

Diffraction Grating – a periodically structured optics component that splits and diffracts visible light into different beams propagating in different directions.

Delaunay Triangulation – Also known as Delone Triangulation, is a form of computational geometry that extends metrics of Euclidean distance. It maximizes triangular vertex minimums in a plane for any given set of discrete points \mathbf{P} within a plane $DT(\mathbf{P})$ that extends to $>3D$ analysis. It is oriented such that no point of a reference triangle is within a navigational circumcircle for any triangle in the reference set. There is no navigational reference for a linear set of points. >4 points on a single circle (e. g. rectangular vertex) do not provide orientation data, where both reference positioning quadrangles satisfy the computational condition with both quadrangles retaining empty interiors.

Delaunay Tessellation Field Estimator – a analytic tool for volume-covering, continuous density, or intensity fields from a discretized point for reconstructions in astrophysics.

Epidemiological – Medicine Science of incidence, distribution, and diseases control modeling, planning, & response.

Exoplanet – Planets other than Earth, particularly those outside the Solar system.

Exobiology - A field of biological science focused on the topics of the universal origins of life, evolution, intergalactic supercluster distribution, & potential futures.

Fermions – a Fermi and Dirac statistically obedient elementary particles with half-integral spin including protons, nucleons, quarks, leptons, and baryons related to matter.

Fundamental Domain – a spatial subset containing exactly one point from each orbit of action (e. g. Voronoi Tessellation Diagrams). Images of a single point exposed to group action induce a novel spatial structure preserving orbital transformations related to the topological space and group spatial operations.

Geohazard – Is a geological situation that can cause widespread damage, i.e. tsunami, Earthquake, sinkhole.

Geoheritage – Is the relationship between Earth & human evolution, and its effects on regional cultures & developments

Geomorphology – The study of planets' landforms in relation to their lithic formations.

Geospatial – Data that is specific to a certain (x, y, z) vector coordinate referenced position, orientation, and trajectory.

Ghyben-Herzberg Relationship - for every foot of fresh water in an unconfined aquifer above sea level, there will be forty feet of fresh water in the aquifer below sea level.

Hydrogeochemical – The chemical composition of water relating to the chemicals in it and the host matrix chemical composition where it is located on the Earth.

In Situ – In the natural or original location.

Karst – Land made of soluble rocks such as: dolomite, limestone and gypsum that contains caves, sinkholes, and aquifers.

Kissing Number – a geometrically defined number of non-overlapping unit spheres arranged with each touching a common unit sphere. The interface number is the same for every sphere in axiomatic lattice packing and casual in random-space packing.

LaGrangian Point- a location in spacetime where the combinatorial gravitational forces of two or more bodies equal the centrifugal force felt by a much smaller co-orbiting body (e.g. Earth, Moon, & Sun).

Lithostratigraphic – Scientific study of rock deposition by layer, or strata for time-series profile of evolutionary developments.

Magnon – a boson obedient, quasiparticle that has a fixed energy, crystalline structure, and lattice momentum that represents electron spin structure and collective excitation measured as a spinning wave.

Many-Body Problem – a large category of physical problems pertaining to quantum dynamics related to numerous particle interactions from 3 to infinity with induced entanglement and data storage via the quantum wave-function acting as a complicated object preventing accurate remote sensing measurements.

Microbiome - The microorganisms that live in a certain location.

Niche Construction Theory – Theory of Evolutionary Biology that as an organism modifies its environment and the subsequent environmental changes, affect both coevolutionary trajectories for the environment and organismal communities.

Oximetry – heart beat pulse monitoring device that utilizes detects patient blood sample oxygen saturation and blood volume by skin illumination to detect changes in light absorption. The datasets are used to produce an optical volumetric measurement of an organ call a photoplethysmogram.

Paleobiogeography – Study of the effect of geological location and features on prehistoric animals and planets.

Phenomenological – States that it's a phenomenon and not a present state.

Phonon – a periodic elastic condensed matter collective excitation arrangement of atoms via vibrations.

Photon – an elementary particle serving as the quantum of electrodynamic fields magnetic radiation and force with zero rest mass and speed of light velocity in vacuums via complementarity.

Phreatic – Water filled karst.

Plasmon – an individually harmonically quantized quasiparticle plasma oscillation.

Polaron – a quasiparticle representing electronic and atomic iterations in solid materials, where electrons convert to photons

Quasicrystal – Also called quasi-periodic crystals, is an ordered material structure that is aperiodic. The crystalline pattern fills all space continuously and lacks translational symmetry. These structures extend non-traditional restriction theorem limits, with Bragg diffractions pattern with symmetric ordering beyond 2, 3, 4, 5, and 6-fold rotational symmetries, for instance 16-fold.

Quasiparticle - a type of emergent phenomena that occurs when a microscopically complicated systems free spaces seems to operate as if it possesses weakly interacting particles.

Quasi-triangulation – a topological space-time navigational reference utilizing geometric subdivisions into simplices, vertices are arbitrary sloped line segments that represent an objects position. These relate to characteristics of Delaunay Triangulation in Apollonian sphere packing.

Radiometric – The measurement of radioactivity which tells the age of rocks, or carbon.

Random Matrix Theory – a mathematically represented probabilistic physical system with some, or all elements, that are inherently causal, stochastic, or chaotic producing unexpected novel systems.

Seiferometry – An analytic technique that determines the topological composition and structure of quantum pulse knotting due to fluid vortices via Seifert tori oscillation.

Snark – a distinct 4 chromatic-edge biconnected cut-edge cubic diagram where edges of a tree are bridges. It contains a bridge if, and only if, it contains an articulator vertex, it is not a biconnected graph if it does not contain a vertex of articulation.

Spectrometry - an analytical technique that determines the composition and structure of a material by measuring the mass to charge ratio of charged particles.

Speleogenesis – Creation & development of caves.

Speleonator – Latin derivative logomeme for cave conjoined with swimmer – cave-diver.

Speleonaut – Latin derivative cave sailor attributed to Jochen Hasenmayer & his cave submarine

Speleothem – A structure that is formed in a cave geohydrochemical dissolution, deposition, or mechanical weathering by mineral deposits.

Trojan Point – a type of Lagrangian object that makes up two of five types of Lagrangian points, that are one type of co-orbital object with arrangements related to relative barycenter of the co-orbital objects.

Unruh Effect – a quantum dynamics prediction that an accelerating sensor will observe blackbody radiation where an inertial sensor would detect none.

Voronoi Tessellation Diagram – a partitioned topological space segmented into regions based on select subset distances to specified points (e. g. seeds, or generators), where each region consists of all points closer to that generator than any other cell. A set of points is dualistic to a Delaunay triangulator.

Xenobiology – Life chemistry based on different base elemental compositions due to differential environmental composition & (Nobel gas law) $Pv=NRt$ on potential organismal evolutionary trajectories.

Appendix C. Analog Martian & Terrestrial Atmospheric Environmental Contexts

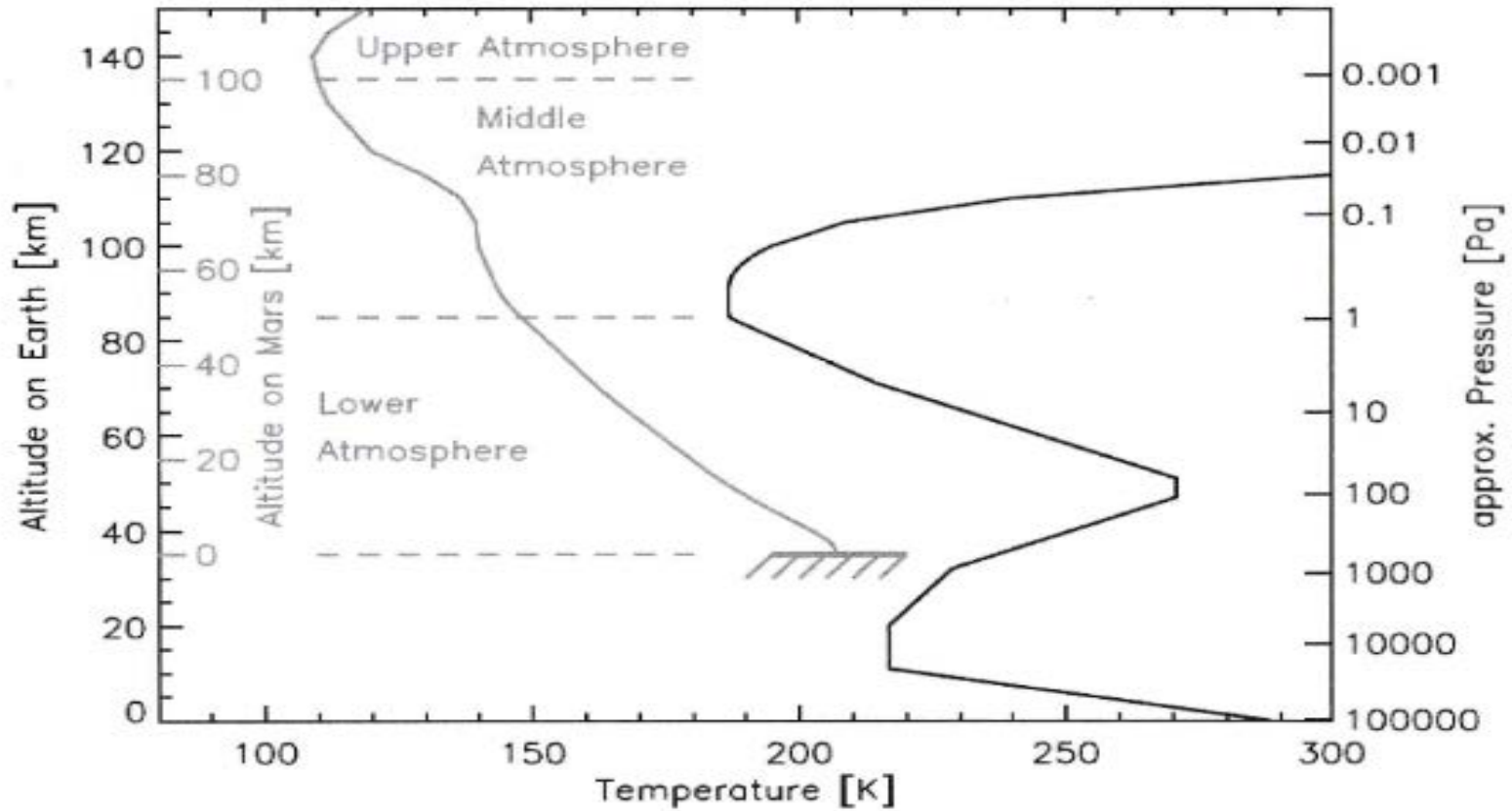
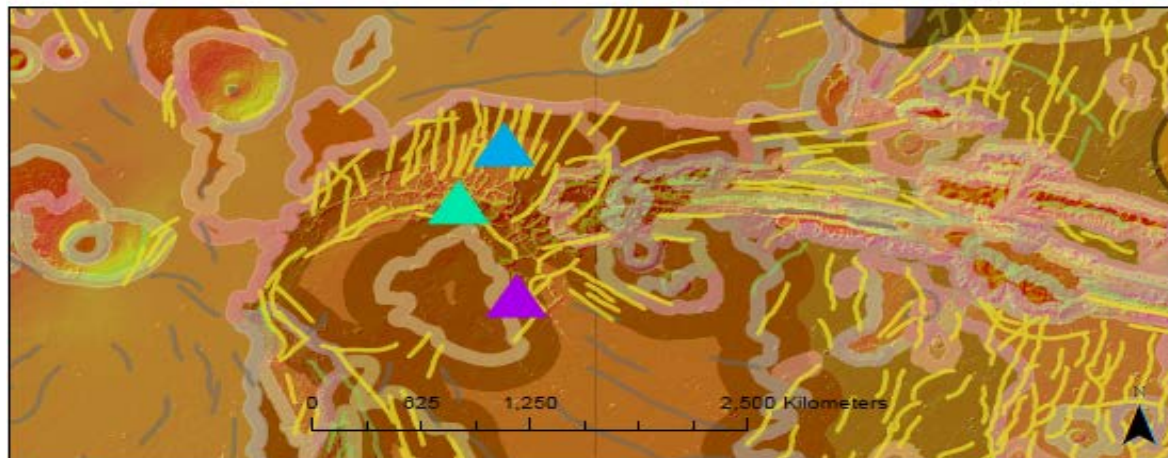
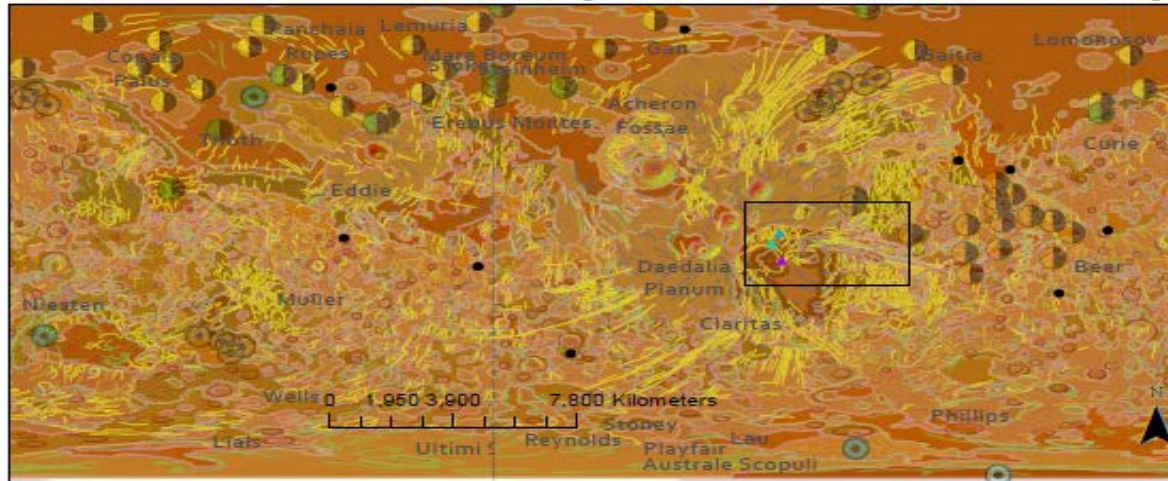


Figure 21: Standard temperature profiles vs. altitude for Earth (black, based on the US standard atmosphere) and Mars (gray, based on the MCS temperature climatology in the non-dusty season in Haberle et al., 2017). The surface pressure on Mars roughly corresponds to the atmospheric pressure on Earth found at 35 km altitude, hence the altitude scale for Mars was offset by 35 km with respect to the altitude scale for Earth. The pressure scale is only approximate due to the differences in atmospheric temperatures.

Appendix D. Martian Kart of Noctis Labyrinthus and Robotic RS Survey Geohazards

Martian Karst of Noctis Labyrinthus and Unmanned System Survey Geohazards



Unmanned Systems Landing Sites

NAME

- MER A
- MER B
- MSL
- Mars 2
- Mars 6
- PHX
- Pathfinder
- Viking 1
- Viking 2

Feature of Interest

Late Hesperian Volcanic Unit

- ▲ Noctis Fossae
- ▲ Noctis Labyrinthus
- ▲ Noctis Tholus

Karst Units

Pseudokarst

Eboulisation

- Amazonian & Noachian Apron
- Amazonian Polar Unit
- Early Amazonian Basin
- Late Amazonian Polar Cap

Eukarst

Solution

- Hesperian Transition
- Late Hesperian Lowland
- Middle Amazonian Lowland

Karst Lineament

Ridge/Collapse

- Tectonic

Global Structure

Origin

- Eolian
- Erosional
- Fluvial
- Impact
- Tectonic
- Volcanic

Soil Saturation/Subsurface Karst

Value

- 236
- 1

Credits NASA JPL, ASU HiRISE, NASA THEMIS, PIGWAS, USGS
 Author: Stephen A. Daire
 Date: 04/27/2018

Spatial Reference
 GCS: GCS Mars 2000
 Datum: Mars 2000
 Units: Degree

Appendix E. International Union of Geological Science Holocene Subdivisions (Cohen et al 2018 update).

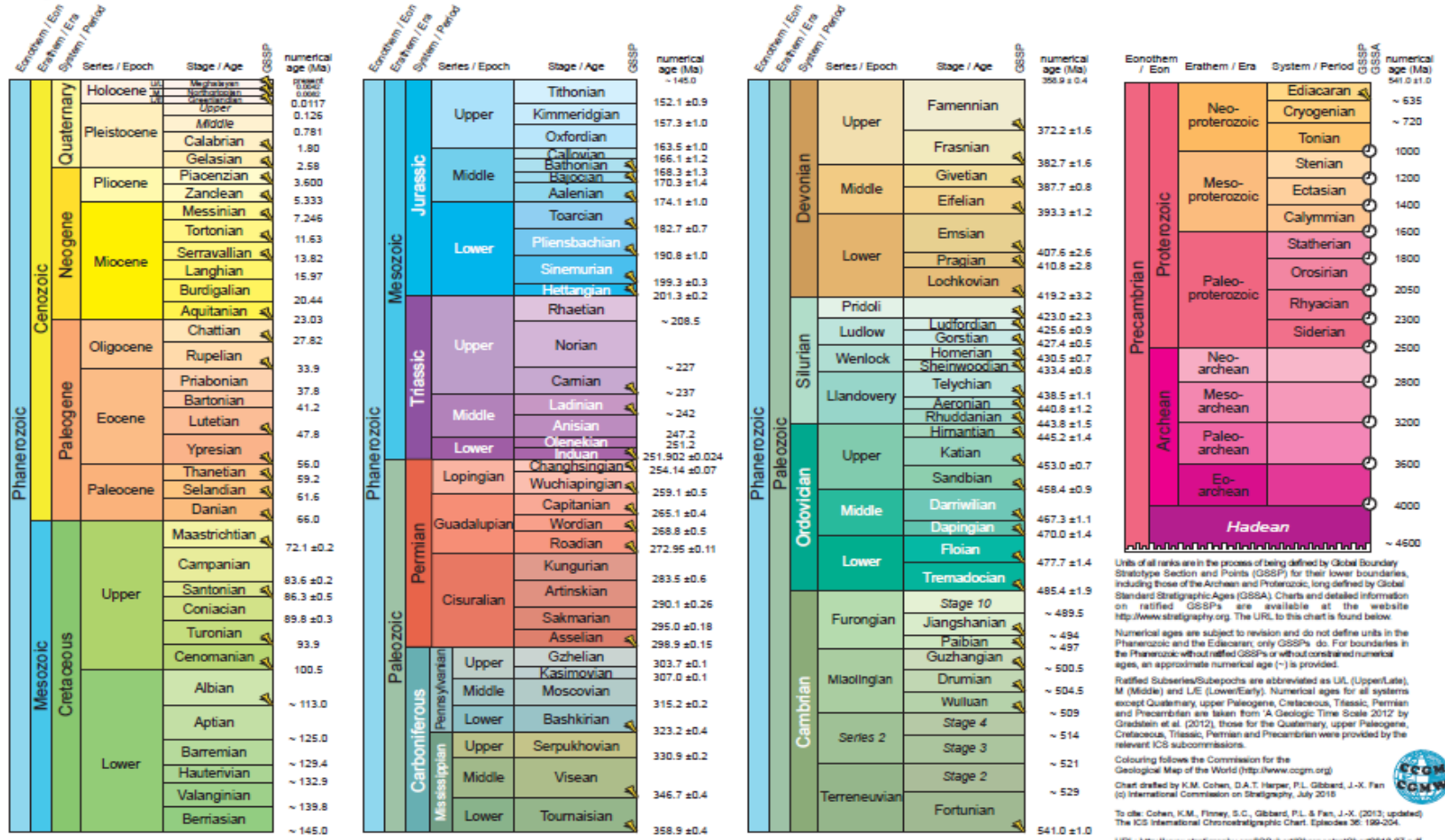


INTERNATIONAL CHRONOSTRATIGRAPHIC CHART

www.stratigraphy.org

International Commission on Stratigraphy

v 2018/07



Appendix F. Karst Geohydrological FOI Datasets & Definitions Table

Karst Geohydrological FOI Datasets & Definitions			
Morphological Entity	Formational Event	Characteristics	Features
Karst	Various natural dynamic dissolution and erosion processes on soluble rock (primarily carbonate rock).	A range of cryptic superficial and subterranean topological structures.	Superficial: bare rock, closed depressions, cenotes/dolines/sinkholes, rock shelters, subsidence, sinking streams, sinkhole lakes, springs, and cave entrances. Subsurface: chambers, halls, conduits, stalagmites, stalactites, and caverns.
Epikarst	Various natural dynamic dissolution and erosion processes on soluble rock (primarily carbonate rock).	Enhanced porosity on or near the surface or at the soil/bedrock contact of many karst landscapes.	Seasonally correlated saturation content, high dissolution and weathering rate, and proximate to the surface. Superficial: bare rock, closed depressions, cenotes/dolines/sinkholes, rock shelters, subsidence, sinking streams, sinkhole lakes, springs, and cave entrances. Subsurface: chambers, halls, conduits, stalagmites, stalactites, and caverns.
Pseudokarst	Natural and Anthropogenic non-dissolution events including thermal (lava and ice), anthropogenic	A topological network formed from non-dissolution weathering. Pervasive in areas of development and production. Can develop within a single	Small areas range from cm to tens of meters in scale and include dissolution from acid spill or leak, broken subsurface infrastructure, boring, and erosion modification. Large scale features range from tens of meters to regional scopes of hundreds of thousands of cubic meters. Impacts

	(liquid extraction and injection, mining, tunneling, production, and development).	significant stochastic perturbation. Anthropogenic formation is divided into small and large area of effect.	include resource extraction induced subsidence and collapse, regional and intercontinental infrastructure, and industrial pollution release.
Paleokarst	Paleokarst are identified as inactive karst features, in geological terms, removed from the dissolution or formational process. These are discovered from exposure from tectonic uplift or subsidence, sea-level fluctuation, road cuts, sinkhole development, and/or high mountain erosion. They can be reactivated due to natural and anthropogenic processes.	The importance of paleokarst is multifactorial. Prior geophysical research has identified economic geochemical resources of karst regions. New understanding and developments in GIST in the areas of climate science, geohazard, and geospatial modeling are promoting use of these datasets. Individual karst features can pose a duality of activity and inactivity, features in phreatic caves are active on the surface and inactive at the core. These are sampled and utilized in palaeoclimatological studies for radiometric dating calibration.	Various natural products of dynamic dissolution and erosion processes over geologic time on soluble rock (primarily carbonate rock). Minerals and chemicals of economic value are related to these formations' stratigraphy. They can be uplifted or buried and are typically inactive features or systems. Human or natural activity can reactivate these dissolution and erosion.

Deep Karst	Various natural dynamic geothermal, mechanical, uplift, subsidence, dissolution, and erosion processes on soluble rock (primarily carbonate rock).	Depth is 100m or greater from the surface.	Various natural products of dynamic dissolution and erosion processes over geologic time on soluble rock (primarily carbonate rock). Minerals and chemicals of economic value are related to these formations' stratigraphy. They can be uplifted or buried and are typically inactive features or systems. Human can reactivate these dissolution and erosion.	
Saturation Zone Typology				
	Conduit & Matrix Inundation	Depth of Features from Surface	Geomorphological Features of Interest	Plasma Chemical Trace Profiles
Vadose	Air filled/ Temporary Groundwater Flow	Within cm of the surface to several km, depending upon the proximity to the coast, formation matrix, and mode or modes of formation.	<p>Closed depressions, cenotes/dolines/sinkholes, rock shelters, subsidence, sinking streams, sinkhole lakes, springs, and cave entrances.</p> <p>Chambers, halls, conduits, stalagmites, stalactites, and caverns of various forms.</p>	<p>Aqueous: Hydrons $^1\text{H}^+$, $^2\text{H}^+$, $^3\text{H}^+$; Hydrides H^-; Fresh Water H_2O; CaCO_3 Calcium Carbonate; NaCl Sodium Chloride; Ca^{2+} Calcium Ions; Sodium Hypochlorite NaOCl; Carbonic Acid H_2CO_3; Sulfur Dioxide H_2SO_3;</p> <p>Gaseous: Hydrogen Sulfide H_2S; Carbon Dioxide CO_2; Radon ^{222}Rn; Methane CH_4;</p> <p>Solid: $^{234}\text{Uranium}$-$^{230}\text{Thorium}$; $\delta^{18}\text{Oxygen}$-$\delta^{16}\text{Oxygen}$; $\delta^{13}\text{Carbon}$- $\delta^{12}\text{Carbon}$;</p>

Epiphreatic	Seasonally/ Periodically/ Cyclically Air filled to submerged.	Within cm of the surface to several km, depending upon the proximity to the coast, formation matrix, and mode or modes of formation.	Chambers, halls, conduits, stalagmites, stalactites, and caverns of various forms.	<p>Aqueous: Hydrons $^1\text{H}^+$, $^2\text{H}^+$, $^3\text{H}^+$; Hydrides H^-; Fresh Water H_2O; Sodium Hypochlorite NaOCl^-; Carbonic Acid H_2CO_3; Sulfur Dioxide SO_2; Methane CH_4 Sulfurous Acid H_3SO^-</p> <p>Gaseous: Hydrogen Sulfide H_2S; Radon ^{222}Rn; Methane CH_4;</p>
Phreatic	Totally submerged in watertable.	Within cm of the surface to several km, depending upon the proximity to the coast, formation matrix, and mode or modes of formation.	Chambers, halls, conduits, stalagmites, stalactites, and caverns of various forms.	<p>Aqueous: Hydrons $^1\text{H}^+$, $^2\text{H}^+$, $^3\text{H}^+$; Hydrides H^-; Fresh Water H_2O; Sodium Hypochlorite NaOCl^-; Carbonic Acid H_2CO_3; Sulfur Dioxide SO_2; Methane CH_4 Sulfurous Acid H_3SO^-</p> <p>Gaseous: Hydrogen Sulfide H_2S; Radon ^{222}Rn; Methane CH_4;</p>
Deep Phreatic	Totally submerged in water table.	Hundreds of m from surface, depending upon the proximity to the coast, formation matrix, and mode or modes of formation.		<p>Aqueous: Hydrons $^1\text{H}^+$, $^2\text{H}^+$, $^3\text{H}^+$; Hydrides H^-; Fresh Water H_2O; Sodium Hypochlorite NaOCl^-; Carbonic Acid H_2CO_3; Sulfur Dioxide SO_2; Methane CH_4 Sulfurous Acid H_3SO^-</p> <p>Gaseous: Hydrogen Sulfide H_2S; Radon ^{222}Rn; Methane CH_4;</p>
Speleothem Structure Typology				

	Formation Hydrodynamics	Geomorphological Result	Characteristics
Active Hydraulics	<ul style="list-style-type: none"> • Droplets • Running • Submersion • Upwelling • Evaporation • Capillary • Condensation • Expansion 	<p>Crystals:</p> <ul style="list-style-type: none"> • Dogtooth Spar – calcite crystal similar to canine teeth that precipitate from water • Frostwork – evaporite calcite or aragonite needles, that can form of popcorn or Boxwork, in high airflow sections • Anthodites – crystalline aragonite, or gypsum, quill or feather needle clusters that radiate from a single base • Cryogenic calcite – loose uncemented crystals of 1mm to >1cm grains on the floor, generation occurring via mineral separation through cycles of water freeze <p>Dripstone:</p> <ul style="list-style-type: none"> • Stalactites <ul style="list-style-type: none"> a) Soda Straws – hollow interior with water dripping through, crystallization occurs from the outside inwards b) Helictites – structures formed from high water pressure forcing soda straws in curling, twisting, horizontal, and vertical antigravity patterns c) Chandeliers – a series of small thin stalactites of variable lengths in clusters on the ceiling • Stalagmites <ul style="list-style-type: none"> a) Broomstick b) Totem Pole – diameter is nearly identical to the formative stalactite without connecting c) Fried Egg • Columns – stalactites and stalagmites that have merged <p>Flowstone – a type of formation similar to a flowing stone waterfall where water seeps from a wall onto rocks and finally the floor:</p> <ul style="list-style-type: none"> • Draperies/Curtains – folded sheets along slanted walls and ceilings 	<p>Ceilings, walls, floors: Formations from flow stone.</p>

		<p>a) Bacon – multicolor red and yellow draperies</p> <ul style="list-style-type: none"> • Rimstone Dams/Gours – crystalline blocks that form in flow stone and form pools of water on the floor • Stone Waterfalls – areas of past water flow vertically from one level of cave floor to another <p>Speleogens:</p> <ul style="list-style-type: none"> • Pillars – connected stalactites and stalagmites • Scallops – a gentle downstream slope and a harsh upstream slope producing an asymmetrical depression inversely proportional to flow velocity, 1cm to >1m in size • Boneyard – labyrinths of limestone cavities • Boxwork – thin blades of calcite formed by preferential erosion of into a honeycomb or box pattern on the surface of veins of metamorphic or igneous rock. <p>Other:</p> <ul style="list-style-type: none"> • Popcorn – calcite sphere clusters that form on the walls of flooded caves. • Pearls – stone spheres formed overtime as drip layers around grains of sand in water small pools, bb to ping-pong ball sized • Calcite Rafts – flat sheets that form of the surface of evaporating pools of water and then skin to the floor at negative buoyancy • Snottites – stalactites or microbial colonies hanging from the ceiling that are non-rigid, which flex and bend with flowing water or air • Moonmilk – actinomyces colonies habituating on cave floors the resemble wet plaster of Paris in texture, similar to flow stone 	
--	--	---	--

<p>Minimal Hydraulic Flow.</p>	<ul style="list-style-type: none"> • Droplets • Running • Submersion • Upwelling • Evaporation • Capillary • Condensation • Expansion 	<p>Crystals:</p> <ul style="list-style-type: none"> • Dogtooth Spar • Frostwork • Anthodites • Cryogenic calcite <p>Dripstone:</p> <ul style="list-style-type: none"> • Stalactites <ul style="list-style-type: none"> d) Soda Straws e) Helictites f) Chandeliers • Stalagmites <ul style="list-style-type: none"> d) Broomstick e) Totem Pole f) Fried Egg • Columns <p>Flowstone:</p> <ul style="list-style-type: none"> • Draperies/Curtains <ul style="list-style-type: none"> b) Bacon • Rimstone Dams/Gours • Stone Waterfalls <p>Speleogens:</p> <ul style="list-style-type: none"> • Pillars • Scallops • Boneyard • Boxwork <p>Other:</p> <ul style="list-style-type: none"> • Popcorn • Pearls • Calcite Rafts 	<p>Formations from splashing. Ceilings, walls, floors: Formations from flow stone.</p>
---------------------------------------	---	--	--

		<ul style="list-style-type: none"> • Snottites 	
No Hydraulic Flow		Other: <ul style="list-style-type: none"> • Popcorn • Pearls • Calcite Rafts • Moonmilk 	Formation from stagnant water, bioperturbation, tectonic shifting,
Cenote/Doline/Sinkhole Geomorphological Formation Mechanisms			
	Classifications of Collapse Dynamic	Post Depositional Result	Types
Natural	Hydrologic: <ul style="list-style-type: none"> • Drought • Flooding • Sea-Level Fluctuations • Cryogenic Geologic: <ul style="list-style-type: none"> • Earthquake • Volcanic Eruption Astronomical: <ul style="list-style-type: none"> • Celestial Body Impact 	Crystals: <ul style="list-style-type: none"> • Dogtooth Spar • Frostwork • Moonmilk • Anthodites • Cryogenic calcite Dripstone: <ul style="list-style-type: none"> • Stalactites <ul style="list-style-type: none"> g) Soda Straws h) Helictites i) Chandeliers • Stalagmites <ul style="list-style-type: none"> g) Broomstick h) Totem Pole i) Fried Egg • Columns Flowstone: <ul style="list-style-type: none"> • Draperies/Curtains <ul style="list-style-type: none"> c) Bacon • Rimstone Dams/Gours • Stone Waterfalls 	Cap Rock

		<p>Speleogens:</p> <ul style="list-style-type: none"> • Pillars • Scallops • Boneyard • Boxwork <p>Other:</p> <ul style="list-style-type: none"> • Popcorn • Pearls • Calcite Rafts • Snottites 	
Anthropogenic	<p>Hydrologic:</p> <ul style="list-style-type: none"> • Pumping • Public/Industrial Ponds, Lakes, and Reservoirs • Run-off Distribution <p>Geologic:</p> <ul style="list-style-type: none"> • Blasting • Drilling • Road Development • Building Construction 	<p>Crystals:</p> <ul style="list-style-type: none"> • Dogtooth Spar • Frostwork • Moonmilk • Anthodites • Cryogenic calcite <p>Dripstone:</p> <ul style="list-style-type: none"> • Stalactites <ul style="list-style-type: none"> j) Soda Straws k) Helictites l) Chandeliers • Stalagmites <ul style="list-style-type: none"> j) Broomstick k) Totem Pole l) Fried Egg • Columns <p>Flowstone:</p> <ul style="list-style-type: none"> • Draperies/Curtains <ul style="list-style-type: none"> d) Bacon • Rimstone Dams/Gours • Stone Waterfalls 	

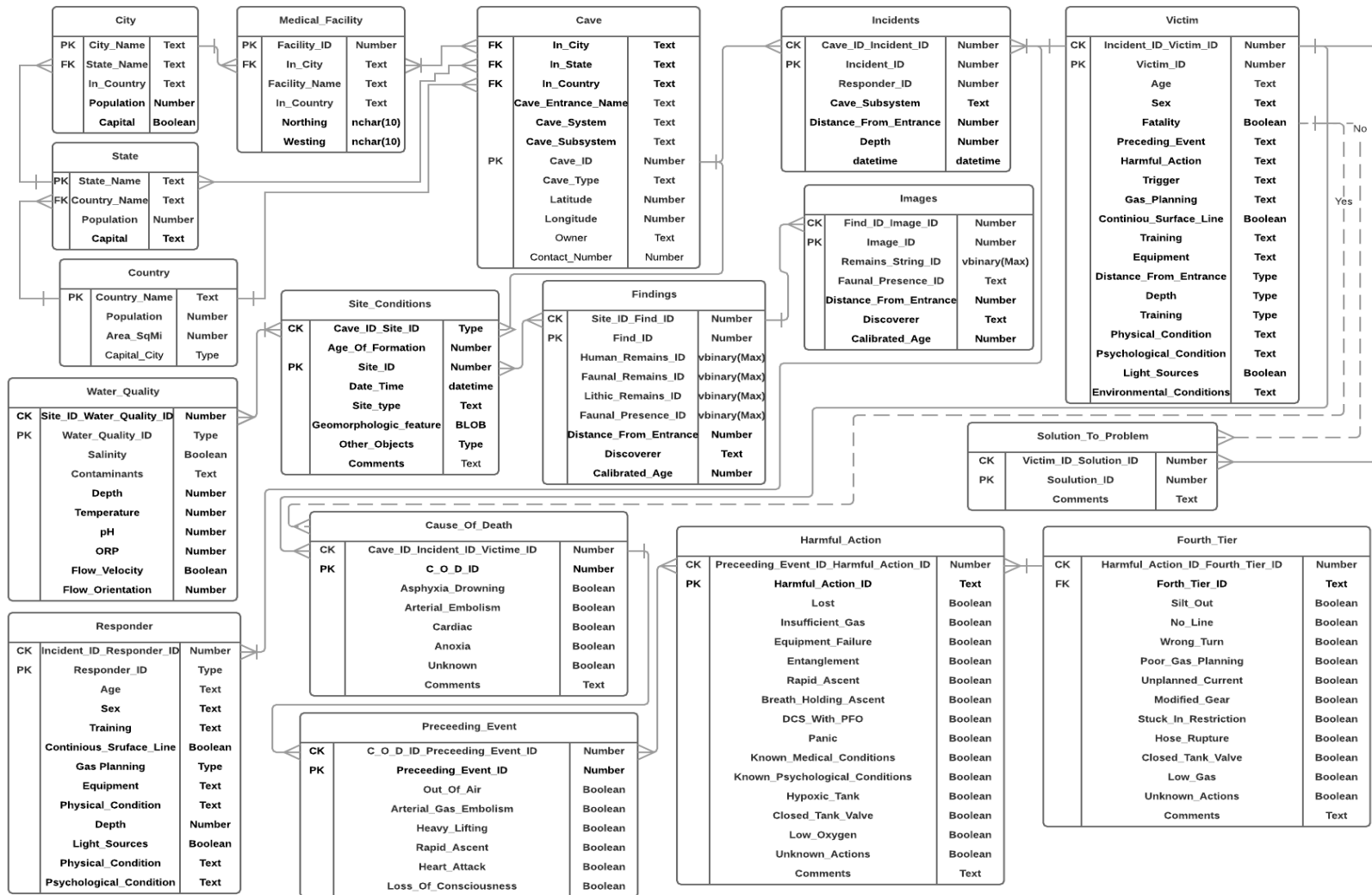
		<p>Speleogens:</p> <ul style="list-style-type: none"> • Pillars • Scallops • Boneyard • Boxwork <p>Other:</p> <ul style="list-style-type: none"> • Popcorn • Pearls • Calcite Rafts • Snottites 	
No Hydraulic Flow		<p>Other:</p> <ul style="list-style-type: none"> • Popcorn • Pearls • Calcite Rafts 	

Appendix G. Microsoft Access Karst Database.

The screenshot shows the Microsoft Access interface with the 'Findings' table open. The ribbon is set to 'Table Tools' with the 'Table' tab selected. The ribbon groups include Filter, Sort & Filter, Records, Find, and Text Formatting. The table data is as follows:

Osteological_Remains	Osteological_Remains	Human_Genus/Species	Cenote Entrance	Cave Subsystem	Cave System	Distance From	Depth (m)	Discoverer	Calibrated
0	0	Taj Mahal	Taj Mahal	Taj Mahal	0	27			
1	0	Naharon	Naranjal	Ox Bel Ha	368	23	G. Walten and		
2	0	Palmas	Muknal	Muknal	174	24	J. Coke		
3	0	El Templo			185	10	S. Gerrard, C. K		
4	0	Chan Hol-1	Chan Hol	Chan Hol	547	8	A. Kampe, T. K		
5	0	Chan Hol-2	Chan Hol	Chan Hol	1240	8	H. Gust		
6	0	Palmas	Muknal	Muknal	210	33	J. Aviles		
7	0	Pat Jacinto	Dos Ojos	Dos Ojos	47	30	Unknown		
8	0	Pat Jacinto	Dos Ojos	Dos Ojos	12	45	Unknown		
*	0				0	0			

Appendix H. ERD of cave system datasets (Daire et al. 2017).



Appendix I. GIST Project Schedule for ULS Cave Survey Deployment Table

GIST Project Schedule for ULS Cave Survey Deployment			
Week of	USC Event	Tasks	Deliverables
20-Aug	Semester Starts	1) Laser Scanner Order 2) Shipping Period 3) Methods Research 4) Logistical Planning 5) Deployment Considerations	1) Resume 2) Photo 3) Thesis Timetable 4) Biography
27-Aug		1) Prepare survey files 2) Prepare geodatabase (GDB) elements 3) Review Proposal 4) Prepare and modify existing QAC Agisoft .las and .laz Orthophoto elements 5) Pack gear	1) Develop ULS cave survey methods a) Scientists-sensor-environment interactions, concerns, and dynamics b) NASA PSTAR research benefits, potentials, and concerns c) analogs in terms of LSS procedures d) Command, Control, Communications, Computers, Collaboration, Intelligence, and Interoperability (C ⁵ I ²) for human & robotic remote sensing deployment and survey apparatus, developments, techniques, and expected outcomes
3-Sep		1) Receive and test ULS 2) Depart for Mexico Arrival at host organization to deposit equipment and prepare laboratory/scanning space 5) Begin Institute of International Astronautic Studies - Project Polar Suborbital Science in the Upper Mesosphere (PoSSUM) Academy online course work.	1) Deploy, Test, & Calibrate ULS a) update scientist-sensor-environment interactions and concerns for analogous NASA PSTAR C ⁵ I ² for human and robotic remote sensing deployment and survey apparatus ergonomics, developments, techniques, needs, & expected outcomes 2) Begin Project PoSSUM course work and reflect on analog environments for scientific astronauts and speleonauts.

		<p>6) Test & Calibrate ULS in lab and with water quality tests daily</p> <p>7) Develop and test 3DGIS models.</p> <p>8) Two days of team debriefs on ULS training in class room of Under the Jungle Dive Shop, land exercises, and survey at the cenote mouth, and open water to determine needs, concerns, and solutions for unexpected problems with FTP</p>	<p>3) conduct LiDAR and PhoDAR scans in laboratory of fractal markers, paleontological and geomorphological evidence assemblage for virtual reality lab (VRL) elements</p>
10-Sep		<p>Technical work</p> <p>1) Prepare existing PhoDAR las/.laz files in ArcGIS Cave GDB</p> <p>2) Test & Calibrate ULS with water quality tests daily</p> <p>3) Continue Project PoSSUM course work</p> <p>4) Develop and test 3DGIS models.</p>	<p>1) Initial LiDAR and PhoDAR model development of interior cross-sections for comparison</p> <p>2) Comparison of the initial real-time results along with water chemistry datasets for refractive index distortions, TPU, surveyor impacts, etc. for reassessment of redeployment via 2G Robotics ULScanner Application in real-time</p>
17-Sep		<p>Technical work</p> <p>1) Two nights of surface LiDAR surveys</p> <p>2) One day of survey site line and target placement via PhoDAR and water quality collection</p> <p>3) Three days of diving for contiguous site ULS surveys of individually parameterized calibrations</p> <p>4) Scan i) open-air ii) fresh water, and iii) salt water.</p> <p>5) AOI a) karst face, b) doline cross-section, c) open water sweep, d) survey line stations, e) fractal spatio-spectrometric marker, & f) FOIs.</p> <p>5) Test & Calibrate ULS with water quality tests & fractal spatio-spectrometric marker daily</p> <p>6) Continue Project PoSSUM course work</p> <p>7) Develop and test 3DGIS models.</p>	<p>1) Comparisons of initial real-time results along with water chemistry datasets for refractive index distortions, TPU, etc. for review and reassessment for redeployment</p> <p>2) Develop ≥ 3 BRCA map and comparative results of the 3 contiguous models to provide hydrochemistry data and photoplethysmogram point cloud data as anticipated spatio-spectrometric surface area, vector color, and million of points per line lidar pulse accuracy for orthophoto modeling surpass previous surveying obstacles and create novel imaging errors and artifacts</p> <p>3) Assessment of ULS data on surveying for a clear stratigraphic cross-section, fossilized bone, limestone firepits, Streptomyces colonies biomolecular signatures, possible pharmaceutical, pollution products, etc.</p>

<p>24-Sep</p>	<p>Technical work</p> <ol style="list-style-type: none"> 1) ULS calibration testing on AOI 2) Additional FOI surveys, if initial results from on-the-fly sensor calibration by the surface support technician during initial week provide satisfactory results 3) Test & Calibrate ULS with water quality tests daily 4) Continue Project PoSSUM Online course work 5) Develop and test 3D GIS models. 6) Pack to Leave 7) Team Final Debrief on Survey project outcomes 8) Travel to Embry-Riddle University Daytona, Florida for PoSSUM Academy Scientist-Astronaut Courses <p>a) DAY ONE 27th: ACADEMIC INSTRUCTION AND SIMULATOR OPERATIONS Objectives: To understand principles of the PoSSUM Program and gain a general understanding of the mesosphere, noctilucent cloud dynamics, observational methods and history, noctilucent cloud structures, aerospace physiology, and life support systems (LSS) relevant to suborbital flight.</p> <p>Topics covered: Overview of the PoSSUM program (1 hr) , Science of the Mesosphere (1 hr), Fundamentals of Remote Sensing (1 hr), Basic Noctilucent Cloud Science (1 hr), PoSSUM Instrumentation Operations (1 hr), Imaging</p>	<ol style="list-style-type: none"> 1) ≥ 3 BRCA map and comparative results of the 3 contiguous models provide detailed geohydrochemical isotopic point cloud data as anticipated spatio-spectrometric surface area, vector color, and thousands of points per line lidar pulse accuracy for orthophoto modeling 2) Initial write ups from dive logs, wet notes, equipment, concerns, video evidence, etc. 3) Consolidation of dive computer dive profile graphs to correlate to the LiDAR and PhoDAR models 4) Development of PoSSUM course materials and experiential notes from courses into analog transliteration for subsurface to supraorbital planetary survey considerations 4) Development of Informal Hand drawn ULS index
----------------------	--	---

		<p>Noctilucent Clouds from Suborbital Spacecraft (1 hr), Imaging Noctilucent Clouds from the International Space Station (1 hr), Aerospace Physiology (1 hr), and Life Support Systems (1 hr).</p> <p>Evening Seminar: PoSSUM Suborbital Simulator Operations Instructors: Dr. Jason Reimuller, Dr. Erik Seedhouse, Dr. Dave Fritts</p> <p>b) DAY TWO: HYPOXIA EFFECTS AND POSSUMCAM OPERATIONS Objectives:</p> <ol style="list-style-type: none"> 1) Overview of PoSSUM instrumentation and operational concepts, and operations of the PoSSUMCam system. 2) To recognize off-nominal environments and that physiological hypoxia responses are individually experienced for contingency awareness in environments with a spacesuit. <p>Training Elements:</p> <ol style="list-style-type: none"> 1) Comprehensive training geared towards the effective use of the PoSSUMCam system and other PoSSUM instrumentation in a classroom environment. 2) Hypoxia awareness training at altitudes equivalent to 25,000 feet in a high-altitude chamber at Southern AeroMedical Institute Flight Operations Facility in Melbourne, Florida, capable of simulating space missions in hypoxic or hyperoxic environments. 	
--	--	--	--

		<p>Evening Seminar: Spaceflight Physiology, Dr. Perry Bechtle Instructors: Dr. Paul Buza, Van Wampler, Parker Rice</p>	
1-Oct		<p>Complete All Technical Work a) DAY THREE: SPACESUIT TRAINING AND POSSUM MISSION SIMULATION Objectives: 1) To don, doff, pressurize, and operate effectively in spacesuits while in confined environments that simulate actual missions. 2) To perform effective Crew Resource Management (CRM) techniques and procedural training in simulators designed specifically for Project PoSSUM, administered at the Embry-Riddle University. 3) Introduction to Spacesuit Contingency Operations, including decompression, smoke, hazardous environments, post-landing scenarios, egress, sea survival systems, capsule egress fundamentals, and aircraft ejection systems. Training Elements: 1) Comprehensive training in mission-qualified spacesuits train in donning, doffing, pressurizing, preflight safety checking, and basic RS operations using a spacesuit in a suborbital spacecraft mesospheric cloud tomography experiment.</p>	<ol style="list-style-type: none"> 1) Development of PoSSUM course materials and experiential notes from courses into analog transliteration for subsurface to supraorbital planetary survey considerations 2) Revision of Informal Hand drawn ULS Index Model

	<p>2) Crew Resource Management training in PoSSUM mission simulation simulating noctilucent cloud research mission operates of PoSSUM scientific instrumentation in a real-time analog environment.</p> <p>3) Introduction to Spacesuit Contingency Operations, including decompression, smoke, hazardous environments, post-landing scenarios, egress, sea survival systems, capsule egress fundamentals, and aircraft ejection systems. Evening Seminar: Spacesuit Operations, Nikolay Moiseev Instructors: Nikolay Moiseev, Chris Lundeen, Van Wampler, Gavin James, and Parker Rice</p> <p>b) DAY FOUR: HIGH-G (ASCENT AND RE-ENTRY) OPERATIONS, MITIGATION METHODS, AND BIOMETRIC SYSTEM OPERATIONS Objectives:</p> <p>1) To perform optimally in a high-G environment, mitigating G-induced blackouts through the use of anti-G equipment and anti g-force stress maneuver (AGSM) breathing techniques.</p> <p>2) To effectively understand and manage individual physiological responses to high-G and changing-G environments through biometric analysis.</p> <p>Training Elements:</p>	
--	--	--

	<p>1) High-G and microgravity Space Physiology flight with Patty Wagstaff Instructors using a Super Decathlon aerobatic aircraft, student using instrumentation while learning how to use mechanical countermeasures and breathing techniques to mitigate high-G ascent and re-entry environments.</p> <p>2) High-G and microgravity Space Physiology flight with Patty Wagstaff instructors using an Extra 300 aerobatic aircraft with scientist-astronaut candidates acting as pilots and RS operators (taking videos) while performing aerobatic maneuvers</p> <p>3) Anti-G Garment training, donning, and doffing</p> <p>4) Comprehensive biometric analysis in aerospace physiology during training activities, including pulse oximetry, blood pressure, blood volume, and an Electroencephalogram (EEG) scans.</p> <p>Instructors: Patty Wagstaff, Alan Moore, Tim Plunkett, Jeff Rochelle</p> <p>c) DAY FIVE: REMEDIAL INSTRUCTION AND EVALUATIONS</p> <p>Objectives:</p> <p>1) Introduction to Virtual and Augmented reality for space missions</p> <p>2) To introduce specialized topics pertaining to aeronomy and astronautics and to review and evaluate academic instruction administered through the previous four days.</p>	
--	--	--

		<p>2) To complete all objectives which could not be completed in the previous days due to inclement weather or other contingencies.</p> <p>· Evening Seminar: Graduation Instructors: Dr. Jason Reimuller</p>	
5-Oct		<p>Write manuscript</p> <p>1) Editing and additional content development on topics</p> <p>a) ULS data quality resulting from methods, b) comparisons and overlays of lidar and photogrammetry datasets for modeling, and c) scientists-sensor-environment interactions and concerns</p> <p>3) Return from Project Polar Suborbital Science in the Upper Mesosphere</p>	<p>1) Development of PoSSUM course materials and experiential notes from courses into analog transliteration for subsurface to supraorbital planetary survey considerations</p> <p>2) Revision of Informal Hand drawn ULS Index Model</p>
8-Oct		<p>Write manuscript</p> <p>1) Needs significant revision and expansion on</p> <p>a) discussion of scientists-sensor-environment interactions and concerns</p> <p>b) ULS pulse calibration index</p> <p>c) Related quantum optics electrodynamic discussion</p> <p>d) Semiformal model of ULS wave-particle propagation and detection.</p>	<p>1) Development of PoSSUM course materials and experiential notes from courses into analog transliteration for subsurface to supraorbital planetary survey considerations</p> <p>2) Revision of Informal Hand drawn ULS Index Model</p>
15-Oct		<p>Write manuscript</p> <p>1) Needs editing and additional content on topics</p> <p>a) ULS data quality resulting from methods, b) comparisons and overlays of datasets for modeling,</p>	<p>1) Development of PoSSUM course materials and experiential notes from courses into analog transliteration for subsurface to supraorbital planetary survey considerations</p> <p>2) Revision of Informal Hand drawn ULS Index Model</p>

		and c) scientists-sensor-environment ULS interactions and concerns om underwater caves and aphotic vacuum space. 2) Research on observed QED phenomena related to Informal Hand drawn ULS Imaging Calibration Index Model	
22-Oct		Write manuscript 1) Needs editing and additional content on topics a) ULS data quality resulting from methods, b) comparisons and overlays of datasets for modeling, and c) scientists-sensor-environment ULS interactions and concerns om underwater caves and aphotic vacuum space. 2) Research on Observed Phenomena presented from Informal Hand drawn ULS Index Model	1) Development of PoSSUM course materials and experiential notes from courses into analog transliteration for subsurface to supraorbital planetary survey considerations 2) Revision of Informal Hand drawn ULS Index Model
29-Oct		Write manuscript 1) Needs editing and additional content on topics a) ULS data quality resulting from methods, b) comparisons and overlays of datasets for modeling, and c) scientists-sensor-environment ULS interactions and concerns om underwater caves and aphotic vacuum space.	1) Development of PoSSUM course materials and experiential notes from courses into analog transliteration for subsurface to supraorbital planetary survey considerations 2) Revision of Informal Hand drawn ULS Index Model
5-Nov		1) Needs editing and additional content on topics a) ULS data quality resulting from methods, b) comparisons and overlays of datasets for modeling, and c) scientists-sensor-environment ULS interactions and concerns om underwater caves and aphotic vacuum space.	1) Development of Chapters 4 & 5 2) Revision of Informal Hand drawn ULS Index Model
12-Nov		1) Needs editing and additional content on topics a) ULS data quality resulting from methods,	1) Development of Chapters 4 & 5 2) Revision of Informal Hand drawn ULS Index Model

		b) comparisons and overlays of datasets for modeling, and c) scientists-sensor-environment ULS interactions and concerns om underwater caves and aphotic vacuum space.	
19-Nov		1) Needs editing and additional content on topics a) ULS data quality resulting from methods, b) comparisons and overlays of datasets for modeling, and c) scientists-sensor-environment ULS interactions and concerns om underwater caves and aphotic vacuum space.	1) Development of PoSSUM course materials and experiential notes from courses into analog transliteration for subsurface to supraorbital planetary survey considerations 2) Development of Semiformal ULS Pulse Calibration Index Model
26-Nov	Classes end 30-Nov	1) Needs editing and additional content on topics a) ULS data quality resulting from methods, b) comparisons and overlays of datasets for modeling, and c) scientists-sensor-environment ULS interactions and concerns om underwater caves and aphotic vacuum space.	1) Development of PoSSUM course materials and experiential notes from courses into analog transliteration for subsurface to supraorbital planetary survey considerations 2) Development of Semiformal ULS Pulse Calibration Index Model
3-Dec		1) NASA PSTAR research benefits, potentials, and concerns 2) analogous in terms of C^5I^2 for human and robotic (RS) deployment and survey apparatus, developments, techniques, and futures.	1) Revision of scanned research literature 2) Final Development of Semiformal ULS photonic quantum vortex slipstream (PQVS) Pulse Calibration Index Model 3) Revisions of Figure titles, page numbers, and description. 4) Updates for the glossary 5) Revision of thesis abstract
10-Dec		1) NASA PSTAR research benefits, potentials, and concerns 2) analogous in terms of C^5I^2 for human and robotic (RS) deployment and survey apparatus, developments, techniques, and futures.	1) Revision of scanned research literature 2) Final Development of Semiformal ULS PQVS Pulse Calibration Index Model 3) Revisions of Figure titles, page numbers, and description. 4) Updates for the glossary

			5) Revision of thesis abstract
17-Dec		1) NASA PSTAR research benefits, potentials, and concerns 2) analogous in terms of C ⁵ I ² for human and robotic (RS) deployment and survey apparatus, developments, techniques, and futures.	1) Revision of scanned research literature 2) Final Development of Semiformal ULS PQVS Pulse Calibration Index Model 3) Revisions of Figure titles, page numbers, and description. 4) Updates for the glossary 5) Revision of thesis abstract
24-Dec	Deadline for signatures	1) NASA PSTAR research benefits, potentials, and concerns 2) analogous in terms of C ⁵ I ² for human and robotic (RS) deployment and survey apparatus, developments, techniques, and futures.	1) Revision of scanned research literature 2) Final Development of Semiformal ULS PQVS Pulse Calibration Index Model 3) Revisions of Figure titles, page numbers, and description. 4) Updates for the glossary 5) Revision of thesis abstract
28-Dec	Upload Deadline	1) Revise a) Abstract b) Tables c) Figure titles d) Figure descriptions	1) Revision of scanned research literature 2) Revisions of Figure titles, page numbers, and description. 4) Updates for the glossary 5) Revision of thesis abstract
11-Jan		2) Revise e) Abstract f) Tables	1) Defense
24-Jan		3) Revise g) Abstract h) Tables	1) Collect signatures and upload
14-Feb		4) Revise i) Appendix j) Index k) Tables	1) Revise Upload

Appendix J. Project Field Survey, Dive Plan, & Crew Procedures Table

Project Field Survey Dive Plan & Crew Procedures	
Location:	Xpu Ha, Quintana Roo, Mexico
AOI:	Sistema Taj Mahal, Cenote Taj Mahal, Sugarbowl Conduit, Deep Bone Room
Date:	09/18/2018 – 9/26/2018
Risk Assessment:	Christine Loew, Marcelin Nebenhaus, Natalie Gibbs, & Jeronimo Aviles
Compiled by:	Stephen A. Daire
Checked by:	Stephen A. Daire, Christine Loew, Natalie Gibbs, & Jeronimo Aviles
Purpose:	<p>Purpose Conducting a series of underwater laser, photogrammetric, and water quality scans of one submerged cave site of interest; Testing and evaluation of ULS performance in phreatic caves with the goal of providing a detailed site map and field evidence for considerations on efficacy of use within a similar context for their environmental and site recording qualities, characteristics, concerns, and impacts. A safe survey will take precedence over all other goals for the assessment. Operations will not take place unless the surveyors and dive supervisor are all comfortable with the on-site conditions, team dynamics, and contingency planning.</p> <p>As such, this case study will look to primarily determine and achieve:</p> <ol style="list-style-type: none"> a. Use ideal scan settings to calibrate the scanner at 1m range of a selected prominent feature of the in ambient/open-water and aphotic cave environments by conducting a series of scans at different beam intensities. b. Using optimal settings from the test scans, acquire a full scan of a major section of a site of interest in a non-ambient light test environment c. Using test scan calibrated settings, an optimal scan of a sample of in a non-ambient light environment d. Corresponding DSLR photogrammetric recordings using targets measured with ISO certified scale and fractal marbles

- e. A comprehensive cultural and natural resource comparison of the quality of the video, point cloud, mesh, and texture created by each of the recordings.
- f. Researching and developing a comprehensive and cohesive geographic information system for the creation of long-term GDBs for geoarchaeological resource management and urban planning.

The following may also be accomplished (in order of priority time permitting): An underwater laser scan of the entire AOI cavern surrounding the site of interest

- a. Laser and photogrammetry test scans of terrestrial AOI in ambient and non-ambient light
- b. Laser and photogrammetry test scans at two additional ranges of a FOI in ambient and non-ambient light
- c. Laser test and photogrammetry scans at an optimal scanning range of the other AOI cave lines not chosen to be scanned in ambient and non-ambient light
- d. Laser and photogrammetry test scans at two additional ranges of the other cave sites not chosen to be scanned in ambient and non-ambient light

Achievement of the primary objectives will forward production of 3D phreatic cave maps and models of unprecedented geovisual precision and accuracy to exhibit, digitally preserve, and enhance the interpretation of phreatic cave geoheritage. These will provide new narratives on caves and evolutionary biology for patrons, institutions, the public, and stakeholders interested in the materials. Moreover, it will provide the basis for follow-up scans of these sites to monitor their site processes of formation, evolution, and rates of degradation as a time-series.

The project will take place in accordance with the community standard for Scientific Diving. The core members of the team will consist of Stephen Daire, Christine Loew, and Jeronimo Aviles. All core members of the team are appropriately qualified to Technical Diving International Sidemount Cave Diving or equivalent and have an extensive amount of field experience as remote sensing operators, underwater cave survey, and scientific divers. By commencement of the project, the entire team will have current Diver Medical, First Aid, CPR and O2 provider certificates, the copies of which, will be kept on file. All those taking part in the operations are familiar with the dive site, local hazards, regionally applicable first response procedures, and locations of medical facilities. The entire team is also informed, trained, and practiced in the requisite dive equipment and techniques necessary to

	safely fulfil all operational aims, and contend with and mitigate all contingencies that arise from Murphy's Law during underwater exploration. Much of this equipment will be supplied by the divers personally primarily for the survey aspect of the project (see the accompanying documents).																				
Divers & Certifications:	<table border="0"> <thead> <tr> <th><i>Crew Member Name</i></th> <th><i>Qualification</i></th> <th><i>Medical Type</i></th> <th><i>Certifications</i></th> </tr> </thead> <tbody> <tr> <td>Stephen Daire</td> <td>TDI Full Cave Diver</td> <td>AAUS Medical</td> <td>1st Aid, CPR, O₂</td> </tr> <tr> <td>Christine Loew</td> <td>TDI Cave Instructor</td> <td>Dive Medical</td> <td>1st Aid, CPR, O₂</td> </tr> <tr> <td>Natalite Gibbs</td> <td>TDI Cave Instructor</td> <td>Dive Medical</td> <td>1st Aid, CPR, O₂</td> </tr> <tr> <td>Marcelin Nebenhaus</td> <td>TDI Cave Instructor</td> <td>Dive Medical</td> <td>1st Aid, CPR, O₂</td> </tr> </tbody> </table> <p>Crew Positions Operation Supervisor: Stephen A. Daire Diver 1 : Marceline Nebenhaus Diver 2: Natalie Gibbs Diver 3: Christine Loew Diver 4: Jeronimo Aviles Surface Support: Rory OKeefe</p> <p>* Diver 3 and 4 will transition for divers 1 and 2 based on available time, geospatial restrictions, and safety constraints.</p>	<i>Crew Member Name</i>	<i>Qualification</i>	<i>Medical Type</i>	<i>Certifications</i>	Stephen Daire	TDI Full Cave Diver	AAUS Medical	1 st Aid, CPR, O ₂	Christine Loew	TDI Cave Instructor	Dive Medical	1 st Aid, CPR, O ₂	Natalite Gibbs	TDI Cave Instructor	Dive Medical	1 st Aid, CPR, O ₂	Marcelin Nebenhaus	TDI Cave Instructor	Dive Medical	1 st Aid, CPR, O ₂
<i>Crew Member Name</i>	<i>Qualification</i>	<i>Medical Type</i>	<i>Certifications</i>																		
Stephen Daire	TDI Full Cave Diver	AAUS Medical	1 st Aid, CPR, O ₂																		
Christine Loew	TDI Cave Instructor	Dive Medical	1 st Aid, CPR, O ₂																		
Natalite Gibbs	TDI Cave Instructor	Dive Medical	1 st Aid, CPR, O ₂																		
Marcelin Nebenhaus	TDI Cave Instructor	Dive Medical	1 st Aid, CPR, O ₂																		
Dive Support/ Surface Transport:	A 10ft Make: Ford Type: F-150 Vehicles will only be driven by those with appropriate experience and qualifications. Provider: Under the Jungle Contact Numbers: nat@underthejungle.com																				
Project Time Table:	The quality of a scan, and therefore, its efficacy of use in depends on a variety of operational variables, but primarily its beam intensity setting has been determined through Phase I tests to be the most influential. Those results also demonstrate that the scanning performs at its absolute best in clear water with diffuse light. A function of beam intensity (BI) to resolution and accuracy of scans at different beam intensities will be conducted to compare against photogrammetry scans on the site of interest for 3D modeling. Additionally, after reviewing which BI provides the best imagery and the least environmental impact, a final scan at that BI will take place using the highest ambient light filtration setting at the highest sampling rate to try and achieve the best results. The goal will be to establish ideal beam intensity and light filtration settings for an ambient light environment of the site. Below is the approximate daily time table for surveying, with considerations made to																				

other dive teams in the area. Therefore, a function of beam intensity to resolution and accuracy of five (5) scans at different beam intensities will be conducted in the most ideal scanning conditions (i.e. non-ambient light and in extremely clear visibility of at least 3m+). The results will then establish an index beam intensity setting for a subsequent 360-degree scans of an entire AOI.

18th September 2018 – 26th September 2018

0900 Wake up & pack gear into trucks

1000 Depart headquarters (HQ) at Under the Jungle Dive shop

1045 Arrive on Site, establish site, Set-up dive equipment/survey gear, Computer prep and perform scan test on dock.

1115 Divers 1 and 2 in the water

Diver 1 and Diver 2 buoyancy check.

Diver 1 and Diver 2 If all OK, proceed down the cave line.

Diver 1 and Diver 2 give okay once on bottom, okay to DSO

Diver 1 takes tape measure and secures end to bottom of shot

Diver 1 unreels tape and both divers proceed to feature that is going to be scanned

Diver 1 and 2 reach scanning sites

Diver 1 puts tape and reel down, lays levelling rod down in place and places reference cubes on structure to be scanned, Secchi Disk at the foot of the structure to be scanned.

Diver 1 takes tape reel and measures far tip of levelling rod from base of mooring shot, notes and reports this distance to topside recorder, reports temperature, depth at site, current and visibility.

Diver 2 puts ULS with tripod aside and takes photos of all this process for Methodology

Diver 1 moves tripod positioning fractal plumb bob over the range mark, takes a water sample, Diver 2 photographs process

1124 Diver 1 signals to get behind the laser, to turn all lights off and instructs topside to begin a scan and record the start time, beam intensity, scan angle, etc. Diver 1 will initiate 1 gentle pull on the ULS cable to start a scan, two pulls to stop scan

1125 Scanning begins at 20% Beam Intensity.

	<p>1137 Scanning ends.</p> <p>1138 Scanning begins at 40% beam intensity.</p> <p>1145 Scanning ends.</p> <p>1146 Scanning begins at 60% beam intensity.</p> <p>1153 Scanning ends. (Divers 1 and 2 signals to each other and topside okay to follow line back to surface) (Divers leave the scanning area).</p> <p>1154 Scanning begins at 80% BI.</p> <p>1155 Divers reach the shot, signal OK to each other and topside to ascend</p> <p>1157 Divers reach 3m depth, perform safety stop for 5min</p> <p>1201 Scanning ends.</p> <p>1202 Divers reach surface (total dive time 90 min); Scanning begins at 100% BI.</p> <p>1207 Second dive team enters the water.</p> <p>1209 Scanning ends. Divers reach the bottom of the shot, give OK to proceed to scanning site</p> <p>1210 Scanning begins with highest ambient light filtration and sampling rate</p> <p>1211 Divers reach site. Both divers monitor progress of the scan</p> <p>1217 Scanning ends</p> <p>1217 Diver 1 takes a final water sample, reports temperature and visibility with lights on. Diver 2 takes photos and video of the process with lights on. Diver 1 gathers survey materials. Diver 1 and Diver 2 signal OK that they are ready to proceed back to the shot line. Diver 1 reels in tape back to the shot with goody bags and survey equipment. Diver 2 follows carrying Tripod and Camera.</p> <p>1227 Divers 1 and 2 reach the shot, signal OK to each other to ascend, Diver 1 notifies topside that the team is ascending shot.</p> <p>1229 Divers 1 and 2 begin safety stop during dive at 3m on return transit</p> <p>1236 Divers reach surface (total dive time 90 min); debrief DSO (Daire)</p> <p>1236 1955 Pack up and secure all items on deck</p> <p>1255 Leave site, head back to HQ</p> <p>1340 Arrival at HQ; Offload equipment</p> <p>1410 End of Operations</p> <p>Deviations to the plan: A dive the next day may be needed to capture more photos and/or to retrieve survey equipment left on bottom. If there is enough time, video may be taken in addition to still shots.</p>
Remote Sensing Surveys:	Figure x.1 Figure x.2

	<p>Figure x.3 Figure x.4</p>
<p>Dive Recording Stages & Plans:</p>	<p>Equipment List (Some of these are not to be used on every dive) Note in bold supplied by either the: (Researcher; PI) (Protean Solutions; PS) (Personal; PL) Water quality scans are implied and will be conducted upon each survey.</p> <p>Diving 3 sets of: Mask, Snorkel, Fins 3 sets of: BCD and Regulators 3 sets of dive weights (approx. 12 - 15lbs each) 3 dive belts 2 x Dive Computer 2 x Dive Knives Dive Watches 1 Compasses Wetsuits (3-5mm)/Drysuits 6 sets of 2 x 80ft³ aluminum tanks of EANx32 2 dive reels (250m) 1 safety reel (15m) 2 jump reels (20m)</p> <p>Survey and Recording 1 Cannon Rebel camera 2 50k lumen underwater lights 1 Slate, pencil & laminated map of dive site 3 wrist slates (BNP) or (PI) 3 laptop (PI) 5 fractal reference cubes 1 plumb bob tripod (PI) 2 Handheld GPS (PI) 1 Underwater Laser Scanner 1 Water Quality Sample Container</p>

Surface

- 2500mA Solar Panel
- 12W Compact Solar Panel
- Power strip
- Water Sample Bottles
- Drinking Water Rain Fly
- Light Money Reel
- Car/Boat Battery
- Car Outlet Converter
- Power Strip
- Computer
- Computer Charger
- Wireless Mouse
- Wireless Mouse USB
- ULS 200
- ULS 200 Junction Box
- ULS Power Cable
- ULS USB Cable
- ULS Data Cable
- ULS Cable Velcro
- Solar Panel Small
- Solar Panel Large
- USB 8-Port
- Stopwatch
- 4 in 1 Charger
- Water
- Sun Screen
- Bug Spray

Site Safety Equipment

1 80ft³ aluminium tank of 100% O₂/ Individual Stage Tank per diver.

	<p>1 First Aid Kit 1 Mobile Phone</p>
Site Description:	<p><i>Location:</i> N 20.48412 W 087.27805 (Geospatial Reference: WGS 84) <i>Elevation:</i> .3m <i>Distance from nearest shore:</i> Exit A at 50m with a 6m climb, exit B at 75m with a climb, and exit C with a 150m submerged swim. <i>Water temperature:</i> 22C <i>Visibility:</i> 20m <i>Depth range:</i> 0 to -25m <i>Bottom Composition:</i> Dissolution Paleosols, ceiling cave-in, & speleothems <i>Underwater Obstructions:</i> 1 Single File/ Head to Toe restriction <i>Entry and Exit points:</i> Cenote Taj Mahal watertable access point, Cenote Sugar Bowl 114m from Taj Mahal then 6m rope ladder/repel to watertable <i>Flow Range:</i> Northwest to Southeast <i>Flow strength:</i> 3km/hr (with no rainfall) <i>Storm Surge:</i> +2-5k/hr</p>
Dive Plan Survey:	<p>Prior to entering the water, on-site conditions will be assessed to determine whether it will be safe enough to conduct a survey of the site. Of primary consideration will be any indicators of bad weather arising and probability of postponing work, active dive teams on the survey line, equipment malfunction, or dive team member concerns. The team will be composed of four crew members, the diver supervisor will enter the open-water to conduct test scans and educates diver 1 and 2 on deployment and concerns. The visual assessment of the site, survey line and marker preparation, and general measurements of notable features that would be most suitable for a possible follow-up underwater laser scanning will be conducted by diver 1 and 2. The dive supervisor will act as a safety officer whose sole duty will be to remain on deck, monitor site conditions and ensure the safety of the surveyors.</p> <p>The divers 1 and 2 will enter the water and will signal an “OK” to the supervisor that they are clear to perform the survey moving along the site, the surveyors will not perform the survey until the supervisor gives a signal of OK and all clear to start operations. The surveyors will have a laminated map from Mr. Nebenhaus of the dive site available from Protean. If possible, the team will mark possible locations for the scanning deployment, FOI targets for scanning, environmental notations (current, visibility, water quality, etc.) and may also mark down areas of concern or inaccessibility.</p>

	<p>The entire survey is not planned to exceed 30 hours along the estimated 50m length of the site and could be considerably shorter depending on what is observed and the data collection rate of the ULS-200.</p> <p>At the end of the survey the diver 1 will swim to the exit, doff gear as well as passing any measuring equipment up to the supervisor. When OK, Divers 1 and 2 will exit the water.</p>
<p>Dive Plan:</p>	<p>Afternoon Dive / Underwater Laser Scan Site: Basic Equipment: (Diver 1), (Diver 2)</p> <p>Dive Team 1: Diver 1 (Nebenhaus), Diver 2 / (Gibbs) Topside Support: Dive Supervisor (Daire), Data Recorder (Rory OKeefe) Dive Team 2: Diver 1 (Nebenhaus), Diver 2 (Loew) Topside Support: Dive Supervisor (Daire), Data Recorder (Rory OKeefe)</p> <p>Estimated Duration of Dives: (1st) approximately 90 minutes (2nd) 90 minutes. Total: _3 hour and _0 minutes. Total Dive Operation: Approximately 6 hours</p> <p>Objectives:</p> <ul style="list-style-type: none"> • 6 total scans of 7 minutes with the last performing and ambient light filtration scan of a prominent distinguishing feature at a TBD Range (likely 1.5m) • 2 turbidity readings; 1 before and after the final scan • 2 salinity readings; 1 before and after the final scan • 2 temperature readings; 1 before and after the final scan • 2 light readings (in lumens); 1 before and after the final scan • 2 visibility readings; 1 before and after the final scan
<p>Goals:</p>	<p>Divers and their Equipment on Site:</p> <p>Lead Divers 1 (Nebenhaus): Levelling bubble, wrist slate for notes, tending the ULS and cable frequently (especially while on the move) to ensure that it does not become snagged on obstructions during the dive operation.</p> <p>Diver 2 (Gibbs): Nikon D90 DSLR camera, lights, wrist slate for notes drone</p> <p>Note: Dive Supervisor/DSO will remain on surface always constantly monitoring weather conditions, and any other safety hazards.</p>

Example Dive Procedure (Times may not be exact):

1000 Depart HQ

1045 Arrive on Site, establish site, Set-up dive equipment/survey gear, Computer prep and perform scan test on dock.

1115 Divers 1 and 2 in the water

Diver 1 and Diver 2 buoyancy check.

Diver 1 and Diver 2 If all OK, proceed down the cave line.

Diver 1 and Diver 2 give okay once on bottom, okay to DSO

Diver 1 takes tape measure and secures end to bottom of shot

Diver 1 unreels tape and both divers proceed to feature that is going to be scanned

Diver 1 and 2 reach scanning sites

Diver 1 puts tape and reel down, lays levelling rod down in place and places reference cubes on structure to be scanned, Secchi Disk at the foot of the structure to be scanned.

Diver 1 takes tape reel and measures far tip of levelling rod from base of mooring shot, notes and reports this distance to topside recorder, reports temperature, depth at site, current and visibility.

Diver 2 puts ULS with tripod aside and takes photos of all this process for Methodology

Diver 1 moves tripod positioning fractal plumb bob over the range mark, takes a water sample, Diver 2 photographs process

1124 Diver 1 signals to get behind the laser, to turn all lights off and instructs topside to begin a scan and record the start time, beam intensity, scan angle, etc. Diver 1 will initiate 1 gentle pull on the ULS cable to start a scan, two pulls to stop scan

1125 Scanning begins at 20% Beam Intensity.

1137 Scanning ends.

1138 Scanning begins at 40% beam intensity.

1145 Scanning ends.

1146 Scanning begins at 60% beam intensity.

1153 Scanning ends. (Divers 1 and 2 signals to each other and topside okay to follow line back to surface) (Divers leave the scanning area).

	<p>1154 Scanning begins at 80% BI. 1155 Divers reach the shot, signal OK to each other and topside to ascend 1157 Divers reach 3m depth, perform safety stop for 5min 1201 Scanning ends. 1202 Divers reach surface (total dive time 90 min); Scanning begins at 100% BI. 1207 Second dive team enters the water. 1209 Scanning ends. Divers reach the bottom of the shot, give OK to proceed to scanning site 1210 Scanning begins with highest ambient light filtration and sampling rate 1211 Divers reach site. Both divers monitor progress of the scan 1217 Scanning ends 1217 Diver 1 takes a final water sample, reports temperature and visibility with lights on. Diver 2 takes photos and video of the process with lights on. Diver 1 gathers survey materials. Diver 1 and Diver 2 signal OK that they are ready to proceed back to the shot line. Diver 1 reels in tape back to the shot with goody bags and survey equipment. Diver 2 follows carrying Tripod and Camera. 1227 Divers 1 and 2 reach the shot, signal OK to each other to ascend, Diver 1 notifies topside that the team is ascending shot. 1229 Divers 1 and 2 begin safety stop during dive at 3m on return transit 1236 Divers reach surface (total dive time 90 min); debrief DSO (Daire) 1236 1955 Pack up and secure all items on deck 1255 Leave site, head back to HQ 1340 Arrival at HQ; Offload equipment 1410 End of Operations</p> <p>Deviations to the plan: A dive the next day may be needed to capture more photos and/or to retrieve survey equipment left on bottom. If there is enough time, video may be taken in addition to still shots.</p>
Dive Plan:	<p>Underwater Laser Scan Site: Sistema Taj Mahal Dive Equipment: Diver 1 Marcelin Nebenhaus, Diver 2 Natalie Gibbs</p> <p>Dive Team: Diver 1, Diver 2 Topside Support: Dive Supervisor/Data Recorder Dive Team: Diver 1, Diver 2 Topside Support: Dive Supervisor/Data Recorder</p>

	<p>Estimated Duration of Dives: (1st) approximately 90 minutes; (2nd) 90 minutes. Total: _3 hour and _0 minutes. Total Dive Operation: Approximately 6 hours</p> <p>Objectives:</p> <ul style="list-style-type: none"> • 5 total scans of 7 minutes each of a prominent distinguishing feature at a TBD Range (likely 1.5m) • 2 turbidity readings; 1 before and after the final scan • 2 salinity readings; 1 before and after the final scan • 2 temperature readings; 1 before and after the final scan • 2 visibility readings; 1 before and after the final scan
<p>Goals:</p>	<p>Survey Equipment (by diver): Diver 1 (Nebenhaus): Levelling Rod, Tape Measure, References, water sample bottle, GoPro mount to mask, small light mount to mask, wrist slate for notes Diver 2 (Loew): Nikon D90 DSLR camera, small light, wrist slate for notes Dive Supervisor/DSO Daire: Will remain on deck at all times constantly monitoring weather conditions, boat traffic and any other safety hazards. Will be the primary driver of the boat and will be tending the ULS-200 cable frequently (especially while divers are on the move) to ensure that it does not become snagged on obstructions during the dive operation.</p> <p>Dive Procedure (Times may not be exact) (Sunset circa 17:00) 1700 Depart HQ 1745 Arrive on Site 1745 Establish work area, Set-up dive equipment/survey gear, ULS/Computer prep and perform scan test on deck, 1815 Divers 1 and 2 in the water Diver 1 and Diver 2 buoyancy check Diver 1 and Diver 2 If all OK, proceed down the cave line with lights on. Diver 1 and Diver 2 give okay once on bottom, okay to DSO Diver 1 takes tape measure and secures end to cave line</p>

	<p>Diver 1 unreels tape and both divers proceed to feature that is going to be scanned</p> <p>Diver 1 and 2 reach scanning site</p> <p>Diver 1 puts tape and reel down, lays levelling rod down in place and places reference cubes on structure to be scanned, at the foot of the structure to be scanned.</p> <p>Diver 1 takes tape reel and measures far tip of levelling rod from base of mooring shot, notes and reports this distance to topside recorder, reports temperature, depth at site, current and visibility.</p> <p>Diver 2 takes photos of all this process for Methodology</p> <p>Diver 1 positioning plumb bob over the (TBD) range mark, takes a water sample, Diver 2 photographs process</p> <p>1824 Diver 1 signals to get behind the laser, to turn all lights off and instructs topside to begin a scan and record the start time, beam intensity, scan angle, etc... If comms fail, Diver 1 will initiate 1 gentle pull on the ULS cable to start a scan, two pulls to stop scan</p> <p>1825 Scanning begins at 20% Beam Intensity.</p> <p>1837 Scanning ends.</p> <p>1838 Scanning begins at 40% beam intensity.</p> <p>1845 Scanning ends.</p> <p>1846 Scanning begins at 60% beam intensity.</p> <p>1853 Scanning ends. (Divers 1 and 2 signals to each other and topside okay to follow tape back to shot) (Divers leave the scanning area).</p> <p>1854 Scanning begins at 80% BI.</p> <p>1855 Divers reach the shot, signal OK to each other and topside to ascend</p> <p>1857 Divers reach 3m depth, perform safety stop for 5min</p> <p>1901 Scanning ends.</p> <p>1902 Divers reach surface (total dive time 90 min); Scanning begins at 100% BI.</p> <p>1907 Second dive team enters the water.</p> <p>1909 Scanning ends. Divers reach the bottom of the shot, give OK to proceed to scanning site</p> <p>1911 Divers reach site</p> <p>1912 Diver 1 takes a final water sample, reports temperature and visibility with lights on. Diver 2 takes photos and video of the process with lights on. Diver 1 gathers survey materials. Diver 1 and Diver 2 signal OK that</p>
--	---

	<p>they are ready to proceed back to the shot line. Diver 1 reels in tape back to the shot with goody bags and survey equipment. Diver 2 follows carrying Camera.</p> <p>1922 Divers 1 and 2 reach the shot, signal OK to each other to ascend, Diver 1 notifies topside that the team is ascending shot.</p> <p>1924 Divers 1 and 2 reach 3m Depth, begin safety stop of 5min</p> <p>1929 Divers reach surface (total dive time 90 min; debrief DSO)</p> <p>1930 Pack up and secure all items on deck</p> <p>1945 Leave site head back to basecamp</p> <p>2030 Arrival at Basecamp; Offload equipment</p> <p>2100 End of Operations</p>
<p>Dive Plan:</p>	<p>Type: Cave Dive / Underwater Laser Scan Site: Taj Mahal Dive Equipment: (Diver 1), (Diver 2)</p> <p>Dive Team 1: Diver 1 (Nebenhaus), Diver 2 / (Gibbs) Topside Support: Dive Supervisor (Daire), Data Recorder (OKeefe) Dive Team 2: Diver 1 (Nebenhaus), Diver 2 (Gibbs) Topside Support: Dive Supervisor (Daire), Data Recorder (OKeefe)</p> <p>Estimated Duration of Dives: (1st) approximately 90 minutes (2nd) 90 minutes. Total: _3 hour and 0 minutes Total Dive Operation: Approximately 3 hours and 0 minutes</p> <p>Objectives:</p> <ul style="list-style-type: none"> • Approximately 5, 7-minute scans at a range (TBD) of an entire section • 1 turbidity reading before and at the end of all scans • 1 salinity reading before and at the end of all scans • 1 temperature reading before and at the end of all scans • 1 visibility reading before and at the end of all scans
<p>Goals:</p>	<p>The quality of scan, and therefore, its efficacy of use in underwater archaeology depends on a variety of operational variables, but primarily its beam intensity setting within a range of (.38m – 2.5m) has been determined through Phase I tests to be the most influential. Those results also demonstrate that the underwater</p>

laser scanner performs at its absolute best in a clear water setting with an absence of light. Therefore, a function of beam intensity to resolution and accuracy of five (5) scans at different beam intensities will be conducted in the most ideal scanning conditions (i.e. non-ambient light and in extremely clear visibility of at least 3m+). The results will then establish an ideal beam intensity setting for a subsequent 360-degree scan of an entire section.

Survey Equipment (by diver):

Diver 1 (Nebenhaus): Levelling Rod, Tape Measure, References, water sample bottle, GoPro mount to helmet, lights mount to helmet, wrist slate for notes

Diver 2 (Gibbs): Nikon D90 DSLR camera, small light, wrist slate for notes

Dive Supervisor/DSO (Daire): Will be tending the ULS-200 cable frequently (especially while divers are on the move to ensure that it does not become snagged on obstructions during the dive operation.

Dive Procedure (Times may not be exact) (Sunset circa 1700):

1000 Depart Basecamp

1045 Arrive on Site

1045 Establish work area, Set-up dive equipment/survey gear, ULS/Computer prep and perform scan test on deck,

1115 Divers 1 and 2 in the water

Diver 1 and Diver 2 buoyancy check

Diver 1 and Diver 2 If all OK, proceed down the cave line with lights on.

Diver 1 and Diver 2 give okay once on bottom, okay to DSO

Diver 1 takes tape measure and secures end to cave line

Diver 1 unreels tape and both divers proceed to feature that is going to be scanned

Diver 1 and 2 reach scanning site

Diver 1 puts tape and reel down, lays levelling rod down in place and places reference cubes on structure to be scanned, at the foot of the structure to be scanned.

Diver 1 takes tape reel and measures far tip of levelling rod from base of mooring shot, notes and reports this distance to topside recorder, reports temperature, depth at site, current and visibility.

	Diver 2 takes photos of all this process for Methodology
	Diver 1 positioning plumb bob over the TBD range mark, takes a water sample, Diver 2 photographs process
1124	Diver 1 signals to get behind the laser, to turn all lights off and instructs topside to begin a scan and record the start time, beam intensity, scan angle, etc... If comms fail, Diver 1 will initiate 1 gentle pull on the ULS cable to start a scan, two pulls to stop scan
1125	Scanning begins at 20% Beam Intensity.
1137	Scanning ends.
1138	Scanning begins at 40% beam intensity.
1145	Scanning ends.
1146	Scanning begins at 60% beam intensity.
1153	Scanning ends. (Divers 1 and 2 signals to each other and topside okay to follow tape back to shot) (Divers leave the scanning area).
1154	Scanning begins at 80% BI.
1155	Divers reach the shot, signal OK to each other and topside to ascend
1157	Divers reach 3m depth, perform safety stop for 5min
1201	Scanning ends.
1202	Divers reach surface (total dive time 90 min); Scanning begins at 100% BI.
1207	Second dive team enters the water.
1209	Scanning ends. Divers reach the bottom of the shot, give OK to proceed to scanning site
1211	Divers reach site
1212	Diver 1 takes a final water sample, reports temperature and visibility with lights on. Diver 2 takes photos and video of the process with lights on. Diver 1 gathers survey materials. Diver 1 and Diver 2 signal OK that they are ready to proceed back to the shot line. Diver 1 reels in tape back to the shot with goody bags and survey equipment. Diver 2 follows carrying Camera.
1222	Divers 1 and 2 reach the shot, signal OK to each other to ascend,

	<p>Diver 1 notifies topside that the team is ascending shot.</p> <p>1224 Divers 1 and 2 reach 3m Depth, begin safety stop of 5min</p> <p>1229 Divers reach surface (total dive time ___min; debrief DSO</p> <p>1230 Pack up and secure all items on deck</p> <p>1245 Leave site head back to basecamp</p> <p>1330 Arrival at Basecamp; Offload equipment</p> <p>1400 End of Operations</p>
Dive Plan:	<p>Type: Cave Dive / Underwater Laser Scan</p> <p>Site:</p> <p>Dive Equipment: (Diver 1), (Diver 2)</p> <p>Dive Team 1: Diver 1 (Nebenhaus), Diver 2 / (Gibbs)</p> <p>Topside Support: Dive Supervisor (Daire), Data Recorder (OKeefe)</p> <p>Dive Team 2: Diver 1 (Nebenhaus), Diver 2 (Gibbs)</p> <p>Topside Support: Dive Supervisor (Daire), Data Recorder (OKeefe)</p> <p>Estimated Duration of Dive: Approximately _90_ minutes</p> <p>Total Dive Operation: Approximately 6 hours and 0 minutes</p> <p>Objectives:</p> <ul style="list-style-type: none"> • 1 scan covering .5m² at a range of .5m for approximately 35 minutes at the highest resolution setting • 2 turbidity readings; 1 before and after the scan • 2 salinity readings; 1 before and after the scan • 2 temperature readings; 1 before and after the scan • 2 visibility readings; 1 before and after the scan
Goals:	<p>A .5m² section of a site will be laser scanned at close range and at the highest resolution setting possible based on previous tests in a non-ambient light environment. The data will then be used as a means to identify and track karst matrix degradation rates over time with a follow-up scans in the subsequent years to help better determine the overall preservation status of the cave site.</p>
Procedure:	<p>Survey Equipment (by diver):</p>

	<p>Lead Diver 1 (Nebenhaus): GoPro mount to mask, small light mount to mask, wrist slate for notes</p> <p>Diver 2 (Gibbs): Nikon D90 DSLR camera, small light, wrist slate for notes</p> <p>Dive Supervisor/DSO (Daire): Will remain on deck at all times constantly monitoring weather conditions and will be tending the ULS-200 cable frequently (especially while divers are on the move) to ensure that it does not become snagged on obstructions during the dive operation.</p> <p>Example Dive Procedure (Times may not be exact):</p> <p>1030 Depart HQ</p> <p>1115 Arrive on Site; Establish work area, Set-up dive equipment/survey gear, ULS/Computer prep and perform scan test</p> <p>1145 Divers 1 and 2 in the water</p> <p style="padding-left: 40px;">Diver 1 and Diver 2 buoyancy check</p> <p style="padding-left: 40px;">Diver 1 and Diver 2 If all OK, proceed down</p> <p>1246 Diver 1 and Diver 2 give okay once on bottom, okay to DSO</p> <p style="padding-left: 40px;">Diver 1 secures end of tape to bottom</p> <p style="padding-left: 40px;">Diver 1 unreels tape and both divers proceed to wood plank that is going to be scanned</p> <p style="padding-left: 40px;">Diver 1 and 2 reach scanning site</p> <p style="padding-left: 40px;">Diver 1 puts tape and reel down, places reference cubes on and adjacent to section of plank to be scanned.</p> <p style="padding-left: 40px;">Diver 1 takes tape reel and measures nearest cube to the shot and reports this distance to topside recorder, reports temperature, depth at site, current and visibility.</p> <p style="padding-left: 40px;">Diver 2 puts ULS with tripod aside and takes photos of all this process for Methodology</p> <p style="padding-left: 40px;">Diver 1 moves tripod with ULS over the estimated center of the scan area and takes a water sample, Diver 2 photographs process.</p> <p>1354 Diver 1 signals to get behind the laser, to turn all lights off and instructs topside to begin a scan and record the start time, beam intensity, scan angle, etc...</p>
--	---

	<p>1455 Scanning begins at TBD beam intensity. 1530 Scanning ends. Diver 1 takes a final water sample, reports temperature and visibility with lights on, records on wrist slate. Diver 2 takes photos and video of the process with lights on. Diver 1 and Diver 2 carefully gather all survey materials. 1633 Diver 1 and Diver 2 signal OK that they are ready to proceed back to the shot. Diver 1 reels in tape back to the shot with goody bags and survey equipment. Diver 2 follows carrying Camera. 1735 Divers 1 and 2 reach the shot, signal OK to each other to ascend. Diver 1 notifies topside that the team is ascending shot. 1836 Divers 1 and 2 reach the surface, no safety stop required (total est. dive time: 51min). Debrief DSO, pack up and secure all items on deck 1945 Leave site head back to HQ 2030 Arrival at HQ; Offload equipment 2100 End of Operations</p> <p>Deviations from the plan: If time permits, photogrammetry of the same section of plank that was scanned will be conducted during an afternoon or check out dive, emergencies stop all project activities.</p>
<p>Dive Plan:</p>	<p>Cave Dive / Underwater Laser Scan Site: Dive Equipment: (Diver 1), (Diver 2)</p> <p>Dive Team 1: Diver 1 (Nebenhaus), Diver 2 (Gibbs) Topside Support: Dive Supervisor (Daire), Data Recorder (OKeefe) Dive Team 2: Diver 1 (Nebenhaus), Diver 2 (Gibbs) Topside Support: Dive Supervisor (Daire), Data Recorder (OKeefe)</p> <p>Estimated Duration of Dives: (1st) approximately 90 minutes (2nd) 90 minutes. Total: 3 hour and 0 minutes. Total Dive Operation: Approximately 3 hours</p> <p>Estimated Duration of Dive Operation: 6 Hours</p>

	<p>Objectives:</p> <ul style="list-style-type: none"> • 15 scans of 5 minutes each of a prominent distinguishing feature at ranges of .50m, 1.50m, and 2.5m • 1 turbidity reading at the start and end of all scanning • 1 salinity reading at the start and end of all scanning • 1 temperature reading at the start and end of all scanning • 1 visibility reading at the start and end of all scanning
<p>Goals:</p>	<p>Determine function of beam intensity to range to quality of scan (resolution and accuracy) operational index scanning conditions (i.e. aphotic and clear visibility of at least 5m+).</p>
<p>Dive Plan:</p>	<p>Survey Equipment (by diver): Lead Diver 1 (Nebenhaus): Levelling Rod, Tape Measure, Goody Bag w/ Container of 9 References, Secchi Disk, two water sample bottles, GoPro mount to mask, small light mount to mask, wrist slate for notes Diver 2 (Gibbs): DSLR camera, ULS-200 w/tripod, small light, wrist slate for notes Dive Supervisor/DSO (Daire): Will remain on deck at all times constantly monitoring weather conditions, boat traffic and any other safety hazards. Will be the primary driver of the boat and will be tending cable frequently (especially while divers are on the move) to ensure that it does not become snagged on obstructions or the prop during the dive operation.</p> <p>0950 Depart HQ 1030 Arrive at Basecamp 1130 – 2000 Head to and establish site, Set-up dive equipment/survey gear, Computer prep and perform scan test on deck 1200 Divers 1 and 2 in the water Diver 1 and Diver 2 buoyancy check Diver 1 and Diver 2 If all OK, proceed down Diver 1 and Diver 2 give okay once on bottom Diver 1 takes tape measure and secures end to bottom of shot Diver 1 unreels tape and both divers proceed to feature that is going to be scanned</p>

	<p>Diver 1 and 2 reach scanning site</p> <p>Diver 1 puts tape and reel down, lays levelling rod down in place and sets reference cubes on structure to be scanned at the foot of the structure to be scanned.</p> <p>Diver 1 takes tape and measures far tip of levelling rod from base of mooring shot, notes and reports this distance to topside recorder, reports temperature, depth at site, current and visibility.</p> <p>Diver 2 takes photos of all this process for Methodology</p>
1215	Diver 1 moves positioning plumb bob over the .50m mark, takes a water sample, Diver 2 photographs process
1219	Diver 1 signals to get behind the laser, to turn all lights off and instructs topside to begin a scan and record the start time, beam intensity, scan angle, etc... 1 will initiate 1 pull on the ULS cable to start a scan, two pulls to stop scan
1220	scanning begins at 20% Beam Intensity.
1225	scanning ends.
1226	scanning begins at 40% BI
1231	scanning ends.
1232	scanning begins at 60% BI
1237	scanning ends.
1238	scanning begins at 80% BI
1243	scanning ends.
1244	scanning begins at 100% BI
1249	scanning ends. Diver 1 reports to topside scanning has ended, confirmation from topside.
1250	Diver moves the scanner back to the 1.5m mark. Diver 2 photographs and takes video of the process. Diver 1 reports temperature and visibility with light on, signals to topside to begin scan at 20% BI. Lights off.
1252	Scanning Begins. Topside and Diver 1 confirm scan taking place. Diver 1 and Diver 2 signal OK that they are ready to proceed back to the caveline. Diver 1 and 2 follow tape back to the shot. Divers

	take great care not to disrupt the scanning process and get entangled in either the tape or the ULS cable while moving to shot.
1256	Divers 1 and 2 reach the shot, signal okay to each other to ascend shot, Diver 1 notifies topside that the team is ascending shot and to continue with 40% BI scan at 2057. Divers 1 and 2 ascend shot and reach surface. (Dive Team 1; End of Dive: 90 min)
1257	Divers 1 (Nebenhaus) and 2 (Gibbs) debrief DSO (Daire). Diver 1 consults with topside recorder, scan of 40% BI begins. Diver 1 takes over (briefly) as recorder and instructs Diver 2 on how to start/stop recordings and log entries as Data Recorder. Diver 1 and Diver 2 in the water.
1303	Scanning at 60% BI begins. Briefing by Diver 1 (Nebenhaus) to Diver 2 (Gibbs) for second dive and objectives
1308	Scanning ends.
1309	Scanning at 80% BI begins. Dive Team 2; Diver 1 (Nebenhaus) and Diver 2 (Gibbs) enter the water, diver checks, etc....
1310	Divers descend down shot
2011	Divers on bottom, signals of okay to each other and through water comms to DSO
1312	Divers carefully make their way to ULS-200 following the tape and locating ULS cable taking care not to entangle in either one.
1315	Scanning ends. Divers arrive at site and monitor progress of next scan.
1316	Scanning at 100% BI begins.
1321	Scanning ends. Diver 1 moves ULS-200 to 2.5m range, reports temperature and visibility with light on by looking at Secchi Disk. Instructs topside to begin scan. Diver 2 videos and photos process. Diver lights off.
1323	Scanning Begins. Divers monitor scanning
1328	Scanning Ends. Diver 1 confirms end of scan with topside, takes second water sample, and divers pack up survey equipment. Diver 1 gathers: Targets, Reference Cubes, reels, markers, and bubble

	<p>level. Diver 2: Secures DSLR camera and ULS-200</p> <p>1335 Divers 1 and 2 signals OK to travel back to the shot and to DSO, with Diver 1 reeling in the tape.</p> <p>1340 Divers 1 and 2 reach the shot, signal OK and to DSO through Comms to ascend the shot</p> <p>1341 Divers 1 and 2 reach the surface signal OK, hand equipment to DSO, brief DSO (Est. Total Dive Time: 31 min)</p> <p>1343 Pack up and secure all items on deck</p> <p>1353 Leave site head back to basecamp</p> <p>1338 Arrival; Offload equipment</p> <p>1400 End of Operations</p>
Dive Plan:	<p>Afternoon Dive / Diver Deployed ULS Scan Site: Taj Mahal Dive Equipment: (Diver 1), (Diver 2)</p> <p>Dive Team 1: Diver 1 (Nebenhaus), Diver 2 (Gibbs) Topside Support: Dive Supervisor (Daire), Data Recorder: (OKeefe)</p> <p>Max estimated Duration of Dives: approximately 45 minutes Max estimated Duration of Dive Operation: 3 Hours and 30 minutes</p> <p>Objectives:</p> <ul style="list-style-type: none"> • 4 scans of 7 minutes each of a prominent distinguishing feature • 1 turbidity reading at the start and end of all scanning • 1 salinity reading at the start and end of all scanning • 1 temperature reading at the start and end of all scanning • 1 visibility reading at the start and end of all scanning
Goals:	<p>The quality of a scan is mostly dependent on a series of environmental variables: salinity, pressure (Depth), temperature and turbidity. Readings for these will be taken before and after scanning. Operational considerations include: range, ping rate, and rotational step per second. A tripod with a pan and tilt mechanism at 1.5m of range with the finest rotational step of .5 degrees per second and a recorded ping rate to obtain the best imagery possible to compare to photogrammetry and underwater laser scanned outputs for resolution and accuracy using</p>

	<p>the fractal reference cubes. Along with two Targets (A and B) will also be positioned at the foot of the feature to gauge accuracy and to aid in registration of the point clouds generated. Each of the four (4) scans around the feature will take approximately 5 minutes to conduct and one (1) minute to reposition for the next scan resulting in a total estimated scan time of approximately 90 minutes.</p> <p>Survey Equipment (by diver): Lead Diver 1 (Nebenhaus): Goody Bag w/ Container of 9 References (A and B), Secchi Disk, two water sample bottles, GoPro mount to mask, wrist slate for notes, Tape and Reel, Levelling Rod Diver 2 (Gibbs): DSLR camera, ULS w/tripod, wrist slate for notes, Dive Supervisor/DSO (Daire): Will remain on deck at all times constantly monitoring weather conditions, boat traffic and any other safety hazards. Will be the primary driver of the boat and will be tending the cable frequently (especially while divers are on the move) to ensure that it does not become snagged on obstructions or the prop during the dive operation.</p>
<p>Procedure:</p>	<p>1000 Depart 1045 Arrive on Site 1115 Establish workspace, Set-up dive equipment/survey gear, Computer. 1115 Divers 1 and 2 in the water Diver 1 and Diver 2 buoyancy check, through water check Diver 1 and Diver 2 If all OK, proceed down the shot line with lights on. Diver 1 and Diver 2 give okay once on bottom, okay to DSO Diver 1 takes tape measure and secures end to bottom of shot Diver 1 unreels tape and both divers proceed to feature that is going to be scanned Diver 1 and 2 reach scanning sites Diver 1 puts tape and reel down, lays levelling rod down in place and sets reference cubes on structure to be scanned, Secchi Disk down at the foot of the structure to be scanned.</p>

	<p>Diver 1 takes tape and measures far tip of levelling rod from base of mooring shot, notes and reports this distance to topside recorder, reports temperature, depth at site, current and visibility.</p> <p>Diver 2 puts ULS with tripod aside and takes photos of all this process for Methodology</p>
1120	Diver 1 moves tripod with BV positioning plumb bob over the 1.5m mark, takes a water sample, Diver 2 photographs process
1125	Diver 1 signals to get behind the sonar and instructs topside to begin a scan. Diver 1 will initiate 1 pull on the ULS cable to start a scan, two pulls to stop scan. Process is repeated four times, moving scanner around the feature to be scanned at a range of 1.5m
1150	Scanning Ends. Diver 1 confirms end of scan with topside, takes second water sample, and divers pack up survey equipment. Diver 1 collect: Photogrammetry targets, Reference Cubes and Levelling Rod. Diver 2: Secures DSLR camera and ULS
1155	Divers 1 and 2 collect OK to travel back to the shot and to DSO, with Diver 1 reeling in the tape.
1158	Divers 1 and 2 reach the shot, signal OK and to DSO through Comms to ascend the shot
1200	Divers 1 and 2 reach the surface, signal OK, hand equipment to DSO, brief DSO (Est. Total Dive Time: 31 min)
1210	Pack up and secure all items on deck
1215	Leave site head back to
1300	Arrival; Offload equipment
1330	End of Operations

Agisoft PhotoScan

**Processing Report
10 September 2018**



Survey Data

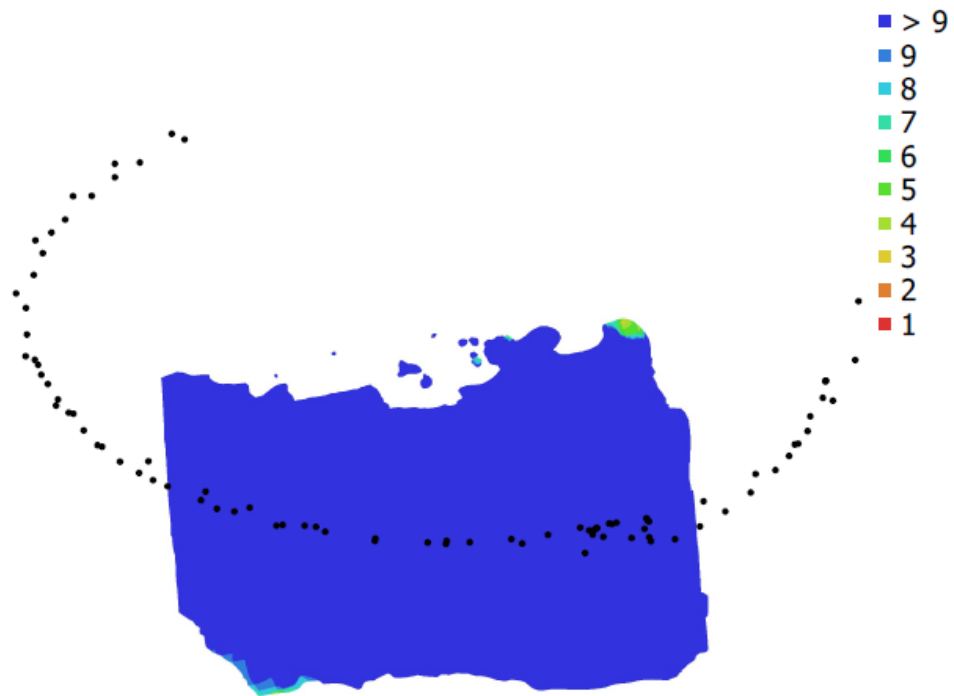


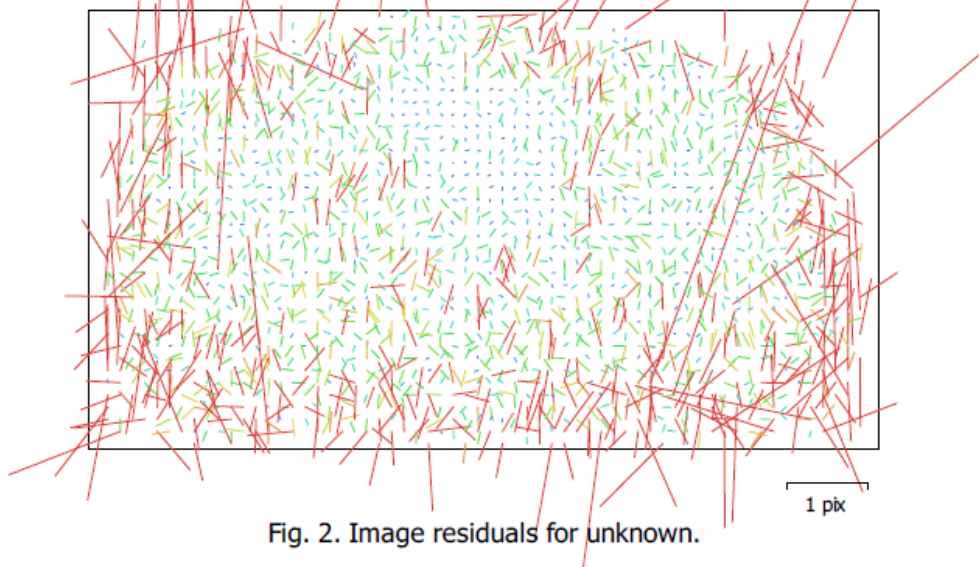
Fig. 1. Camera locations and image overlap.

Number of images:	88	Camera stations:	88
		Tie points:	20,378
		Projections:	48,568
		Reprojection error:	1.29 pix

Camera Model	Resolution	Focal Length	Pixel Size	Precalibrated
unknown	1920 x 1080	unknown	unknown	No

Table 1. Cameras.

Camera Calibration



unknown
88 images

Type **Frame** Resolution **1920 x 1080** Focal Length **unknown** Pixel Size **unknown**

	Value	Error	F	Cx	Cy	K1	K2	K3	P1	P2
F	1797.26	3.6	1.00	0.07	-0.41	0.27	-0.23	0.27	0.04	-0.21
Cx	7.21129	2.8		1.00	0.00	-0.12	0.17	-0.21	0.78	0.10
Cy	-0.542352	4			1.00	-0.01	-0.02	0.04	-0.00	0.60
K1	0.228024	0.008				1.00	-0.95	0.90	-0.10	-0.03
K2	-1.49425	0.057					1.00	-0.98	0.15	-0.05
K3	2.79658	0.13						1.00	-0.18	0.05
P1	-0.00329513	0.00057							1.00	0.09
P2	0.00338323	0.00059								1.00

Table 2. Calibration coefficients and correlation matrix.

Digital Elevation Model

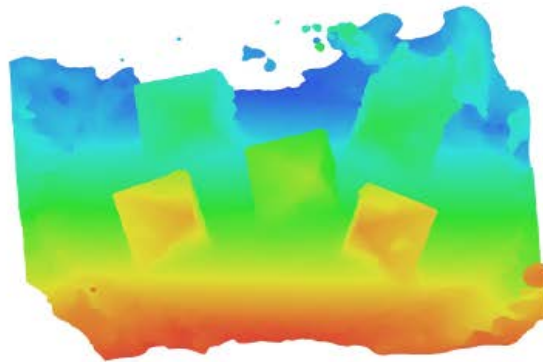


Fig. 3. Reconstructed digital elevation model.

Processing Parameters

General	
Cameras	88
Aligned cameras	88
Point Cloud	
Points	20,378 of 39,774
RMS reprojection error	0.182175 (1.28845 pix)
Max reprojection error	0.554788 (20.6606 pix)
Mean key point size	6.36154 pix
Point colors	3 bands, uint8
Key points	No
Average tie point multiplicity	2.85199
Alignment parameters	
Accuracy	High
Generic preselection	Yes
Key point limit	40,000
Tie point limit	4,000
Adaptive camera model fitting	No
Matching time	6 minutes 9 seconds
Alignment time	45 seconds
Dense Point Cloud	
Points	474,065
Point colors	3 bands, uint8
Reconstruction parameters	
Quality	Medium
Depth filtering	Aggressive
Depth maps generation time	1 minutes 41 seconds
Dense cloud generation time	2 minutes 22 seconds
Model	
Faces	59,999
Vertices	30,429
Vertex colors	3 bands, uint8
Texture	4,096 x 4,096, 4 bands, uint8
Reconstruction parameters	
Surface type	Arbitrary
Source data	Dense
Interpolation	Enabled
Quality	Medium
Depth filtering	Aggressive
Face count	60,000
Processing time	15 seconds
Texturing parameters	
Mapping mode	Generic
Blending mode	Mosaic
Texture size	4,096 x 4,096
Enable hole filling	Yes
Enable ghosting filter	Yes
UV mapping time	25 seconds
Blending time	59 seconds
Software	
Version	1.4.3 build 6529
Platform	Windows 64

Appendix L. Philosophies, Procedures, & Tools for Subaquatic Survey & Survival

Deployment Philosophies & Techniques for Subaquatic Survey & Survival				
Objectives				
Good (Gas)	1) Confirm Gas & Reserve 2) Two Independent 1 st stages			
Deployment (Decompression)	1) Compare Theoretical/ Actual Gas Supply 2) Use two dive computers			
Main (Mission)	1) Safe Return 2) Team plans together 3) All team agrees upon dive plan 4) Team dives the plan			
Objective (O₂)	1) Analyzed Labeled (Tank-Top/Tank-Side/Regulator) 2) Computer set for gasses			
Is (Inert Gas Narcosis)	1) Perceive Risks 2) Dive no deeper than plan 3) Diver no deeper than need			
To (Thermal Exposure)	1) Suit adequate for dive 2) Inspect seals, valves, zippers			
Live (Logistics)	1) Who, What, When, Where, Why, How, and Via 2) Establish dive, project, gear, and crew managers			
No-Tox Etiquette & Procedures for LSS Narcosis Mitigation				
Note	Observe	Turn	Orient	Examine
Tank Bottle 1) Name 2) Depth 3) Gas O ₂ -N ₂ %	Actual PPO ₂ / Max PPO ₂ Valves Open/Closed Tank Pressure	Pressurize hose Valves from Open to Close	2nd Stage on BCD Test Bottles Switch Bottles	Team Bottles 1) Name 2) Depth 3) Gas O ₂ -N ₂ %
Gas Toxicity Equations for Planning Oxygen & Nitrogen Operational Exposures				
Equivalent Air Depth	Partial pressure O ₂	Max Depth, Z	Contingency Depth	
$= ((1 - O_2\%) (Z+33)/.79) - 33$	$= ((Z + 33)/33) (O_2\%)$	$= (46.2/O_2\%) - 33$	$= (52.8/O_2\%) - 33$	
Subaquatic Psychological Condition & Pre-Survey Procedure				
Being (BCD)	Wary (Weight)	Reduces (Releases)	Grievous (Gas)	Failures (Final)
1) Gear Placement & Assembly 2) Type & Volume 3) Inflators	1) Mass 2) Distribution 3) Trim 4) Securing	1) Operate 2) Break-away 3) Fasten	1) Analyze Gas O ₂ -N ₂ % 2) Test Self-Contained Breathing/ Rebreathing Apparatus	1) Head-To-Toe Check 2) Missing Gear 3) Team Check

Appendix M. Nebenhaus, Mayor, Daire, & Loew Spatial Datasets of Sistema Taj Mahal

Spatial Datasets	
AOI	Sistema Taj Mahal, Cenote Taj Mahal, Deep Bone Room. Xpu Ha, Quintana Roo, México.
Datasets	.CSV, .JPEG, .TML, .OBJ, .SVG files of various size, composition, and focus.
Attributes	Geospatial survey for xyz & isotopic geomorphological and geoheritage data
FOI	Data permission granted with stipulations of citation sourcing, and community standards for cave etiquette on non-disclosure of maps for conservation and accident prevention. Deviation occurs over mapping distances, bowing of cave line, and estimation of center fit line is based on approximation of room size, light capacity, and speleothem density.
Points & Projections	<p>Nebenhaus, M. 2017: Elevation: 10.0m Decimal Degree: Latitude: 20.483786 Longitude: -87.27680645984722 Degrees, Minutes, Seconds: Latitude: 20 29 01.6296 N Longitude: 87 16 26.5033 W UTM: 16Q Easting 471134 Northing 2265043</p> <p>Mayor, D. 2017: Elevation: 9.9m Decimal Degree: Latitude: 20.48369 Longitude: -87.27692 Degrees, Minutes, Seconds: Latitude: 20 29 01.2840 N Longitude: 87 16 36.9120 W UTM: 16Q Easting 471122.1 Northing 2265032.3</p> <p>Daire, S. A. and Loew, C. 2018: Elevation: 10.0m Decimal Degree: Latitude: 20.483786 Longitude: -87.27680645984722 Degrees, Minutes, Seconds: Latitude: 20 29 01.6296 N Longitude: 87 16 26.5033 W UTM: 16Q Easting 471134 Northing 226504</p>
Sources: Nebenhaus, M. 2017. Mayor, D. 2017. Daire, S. A. Loew, C. Nolasco, E. 2017. Daire, S. A. Loew, C. 2018	

Appendix N. Laser Classification & Safety Datasheet

Laser Classes & Considerations	Class	Notes
Classifications ANSI & IEC	3	
<i>Sub-Class</i>	<i>3R</i>	
U. S. FDA	Class IIIa (Definition is different, but results are similar)	Newer ANSI/IEC number classes are now preferred over older FDA Roman numeral classes.
Human-accessible laser power (for visible light)	For visible light, emits beam between 1 and 4.99 milliwatts.	Non-laser visible lasers emitting infrared or ultraviolet (UV) are included in this chart. Only visible lasers are discussed.
Caution/warning indication Label descriptive text	CAUTION Avoid direct eye contact	For visible-light lasers, the word “light” can be used instead of “radiation.” The latter is more accurate for lasers emitting infrared and UV radiation.
EYE AND SKIN HAZARDS Eye hazard for intraocular exposure (having a direct or reflected beam enter the eye)	Unintentional or accidental exposure to direct or reflected beam has a low risk.	Avoid eye exposure to a direct or reflected laser beam, within the NOHD. The closer you are to the laser, the greater the chance of hazard and the more serious the injury potential. Dark materials which absorb heat, and lightweight materials such as paper and fabric, are most easily
Maximum or typical Nominal Ocular Hazard Distance (for 1 milliradian beam, exposure time less than ¼ second)	Avoid intentional exposure to direct or reflected beam. NOHD of 4.99 mW beam: 52 ft (16m)	
Eye hazard for diffuse reflection exposure (looking at the laser “dot” scattered off a surface)	None	
Skin burn hazard	None	
Materials burn hazard	None	
VISUAL INTERFERENCE DISTANCES		Value given for 555 nm, the green wavelength that appears brightest to the light-adapted human eye. This gives the

Maximum or typical flash blindness distance (FAA 100 uW/cm ² , for 1 milliradian beam, 555 nm green light)	For a 4.99 mW beam: 261 ft (80 m)	longest hazard distance. To approximate for led laser light, divide the distance by about 5; for blue, divide by 20.
Maximum or typical glare distance (FAA 5 uW/cm ² , for 1 milliradian beam, 555 nm green light)	1,169 ft (356 m)	See above
Maximum or typical distraction distance (FAA 0.05 uW/cm ² , for 1 milliradian beam, 555 nm green light)	11,689 ft (3,563 m)	See above
Technical Notes	Class 3R is either: (1) From 1 to 4.99 mW into a 7mm aperture (e.g. pupil of the eye) or (2) five times the Class 2 limit of 2.5 mW/cm ² , which works out to be 12.5 mW/cm ² . The second method is used by LaserSafetyFacts to determine NOHD.	

Source: LaserSafetyFacts.com, 2018

Appendix O. Exported AgiSoft DTM for Full Cave Photoplethysmogram in Cloudcompare

[18:33:39] [Global Shift] Max abs. coord = 1e+4 / max abs. diag = 1e+6
[18:33:39] [ccColorScalesManager] Found 2 custom scale(s) in persistent settings
[18:33:39] [Plugins] Plugin lookup dirs: C:/Program Files/CloudCompareStereo/plugins
[18:33:39] Found plugin: Animation (QANIMATION_PLUGIN.dll)
[18:33:39] Found plugin: Blur (shader) (QBLUR_PLUGIN.dll)
[18:33:39] Found plugin: CEA virtual broom (QBROOM_PLUGIN.dll)
[18:33:39] Found plugin: CANUPO classification (QCANUPO_PLUGIN_DLL.dll)
[18:33:39] Found plugin: Compass (QCOMPASS_PLUGIN.dll)
[18:33:39] Found plugin: Mesh Boolean Operations (QCORK_PLUGIN.dll)
[18:33:39] Found plugin: CSF Filter (QCSF_PLUGIN.dll)
[18:33:39] Found plugin: CSV Matrix I/O filter (QCSV_MATRIX_IO_PLUGIN.dll)
[18:33:39] Found plugin: DotProduct I/O filter (QDOT_PRODUCT_IO_PLUGIN.dll)
[18:33:39] Found plugin: E.D.L. (shader) (QEDL_PLUGIN.dll)
[18:33:39] Found plugin: Ellipser (Ellipse marking) (QELLIPSER_PLUGIN.dll)

[18:33:39] Found plugin: Facet/fracture detection (QFACETS_PLUGIN_DLL.dll)
 [18:33:39] Found plugin: Hough Normals Computation (QHOUGH_NORMALS_PLUGIN.dll)
 [18:33:39] Found plugin: Hidden Point Removal (QHPR_PLUGIN.dll)
 [18:33:39] Found plugin: LAS FWF I/O filter (QLAS_FWF_IO_PLUGIN.dll)
 [18:33:39] Found plugin: M3C2 distance (QM3C2_PLUGIN_DLL.dll)
 [18:33:39] Found plugin: PCL I/O filter (QPCL_IO_PLUGIN.dll)
 [18:33:39] Found plugin: PCL wrapper (QPCL_PLUGIN.dll)
 [18:33:39] Found plugin: P.C.V. (Ambient Occlusion) (QPCV_PLUGIN.dll)
 [18:33:39] Found plugin: Photoscan I/O filter (QPHOTOSCAN_IO_PLUGIN.dll)
 [18:33:39] Found plugin: Poisson Surface Reconstruction (QPOISSON_RECON_PLUGIN.dll)
 [18:33:39] Found plugin: RANSAC Shape Detection (QRANSAC_SD_PLUGIN.dll)
 [18:33:39] Found plugin: RDB I/O filter (QRDB_IO_PLUGIN.dll)
 [18:33:39] Found plugin: Riegl I/O filter (QRIEGL_IO_PLUGIN.dll)
 [18:33:39] Found plugin: Surface of Revolution Analysis (QSRA_PLUGIN.dll)
 [18:33:39] Found plugin: S.S.A.O. (shader) (QSSAO_PLUGIN.dll)
 [18:33:39] [Plugin][CSV Matrix I/O filter] New file extension(s) registered: CSV
 [18:33:39] [Plugin][DotProduct I/O filter] New file extension(s) registered: DP
 [18:33:39] [Plugin][LAS FWF I/O filter] New file extension(s) registered: LAS
 [18:33:39] [Plugin][PCL I/O filter] New file extension(s) registered: PCD
 [18:33:39] [Plugin][Photoscan I/O filter] New file extension(s) registered: PSZ
 [18:33:39] [Plugin][RDB I/O filter] New file extension(s) registered: RDBX
 [18:33:39] [Plugin][Riegl I/O filter] New file extension(s) registered: RDS
 [18:33:39] [ccGLWindow] Perspective is off by default
 [18:33:39] [3D Mouse] Could not open a 3DxWare device
 [18:33:39] CloudCompare started!
 [18:33:39] [ccCompass] ccCompass plugin initialized successfully.
 [18:33:40] [3D View 1] Graphics card manufacturer: Intel
 [18:33:40] [3D View 1] Renderer: Intel(R) UHD Graphics 630
 [18:33:40] [3D View 1] GL version: 4.5.0 - Build 23.20.16.5018
 [18:33:40] [3D View 1] GLSL Version: 4.50 - Build 23.20.16.5018
 [18:33:40] [3D View 1] VBOs available
 [18:33:40] [3D View 1] Shaders available
 [18:33:40] [3D View 1] GL filters available
 [18:33:40] [3D View 1] Color ramp shader loaded successfully
 [18:33:40] [3D View 1] Stereo mode: not supported
 [18:33:40] [ccGLWindow] 3D view initialized
 [18:33:40] [Global Shift] Max abs. coord = 1e+4 / max abs. diag = 1e+6
 [18:34:14] [I/O] File 'D:/594b_12-10-2018/Daire-594b-Thesis-DATA/Day_2/LiDAR/2018-9-21-Deep-Bone-Room/2018-9-21-15-25-12_deep_bone_hoz.2Gs.xyz' loaded successfully
 [18:34:14] [VBO] VBO(s) (re)initialized for cloud '2018-9-21-15-25-12_deep_bone_hoz - Cloud' (0.07 Mb = 100.00% of points could be loaded)
 [18:34:16] [I/O] File 'D:/594b_12-10-2018/Daire-594b-Thesis-DATA/Day_2/LiDAR/2018-9-21-Deep-Bone-Room/2018-9-21-15-49-31_deep_bone_hoz2.2Gs.xyz' loaded successfully
 [18:34:16] [VBO] VBO(s) (re)initialized for cloud '2018-9-21-15-49-31_deep_bone_hoz2 - Cloud' (13.22 Mb = 100.00% of points could be loaded)

[18:34:18] [I/O] File 'D:/594b_12-10-2018/Daire-594b-Thesis-DATA/Day_2/LiDAR/2018-9-21-Deep-Bone-Room/2018-9-21-15-52-23deepbonehoz2.2Gs.xyz' loaded successfully
[18:34:18] [VBO] VBO(s) (re)initialized for cloud '2018-9-21-15-52-23deepbonehoz2 - Cloud' (14.39 Mb = 100.00% of points could be loaded)
[18:34:20] [I/O] File 'D:/594b_12-10-2018/Daire-594b-Thesis-DATA/Day_2/LiDAR/2018-9-21-Deep-Bone-Room/2018-9-21-15-57-7_deep_bone_vert2.2Gs.xyz' loaded successfully
[18:34:20] [VBO] VBO(s) (re)initialized for cloud '2018-9-21-15-57-7_deep_bone_vert2 - Cloud' (12.53 Mb = 100.00% of points could be loaded)
[18:34:21] [I/O] File 'D:/594b_12-10-2018/Daire-594b-Thesis-DATA/Day_2/LiDAR/2018-9-21-Deep-Bone-Room/2018-9-21-16-18-4_deep_bone_hor3.2Gs.xyz' loaded successfully
[18:34:22] [VBO] VBO(s) (re)initialized for cloud '2018-9-21-16-18-4_deep_bone_hor3 - Cloud' (13.71 Mb = 100.00% of points could be loaded)
[18:34:23] [I/O] File 'D:/594b_12-10-2018/Daire-594b-Thesis-DATA/Day_2/LiDAR/2018-9-21-Deep-Bone-Room/2018-9-21-16-28-38_deep_bone_vert3.2Gs.xyz' loaded successfully
[18:34:23] [VBO] VBO(s) (re)initialized for cloud '2018-9-21-16-28-38_deep_bone_vert3 - Cloud' (13.70 Mb = 100.00% of points could be loaded)
[18:34:24] [I/O] File 'D:/594b_12-10-2018/Daire-594b-Thesis-DATA/Day_2/LiDAR/2018-9-21-Deep-Bone-Room/2018-9-21-16-38-46_deep_Bone_hoz_4.2Gs.xyz' loaded successfully
[18:34:25] [VBO] VBO(s) (re)initialized for cloud '2018-9-21-16-38-46_deep_Bone_hoz_4 - Cloud' (13.77 Mb = 100.00% of points could be loaded)
[18:34:26] [I/O] File 'D:/594b_12-10-2018/Daire-594b-Thesis-DATA/Day_2/LiDAR/2018-9-21-Deep-Bone-Room/2018-9-21-16-44-17_deep_bone_vert4.2Gs.xyz' loaded successfully
[18:34:26] [VBO] VBO(s) (re)initialized for cloud '2018-9-21-16-44-17_deep_bone_vert4 - Cloud' (13.70 Mb = 100.00% of points could be loaded)
[18:34:27] [I/O] File 'D:/594b_12-10-2018/Daire-594b-Thesis-DATA/Day_2/LiDAR/2018-9-21-Deep-Bone-Room/2018-9-21-16-53-18_deep_bone_horz_5.2Gs.xyz' loaded successfully
[18:34:28] [VBO] VBO(s) (re)initialized for cloud '2018-9-21-16-53-18_deep_bone_horz_5 - Cloud' (14.32 Mb = 100.00% of points could be loaded)
[18:34:29] [I/O] File 'D:/594b_12-10-2018/Daire-594b-Thesis-DATA/Day_2/LiDAR/2018-9-21-Deep-Bone-Room/2018-9-21-17-0-0_Deep_Bone_Vert_6.2Gs.xyz' loaded successfully
[18:34:29] [VBO] VBO(s) (re)initialized for cloud '2018-9-21-17-0-0_Deep_Bone_Vert_6 - Cloud' (13.49 Mb = 100.00% of points could be loaded)
[18:34:30] [I/O] File 'D:/594b_12-10-2018/Daire-594b-Thesis-DATA/Day_2/LiDAR/2018-9-21-Deep-Bone-Room/2018-9-21-17-34-41_deep_bone_horz7.2Gs.xyz' loaded successfully
[18:34:31] [VBO] VBO(s) (re)initialized for cloud '2018-9-21-17-34-41_deep_bone_horz7 - Cloud' (13.71 Mb = 100.00% of points could be loaded)
[18:35:43] [Load] Can't guess file format: unhandled file extension 'zip'
[18:36:52] [Load] Can't guess file format: unhandled file extension 'xml'
[18:36:54] [Load] Can't guess file format: unhandled file extension 'xml'
[18:36:55] [Load] Can't guess file format: unhandled file extension 'xml'
[18:36:55] [OBJ] D:/594b_12-10-2018/Daire-594b-Thesis-DATA/2018_Survey_May/Cenote_Taj_Ma_Hal/Full Site Final Alignments/Chamber_Survey_Line_Paleontological_SO4_FOI.obj
[18:36:58] [OBJ] 93073 points, 0 faces
[18:36:58] [OBJ] 0 tex. coords, 93073 normals

[18:36:58] [I/O] File 'D:/594b_12-10-2018/Daire-594b-Thesis-DATA/2018_Survey_May/Cenote_Taj_Ma_Hal/Full Site Final Alignments/Chamber_Survey_Line_Paleontological_SO4_FOI.obj' loaded successfully
[18:36:58] [VBO] VBO(s) (re)initialized for cloud 'vertices' (1.07 Mb = 100.00% of points could be loaded)
[18:36:58] [OBJ] D:/594b_12-10-2018/Daire-594b-Thesis-DATA/2018_Survey_May/Cenote_Taj_Ma_Hal/Full Site Final Alignments/Chamber_Line_End_SO4_FOI.obj
[18:37:31] [OBJ] 3998248 points, 0 faces
[18:37:31] [OBJ] 0 tex. coords, 3998248 normals
[18:37:31] [I/O] File 'D:/594b_12-10-2018/Daire-594b-Thesis-DATA/2018_Survey_May/Cenote_Taj_Ma_Hal/Full Site Final Alignments/Chamber_Line_End_SO4_FOI.obj' loaded successfully
[18:37:32] [VBO] VBO(s) (re)initialized for cloud 'vertices' (45.76 Mb = 100.00% of points could be loaded)
[18:37:32] [OBJ] D:/594b_12-10-2018/Daire-594b-Thesis-DATA/2018_Survey_May/Cenote_Taj_Ma_Hal/Full Site Final Alignments/Corridor_Line_SO4_FOI.obj
[18:37:36] [OBJ] 450612 points, 0 faces
[18:37:36] [OBJ] 0 tex. coords, 450612 normals
[18:37:36] [I/O] File 'D:/594b_12-10-2018/Daire-594b-Thesis-DATA/2018_Survey_May/Cenote_Taj_Ma_Hal/Full Site Final Alignments/Corridor_Line_SO4_FOI.obj' loaded successfully
[18:37:36] [VBO] VBO(s) (re)initialized for cloud 'vertices' (5.16 Mb = 100.00% of points could be loaded)
[18:37:36] [OBJ] D:/594b_12-10-2018/Daire-594b-Thesis-DATA/2018_Survey_May/Cenote_Taj_Ma_Hal/Full Site Final Alignments/Chamber_Walls_SO4_FOI.obj
[18:37:54] [OBJ] 2282754 points, 0 faces
[18:37:54] [OBJ] 0 tex. coords, 2282754 normals
[18:37:54] [I/O] File 'D:/594b_12-10-2018/Daire-594b-Thesis-DATA/2018_Survey_May/Cenote_Taj_Ma_Hal/Full Site Final Alignments/Chamber_Walls_SO4_FOI.obj' loaded successfully
[18:37:55] [VBO] VBO(s) (re)initialized for cloud 'vertices' (26.12 Mb = 100.00% of points could be loaded)
[18:38:07] [I/O] File 'D:/594b_12-10-2018/Daire-594b-Thesis-DATA/2018_Survey_May/Cenote_Taj_Ma_Hal/Full Site Final Alignments/Chamber_Line_End_SO4.txt' loaded successfully
[18:38:08] [VBO] VBO(s) (re)initialized for cloud 'Chamber_Line_End_SO4 - Cloud' (57.20 Mb = 100.00% of points could be loaded)
[18:38:08] [I/O] File 'D:/594b_12-10-2018/Daire-594b-Thesis-DATA/2018_Survey_May/Cenote_Taj_Ma_Hal/Full Site Final Alignments/Chamber_Line_End_SO4_FOI.jpg' loaded successfully
[18:38:27] [AsciiFilter::Load] Line 1 is corrupted (found 1 part(s) on 7 expected)!

[18:38:34] [I/O] File 'D:/594b_12-10-2018/Daire-594b-Thesis-DATA/2018_Survey_May/Cenote_Taj_Ma_Hal/Full Site Final Alignments/Chamber_Line_End_SO4.pts' loaded successfully
[18:38:35] [VBO] VBO(s) (re)initialized for cloud 'Chamber_Line_End_SO4 - Cloud' (57.20 Mb = 100.00% of points could be loaded)
[18:38:37] [AsciiFilter::Load] Line 1 is corrupted (found 1 part(s) on 7 expected!)
[18:38:37] [I/O] File 'D:/594b_12-10-2018/Daire-594b-Thesis-DATA/2018_Survey_May/Cenote_Taj_Ma_Hal/Full Site Final Alignments/Chamber_Survey_Line_Paleontological_SO4_FOI.pts' loaded successfully
[18:38:37] [VBO] VBO(s) (re)initialized for cloud 'Chamber_Survey_Line_Paleontological_SO4_FOI - Cloud' (1.33 Mb = 100.00% of points could be loaded)
[18:38:38] [AsciiFilter::Load] Line 1 is corrupted (found 1 part(s) on 7 expected!)
[18:38:42] [I/O] File 'D:/594b_12-10-2018/Daire-594b-Thesis-DATA/2018_Survey_May/Cenote_Taj_Ma_Hal/Full Site Final Alignments/Chamber_Walls_SO4_FOI.pts' loaded successfully
[18:38:42] [VBO] VBO(s) (re)initialized for cloud 'Chamber_Walls_SO4_FOI - Cloud' (32.66 Mb = 100.00% of points could be loaded)
[18:38:43] [AsciiFilter::Load] Line 1 is corrupted (found 1 part(s) on 7 expected!)
[18:38:44] [I/O] File 'D:/594b_12-10-2018/Daire-594b-Thesis-DATA/2018_Survey_May/Cenote_Taj_Ma_Hal/Full Site Final Alignments/Corridor_Line_SO4_FOI.pts' loaded successfully
[18:38:44] [VBO] VBO(s) (re)initialized for cloud 'Corridor_Line_SO4_FOI - Cloud' (6.45 Mb = 100.00% of points could be loaded)
[18:38:44] [OBJ] D:/594b_12-10-2018/Daire-594b-Thesis-DATA/2018_Survey_May/Cenote_Taj_Ma_Hal/Full Site Final Alignments/Day_3_AOI_Complete_Deep_Bone_Room.obj
[18:38:45] [OBJ] 35339 points, 0 faces
[18:38:45] [OBJ] 0 tex. coords, 35339 normals
[18:38:45] [I/O] File 'D:/594b_12-10-2018/Daire-594b-Thesis-DATA/2018_Survey_May/Cenote_Taj_Ma_Hal/Full Site Final Alignments/Day_3_AOI_Complete_Deep_Bone_Room.obj' loaded successfully
[18:38:45] [VBO] VBO(s) (re)initialized for cloud 'vertices' (0.40 Mb = 100.00% of points could be loaded)
[18:38:46] [I/O] File 'D:/594b_12-10-2018/Daire-594b-Thesis-DATA/2018_Survey_May/Cenote_Taj_Ma_Hal/Full Site Final Alignments/Day_3_AOI_Complete_Deep_Bone_Room.txt' loaded successfully
[18:38:46] [VBO] VBO(s) (re)initialized for cloud 'Day_3_AOI_Complete_Deep_Bone_Room - Cloud' (0.51 Mb = 100.00% of points could be loaded)
[18:38:46] [LAS] D:/594b_12-10-2018/Daire-594b-Thesis-DATA/2018_Survey_May/Cenote_Taj_Ma_Hal/Full Site Final Alignments/Day_3_AOI_Complete_Deep_Bone_Room.las - signature: LASF
[18:38:47] [LAS] Cloud has been recentered! Translation: (1000.00 ; 1000.00 ; 1000.00)
[18:38:47] [LAS] Color components are coded on 16 bits
[18:38:47] [LAS] All 'User Data' values were the same (0)! We ignored them...

[18:38:47] [LAS] All 'Scan Angle Rank' values were the same (0)! We ignored them...
[18:38:47] [LAS] All 'Flightline Edge' values were the same (0)! We ignored them...
[18:38:47] [LAS] All 'Number of Returns' values were the same (1)! We ignored them...
[18:38:47] [LAS] All 'Return Number' values were the same (1)! We ignored them...
[18:38:47] [LAS] All 'Classification' values were the same (0)! We ignored them...
[18:38:47] [I/O] File 'D:/594b_12-10-2018/Daire-594b-Thesis-DATA/2018_Survey_May/Cenote_Taj_Ma_Hal/Full Site Final Alignments/Day_3_AOI_Complete_Deep_Bone_Room.las' loaded successfully
[18:38:47] [VBO] VBO(s) (re)initialized for cloud 'Day_3_AOI_Complete_Deep_Bone_Room - Cloud' (0.51 Mb = 100.00% of points could be loaded)
[18:38:48] [LAS] D:/594b_12-10-2018/Daire-594b-Thesis-DATA/2018_Survey_May/Cenote_Taj_Ma_Hal/Full Site Final Alignments/Day_3_AOI_Complete_Deep_Bone_Room.laz - signature: LASF
[18:38:49] [LAS] Cloud has been recentered! Translation: (1000.00 ; 1000.00 ; 1000.00)
[18:38:49] [LAS] Color components are coded on 16 bits
[18:38:49] [LAS] All 'User Data' values were the same (0)! We ignored them...
[18:38:49] [LAS] All 'Scan Angle Rank' values were the same (0)! We ignored them...
[18:38:49] [LAS] All 'Flightline Edge' values were the same (0)! We ignored them...
[18:38:49] [LAS] All 'Number of Returns' values were the same (1)! We ignored them...
[18:38:49] [LAS] All 'Return Number' values were the same (1)! We ignored them...
[18:38:49] [LAS] All 'Classification' values were the same (0)! We ignored them...
[18:38:49] [I/O] File 'D:/594b_12-10-2018/Daire-594b-Thesis-DATA/2018_Survey_May/Cenote_Taj_Ma_Hal/Full Site Final Alignments/Day_3_AOI_Complete_Deep_Bone_Room.laz' loaded successfully
[18:38:49] [VBO] VBO(s) (re)initialized for cloud 'Day_3_AOI_Complete_Deep_Bone_Room - Cloud' (0.51 Mb = 100.00% of points could be loaded)
[18:38:50] [AsciiFilter::Load] Line 1 is corrupted (found 1 part(s) on 7 expected)!
[18:38:50] [I/O] File 'D:/594b_12-10-2018/Daire-594b-Thesis-DATA/2018_Survey_May/Cenote_Taj_Ma_Hal/Full Site Final Alignments/Day_3_AOI_Complete_Deep_Bone_Room.pts' loaded successfully
[18:38:50] [VBO] VBO(s) (re)initialized for cloud 'Day_3_AOI_Complete_Deep_Bone_Room - Cloud' (0.51 Mb = 100.00% of points could be loaded)
[18:42:36] [Load] Can't guess file format: unhandled file extension '2Gs'
[18:42:37] [Load] Can't guess file format: unhandled file extension '2Gs'
[18:42:39] [I/O] File 'D:/594b_12-10-2018/Daire-594b-Thesis-DATA/Day_2/LiDAR/2018-9-21-Deep-Bone-Room/2018-9-21-15-25-12_deep_bone_hoz.2Gs.xyz' loaded successfully
[18:42:39] [VBO] VBO(s) (re)initialized for cloud '2018-9-21-15-25-12_deep_bone_hoz - Cloud' (0.07 Mb = 100.00% of points could be loaded)
[18:42:39] [Load] Can't guess file format: unhandled file extension '2Gs'
[18:42:41] [I/O] File 'D:/594b_12-10-2018/Daire-594b-Thesis-DATA/Day_2/LiDAR/2018-9-21-Deep-Bone-Room/2018-9-21-15-49-31_deep_bone_hoz2.2Gs.xyz' loaded successfully
[18:42:41] [VBO] VBO(s) (re)initialized for cloud '2018-9-21-15-49-31_deep_bone_hoz2 - Cloud' (13.22 Mb = 100.00% of points could be loaded)
[18:42:41] [Load] Can't guess file format: unhandled file extension '2Gs'

[18:42:43] [I/O] File 'D:/594b_12-10-2018/Daire-594b-Thesis-DATA/Day_2/LiDAR/2018-9-21-Deep-Bone-Room/2018-9-21-15-52-23deepbonehoz2.2Gs.xyz' loaded successfully
[18:42:43] [VBO] VBO(s) (re)initialized for cloud '2018-9-21-15-52-23deepbonehoz2 - Cloud' (14.39 Mb = 100.00% of points could be loaded)
[18:42:43] [Load] Can't guess file format: unhandled file extension '2Gs'
[18:42:45] [I/O] File 'D:/594b_12-10-2018/Daire-594b-Thesis-DATA/Day_2/LiDAR/2018-9-21-Deep-Bone-Room/2018-9-21-15-57-7_deep_bone_vert2.2Gs.xyz' loaded successfully
[18:42:45] [VBO] VBO(s) (re)initialized for cloud '2018-9-21-15-57-7_deep_bone_vert2 - Cloud' (12.53 Mb = 100.00% of points could be loaded)
[18:42:45] [Load] Can't guess file format: unhandled file extension '2Gs'
[18:42:46] [I/O] File 'D:/594b_12-10-2018/Daire-594b-Thesis-DATA/Day_2/LiDAR/2018-9-21-Deep-Bone-Room/2018-9-21-16-18-4_deep_bone_hor3.2Gs.xyz' loaded successfully
[18:42:47] [VBO] VBO(s) (re)initialized for cloud '2018-9-21-16-18-4_deep_bone_hor3 - Cloud' (13.71 Mb = 100.00% of points could be loaded)
[18:42:47] [Load] Can't guess file format: unhandled file extension '2Gs'
[18:42:48] [I/O] File 'D:/594b_12-10-2018/Daire-594b-Thesis-DATA/Day_2/LiDAR/2018-9-21-Deep-Bone-Room/2018-9-21-16-28-38_deep_bone_vert3.2Gs.xyz' loaded successfully
[18:42:48] [VBO] VBO(s) (re)initialized for cloud '2018-9-21-16-28-38_deep_bone_vert3 - Cloud' (13.70 Mb = 100.00% of points could be loaded)
[18:42:48] [Load] Can't guess file format: unhandled file extension '2Gs'
[18:42:50] [I/O] File 'D:/594b_12-10-2018/Daire-594b-Thesis-DATA/Day_2/LiDAR/2018-9-21-Deep-Bone-Room/2018-9-21-16-38-46_deep_Bone_hoz_4.2Gs.xyz' loaded successfully
[18:42:50] [VBO] VBO(s) (re)initialized for cloud '2018-9-21-16-38-46_deep_Bone_hoz_4 - Cloud' (13.77 Mb = 100.00% of points could be loaded)
[18:42:50] [Load] Can't guess file format: unhandled file extension '2Gs'
[18:42:52] [I/O] File 'D:/594b_12-10-2018/Daire-594b-Thesis-DATA/Day_2/LiDAR/2018-9-21-Deep-Bone-Room/2018-9-21-16-44-17_deep_bone_vert4.2Gs.xyz' loaded successfully
[18:42:52] [VBO] VBO(s) (re)initialized for cloud '2018-9-21-16-44-17_deep_bone_vert4 - Cloud' (13.70 Mb = 100.00% of points could be loaded)
[18:42:52] [Load] Can't guess file format: unhandled file extension '2Gs'
[18:42:53] [I/O] File 'D:/594b_12-10-2018/Daire-594b-Thesis-DATA/Day_2/LiDAR/2018-9-21-Deep-Bone-Room/2018-9-21-16-53-18_deep_bone_horz_5.2Gs.xyz' loaded successfully
[18:42:53] [VBO] VBO(s) (re)initialized for cloud '2018-9-21-16-53-18_deep_bone_horz_5 - Cloud' (14.32 Mb = 100.00% of points could be loaded)
[18:42:53] [Load] Can't guess file format: unhandled file extension '2Gs'
[18:42:55] [I/O] File 'D:/594b_12-10-2018/Daire-594b-Thesis-DATA/Day_2/LiDAR/2018-9-21-Deep-Bone-Room/2018-9-21-17-0-0_Deep_Bone_Vert_6.2Gs.xyz' loaded successfully
[18:42:55] [VBO] VBO(s) (re)initialized for cloud '2018-9-21-17-0-0_Deep_Bone_Vert_6 - Cloud' (13.49 Mb = 100.00% of points could be loaded)
[18:42:55] [Load] Can't guess file format: unhandled file extension '2Gs'
[18:42:56] [I/O] File 'D:/594b_12-10-2018/Daire-594b-Thesis-DATA/Day_2/LiDAR/2018-9-21-Deep-Bone-Room/2018-9-21-17-34-41_deep_bone_horz7.2Gs.xyz' loaded successfully
[18:42:57] [VBO] VBO(s) (re)initialized for cloud '2018-9-21-17-34-41_deep_bone_horz7 - Cloud' (13.71 Mb = 100.00% of points could be loaded)
[18:43:19] [Load] Can't guess file format: unhandled file extension '2Gs'

[18:43:20] [Load] Can't guess file format: unhandled file extension '2Gs'
[18:43:21] [I/O] File 'D:/594b_12-10-2018/Daire-594b-Thesis-DATA/Day_2/LiDAR/2018-9-21-Deep-Bone-Room/2018-9-21-15-25-12_deep_bone_hoz.2Gs.xyz' loaded successfully
[18:43:21] [VBO] VBO(s) (re)initialized for cloud '2018-9-21-15-25-12_deep_bone_hoz - Cloud' (0.07 Mb = 100.00% of points could be loaded)
[18:43:21] [Load] Can't guess file format: unhandled file extension '2Gs'
[18:43:25] [I/O] File 'D:/594b_12-10-2018/Daire-594b-Thesis-DATA/Day_2/LiDAR/2018-9-21-Deep-Bone-Room/2018-9-21-15-49-31_deep_bone_hoz2.2Gs.xyz' loaded successfully
[18:43:25] [VBO] VBO(s) (re)initialized for cloud '2018-9-21-15-49-31_deep_bone_hoz2 - Cloud' (13.22 Mb = 100.00% of points could be loaded)
[18:43:25] [Load] Can't guess file format: unhandled file extension '2Gs'
[18:43:27] [I/O] File 'D:/594b_12-10-2018/Daire-594b-Thesis-DATA/Day_2/LiDAR/2018-9-21-Deep-Bone-Room/2018-9-21-15-52-23deepbonehoz2.2Gs.xyz' loaded successfully
[18:43:27] [VBO] VBO(s) (re)initialized for cloud '2018-9-21-15-52-23deepbonehoz2 - Cloud' (14.39 Mb = 100.00% of points could be loaded)
[18:43:27] [Load] Can't guess file format: unhandled file extension '2Gs'
[18:43:30] [I/O] File 'D:/594b_12-10-2018/Daire-594b-Thesis-DATA/Day_2/LiDAR/2018-9-21-Deep-Bone-Room/2018-9-21-15-57-7_deep_bone_vert2.2Gs.xyz' loaded successfully
[18:43:30] [VBO] VBO(s) (re)initialized for cloud '2018-9-21-15-57-7_deep_bone_vert2 - Cloud' (12.53 Mb = 100.00% of points could be loaded)
[18:43:30] [Load] Can't guess file format: unhandled file extension '2Gs'
[18:43:33] [I/O] File 'D:/594b_12-10-2018/Daire-594b-Thesis-DATA/Day_2/LiDAR/2018-9-21-Deep-Bone-Room/2018-9-21-16-18-4_deep_bone_hor3.2Gs.xyz' loaded successfully
[18:43:33] [VBO] VBO(s) (re)initialized for cloud '2018-9-21-16-18-4_deep_bone_hor3 - Cloud' (13.71 Mb = 100.00% of points could be loaded)
[18:43:33] [Load] Can't guess file format: unhandled file extension '2Gs'
[18:43:35] [I/O] File 'D:/594b_12-10-2018/Daire-594b-Thesis-DATA/Day_2/LiDAR/2018-9-21-Deep-Bone-Room/2018-9-21-16-28-38_deep_bone_vert3.2Gs.xyz' loaded successfully
[18:43:35] [VBO] VBO(s) (re)initialized for cloud '2018-9-21-16-28-38_deep_bone_vert3 - Cloud' (13.70 Mb = 100.00% of points could be loaded)
[18:43:35] [Load] Can't guess file format: unhandled file extension '2Gs'
[18:43:38] [I/O] File 'D:/594b_12-10-2018/Daire-594b-Thesis-DATA/Day_2/LiDAR/2018-9-21-Deep-Bone-Room/2018-9-21-16-38-46_deep_Bone_hoz_4.2Gs.xyz' loaded successfully
[18:43:38] [VBO] VBO(s) (re)initialized for cloud '2018-9-21-16-38-46_deep_Bone_hoz_4 - Cloud' (13.77 Mb = 100.00% of points could be loaded)
[18:43:38] [Load] Can't guess file format: unhandled file extension '2Gs'
[18:43:41] [I/O] File 'D:/594b_12-10-2018/Daire-594b-Thesis-DATA/Day_2/LiDAR/2018-9-21-Deep-Bone-Room/2018-9-21-16-44-17_deep_bone_vert4.2Gs.xyz' loaded successfully
[18:43:41] [VBO] VBO(s) (re)initialized for cloud '2018-9-21-16-44-17_deep_bone_vert4 - Cloud' (13.70 Mb = 100.00% of points could be loaded)
[18:43:41] [Load] Can't guess file format: unhandled file extension '2Gs'
[18:43:43] [I/O] File 'D:/594b_12-10-2018/Daire-594b-Thesis-DATA/Day_2/LiDAR/2018-9-21-Deep-Bone-Room/2018-9-21-16-53-18_deep_bone_horz_5.2Gs.xyz' loaded successfully
[18:43:43] [VBO] VBO(s) (re)initialized for cloud '2018-9-21-16-53-18_deep_bone_horz_5 - Cloud' (14.32 Mb = 100.00% of points could be loaded)

[18:43:43] [Load] Can't guess file format: unhandled file extension '2Gs'
[18:43:45] [I/O] File 'D:/594b_12-10-2018/Daire-594b-Thesis-DATA/Day_2/LiDAR/2018-9-21-Deep-Bone-Room/2018-9-21-17-0-0_Deep_Bone_Vert_6.2Gs.xyz' loaded successfully
[18:43:45] [VBO] VBO(s) (re)initialized for cloud '2018-9-21-17-0-0_Deep_Bone_Vert_6 - Cloud' (13.49 Mb = 100.00% of points could be loaded)
[18:43:45] [Load] Can't guess file format: unhandled file extension '2Gs'
[18:43:47] [I/O] File 'D:/594b_12-10-2018/Daire-594b-Thesis-DATA/Day_2/LiDAR/2018-9-21-Deep-Bone-Room/2018-9-21-17-34-41_deep_bone_horz7.2Gs.xyz' loaded successfully
[18:43:47] [VBO] VBO(s) (re)initialized for cloud '2018-9-21-17-34-41_deep_bone_horz7 - Cloud' (13.71 Mb = 100.00% of points could be loaded)
[18:44:58] [I/O] File 'D:/594b_12-10-2018/Daire-594b-Thesis-DATA/2018_Survey_May/Cenote_Taj_Ma_Hal/Full Site Final Alignments/Chamber_Line_End_SO4.txt' loaded successfully
[18:44:58] [VBO] VBO(s) (re)initialized for cloud 'Chamber_Line_End_SO4 - Cloud' (57.20 Mb = 100.00% of points could be loaded)
[18:44:59] [AsciiFilter::Load] Line 1 is corrupted (found 1 part(s) on 7 expected)!
[18:45:07] [I/O] File 'D:/594b_12-10-2018/Daire-594b-Thesis-DATA/2018_Survey_May/Cenote_Taj_Ma_Hal/Full Site Final Alignments/Chamber_Line_End_SO4.pts' loaded successfully
[18:45:07] [VBO] VBO(s) (re)initialized for cloud 'Chamber_Line_End_SO4 - Cloud' (57.20 Mb = 100.00% of points could be loaded)
[18:45:07] [AsciiFilter::Load] Line 1 is corrupted (found 1 part(s) on 7 expected)!
[18:45:12] [I/O] File 'D:/594b_12-10-2018/Daire-594b-Thesis-DATA/2018_Survey_May/Cenote_Taj_Ma_Hal/Full Site Final Alignments/Chamber_Walls_SO4_FOI.pts' loaded successfully
[18:45:12] [VBO] VBO(s) (re)initialized for cloud 'Chamber_Walls_SO4_FOI - Cloud' (32.66 Mb = 100.00% of points could be loaded)
[18:45:13] [AsciiFilter::Load] Line 1 is corrupted (found 1 part(s) on 7 expected)!
[18:45:13] [I/O] File 'D:/594b_12-10-2018/Daire-594b-Thesis-DATA/2018_Survey_May/Cenote_Taj_Ma_Hal/Full Site Final Alignments/Corridor_Line_SO4_FOI.pts' loaded successfully
[18:45:14] [VBO] VBO(s) (re)initialized for cloud 'Corridor_Line_SO4_FOI - Cloud' (6.45 Mb = 100.00% of points could be loaded)
[18:45:14] [Load] Can't guess file format: unhandled file extension 'xml'
[18:45:15] [Load] Can't guess file format: unhandled file extension 'xml'
[18:45:16] [AsciiFilter::Load] Line 1 is corrupted (found 1 part(s) on 7 expected)!
[18:45:16] [I/O] File 'D:/594b_12-10-2018/Daire-594b-Thesis-DATA/2018_Survey_May/Cenote_Taj_Ma_Hal/Full Site Final Alignments/Chmaber_Survey_Line_Paleontological_SO4_FOI.pts' loaded successfully
[18:45:16] [VBO] VBO(s) (re)initialized for cloud 'Chmaber_Survey_Line_Paleontological_SO4_FOI - Cloud' (1.33 Mb = 100.00% of points could be loaded)
[18:45:16] [OBJ] D:/594b_12-10-2018/Daire-594b-Thesis-DATA/2018_Survey_May/Cenote_Taj_Ma_Hal/Full Site Final Alignments/Day_3_AOI_Complete_Deep_Bone_Room.obj

[18:45:17] [OBJ] 35339 points, 0 faces
[18:45:17] [OBJ] 0 tex. coords, 35339 normals
[18:45:17] [I/O] File 'D:/594b_12-10-2018/Daire-594b-Thesis-DATA/2018_Survey_May/Cenote_Taj_Ma_Hal/Full Site Final Alignments/Day_3_AOI_Complete_Deep_Bone_Room.obj' loaded successfully
[18:45:17] [VBO] VBO(s) (re)initialized for cloud 'vertices' (0.40 Mb = 100.00% of points could be loaded)
[18:45:17] [I/O] File 'D:/594b_12-10-2018/Daire-594b-Thesis-DATA/2018_Survey_May/Cenote_Taj_Ma_Hal/Full Site Final Alignments/Day_3_AOI_Complete_Deep_Bone_Room.txt' loaded successfully
[18:45:17] [VBO] VBO(s) (re)initialized for cloud 'Day_3_AOI_Complete_Deep_Bone_Room - Cloud' (0.51 Mb = 100.00% of points could be loaded)
[18:45:17] [LAS] D:/594b_12-10-2018/Daire-594b-Thesis-DATA/2018_Survey_May/Cenote_Taj_Ma_Hal/Full Site Final Alignments/Day_3_AOI_Complete_Deep_Bone_Room.las - signature: LASF
[18:45:19] [LAS] Cloud has been recentered! Translation: (1000.00 ; 1000.00 ; 1000.00)
[18:45:19] [LAS] Color components are coded on 16 bits
[18:45:19] [LAS] All 'User Data' values were the same (0)! We ignored them...
[18:45:19] [LAS] All 'Scan Angle Rank' values were the same (0)! We ignored them...
[18:45:19] [LAS] All 'Flightline Edge' values were the same (0)! We ignored them...
[18:45:19] [LAS] All 'Number of Returns' values were the same (1)! We ignored them...
[18:45:19] [LAS] All 'Return Number' values were the same (1)! We ignored them...
[18:45:19] [LAS] All 'Classification' values were the same (0)! We ignored them...
[18:45:19] [I/O] File 'D:/594b_12-10-2018/Daire-594b-Thesis-DATA/2018_Survey_May/Cenote_Taj_Ma_Hal/Full Site Final Alignments/Day_3_AOI_Complete_Deep_Bone_Room.las' loaded successfully
[18:45:19] [VBO] VBO(s) (re)initialized for cloud 'Day_3_AOI_Complete_Deep_Bone_Room - Cloud' (0.51 Mb = 100.00% of points could be loaded)
[18:45:19] [LAS] D:/594b_12-10-2018/Daire-594b-Thesis-DATA/2018_Survey_May/Cenote_Taj_Ma_Hal/Full Site Final Alignments/Day_3_AOI_Complete_Deep_Bone_Room.laz - signature: LASF
[18:45:20] [LAS] Cloud has been recentered! Translation: (1000.00 ; 1000.00 ; 1000.00)
[18:45:20] [LAS] Color components are coded on 16 bits
[18:45:20] [LAS] All 'User Data' values were the same (0)! We ignored them...
[18:45:20] [LAS] All 'Scan Angle Rank' values were the same (0)! We ignored them...
[18:45:20] [LAS] All 'Flightline Edge' values were the same (0)! We ignored them...
[18:45:20] [LAS] All 'Number of Returns' values were the same (1)! We ignored them...
[18:45:20] [LAS] All 'Return Number' values were the same (1)! We ignored them...
[18:45:20] [LAS] All 'Classification' values were the same (0)! We ignored them...
[18:45:20] [I/O] File 'D:/594b_12-10-2018/Daire-594b-Thesis-DATA/2018_Survey_May/Cenote_Taj_Ma_Hal/Full Site Final Alignments/Day_3_AOI_Complete_Deep_Bone_Room.laz' loaded successfully
[18:45:20] [VBO] VBO(s) (re)initialized for cloud 'Day_3_AOI_Complete_Deep_Bone_Room - Cloud' (0.51 Mb = 100.00% of points could be loaded)
[18:45:21] [AsciiFilter::Load] Line 1 is corrupted (found 1 part(s) on 7 expected)!

[18:45:21] [I/O] File 'D:/594b_12-10-2018/Daire-594b-Thesis-DATA/2018_Survey_May/Cenote_Taj_Ma_Hal/Full Site Final Alignments/Day_3_AOI_Complete_Deep_Bone_Room.pts' loaded successfully
[18:45:21] [VBO] VBO(s) (re)initialized for cloud 'Day_3_AOI_Complete_Deep_Bone_Room - Cloud' (0.51 Mb = 100.00% of points could be loaded)
[18:46:08] [Load] Can't guess file format: unhandled file extension '2Gs'
[18:46:09] [Load] Can't guess file format: unhandled file extension '2Gs'
[18:46:10] [I/O] File 'D:/594b_12-10-2018/Daire-594b-Thesis-DATA/Day_2/LiDAR/2018-9-21-Deep-Bone-Room/2018-9-21-15-25-12_deep_bone_hoz.2Gs.xyz' loaded successfully
[18:46:10] [VBO] VBO(s) (re)initialized for cloud '2018-9-21-15-25-12_deep_bone_hoz - Cloud' (0.07 Mb = 100.00% of points could be loaded)
[18:46:10] [Load] Can't guess file format: unhandled file extension '2Gs'
[18:46:11] [I/O] File 'D:/594b_12-10-2018/Daire-594b-Thesis-DATA/Day_2/LiDAR/2018-9-21-Deep-Bone-Room/2018-9-21-15-49-31_deep_bone_hoz2.2Gs.xyz' loaded successfully
[18:46:11] [VBO] VBO(s) (re)initialized for cloud '2018-9-21-15-49-31_deep_bone_hoz2 - Cloud' (13.22 Mb = 100.00% of points could be loaded)
[18:46:11] [Load] Can't guess file format: unhandled file extension '2Gs'
[18:46:13] [I/O] File 'D:/594b_12-10-2018/Daire-594b-Thesis-DATA/Day_2/LiDAR/2018-9-21-Deep-Bone-Room/2018-9-21-15-52-23deepbonehoz2.2Gs.xyz' loaded successfully
[18:46:13] [VBO] VBO(s) (re)initialized for cloud '2018-9-21-15-52-23deepbonehoz2 - Cloud' (14.39 Mb = 100.00% of points could be loaded)
[18:46:13] [Load] Can't guess file format: unhandled file extension '2Gs'
[18:46:14] [I/O] File 'D:/594b_12-10-2018/Daire-594b-Thesis-DATA/Day_2/LiDAR/2018-9-21-Deep-Bone-Room/2018-9-21-15-57-7_deep_bone_vert2.2Gs.xyz' loaded successfully
[18:46:14] [VBO] VBO(s) (re)initialized for cloud '2018-9-21-15-57-7_deep_bone_vert2 - Cloud' (12.53 Mb = 100.00% of points could be loaded)
[18:46:14] [Load] Can't guess file format: unhandled file extension '2Gs'
[18:46:16] [I/O] File 'D:/594b_12-10-2018/Daire-594b-Thesis-DATA/Day_2/LiDAR/2018-9-21-Deep-Bone-Room/2018-9-21-16-18-4_deep_bone_hor3.2Gs.xyz' loaded successfully
[18:46:16] [VBO] VBO(s) (re)initialized for cloud '2018-9-21-16-18-4_deep_bone_hor3 - Cloud' (13.71 Mb = 100.00% of points could be loaded)
[18:46:16] [Load] Can't guess file format: unhandled file extension '2Gs'
[18:46:18] [I/O] File 'D:/594b_12-10-2018/Daire-594b-Thesis-DATA/Day_2/LiDAR/2018-9-21-Deep-Bone-Room/2018-9-21-16-28-38_deep_bone_vert3.2Gs.xyz' loaded successfully
[18:46:18] [VBO] VBO(s) (re)initialized for cloud '2018-9-21-16-28-38_deep_bone_vert3 - Cloud' (13.70 Mb = 100.00% of points could be loaded)
[18:46:18] [Load] Can't guess file format: unhandled file extension '2Gs'
[18:46:19] [I/O] File 'D:/594b_12-10-2018/Daire-594b-Thesis-DATA/Day_2/LiDAR/2018-9-21-Deep-Bone-Room/2018-9-21-16-38-46_deep_Bone_hoz_4.2Gs.xyz' loaded successfully
[18:46:19] [VBO] VBO(s) (re)initialized for cloud '2018-9-21-16-38-46_deep_Bone_hoz_4 - Cloud' (13.77 Mb = 100.00% of points could be loaded)
[18:46:19] [Load] Can't guess file format: unhandled file extension '2Gs'
[18:46:21] [I/O] File 'D:/594b_12-10-2018/Daire-594b-Thesis-DATA/Day_2/LiDAR/2018-9-21-Deep-Bone-Room/2018-9-21-16-44-17_deep_bone_vert4.2Gs.xyz' loaded successfully

[18:46:21] [VBO] VBO(s) (re)initialized for cloud '2018-9-21-16-44-17_deep_bone_vert4 - Cloud' (13.70 Mb = 100.00% of points could be loaded)
[18:46:21] [Load] Can't guess file format: unhandled file extension '2Gs'
[18:46:22] [I/O] File 'D:/594b_12-10-2018/Daire-594b-Thesis-DATA/Day_2/LiDAR/2018-9-21-Deep-Bone-Room/2018-9-21-16-53-18_deep_bone_horz_5.2Gs.xyz' loaded successfully
[18:46:22] [VBO] VBO(s) (re)initialized for cloud '2018-9-21-16-53-18_deep_bone_horz_5 - Cloud' (14.32 Mb = 100.00% of points could be loaded)
[18:46:22] [Load] Can't guess file format: unhandled file extension '2Gs'
[18:46:24] [I/O] File 'D:/594b_12-10-2018/Daire-594b-Thesis-DATA/Day_2/LiDAR/2018-9-21-Deep-Bone-Room/2018-9-21-17-0-0_Deep_Bone_Vert_6.2Gs.xyz' loaded successfully
[18:46:24] [VBO] VBO(s) (re)initialized for cloud '2018-9-21-17-0-0_Deep_Bone_Vert_6 - Cloud' (13.49 Mb = 100.00% of points could be loaded)
[18:46:24] [Load] Can't guess file format: unhandled file extension '2Gs'
[18:46:25] [I/O] File 'D:/594b_12-10-2018/Daire-594b-Thesis-DATA/Day_2/LiDAR/2018-9-21-Deep-Bone-Room/2018-9-21-17-34-41_deep_bone_horz7.2Gs.xyz' loaded successfully
[18:46:25] [VBO] VBO(s) (re)initialized for cloud '2018-9-21-17-34-41_deep_bone_horz7 - Cloud' (13.71 Mb = 100.00% of points could be loaded)
[18:48:31] [LAS] D:/594b_12-10-2018/Daire-594b-Thesis-DATA/2018_Survey_May/Cenote_Taj_Ma_Hal/Full Site Final Alignments/Day_3_AOI_Complete_Deep_Bone_Room.laz - signature: LASF
[18:48:35] An error occurred while loading 'Day_3_AOI_Complete_Deep_Bone_Room': process canceled by user
[18:48:45] [I/O] File 'D:/594b_12-10-2018/Daire-594b-Thesis-DATA/2018_Survey_May/Cenote_Taj_Ma_Hal/Full Site Final Alignments/Day_3_AOI_Complete_Deep_Bone_Room.txt' loaded successfully
[18:48:45] [VBO] VBO(s) (re)initialized for cloud 'Day_3_AOI_Complete_Deep_Bone_Room - Cloud' (0.51 Mb = 100.00% of points could be loaded)
[18:48:46] [AsciiFilter::Load] Line 1 is corrupted (found 1 part(s) on 7 expected)!
[18:48:46] [I/O] File 'D:/594b_12-10-2018/Daire-594b-Thesis-DATA/2018_Survey_May/Cenote_Taj_Ma_Hal/Full Site Final Alignments/Day_3_AOI_Complete_Deep_Bone_Room.pts' loaded successfully
[18:48:47] [VBO] VBO(s) (re)initialized for cloud 'Day_3_AOI_Complete_Deep_Bone_Room - Cloud' (0.51 Mb = 100.00% of points could be loaded)
[18:48:47] [AsciiFilter::Load] Line 1 is corrupted (found 1 part(s) on 7 expected)!
[18:48:48] [I/O] File 'D:/594b_12-10-2018/Daire-594b-Thesis-DATA/2018_Survey_May/Cenote_Taj_Ma_Hal/Full Site Final Alignments/Corridor_Line_SO4_FOI.pts' loaded successfully
[18:48:48] [VBO] VBO(s) (re)initialized for cloud 'Corridor_Line_SO4_FOI - Cloud' (6.45 Mb = 100.00% of points could be loaded)
[18:48:49] [AsciiFilter::Load] Line 1 is corrupted (found 1 part(s) on 7 expected)!
[18:48:50] [I/O] File 'D:/594b_12-10-2018/Daire-594b-Thesis-DATA/2018_Survey_May/Cenote_Taj_Ma_Hal/Full Site Final Alignments/Chmaber_Survey_Line_Paleontological_SO4_FOI.pts' loaded successfully

[18:48:50] [VBO] VBO(s) (re)initialized for cloud 'Chmaber_Survey_Line_Paleontological_SO4_FOI - Cloud' (1.33 Mb = 100.00% of points could be loaded)

[18:48:51] [AsciiFilter::Load] Line 1 is corrupted (found 1 part(s) on 7 expected)!

[18:48:55] [I/O] File 'D:/594b_12-10-2018/Daire-594b-Thesis-DATA/2018_Survey_May/Cenote_Taj_Ma_Hal/Full Site Final Alignments/Chamber_Walls_SO4_FOI.pts' loaded successfully

[18:48:55] [VBO] VBO(s) (re)initialized for cloud 'Chamber_Walls_SO4_FOI - Cloud' (32.66 Mb = 100.00% of points could be loaded)

[18:49:06] [I/O] File 'D:/594b_12-10-2018/Daire-594b-Thesis-DATA/2018_Survey_May/Cenote_Taj_Ma_Hal/Full Site Final Alignments/Chamber_Line_End_SO4.txt' loaded successfully

[18:49:07] [VBO] VBO(s) (re)initialized for cloud 'Chamber_Line_End_SO4 - Cloud' (57.20 Mb = 100.00% of points could be loaded)

[18:49:08] [AsciiFilter::Load] Line 1 is corrupted (found 1 part(s) on 7 expected)!

[18:49:16] [I/O] File 'D:/594b_12-10-2018/Daire-594b-Thesis-DATA/2018_Survey_May/Cenote_Taj_Ma_Hal/Full Site Final Alignments/Chamber_Line_End_SO4.pts' loaded successfully

[18:49:16] [VBO] VBO(s) (re)initialized for cloud 'Chamber_Line_End_SO4 - Cloud' (57.20 Mb = 100.00% of points could be loaded)2